Computational Cosmology

Dr Noam I Libeskind

The majority of these notes are credited to Alexander Knebe:

http://popia.ft.uam.es/ACO/lectures.html

A crash course in Computational Cosmology

Dr Noam I Libeskind

A crash course in Computational Cosmology

Dr Noam I Libeskind

Why use computers?
The N body problem

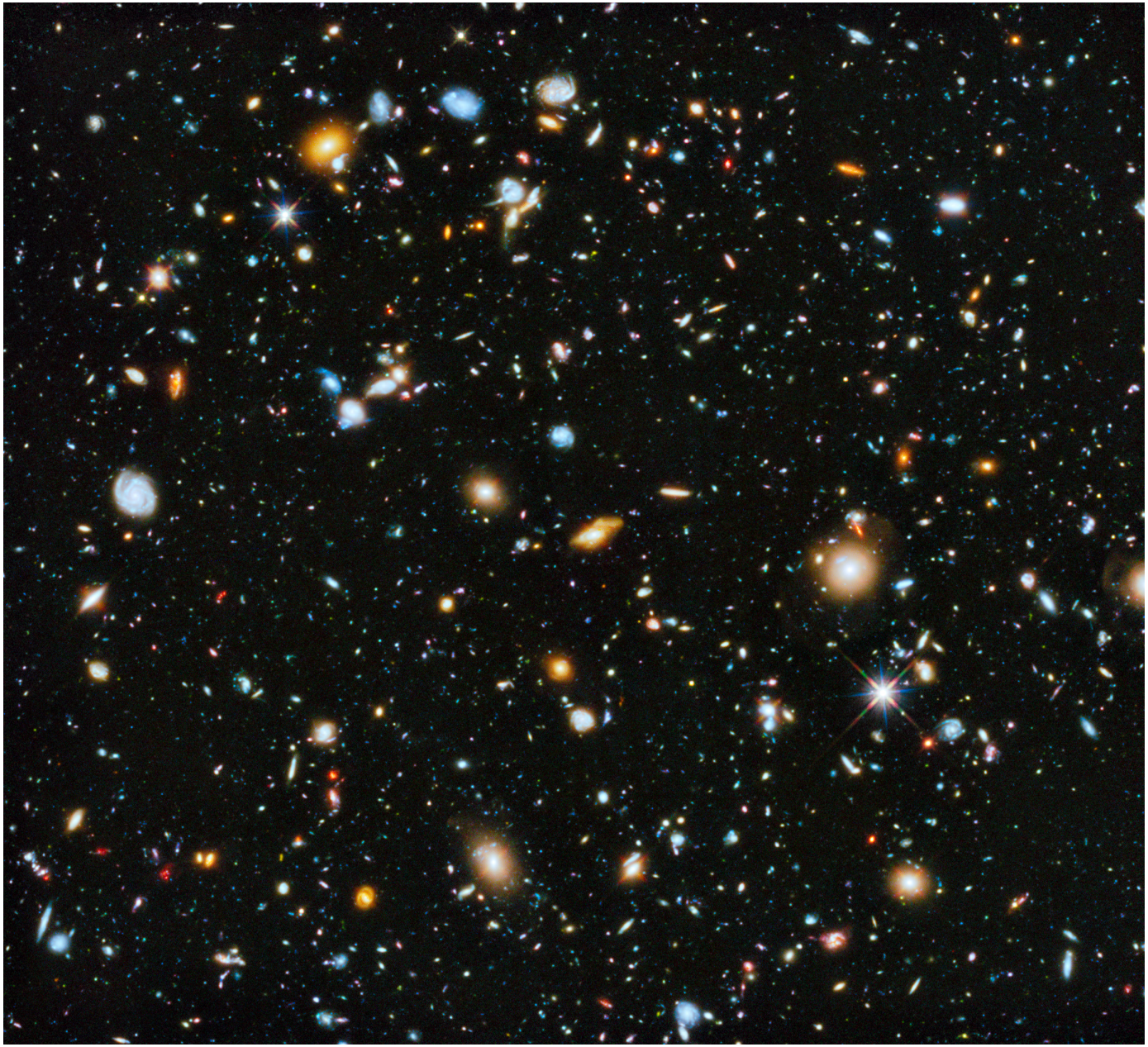

Hubble deep field

Webb field – 50,000 galaxies

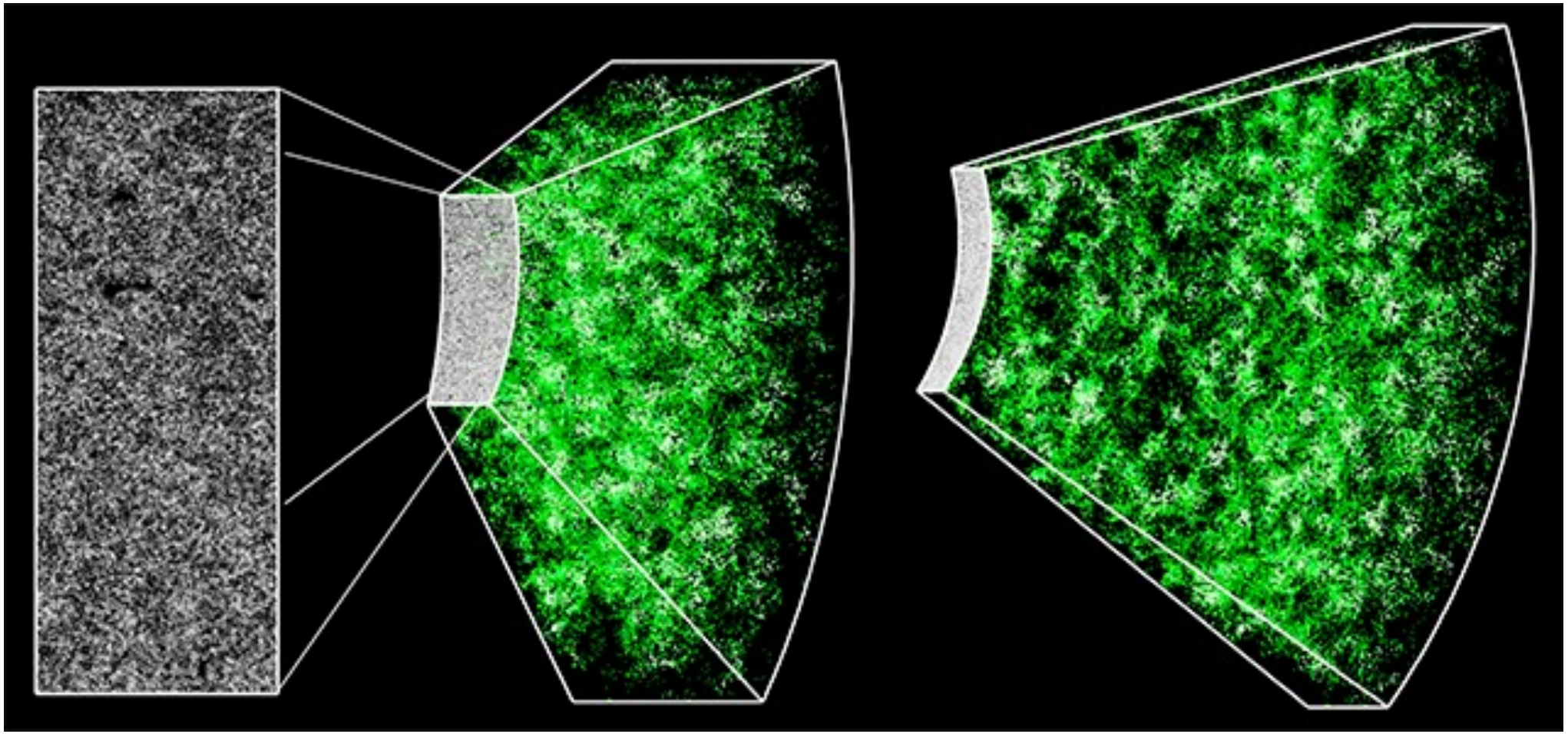

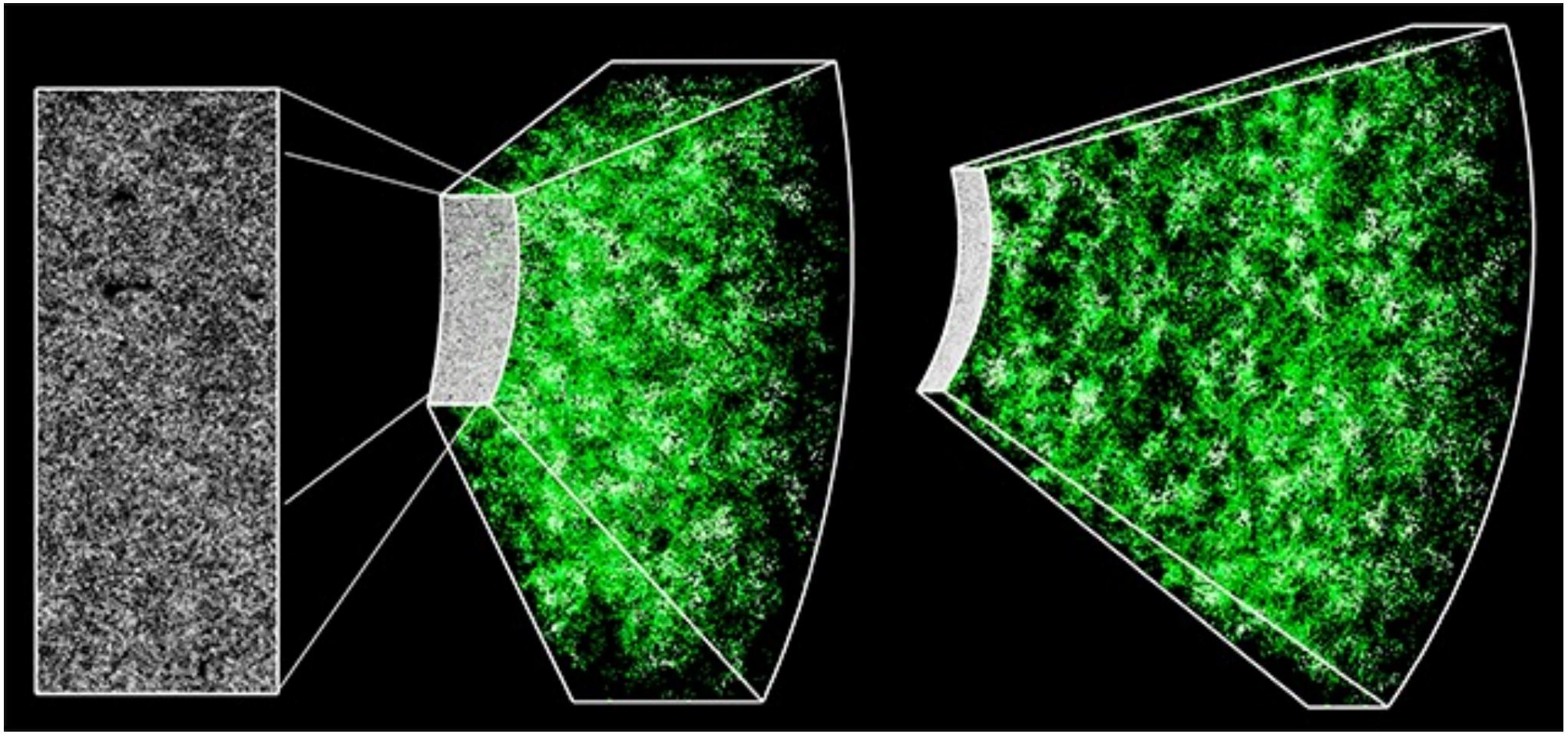

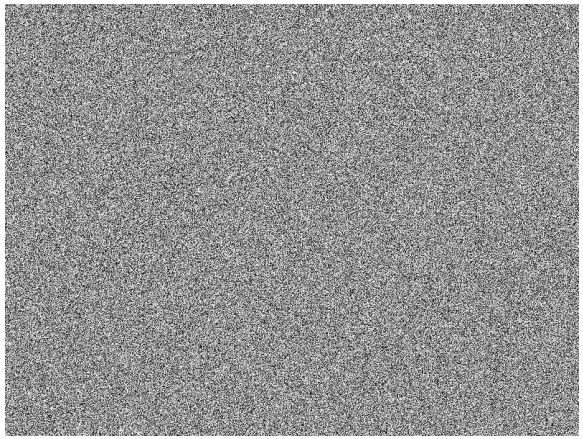

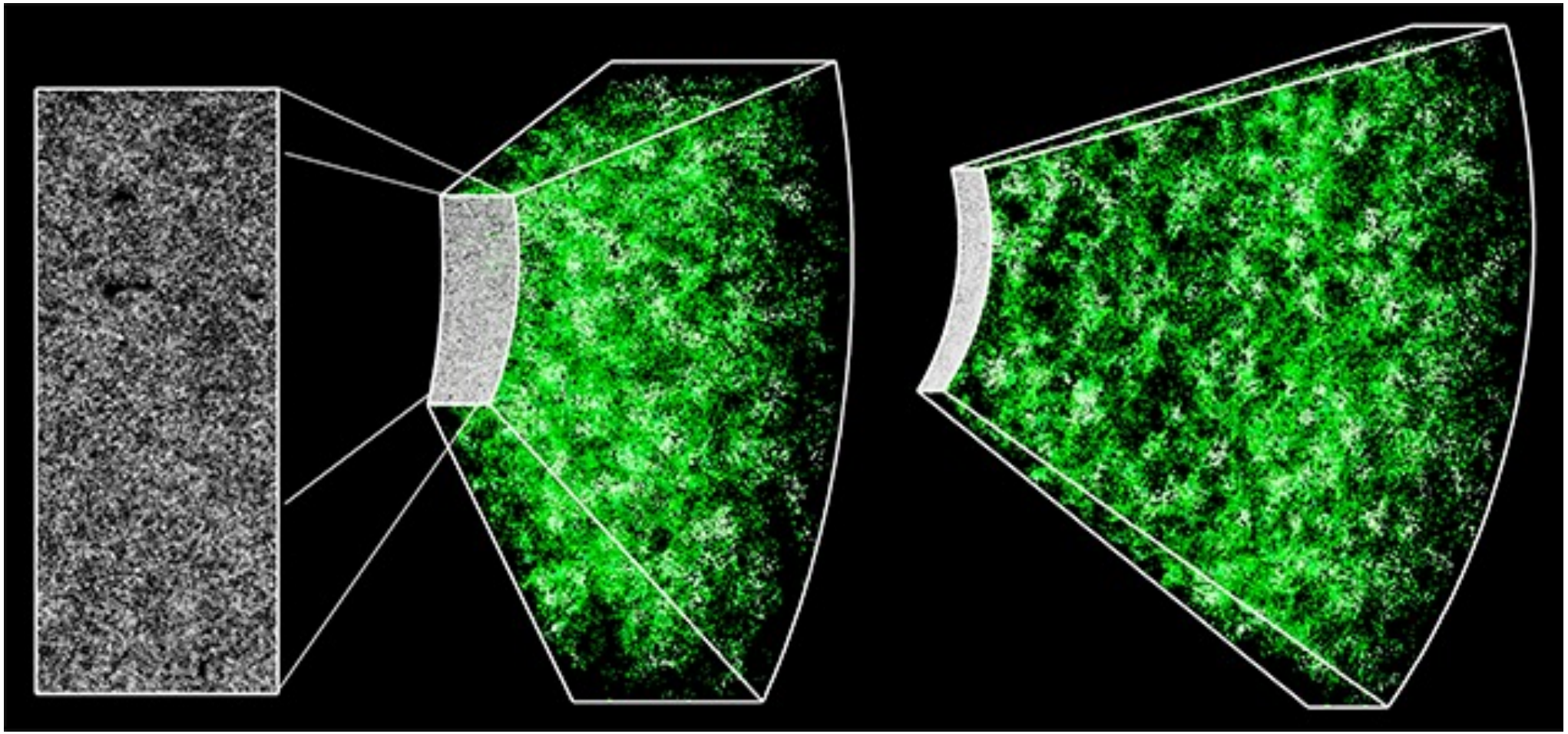

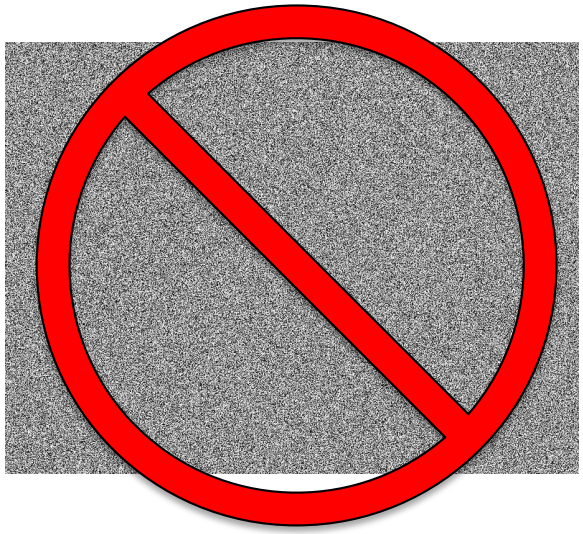

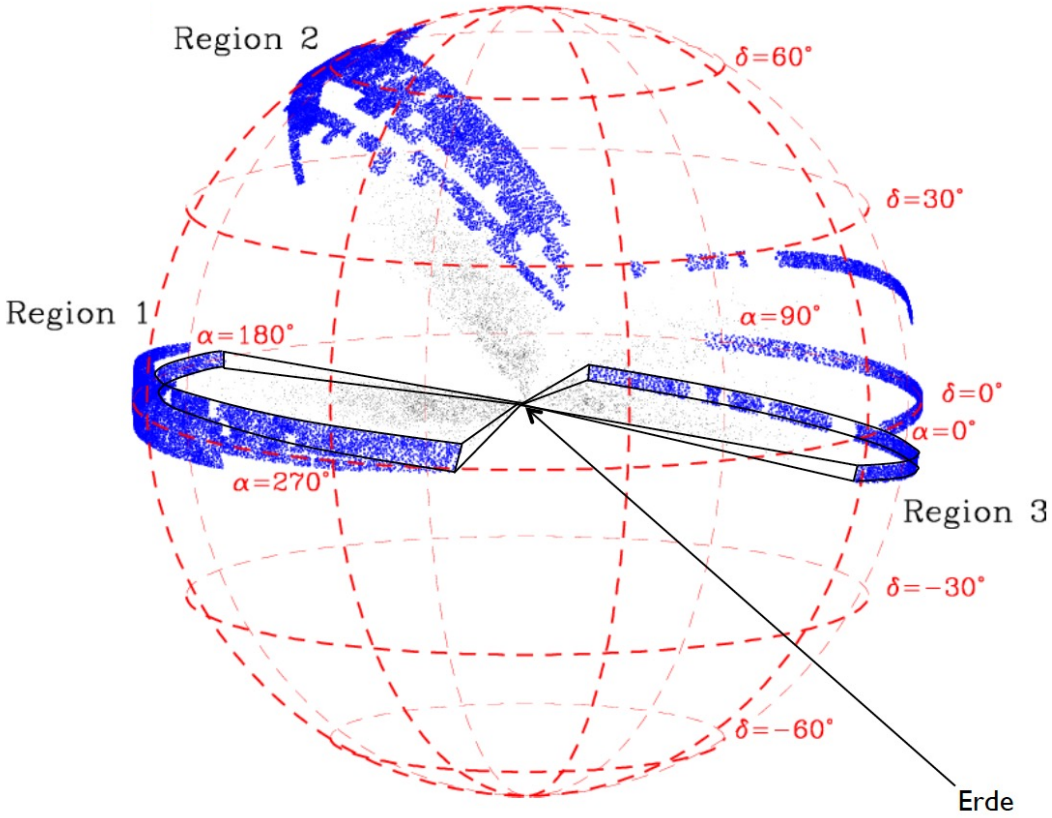
Region 2
δ=60°
δ=30°
Region 1
α=90°
α=180°
δ=0°
α=0°
α=270°
Region 3
δ=−30°
δ=−60°
Erde

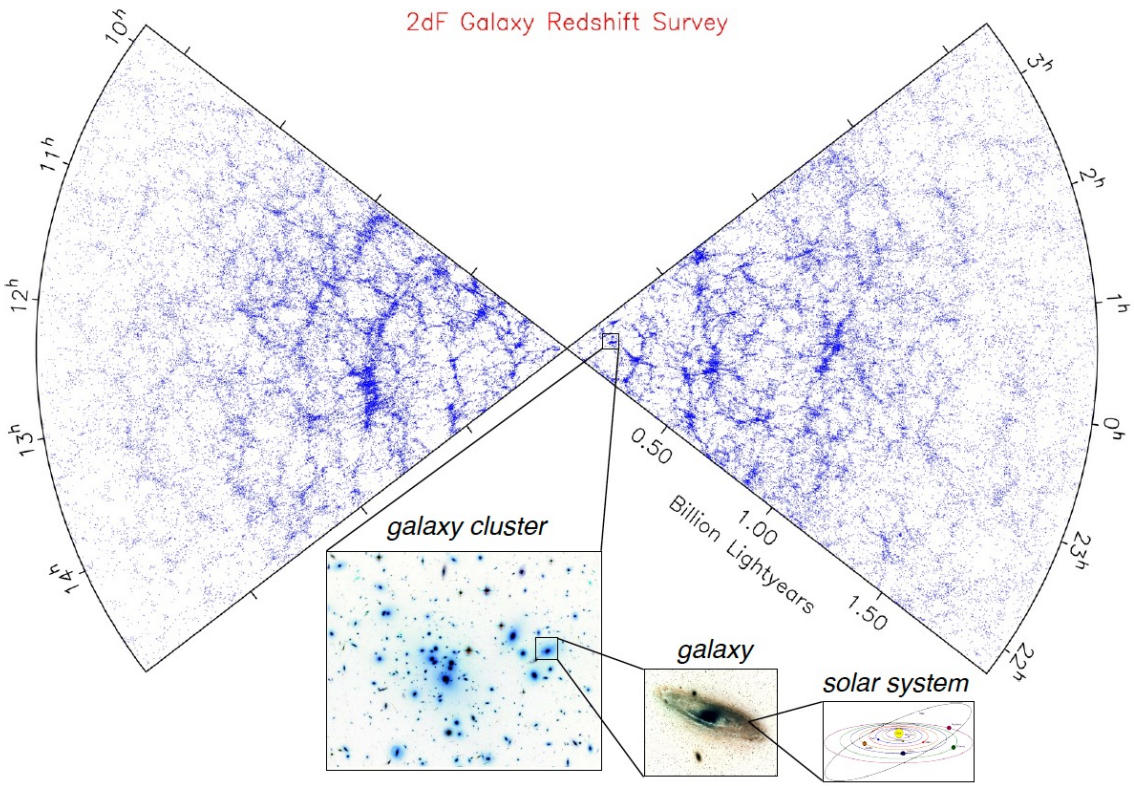
2dF Galaxy Redshift Survey
10h
11h
12h
13h
14h
3h
2h
1h
0h
23h
22h
0.50
1.00
1.50
Billion Lightyears
galaxy cluster
galaxy
solar system

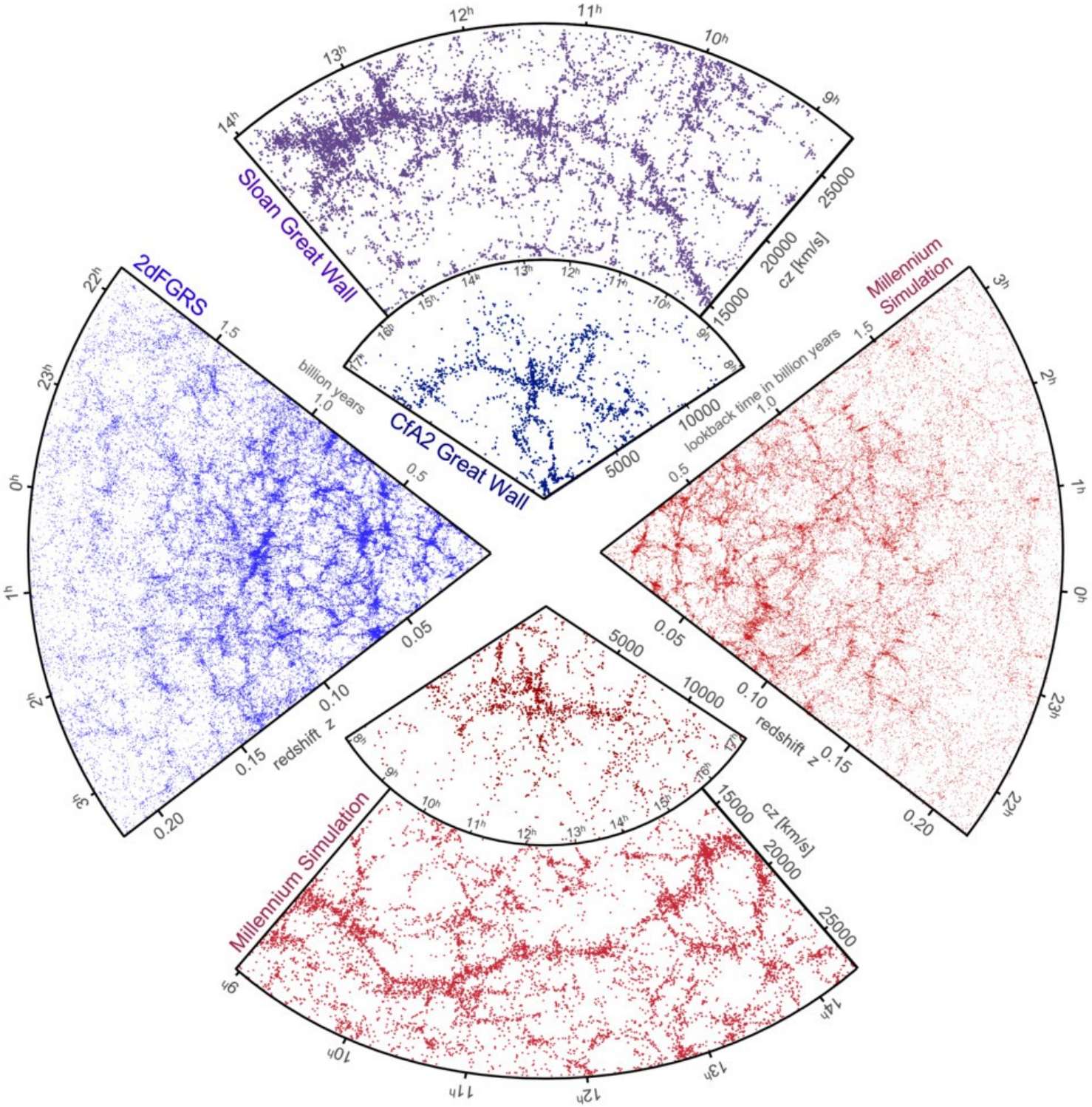
Sloan Great Wall
2dFGRS
CfA2 Great Wall
Millennium Simulation
Millennium Simulation
cz [km/s]
billion years
lookback time in billion years
redshift z

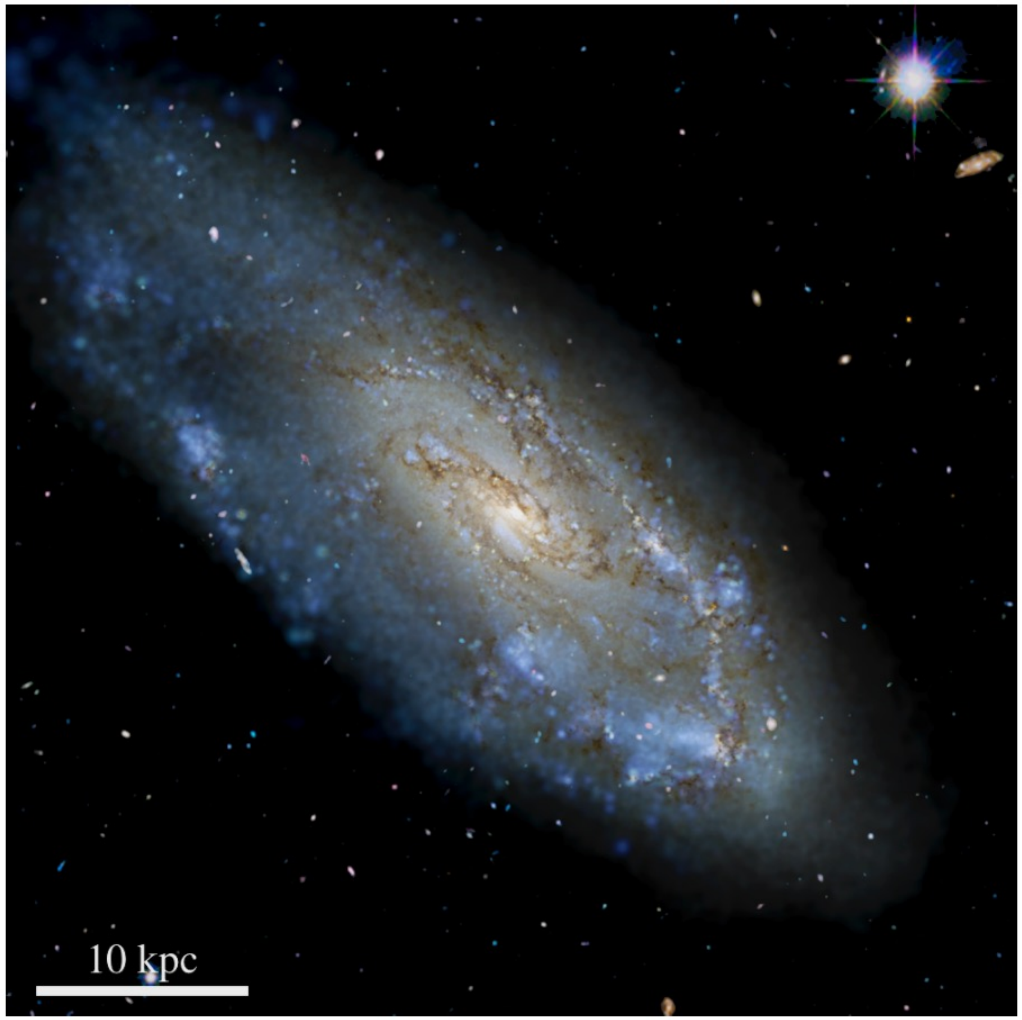

Latte simulation

M31, *Andromeda*

"Dynamical range"

The range of scales that are important. In cosmology its enormous for example

Object	Scale (m)	Scale (Mpc)
Black hole	10^{10}	1e-12
Interstellar distances	10^{16}	1e-8
Small galaxies	10^{20}	0.01
Milky Way halo	10^{21}	0.1
Local Group distances	10^{22}	1
Cluster	10^{23}	10
Large-scale structures	10^{24}	100

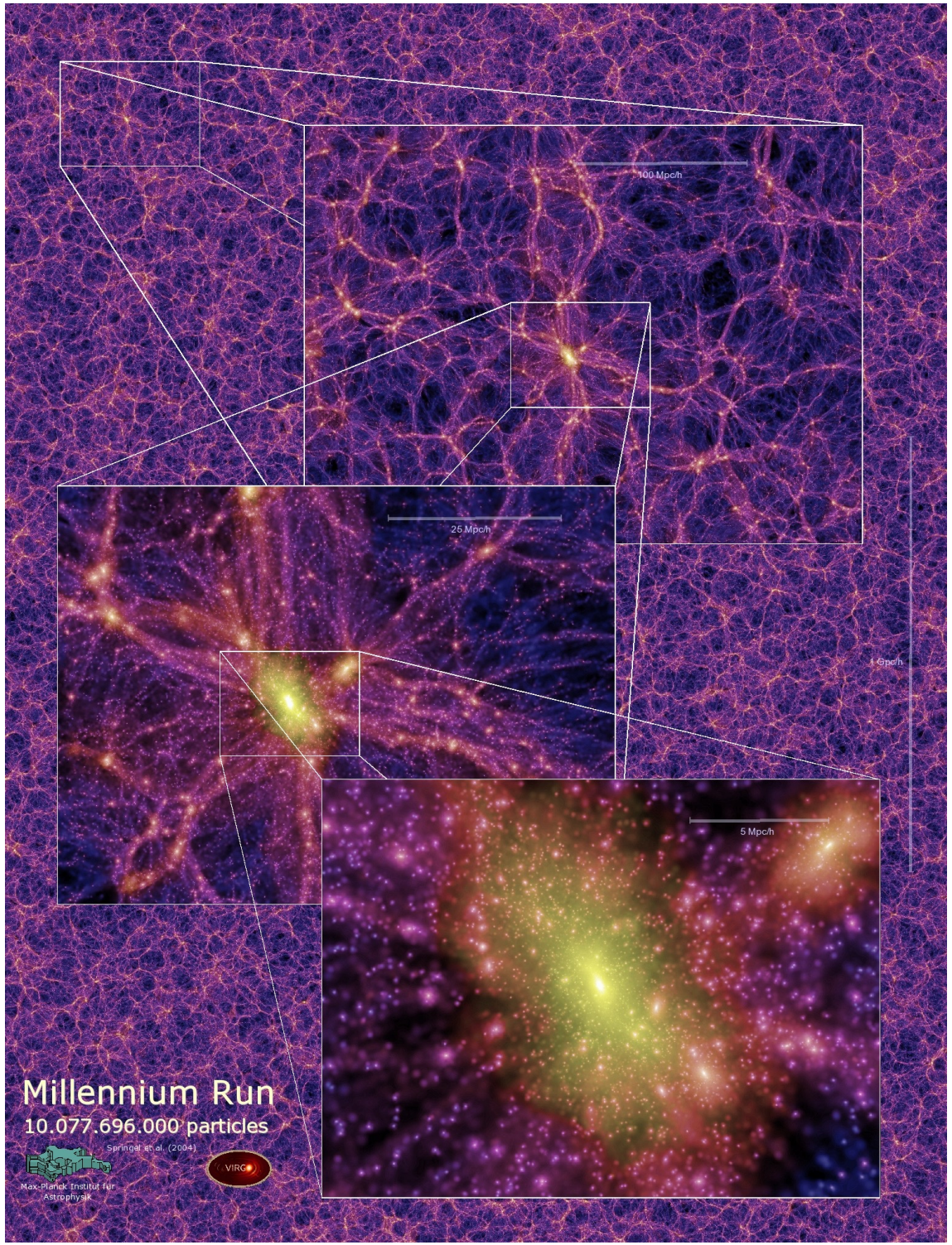

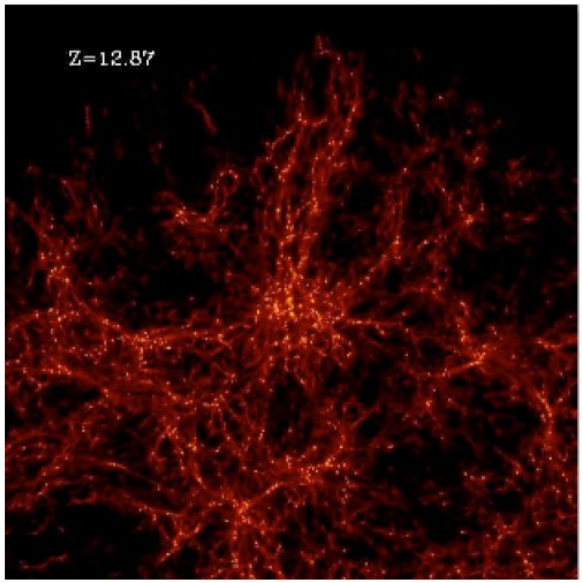

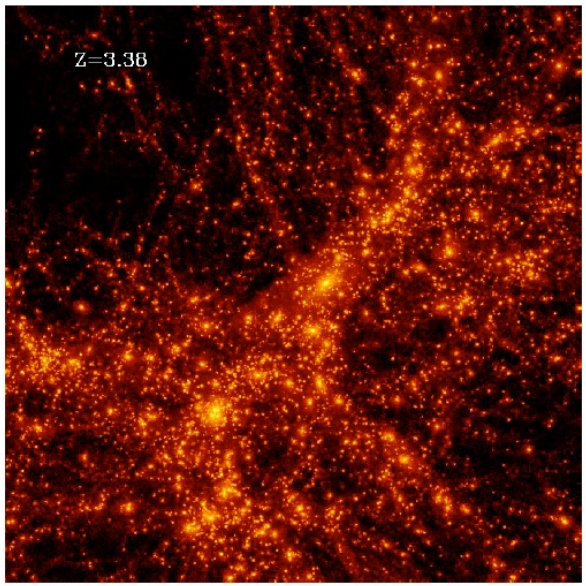

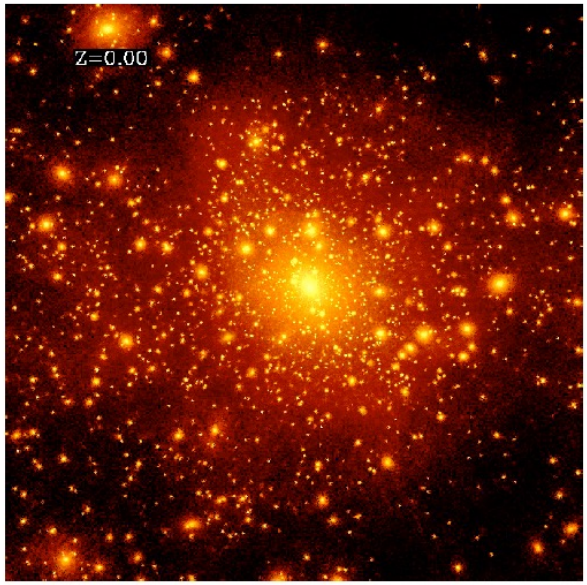

Multi body gravitational dynamics

Complex (but tractable) problem!

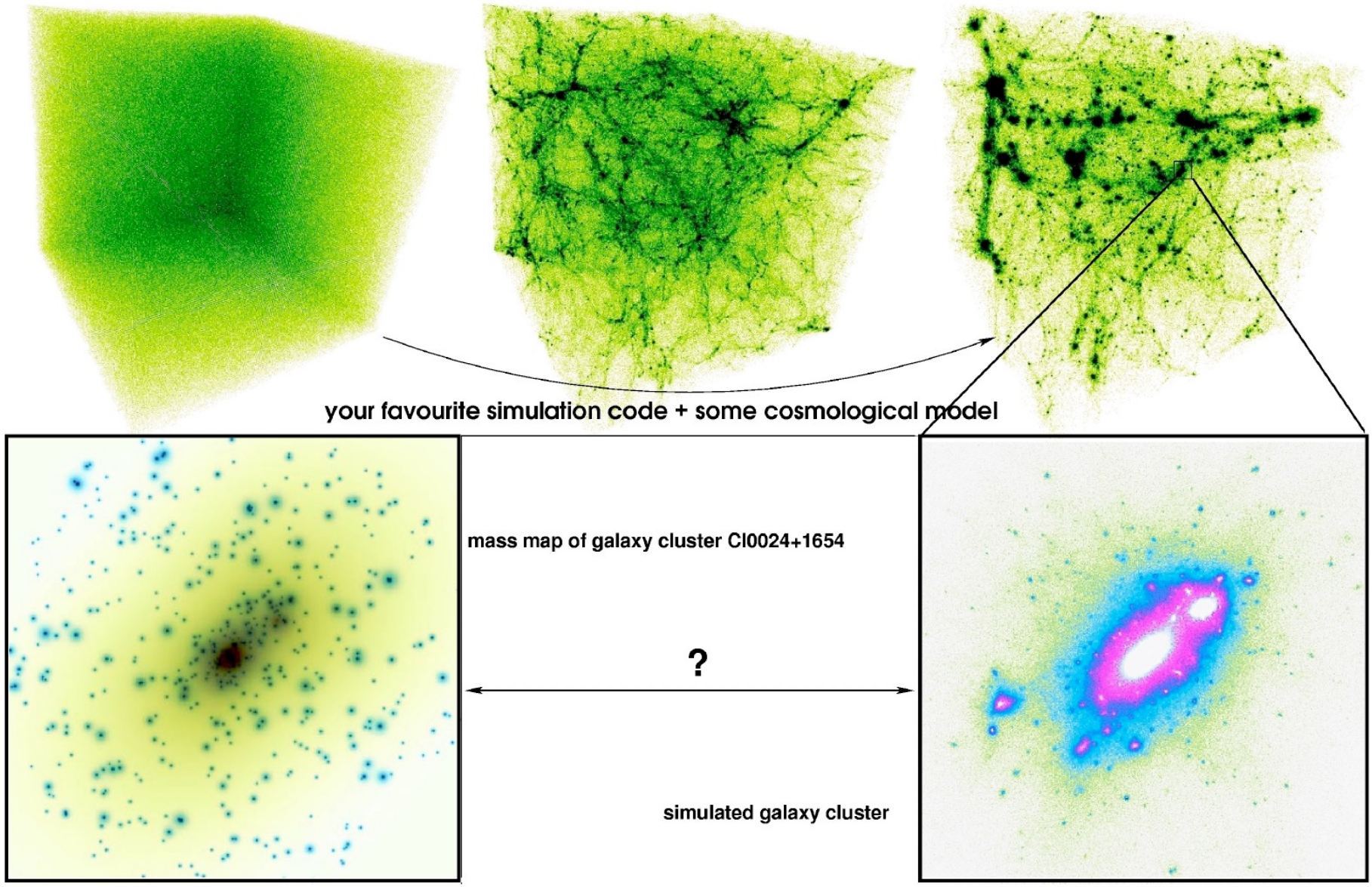
your favourite simulation code + some cosmological model
mass map of galaxy cluster Cl0024+1654
?
simulated galaxy cluster

Roger Penrose, Reinhard Genzel and Andrea Ghez. Credit: Ill. Niklas Elmehed. © Nobel Media.

Monthly Notices of the ROYAL ASTRONOMICAL SOCIETY

MNRAS **495,** 3403–3408 (2020) doi:10.1093/mnras/staa1343
Advance Access publication 2020 May 18

Apparent evidence for Hawking points in the CMB Sky★

Daniel An,[1] Krzysztof A. Meissner,[2] Paweł Nurowski[3]† and Roger Penrose[4]

[1]*Science Department, SUNY Maritime College, 6 Pennyfield Av., Throggs Neck, NY 10465, USA*
[2]*Faculty of Physics, University of Warsaw, Pasteura 5, PL-02-093 Warsaw, Poland*
[3]*Center for Theoretical Physics of PAS, Al. Lotników 32/46, PL-02-688 Warsaw, Poland*
[4]*Mathematical Institute, Oxford University, Radcliffe Observatory Quarter, Woodstock Rd., Oxford OX2 6GG, UK*

Accepted 2020 May 6. Received 2020 May 6; in original form 2019 September 3

ABSTRACT

This paper presents strong observational evidence of numerous previously unobserved anomalous circular spots, of significantly raised temperature, in the cosmic microwave background sky. The spots have angular radii between 0.03 and 0.04 rad (i.e. angular diameters between about 3° and 4°). There is a clear cut-off at that size, indicating that each anomalous spot would have originated from a highly energetic point-like source, located at the end of inflation – or else point-like at the conformally expanded Big Bang, if it is considered that there was no inflationary phase. The significant presence of these anomalous spots, was initially noticed in the *Planck* 70 GHz satellite data by comparison with 1000 standard simulations, and then confirmed by extending the comparison to 10 000 simulations. Such anomalous points were then found at precisely the same locations in the *WMAP (Wilkinson Microwave Anisotropy Probe)* data, their significance was confirmed by comparison with 1000 *WMAP* simulations. *Planck* and *WMAP* have very different noise properties and it seems exceedingly unlikely that the observed presence of anomalous points in the same directions on both maps may come entirely from the noise. Subsequently, further confirmation was found in the *Planck* data by comparison with 1000 FFP8.1 MC simulations (with $l \leq 1500$). The existence of such anomalous regions, resulting from point-like sources at the conformally stretched-out big bang, is a predicted consequence of conformal cyclic cosmology, these sources being the Hawking points of the theory, resulting from the Hawking radiation from supermassive black holes in a cosmic aeon prior to our own.

Key words: cosmic background radiation.

PACS: 04.20.Ha – 04.70.Dy – 98.80.Bp – 98.80.Ft.

Roger Penrose, Reinhard Genzel and Andrea Ghez. Credit: Ill. Niklas Elmehed. © Nobel Media.

Monthly Notices of the ROYAL ASTRONOMICAL SOCIETY

MNRAS **495,** 3403–3408 (2020) doi:10.1093/mnras/staa1343
Advance Access publication 2020 May 18

Apparent evidence for Hawking points in the CMB Sky★

Daniel An,[1] Krzysztof A. Meissner,[2] Paweł Nurowski[3]† and Roger Penrose[4]

[1]*Science Department, SUNY Maritime College, 6 Pennyfield Av., Throggs Neck, NY 10465, USA*
[2]*Faculty of Physics, University of Warsaw, Pasteura 5, PL-02-093 Warsaw, Poland*
[3]*Center for Theoretical Physics of PAS, Al. Lotników 32/46, PL-02-688 Warsaw, Poland*
[4]*Mathematical Institute, Oxford University, Radcliffe Observatory Quarter, Woodstock Rd., Oxford OX2 6GG, UK*

The significant presence of these anomalous spots, was initially noticed in the *Planck* 70 GHz satellite data by comparison with 1000 standard simulations, and then confirmed by extending the comparison to 10 000 simulations.

This paper presents strong observational evidence of numerous previously unobserved anomalous circular spots, of significantly raised temperature, in the cosmic microwave background sky. The spots have angular radii between 0.03 and 0.04 rad (i.e. angular diameters between about 3° and 4°). There is a clear cut-off at that size, indicating that each anomalous spot would have originated from a highly energetic point-like source, located at the end of inflation – or else point-like at the conformally expanded Big Bang, if it is considered that there was no inflationary phase. The significant presence of these anomalous spots, was initially noticed in the *Planck* 70 GHz satellite data by comparison with 1000 standard simulations, and then confirmed by extending the comparison to 10 000 simulations. Such anomalous points were then found at precisely the same locations in the *WMAP (Wilkinson Microwave Anisotropy Probe)* data, their significance was confirmed by comparison with 1000 *WMAP* simulations. *Planck* and *WMAP* have very different noise properties and it seems exceedingly unlikely that the observed presence of anomalous points in the same directions on both maps may come entirely from the noise. Subsequently, further confirmation was found in the *Planck* data by comparison with 1000 FFP8.1 MC simulations (with $l \leq 1500$). The existence of such anomalous regions, resulting from point-like sources at the conformally stretched-out big bang, is a predicted consequence of conformal cyclic cosmology, these sources being the Hawking points of the theory, resulting from the Hawking radiation from supermassive black holes in a cosmic aeon prior to our own.

Key words: cosmic background radiation.

PACS: 04.20.Ha – 04.70.Dy – 98.80.Bp – 98.80.Ft.

Monthly Notices of the ROYAL ASTRONOMICAL SOCIETY

MNRAS **494,** 4168–4186 (2020) doi:10.1093/mnras/staa922
Advance Access publication 2020 April 7

A parameter survey of Sgr A∗ radiative models from GRMHD simulations with self-consistent electron heating

J. Dexter ,[1,2★] A. Jiménez-Rosales,[1★] S. M. Ressler,[3] A. Tchekhovskoy,[4] M. Bauböck,[1] P. T. de Zeeuw,[1] F. Eisenhauer,[1] S. von Fellenberg,[1] F. Gao,[1] R. Genzel,[1,5] S. Gillessen,[1] M. Habibi,[1] T. Ott,[1] J. Stadler,[1] O. Straub[1] and F. Widmann[1]

[1]*Max Planck Institute for Extraterrestrial Physics (MPE), Giessenbachstr 1, D-85748 Garching, Germany*
[2]*JILA and Department of Astrophysical and Planetary Sciences, University of Colorado, Boulder, CO 80309, USA*
[3]*Kavli Institute for Theoretical Physics, University of California Santa Barbara, Kohn Hall, Santa Barbara, CA 93107, USA*
[4]*Center for Interdisciplinary Exploration & Research in Astrophysics (CIERA), Physics & Astronomy, Northwestern University, Evanston, IL 60202, USA*
[5]*Departments of Physics and Astronomy, Le Conte Hall, University of California, Berkeley, CA 94720, USA*

Accepted 2020 March 21. Received 2020 March 20; in original form 2020 February 1

ABSTRACT

The Galactic centre black hole candidate Sgr A∗ is the best target for studies of low-luminosity accretion physics, including with near-infrared (NIR) and submillimetre wavelength long baseline interferometry experiments. Here, we compare images and spectra generated from a parameter survey of general relativistic MHD simulations to a set of radio to NIR observations of Sgr A∗. Our models span the limits of weak and strong magnetization and use a range of sub-grid prescriptions for electron heating. We find two classes of scenarios can explain the broad shape of the submillimetre spectral peak and the highly variable NIR flaring emission. Weakly magnetized 'disc-jet' models where most of the emission is produced near the jet wall, consistent with past work, as well as strongly magnetized (magnetically arrested disc) models where hot electrons are present everywhere. Disc-jet models are strongly depolarized at submillimetre wavelengths as a result of strong Faraday rotation, inconsistent with observations of Sgr A∗. We instead favour the strongly magnetized models, which provide a good description of the median and highly variable linear polarization signal. The same models can also explain the observed mean Faraday rotation measure and potentially the polarization signals seen recently in Sgr A∗ NIR flares.

Key words: accretion, accretion discs – black hole physics – MHD – polarization – radiative transfer – Galaxy: centre.

Monthly Notices of the ROYAL ASTRONOMICAL SOCIETY

MNRAS **495,** 3403–3408 (2020) doi:10.1093/mnras/staa1343
Advance Access publication 2020 May 18

Apparent evidence for Hawking points in the CMB Sky★

Daniel An,[1] Krzysztof A. Meissner,[2] Paweł Nurowski[3]† and Roger Penrose[4]

[1]*Science Department, SUNY Maritime College, 6 Pennyfield Av., Throggs Neck, NY 10465, USA*
[2]*Faculty of Physics, University of Warsaw, Pasteura 5, PL-02-093 Warsaw, Poland*
[3]*Center for Theoretical Physics of PAS, Al. Lotników 32/46, PL-02-688 Warsaw, Poland*
[4]*Mathematical Institute, Oxford University, Radcliffe Observatory Quarter, Woodstock Rd., Oxford OX2 6GG, UK*

Accepted 2020 May 6. Received 2020 May 6; in original form 2019 September 3

ABSTRACT

This paper presents strong observational evidence of numerous previously unobserved anomalous circular spots, of significantly raised temperature, in the cosmic microwave background sky. The spots have angular radii between 0.03 and 0.04 rad (i.e. angular diameters between about 3° and 4°). There is a clear cut-off at that size, indicating that each anomalous spot would have originated from a highly energetic point-like source, located at the end of inflation – or else point-like at the conformally expanded Big Bang, if it is considered that there was no inflationary phase. The significant presence of these anomalous spots, was initially noticed in the *Planck* 70 GHz satellite data by comparison with 1000 standard simulations, and then confirmed by extending the comparison to 10 000 simulations. Such anomalous points were then found at precisely the same locations in the *WMAP (Wilkinson Microwave Anisotropy Probe)* data, their significance was confirmed by comparison with 1000 *WMAP* simulations. *Planck* and *WMAP* have very different noise properties and it seems exceedingly unlikely that the observed presence of anomalous points in the same directions on both maps may come entirely from the noise. Subsequently, further confirmation was found in the *Planck* data by comparison with 1000 FFP8.1 MC simulations (with $l \leq 1500$). The existence of such anomalous regions, resulting from point-like sources at the conformally stretched-out big bang, is a predicted consequence of conformal cyclic cosmology, these sources being the Hawking points of the theory, resulting from the Hawking radiation from supermassive black holes in a cosmic aeon prior to our own.

Key words: cosmic background radiation.

PACS: 04.20.Ha – 04.70.Dy – 98.80.Bp – 98.80.Ft.

Monthly Notices of the ROYAL ASTRONOMICAL SOCIETY

MNRAS **494,** 4168–4186 (2020) doi:10.1093/mnras/staa922
Advance Access publication 2020 April 7

A parameter survey of Sgr A∗ radiative models from GRMHD simulations with self-consistent electron heating

J. Dexter ,[1,2★] A. Jiménez-Rosales,[1★] S. M. Ressler,[3] A. Tchekhovskoy,[4]
M. Bauböck,[1] P. T. de Zeeuw,[1] F. Eisenhauer,[1] S. von Fellenberg,[1] F. Gao,[1]
R. Genzel,[1,5] S. Gillessen,[1] M. Habibi,[1] T. Ott,[1] J. Stadler,[1] O. Straub[1] and F. Widmann[1]

[1]*Max Planck Institute for Extraterrestrial Physics (MPE), Giessenbachstr 1, D-85748 Garching, Germany*
[2]*JILA and Department of Astrophysical and Planetary Sciences, University of Colorado, Boulder, CO 80309, USA*
[3]*Kavli Institute for Theoretical Physics, University of California Santa Barbara, Kohn Hall, Santa Barbara, CA 93107, USA*
[4]*Center for Interdisciplinary Exploration & Research in Astrophysics (CIERA), Physics & Astronomy, Northwestern University, Evanston, IL 60202, USA*
[5]*Departments of Physics and Astronomy, Le Conte Hall, University of California, Berkeley, CA 94720, USA*

Accepted 2020 M

Here, we compare images and spectra generated from a parameter survey of general relativistic MHD simulations to a set of radio to NIR observations of Sgr A∗. (

accretion physics, including with near-infrared (NIR) and submillimetre wavelength long baseline interferometry experiments. Here, we compare images and spectra generated from a parameter survey of general relativistic MHD simulations to a set of radio to NIR observations of Sgr A∗. Our models span the limits of weak and strong magnetization and use a range of sub-grid prescriptions for electron heating. We find two classes of scenarios can explain the broad shape of the submillimetre spectral peak and the highly variable NIR flaring emission. Weakly magnetized 'disc-jet' models where most of the emission is produced near the jet wall, consistent with past work, as well as strongly magnetized (magnetically arrested disc) models where hot electrons are present everywhere. Disc-jet models are strongly depolarized at submillimetre wavelengths as a result of strong Faraday rotation, inconsistent with observations of Sgr A∗. We instead favour the strongly magnetized models, which provide a good description of the median and highly variable linear polarization signal. The same models can also explain the observed mean Faraday rotation measure and potentially the polarization signals seen recently in Sgr A∗ NIR flares.

Key words: accretion, accretion discs – black hole physics – MHD – polarization – radiative transfer – Galaxy: centre.

Monthly Notices of the ROYAL ASTRONOMICAL SOCIETY

MNRAS **495,** 3403–3408 (2020) doi:10.1093/mnras/staa1343
Advance Access publication 2020 May 18

Apparent evidence for Hawking points in the CMB Sky★

Daniel An,[1] Krzysztof A. Meissner,[2] Paweł Nurowski[3]† and Roger Penrose[4]

[1]*Science Department, SUNY Maritime College, 6 Pennyfield Av., Throggs Neck, NY 10465, USA*
[2]*Faculty of Physics, University of Warsaw, Pasteura 5, PL-02-093 Warsaw, Poland*
[3]*Center for Theoretical Physics of PAS, Al. Lotników 32/46, PL-02-688 Warsaw, Poland*
[4]*Mathematical Institute, Oxford University, Radcliffe Observatory Quarter, Woodstock Rd., Oxford OX2 6GG, UK*

Accepted 2020 May 6. Received 2020 May 6; in original form 2019 September 3

ABSTRACT

This paper presents strong observational evidence of numerous previously unobserved anomalous circular spots, of significantly raised temperature, in the cosmic microwave background sky. The spots have angular radii between 0.03 and 0.04 rad (i.e. angular diameters between about 3° and 4°). There is a clear cut-off at that size, indicating that each anomalous spot would have originated from a highly energetic point-like source, located at the end of inflation – or else point-like at the conformally expanded Big Bang, if it is considered that there was no inflationary phase. The significant presence of these anomalous spots, was initially noticed in the *Planck* 70 GHz satellite data by comparison with 1000 standard simulations, and then confirmed by extending the comparison to 10 000 simulations. Such anomalous points were then found at precisely the same locations in the *WMAP (Wilkinson Microwave Anisotropy Probe)* data, their significance was confirmed by comparison with 1000 *WMAP* simulations. *Planck* and *WMAP* have very different noise properties and it seems exceedingly unlikely that the observed presence of anomalous points in the same directions on both maps may come entirely from the noise. Subsequently, further confirmation was found in the *Planck* data by comparison with 1000 FFP8.1 MC simulations (with $l \leq 1500$). The existence of such anomalous regions, resulting from point-like sources at the conformally stretched-out big bang, is a predicted consequence of conformal cyclic cosmology, these sources being the
ting from the Hawking radiation from supermassive black
own.

adiation.

0.Bp – 98.80.Ft.

Monthly Notices of the ROYAL ASTRONOMICAL SOCIETY

MNRAS **494,** 4168–4186 (2020) doi:10.1093/mnras/staa922
Advance Access publication 2020 April 7

A parameter survey of Sgr A∗ radiative models from GRMHD simulations with self-consistent electron heating

J. Dexter,[1,2★] A. Jiménez-Rosales,[1★] S. M. Ressler,[3] A. Tchekhovskoy,[4] M. Bauböck,[1] P. T. de Zeeuw,[1] F. Eisenhauer,[1] S. von Fellenberg,[1] F. Gao,[1] R. Genzel,[1,5] S. Gillessen,[1] M. Habibi,[1] T. Ott,[1] J. Stadler,[1] O. Straub[1] and F. Widmann[1]

[1]*Max Planck Institute for Extraterrestrial Physics (MPE), Giessenbachstr 1, D-85748 Garching, Germany*
[2]*JILA and Department of Astrophysical and Planetary Sciences, University of Colorado, Boulder, CO 80309, USA*
[3]*Kavli Institute for Theoretical Physics, University of California Santa Barbara, Kohn Hall, Santa Barbara, CA 93107, USA*
[4]*Center for Interdisciplinary Exploration & Research in Astrophysics (CIERA), Physics & Astronomy, Northwestern University, Evanston, IL 60202, USA*
[5]*Departments of Physics and Astronomy, Le Conte Hall, University of California, Berkeley, CA 94720, USA*

Accepted 2020 March 21. Received 2020 March 20; in original form 2020 February 1

ABSTRACT

The Galactic centre black hole candidate Sgr A∗ is the best target for studies of low-luminosity accretion physics, including with near-infrared (NIR) and submillimetre wavelength long baseline interferometry experiments. Here, we compare images and spectra generated from a parameter survey of general relativistic MHD simulations to a set of radio to NIR observations of Sgr A∗. Our models span the limits of weak and strong magnetization and use a range of sub-grid prescriptions for electron heating. We find two classes of scenarios can explain the broad shape of the submillimetre spectral peak and the highly variable NIR flaring emission. Weakly magnetized 'disc-jet' models where most of the emission is produced near the jet wall, consistent with past work, as well as strongly magnetized (magnetically arrested disc) models where hot electrons are present everywhere. Disc-jet models are strongly depolarized at submillimetre wavelengths as a result of strong Faraday rotation, inconsistent with observations of Sgr A∗. We instead favour the strongly magnetized models, which provide a good description of the median and highly variable linear polarization signal. The same models can also explain the observed mean Faraday rotation measure and potentially the polarization signals seen recently in Sgr A∗ NIR flares.

Key words: accretion, accretion discs – black hole physics – MHD – polarization – radiative transfer – Galaxy: centre.

Monthly Notices of the ROYAL ASTRONOMICAL SOCIETY

MNRAS **495,** 3403–3408 (2020) doi:10.1093/mnras/staa1343
Advance Access publication 2020 May 18

Apparent evidence for Hawking points in the CMB Sky★

Daniel An,[1] Krzysztof A. Meissner,[2] Paweł Nurowski[3]† and Roger Penrose[4]

[1]*Science Department, SUNY Maritime College, 6 Pennyfield Av., Throggs Neck, NY 10465, USA*
[2]*Faculty of Physics, University of Warsaw, Pasteura 5, PL-02-093 Warsaw, Poland*
[3]*Center for Theoretical Physics of PAS, Al. Lotników 32/46, PL-02-688 Warsaw, Poland*
[4]*Mathematical Institute, Oxford University, Radcliffe Observatory Quarter, Woodstock Rd., Oxford OX2 6GG, UK*

Accepted 2020 May 6. Received 2020 May 6; in original form 2019 September 3

ABSTRACT

This paper presents strong observational evidence of numerous previously unobserved anomalous circular spots, of significantly raised temperature, in the cosmic microwave background sky. The spots have angular radii between 0.03 and 0.04 rad (i.e. angular diameters between about 3° and 4°). There is a clear cut-off at that size, indicating that each anomalous spot would have originated from a highly energetic point-like source, located at the end of inflation – or else point-like at the conformally expanded Big Bang, if it is considered that there was no inflationary phase. The significant presence of these anomalous spots, was initially noticed in the *Planck* 70 GHz satellite data by comparison with 1000 standard simulations, and then confirmed by extending the comparison to 10 000 simulations. Such anomalous points were then found at precisely the same locations in the *WMAP (Wilkinson Microwave*

ıтrophysical Journal, 897:135 (14pp), 2020 July 10 https://doi.org/10.3847/1538-4357/ab980d

ıctic Center IRS 13E: Colliding Stellar Winds or an Intermediate-mass Black Hole?

Zhenlin Zhu[1,2,3,4], Zhiyuan Li[1,2], Anna Ciurlo[5], Mark R. Morris[5], Mengfei Zhang[1,2], Tuan Do[5], and Andrea M. Ghez[5]

chool of Astronomy and Space Science, Nanjing University, Nanjing 210023, People's Republic of China; zhuzl@smail.nju.edu.cn, lizy@nju.edu.cn
Key Laboratory of Modern Astronomy and Astrophysics (Nanjing University), Ministry of Education, Nanjing 210023, People's Republic of China
[3] SRON Netherlands Institute for Space Research, Sorbonnelaan 2, 3584 CA Utrecht, The Netherlands
[4] Leiden Observatory, Leiden University, Niels Bohrweg 2, 2300 RA Leiden, The Netherlands
[5] Department of Physics and Astronomy, University of California, Los Angeles, CA 90095, USA
Received 2020 March 18; revised 2020 May 26; accepted 2020 May 28; published 2020 July 10

Abstract

A small cluster of massive stars residing in the Galactic center, collectively known as IRS 13E, is of special interest due to its close proximity to the central supermassive black hole Sgr A* and the possibility that an embedded intermediate-mass black hole (IMBH) binds its member stars. It has been suggested that colliding winds from two member stars, both classified as Wolf–Rayet type, are responsible for the observed X-ray, infrared, and radio emission from IRS 13E. We have conducted an in-depth study of the X-ray spatial, temporal, and spectral properties of IRS 13E, based on 5.6 Ms of ultradeep Chandra observations obtained over 20 years. These X-ray observations show no significant evidence for source variability. We have also explored the kinematics of the cluster members, using Keck near-infrared imaging and spectroscopic data on a 14 yr baseline that considerably improve the accuracy of the stars' proper motions. The observations are interpreted using three-dimensional hydrodynamical simulations of colliding winds tailored to match the physical conditions of IRS 13E, leading us to conclude that the observed X-ray spectrum and morphology can be well explained by the colliding wind scenario, in the meantime offering no support for the presence of a putative IMBH. An IMBH more massive than a few 10^3 $M_\odot$ is also strongly disfavored by the stellar kinematics.

Unified Astronomy Thesaurus concepts: Galactic center (565); X-ray sources (1822); Stellar winds (1636); Black hole physics (159)

Monthly Notices of the ROYAL ASTRONOMICAL SOCIETY

MNRAS **494,** 4168–4186 (2020) doi:10.1093/mnras/staa922
Advance Access publication 2020 April 7

A parameter survey of Sgr A∗ radiative models from GRMHD simulations with self-consistent electron heating

J. Dexter ,[1,2★] A. Jiménez-Rosales,[1★] S. M. Ressler,[3] A. Tchekhovskoy,[4] M. Bauböck,[1] P. T. de Zeeuw,[1] F. Eisenhauer,[1] S. von Fellenberg,[1] F. Gao,[1] R. Genzel,[1,5] S. Gillessen,[1] M. Habibi,[1] T. Ott,[1] J. Stadler,[1] O. Straub[1] and F. Widmann[1]

[1]*Max Planck Institute for Extraterrestrial Physics (MPE), Giessenbachstr 1, D-85748 Garching, Germany*
[2]*JILA and Department of Astrophysical and Planetary Sciences, University of Colorado, Boulder, CO 80309, USA*
[3]*Kavli Institute for Theoretical Physics, University of California Santa Barbara, Kohn Hall, Santa Barbara, CA 93107, USA*
[4]*Center for Interdisciplinary Exploration & Research in Astrophysics (CIERA), Physics & Astronomy, Northwestern University, Evanston, IL 60202, USA*
[5]*Departments of Physics and Astronomy, Le Conte Hall, University of California, Berkeley, CA 94720, USA*

Accepted 2020 March 21. Received 2020 March 20; in original form 2020 February 1

ABSTRACT

The Galactic centre black hole candidate Sgr A∗ is the best target for studies of low-luminosity accretion physics, including with near-infrared (NIR) and submillimetre wavelength long baseline interferometry experiments. Here, we compare images and spectra generated from a parameter survey of general relativistic MHD simulations to a set of radio to NIR observations of Sgr A∗. We instead favour the strongly magnetized models, which provide a good description of the median and highly variable linear polarization signal. The same models can also explain the observed mean Faraday rotation measure and potentially the polarization signals seen recently in Sgr A∗ NIR flares.

Key words: accretion, accretion discs – black hole physics – MHD – polarization – radiative transfer – Galaxy: centre.

Monthly Notices of the ROYAL ASTRONOMICAL SOCIETY

MNRAS **495,** 3403–3408 (2020) doi:10.1093/mnras/staa1343
Advance Access publication 2020 May 18

Apparent evidence for Hawking points in the CMB Sky★

Daniel An,[1] Krzysztof A. Meissner,[2] Paweł Nurowski[3]† and Roger Penrose[4]

[1]*Science Department, SUNY Maritime College, 6 Pennyfield Av., Throggs Neck, NY 10465, USA*
[2]*Faculty of Physics, University of Warsaw, Pasteura 5, PL-02-093 Warsaw, Poland*
[3]*Center for Theoretical Physics of PAS, Al. Lotników 32/46, PL-02-688 Warsaw, Poland*
[4]*Mathematical Institute, Oxford University, Radcliffe Observatory Quarter, Woodstock Rd., Oxford OX2 6GG, UK*

Accepted 2020 May 6. Received 2020 May 6; in original form 2019 September 3

ABSTRACT

This paper presents strong observational evidence of numerous previously unobserved anomalous circular spots, of significantly raised temperature, in the cosmic microwave background sky. The spots have angular radii between 0.03 and 0.04 rad (i.e. angular diameters between about 3° and 4°). There is a clear cut-off at that size, indicating that each anomalous spot would have originated from a highly energetic point-like source, located at the end of inflation – or else point-like at the conformally expanded Big Bang, if it is considered that there was no inflationary phase. The significant presence of these anomalous spots, was initially noticed in the *Planck* 70 GHz satellite data by comparison with 1000 standard simulations, and then confirmed by extending the comparison to 10 000 simulations. Such anomalous points were then found at precisely the same locations in the *WMAP (Wilkinson Microwave*

TROPHYSICAL JOURNAL, 897:135 (14pp), 2020 July 10 https://doi.org/10.3847/1538-4357/ab980d

CrossMark

ıctic Center IRS 13E: Colliding Stellar Winds or an Intermediate-mass Black Hole?

Zhenlin Zhu[1,2,3,4], Zhiyuan Li[1,2], Anna Ciurlo[5], Mark R. Morris[5], Mengfei Zhang[1,2], Tuan Do[5], and Andrea M. Ghez[5]

chool of Astronomy and Space Science, Nanjing University, Nanjing 210023, People's Republic of China; zhuzl@smail.nju.edu.cn, lizy@nju.edu.cn
Key Laboratory of Modern Astronomy and Astrophysics (Nanjing University), Ministry of Education, Nanjing 210023, People's Republic of China
[3] SRON Netherlands Institute for Space Research, Sorbonnelaan 2, 3584 CA Utrecht, The Netherlands
[4] Leiden Observatory, Leiden University, Niels Bohrweg 2, 2300 RA Leiden, The Netherlands
[5] Department of Physics and Astronomy, University of California, Los Angeles, CA 90095, USA
Received 2020 March 18; revised 2020 May 26; accepted 2020 May 28; published 2020 July 10

Abstract

A small cluster of massive stars residing in the Galactic center, collectively known as IRS 13E, is of special interest

The observations are interpreted using three-dimensional hydrodynamical simulations of colliding winds tailored to match the physical conditions of IRS 13E, leading us to conclude that the observed X-ray spectrum and morphology can be well explained by the colliding wind scenario, in the meantime offering no support for the presence of a putative IMBH.

improve the accuracy of the stars' proper motions. The observations are interpreted using three-dimensional hydrodynamical simulations of colliding winds tailored to match the physical conditions of IRS 13E, leading us to conclude that the observed X-ray spectrum and morphology can be well explained by the colliding wind scenario, in the meantime offering no support for the presence of a putative IMBH. An IMBH more massive than a few 10^3 $M_\odot$ is also strongly disfavored by the stellar kinematics.

Unified Astronomy Thesaurus concepts: Galactic center (565); X-ray sources (1822); Stellar winds (1636); Black hole physics (159)

Monthly Notices of the ROYAL ASTRONOMICAL SOCIETY

MNRAS **494,** 4168–4186 (2020) doi:10.1093/mnras/staa922
Advance Access publication 2020 April 7

A parameter survey of Sgr A∗ radiative models from GRMHD simulations with self-consistent electron heating

J. Dexter,[1,2★] A. Jiménez-Rosales,[1★] S. M. Ressler,[3] A. Tchekhovskoy,[4] M. Bauböck,[1] P. T. de Zeeuw,[1] F. Eisenhauer,[1] S. von Fellenberg,[1] F. Gao,[1] R. Genzel,[1,5] S. Gillessen,[1] M. Habibi,[1] T. Ott,[1] J. Stadler,[1] O. Straub[1] and F. Widmann[1]

[1]*Max Planck Institute for Extraterrestrial Physics (MPE), Giessenbachstr 1, D-85748 Garching, Germany*
[2]*JILA and Department of Astrophysical and Planetary Sciences, University of Colorado, Boulder, CO 80309, USA*
[3]*Kavli Institute for Theoretical Physics, University of California Santa Barbara, Kohn Hall, Santa Barbara, CA 93107, USA*
[4]*Center for Interdisciplinary Exploration & Research in Astrophysics (CIERA), Physics & Astronomy, Northwestern University, Evanston, IL 60202, USA*
[5]*Departments of Physics and Astronomy, Le Conte Hall, University of California, Berkeley, CA 94720, USA*

Accepted 2020 March 21. Received 2020 March 20; in original form 2020 February 1

ABSTRACT

The Galactic centre black hole candidate Sgr A∗ is the best target for studies of low-luminosity accretion physics, including with near-infrared (NIR) and submillimetre wavelength long baseline interferometry experiments. Here, we compare images and spectra generated from a parameter survey of general relativistic MHD simulations to a set of radio to NIR observations of Sgr A∗. Our models span the limits of weak and strong magnetization and use a range of sub-grid prescriptions for electron heating. We find two classes of scenarios can explain the broad shape of the submillimetre spectral peak and the highly variable NIR flaring emission. Weakly magnetized 'disc-jet' models where most of the emission is produced near the jet wall, consistent with past work, as well as strongly magnetized (magnetically arrested disc) models where hot electrons are present everywhere. Disc-jet models are strongly depolarized at submillimetre wavelengths as a result of strong Faraday rotation, inconsistent with observations of Sgr A∗. We instead favour the strongly magnetized models, which provide a good description of the median and highly variable linear polarization signal. The same models can also explain the observed mean Faraday rotation measure and potentially the polarization signals seen recently in Sgr A∗ NIR flares.

Key words: accretion, accretion discs – black hole physics – MHD – polarization – radiative transfer – Galaxy: centre.

Monthly Notices of the ROYAL ASTRONOMICAL SOCIETY

MNRAS **495,** 3403–3408 (2020) doi:10.1093/mnras/staa1343
Advance Access publication 2020 May 18

Apparent evidence for Hawking points in the CMB Sky★

Daniel An,[1] Krzysztof A. Meissner,[2] Paweł Nurowski[3]† and Roger Penrose[4]

[1]*Science Department, SUNY Maritime College, 6 Pennyfield Av., Throggs Neck, NY 10465, USA*
[2]*Faculty of Physics, University of Warsaw, Pasteura 5, PL-02-093 Warsaw, Poland*
[3]*Center for Theoretical Physics of PAS, Al. Lotników 32/46, PL-02-688 Warsaw, Poland*
[4]*Mathematical Institute, Oxford University, Radcliffe Observatory Quarter, Woodstock Rd., Oxford OX2 6GG, UK*

Accepted 2020 May 6. Received 2020 May 6; in original form 2019 September 3

ABSTRACT

This paper presents strong observational evidence of numerous previously unobserved anomalous circular spots, of significantly raised temperature, in the cosmic microwave background sky. The spots have angular radii between 0.03 and 0.04 rad (i.e. angular diameters between about 3° and 4°). There is a clear cut-off at that size, indicating that each anomalous spot would have originated from a highly energetic point-like source, located at the end of inflation – or else point-like at the conformally expanded Big Bang, if it is considered that there was no inflationary phase. The significant presence of these anomalous spots, was initially noticed in the *Planck* 70 GHz satellite data by comparison with 1000 standard simulations, and then confirmed by extending the comparison to 10 000 simulations. Such anomalous points were then found at precisely the same locations in the *WMAP (Wilkinson Microwave*

ıтrophysical Journal, 897:135 (14pp), 2020 July 10 https://doi.org/10.3847/1538-4357/ab980d

ıctic Center IRS 13E: Colliding Stellar Winds or an Intermediate-mass Black Hole?

Zhenlin Zhu[1,2,3,4], Zhiyuan Li[1,2], Anna Ciurlo[5], Mark R. Morris[5], Mengfei Zhang[1,2], Tuan Do[5], and Andrea M. Ghez[5]

chool of Astronomy and Space Science, Nanjing University, Nanjing 210023, People's Republic of China; zhuzl@smail.nju.edu.cn, lizy@nju.edu.cn
Key Laboratory of Modern Astronomy and Astrophysics (Nanjing University), Ministry of Education, Nanjing 210023, People's Republic of China
[3] SRON Netherlands Institute for Space Research, Sorbonnelaan 2, 3584 CA Utrecht, The Netherlands
[4] Leiden Observatory, Leiden University, Niels Bohrweg 2, 2300 RA Leiden, The Netherlands
[5] Department of Physics and Astronomy, University of California, Los Angeles, CA 90095, USA
Received 2020 March 18; revised 2020 May 26; accepted 2020 May 28; published 2020 July 10

Abstract

A small cluster of massive stars residing in the Galactic center, collectively known as IRS 13E, is of special interest due to its close proximity to the central supermassive black hole Sgr A* and the possibility that an embedded intermediate-mass black hole (IMBH) binds its member stars. It has been suggested that colliding winds from two member stars, both classified as Wolf–Rayet type, are responsible for the observed X-ray, infrared, and radio emission from IRS 13E. We have conducted an in-depth study of the X-ray spatial, temporal, and spectral properties of IRS 13E, based on 5.6 Ms of ultradeep Chandra observations obtained over 20 years. These X-ray observations show no significant evidence for source variability. We have also explored the kinematics of the cluster members, using Keck near-infrared imaging and spectroscopic data on a 14 yr baseline that considerably improve the accuracy of the stars' proper motions. The observations are interpreted using three-dimensional hydrodynamical simulations of colliding winds tailored to match the physical conditions of IRS 13E, leading us to conclude that the observed X-ray spectrum and morphology can be well explained by the colliding wind scenario, in the meantime offering no support for the presence of a putative IMBH. An IMBH more massive than a few 10^3 $M_\odot$ is also strongly disfavored by the stellar kinematics.

Unified Astronomy Thesaurus concepts: Galactic center (565); X-ray sources (1822); Stellar winds (1636); Black hole physics (159)

Historical review

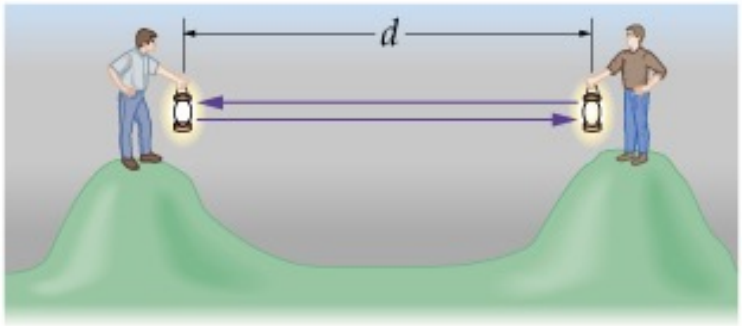

The first paper suggesting simulations of gravity

Erik Holmberg

THE ASTROPHYSICAL JOURNAL

AN INTERNATIONAL REVIEW OF SPECTROSCOPY AND ASTRONOMICAL PHYSICS

VOLUME 94 NOVEMBER 1941 NUMBER 3

ON THE CLUSTERING TENDENCIES AMONG THE NEBULAE

II. A STUDY OF ENCOUNTERS BETWEEN LABORATORY MODELS OF STELLAR SYSTEMS BY A NEW INTEGRATION PROCEDURE

ERIK HOLMBERG

ABSTRACT

In a previous paper[1] the writer discussed the possibility of explaining the observed clustering effects among extragalactic nebulae as a result of captures. The present investigation deals with the important problem of whether the loss of energy resulting from the tidal disturbances at a close encounter between two nebulae is large enough to effect a capture. The tidal deformations of two models of stellar systems, passing each other at a small distance, are studied by reconstructing, piece by piece, the orbits described by the individual mass elements. The difficulty of integrating the total gravitational force acting upon a certain element at a certain point of time is solved by replacing gravitation by light. The mass elements are represented by light-bulbs, the candle power being proportional to mass, and the total light is measured by a photocell (Fig. 1). The nebulae are assumed to have a flattened shape, and each is represented by 37 light-bulbs. It is found that the tidal deformations cause an increase in the attraction between the two objects, the increase reaching its maximum value when the nebulae are separating, i.e., after the passage. The resulting loss of energy (Fig. 6) is comparatively large and may, in favorable cases, effect a capture. The spiral arms developing during the encounter (Figs. 4) represent an interesting by-product of the investigation. The direction of the arms depends on the direction of rotation of the nebulae with respect to the direction of their space motions.

I. THE EXPERIMENTAL ARRANGEMENTS

The present paper is a study of the tidal disturbances appearing in stellar systems which pass one another at small distances. These tidal disturbances are of some importance since they are accompanied by a loss of energy which may result in a capture between the two objects. In a previous paper[1] the writer discussed the clustering tendencies among extragalactic nebulae. A theory was put forth that the observed clustering effects are the result of captures between individual nebulae. The capture theory seems to be able to account not only for double and multiple nebulae but also for the large extragalactic clusters. The present investigation tries to give an answer to the important question of whether the loss of energy accompanying a close encounter between two nebulae is large enough to effect a capture.

A study of tidal disturbances is greatly facilitated if it can be restricted to only two dimensions, i.e., to nebulae of a flattened shape, the principal planes of which coincide with the plane of their hyperbolic orbits. In order to reconstruct the orbit described by

[1] *Mt. W. Contr.*, No. 633; *Ap. J.*, 92, 200, 1940.

The first paper suggesting simulations of gravity

Erik Holmberg

THE ASTROPHYSICAL JOURNAL

AN INTERNATIONAL REVIEW OF SPECTROSCOPY AND ASTRONOMICAL PHYSICS

VOLUME 94 NOVEMBER 1941 NUMBER 3

ON THE CLUSTERING TENDENCIES AMONG THE NEBULAE

II. A STUDY OF ENCOUNTERS BETWEEN LABORATORY MODELS OF STELLAR SYSTEMS BY A NEW INTEGRATION PROCEDURE

ERIK HOLMBERG

ABSTRACT

In a previous paper[1] the writer discussed the possibility of explaining the observed clustering effects among extragalactic nebulae as a result of captures. The present investigation deals with the important problem of whether the loss of energy resulting from the tidal disturbances at a close encounter between two nebulae is large enough to effect a capture. The tidal deformations of two models of stellar systems, passing each other at a small distance, are studied by reconstructing, piece by piece, the orbits described by the individual mass elements. The difficulty of integrating the total gravitational force acting upon a certain element at a certain point of time is solved by replacing gravitation by light. The mass elements are represented by light-bulbs, the candle power being proportional to mass, and the total light is measured by a photocell (Fig. 1). The nebulae are assumed to have a flattened shape, and each is represented by 37 light-bulbs. It is found that the tidal deformations cause an increase in the attraction between the two objects, the increase reaching its maximum value when the nebulae are separating, i.e., after the passage. The resulting loss of energy (Fig. 6) is comparatively large and may, in favorable cases, effect a capture. The spiral arms developing during the encounter (Figs. 4) represent an interesting by-product of the investigation. The direction of the arms depends on the direction of rotation of the nebulae with respect to the direction of their space motions.

I. THE EXPERIMENTAL ARRANGEMENTS

The present paper is a study of the tidal disturbances appearing in stellar systems which pass one another at small distances. These tidal disturbances are of some importance since they are accompanied by a loss of energy which may result in a capture between the two objects. In a previous paper[1] the writer discussed the clustering tendencies among extragalactic nebulae. A theory was put forth that the observed clustering effects are the result of captures between individual nebulae. The capture theory seems to be able to account not only for double and multiple nebulae but also for the large extragalactic clusters. The present investigation tries to give an answer to the important question of whether the loss of energy accompanying a close encounter between two nebulae is large enough to effect a capture.

A study of tidal disturbances is greatly facilitated if it can be restricted to only two dimensions, i.e., to nebulae of a flattened shape, the principal planes of which coincide with the plane of their hyperbolic orbits. In order to reconstruct the orbit described by

[1] *Mt. W. Contr.*, No. 633; *Ap. J.*, 92, 200, 1940.

The first paper suggesting simulations of gravity

Erik Holmberg

THE ASTROPHYSICAL JOURNAL

AN INTERNATIONAL REVIEW OF SPECTROSCOPY AND ASTRONOMICAL PHYSICS

VOLUME 94 NOVEMBER 1941 NUMBER 3

ON THE CLUSTERING TENDENCIES AMONG THE NEBULAE

II. A STUDY OF ENCOUNTERS BETWEEN LABORATORY MODELS OF STELLAR SYSTEMS BY A NEW INTEGRATION PROCEDURE

ERIK HOLMBERG

ABSTRACT

In a previous paper[1] the writer discussed the possibility of explaining the observed clustering effects among extragalactic nebulae as a result of captures. The present investigation deals with the important problem of whether the loss of energy resulting from the tidal disturbances at a close encounter between

by the individual mass elements. The difficulty of integrating the total gravitational force acting upon a certain element at a certain point of time is solved by replacing gravitation by light. The mass elements are represented by light-bulbs, the candle power being proportional to mass, and the total light is measured by a photocell (Fig. 1). The nebulae are assumed to have a flattened shape, and each is represented

of the investigation. The direction of the arms depends on the direction of rotation of the nebulae with respect to the direction of their space motions.

I. THE EXPERIMENTAL ARRANGEMENTS

The present paper is a study of the tidal disturbances appearing in stellar systems which pass one another at small distances. These tidal disturbances are of some importance since they are accompanied by a loss of energy which may result in a capture between the two objects. In a previous paper[1] the writer discussed the clustering tendencies among extragalactic nebulae. A theory was put forth that the observed clustering effects are the result of captures between individual nebulae. The capture theory seems to be able to account not only for double and multiple nebulae but also for the large extragalactic clusters. The present investigation tries to give an answer to the important question of whether the loss of energy accompanying a close encounter between two nebulae is large enough to effect a capture.

A study of tidal disturbances is greatly facilitated if it can be restricted to only two dimensions, i.e., to nebulae of a flattened shape, the principal planes of which coincide with the plane of their hyperbolic orbits. In order to reconstruct the orbit described by

[1] *Mt. W. Contr.*, No. 633; *Ap. J.*, 92, 200, 1940.

“Gravity solver”

Erik Holmberg

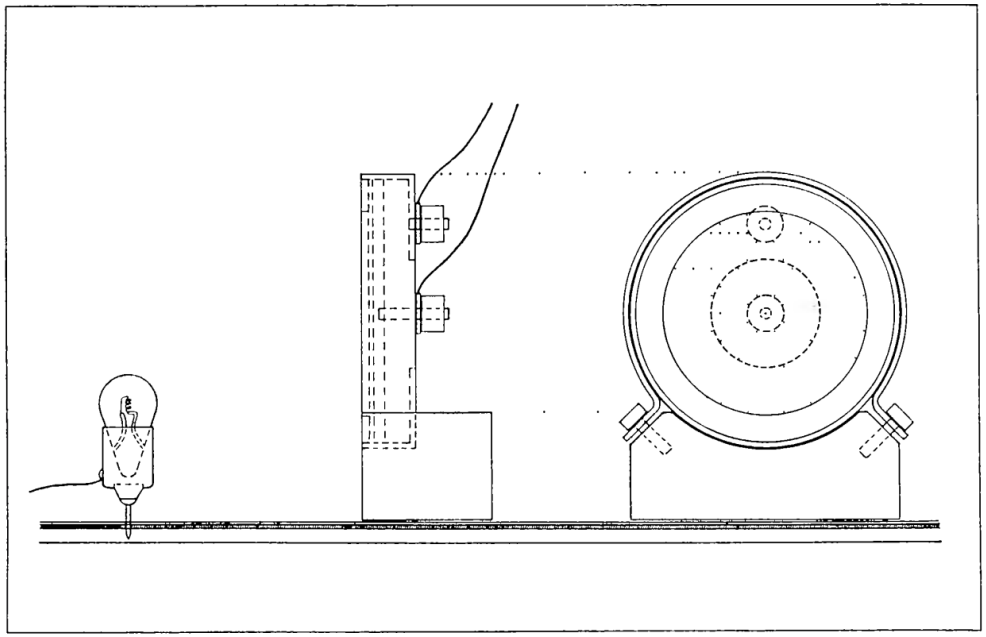

G. 1.—Cross-section of light-bulb and photocell (half-size)

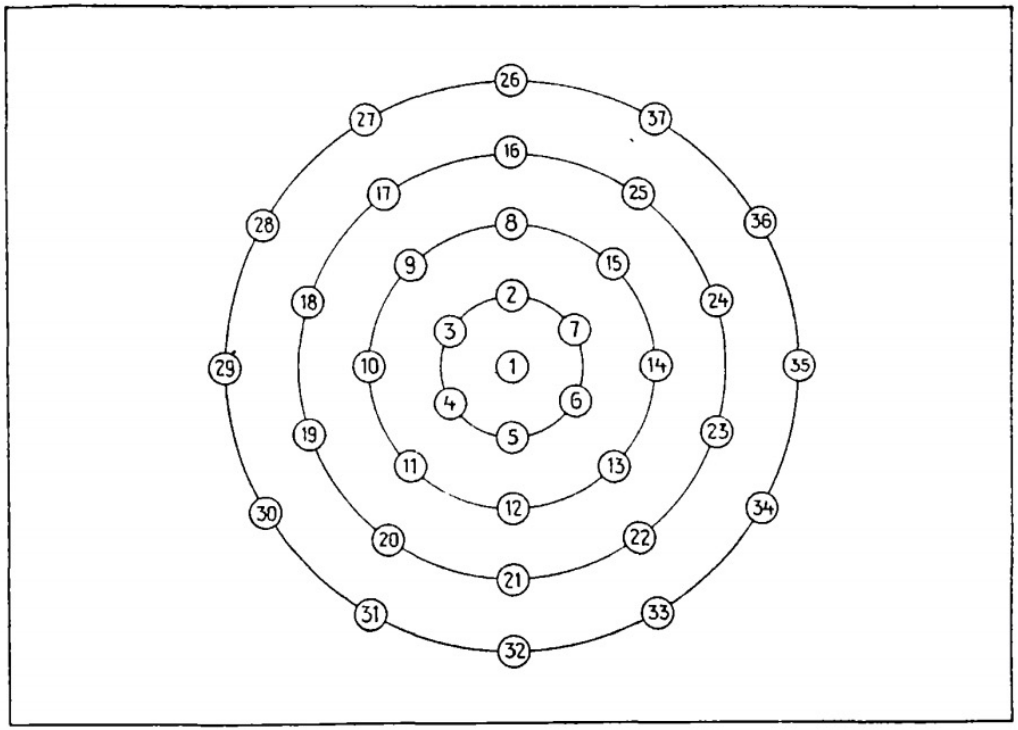

FIG. 3

“Initial conditions”

Light “dilution” is the same as gravity ie ~ r^-2

N = 2x 37

Erik Holmberg

- replacing gravity by light (same $1/r^2$ law)
- formation of tidal features

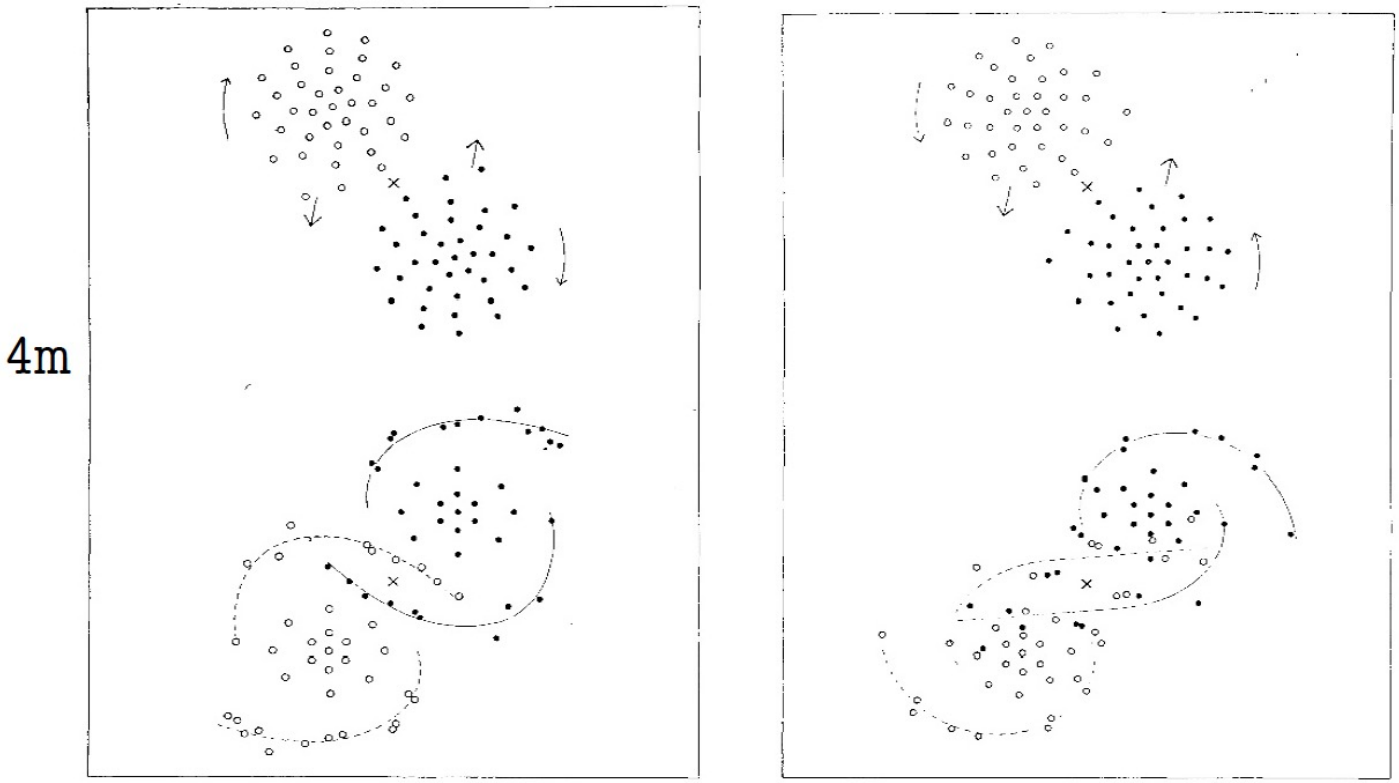

- gravity of N bodies

$$\boxed{m_i \ddot{\vec{r}}_i = \vec{F}(\vec{r}_i) \quad \forall i \in N}$$

- the “brute force approach” scales like N^2:

$$\vec{F}(\vec{r}_i) = -\sum_{i \neq j} \frac{G m_i m_j}{(r_i - r_j)^3} (\vec{r}_i - \vec{r}_j)$$

the summation over (N-1) particles has to be done for all N particles:

$\Rightarrow$ number of floating point operations $\propto$ N(N-1) $\propto N^2$

• gravity of N bodies

$$\boxed{m_i \ddot{\vec{r}}_i = \vec{F}(\vec{r}_i) \quad \forall i \in N}$$

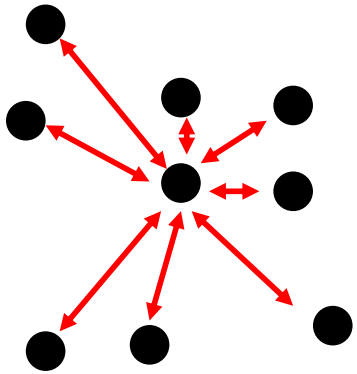

• the "brute force approach" scales like N^2:

N-1

$$\vec{F}(\vec{r}_i) = -\sum_{i \neq j} \frac{G m_i m_j}{(r_i - r_j)^3} (\vec{r}_i - \vec{r}_j)$$

the summation over (N-1) particles has to be done for all N particles:

$\Rightarrow$ number of floating point operations $\propto$ N(N-1) $\propto N^2$

• gravity of N bodies

$$m_i \ddot{\vec{r}}_i = \vec{F}(\vec{r}_i) \quad \forall i \in N$$

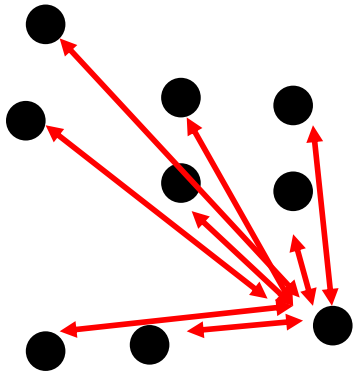

• the "brute force approach" scales like N^2:

(N-1)+(N-1) + ….

$$\vec{F}(\vec{r}_i) = -\sum_{i \neq j} \frac{G m_i m_j}{(r_i - r_j)^3} (\vec{r}_i - \vec{r}_j)$$

the summation over (N-1) particles has to be done for all N particles:

$\Rightarrow$ number of floating point operations $\propto$ N(N-1) $\propto N^2$

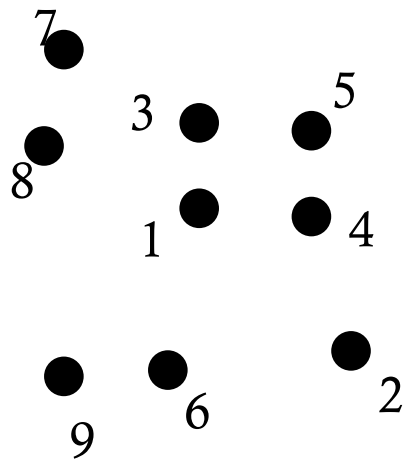

$$\vec{F}(\vec{r}_i) = -\sum_{i \neq j} \frac{G m_i m_j}{(r_i - r_j)^3} (\vec{r}_i - \vec{r}_j)$$

Particle	*r*	Force	acceleration	displacement
1				
2				
…				
N				

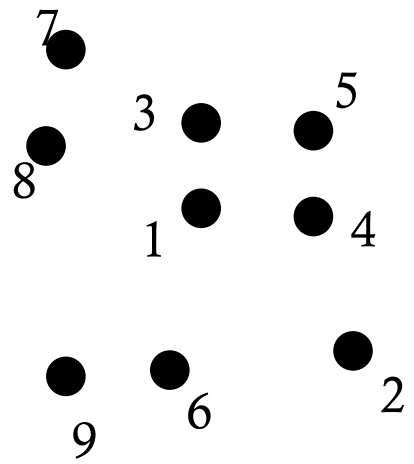

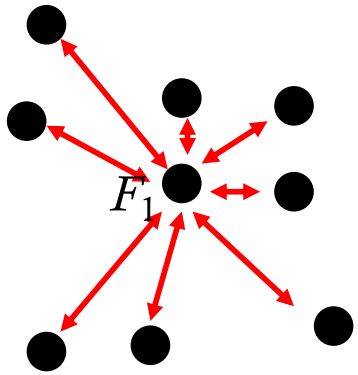

$$\vec{F}(\vec{r}_i) = -\sum_{i \neq j} \frac{G m_i m_j}{(r_i - r_j)^3} (\vec{r}_i - \vec{r}_j)$$

Particle	*r*	Force	acceleration	displacement
1	0	0	0	0
2				
…				
N				

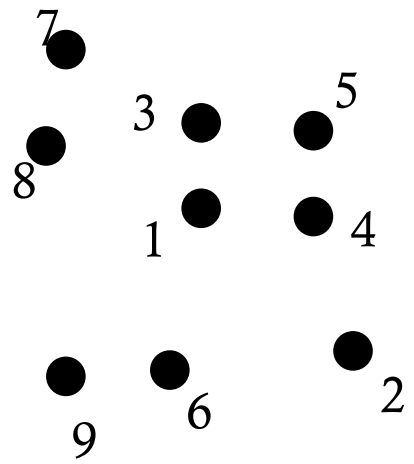

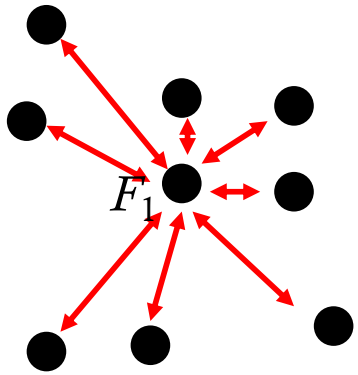

$$\vec{F}(\vec{r}_i) = -\sum_{i \neq j} \frac{G m_i m_j}{(r_i - r_j)^3} (\vec{r}_i - \vec{r}_j)$$

Particle	r	Force	acceleration	displacement
1	0	0	0	0
2	r_2	$F_2 = \mathrm{G}\, m_2 / r_2$	$a_2 = F_2 / m_2$	$\Delta x_2 = a_2 (\Delta t_2)^2$
…				
N	r_N	$F_N = \mathrm{G}\, m_N / r_N$	$a_N = F_N / m_N$	$\Delta x_N = a_N (\Delta t_N)^2$

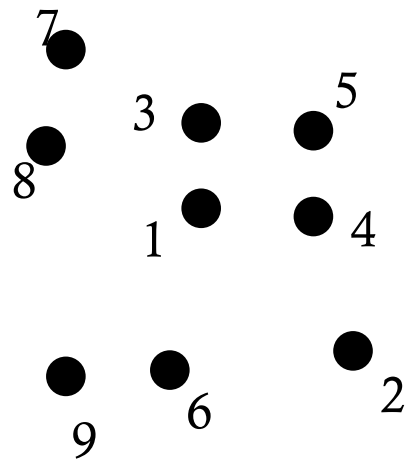

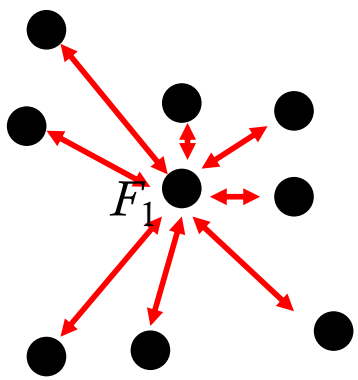

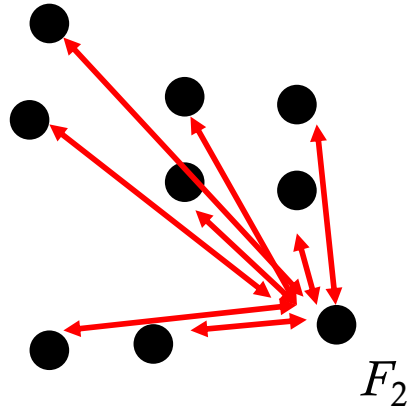

$$\vec{F}(\vec{r}_i) = -\sum_{i \neq j} \frac{G m_i m_j}{(r_i - r_j)^3} (\vec{r}_i - \vec{r}_j)$$

Particle	r	Force	acceleration	displacement
1	r_2	$F_2 = G\, m_2 / r_2$	$a_2 = F_2 / m_2$	$\Delta x_2 = a_2 (\Delta t_2)^2$
2	0	0	0	0
…				
N	r_N	$F_N = G\, m_N / r_N$	$a_N = F_N / m_N$	$\Delta x_N = a_N (\Delta t_N)^2$

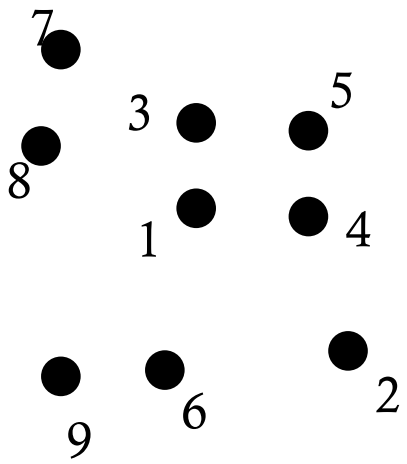
7
3
5
8
1
4
9
6
2

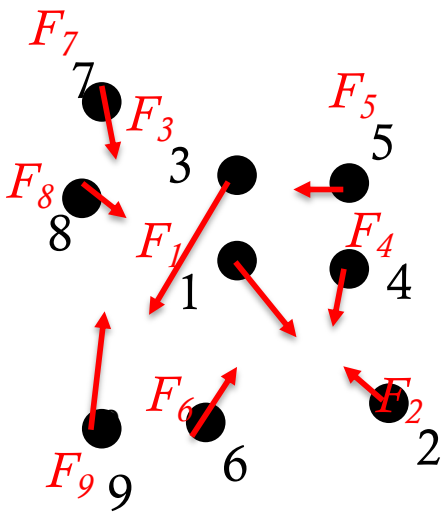
F7
7
F3
F5
5
3
F8
8
F1
F4
1
4
F6
F2
F9
9
6
2

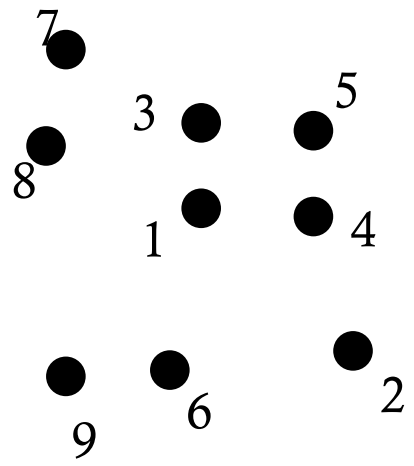

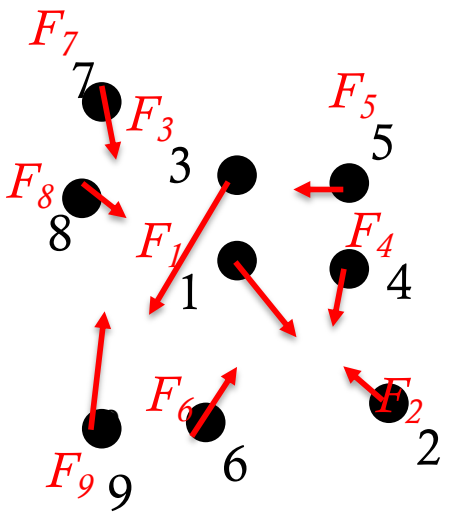

$a_1 = F_1 / m_1$
$\Delta x_1 = a_1 (\Delta t)^2$

$a_2 = F_2 / m_2$
$\Delta x_2 = a_2 (\Delta t)^2$

…

$a_N = F_N / m_N$
$\Delta x_N = a_N (\Delta t)^2$

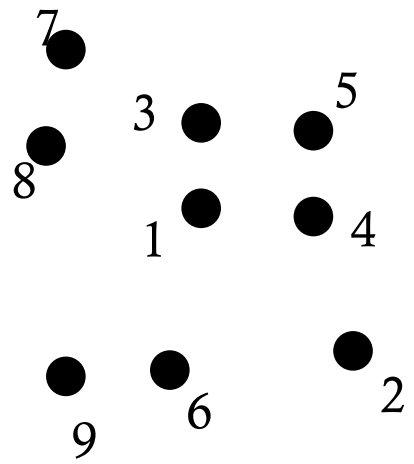

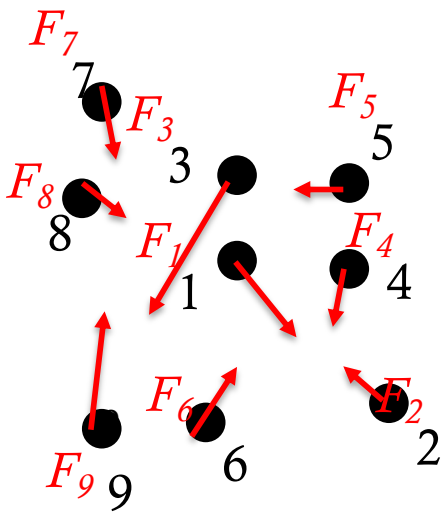

$a_1 = F_1 / m_1$
$\Delta x_1 = a_1 (\Delta t)^2$

$a_1 = F_1 / m_1$
$\Delta x_1 = v_1 \Delta t + a_1 (\Delta t)^2$

$a_2 = F_2 / m_2$
$\Delta x_2 = a_2 (\Delta t)^2$

$a_2 = F_2 / m_2$
$\Delta x_2 = v_2 \Delta t + a_2 (\Delta t)^2$

…

…

$a_N = F_N / m_N$
$\Delta x_N = a_N (\Delta t)^2$

$a_N = F_N / m_N$
$\Delta x_N = v_N \Delta t + a_N (\Delta t)^2$

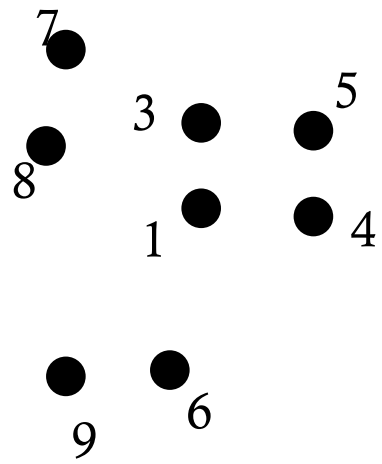
7
3
5
8
1
4
9
6


2

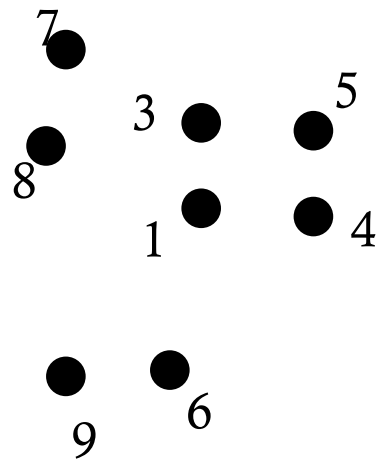

High accelerations

Low acceleration

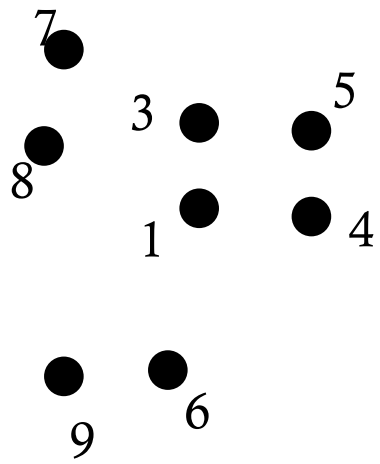

High accelerations

Time step should be small

Low acceleration

Time step can be longer

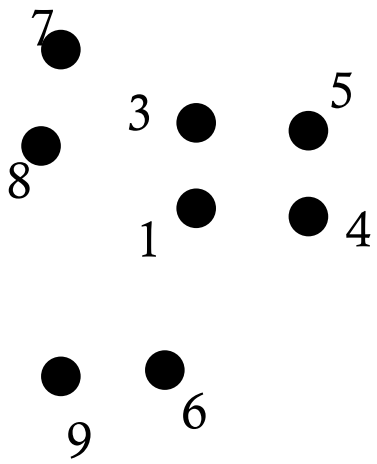

High accelerations

Time step should be small

$$\Delta t = \alpha\sqrt{\epsilon/|\mathbf{a}|}$$

Epsilon – softening
Alpha – “tolerance” paramter

Low acceleration

Time step can be longer

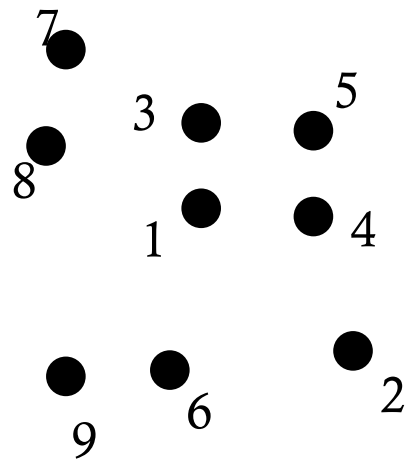

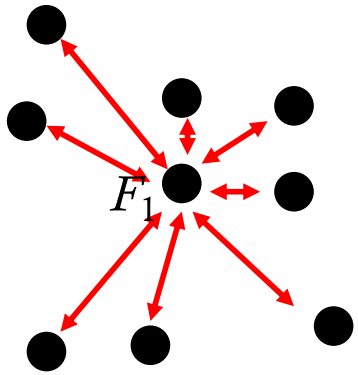

$$\vec{F}(\vec{r}_i) = -\sum_{i \neq j} \frac{G m_i m_j}{(r_i - r_j)^3} (\vec{r}_i - \vec{r}_j)$$

Particle	r	Force	acceleration	Velocity	displacement
1	0	0	0	0	0
2	r_2	$F_2 = G\, m_2 / r_2$	$a_2 = F_2 / m_2$	$\Delta v_2 = a_2 (\Delta t_2)$	$\Delta x_2 = \Delta v_2 \Delta t_2 + a_2 (\Delta t_2)$
…					
N	r_N	$F_N = G\, m_N / r_N$	$a_N = F_N / m_N$	$\Delta v_1 = a_N (\Delta t_N)$	$\Delta x_N = \Delta v_N \Delta t_N + a_N (\Delta t_N)$

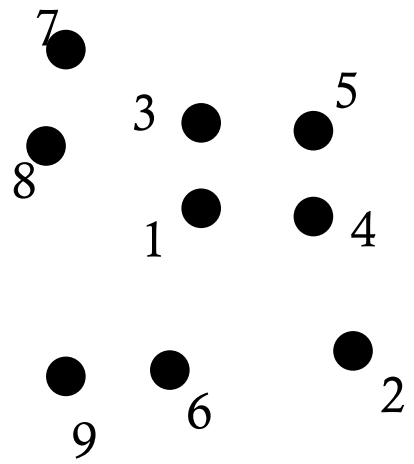

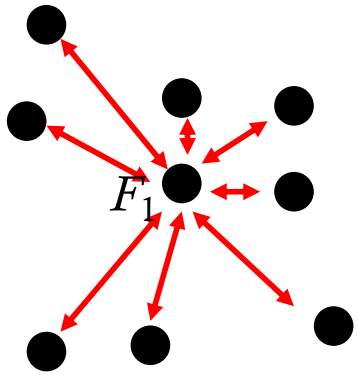

$$\vec{F}(\vec{r}_i) = -\sum_{i \neq j} \frac{G m_i m_j}{(r_i - r_j)^3} (\vec{r}_i - \vec{r}_j)$$

Particle	r	Force	acceleration	Velocity	displacement
1	r_1	$F_1 = G\, m_1 / r_1$	$a_1 = F_1 / m_1$	$\Delta v_1 = v_1 + a_2 (\Delta t_2)$	$\Delta x_2 = \Delta v_2 \Delta t_2 + a_2 (\Delta t_2)$
2	0	0	0	0	0
…					
N	r_N	$F_N = G\, m_N / r_N$	$a_N = F_N / m_N$	$\Delta v_1 = v_N + a_N (\Delta t_N)$	$\Delta x_N = \Delta v_N \Delta t_N + a_N (\Delta t_N)$

• gravity of N bodies

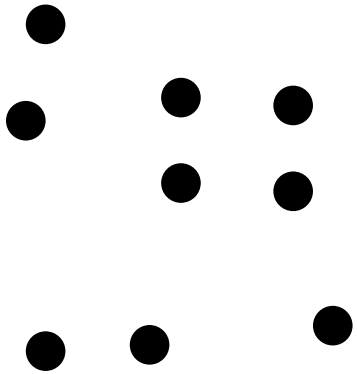

$$\boxed{m_i \ddot{\vec{r}}_i = \vec{F}(\vec{r}_i) \quad \forall i \in N}$$

• the “brute force approach” scales like N^2:

$$\vec{F}(\vec{r}_i) = -\sum_{i \neq j} \frac{G m_i m_j}{(r_i - r_j)^3} (\vec{r}_i - \vec{r}_j)$$

the summation over (N-1) particles has to be done for all N particles:

$\Rightarrow$ number of floating point operations $\propto$ N(N-1) $\propto N^2$

Sverre Aarseth

DYNAMICAL EVOLUTION OF CLUSTERS OF GALAXIES, I

S. J. Aarseth

(Communicated by F. Hoyle)

(Received 1962 November 12)

Summary

Numerical integrations of the classical N-body problem have been carried out on a fast computer for a variety of clusters in the range $N = 25$ to $N = 100$. Newtonian forces are slightly modified to give convergence for collisions. The solutions are completely general and the results are applied to clusters of galaxies. It is found that the moment of inertia increases considerably even if bodies are not lost by ejection. At the same time there is an increase of mass in the central regions. The derived relaxation times are substantially longer than predicted by the theory of Chandrasekhar, but even so there is a deficiency of escapers for $N \gtrsim 50$. Some of the light cluster members are lost when the effect of cosmic expansion is included.

The dynamical formation rate of binaries is found to be small but this is compensated by long life-times for heavy doubles. Radially contracting clusters of irregular shapes are studied and a common feature is the formation of a compact sub-system of high stability. Field galaxies moving through a cluster do not affect the bound members significantly, but there is a likelihood of capture.

In some cases the integration time corresponds to a physical time $\sim 10^{10}$ yrs for a typical model cluster, but maximum errors in total energy may still be $\lesssim 0{\cdot}5$ per cent. The estimated computer time depends on the expression N^2t where t is the physical integration time.

---

1. *Introduction.*—Originally most clusters of galaxies were studied because they provide yard-sticks in the mapping of space. It is now realized that the clues to galaxy formation lie hidden in these island universes and more intensive studies of all their physical properties are being undertaken. Recent work by Abell (1) indicates that there are many different types of clusters, but the most numerous groups are found to contain around 50 visible bright galaxies. In the present paper we are interested in the dynamical behaviour of galaxies as they move about in a cluster and the effect this has on its large-scale evolution.

Given positions, velocities and masses for all cluster members and that the motions are governed by Newton's law, the future coordinates are in principle determined, provided the system is left to itself. Direct solutions of the N-body problem, however, have only been made possible by the introduction of high-speed computers. von Hoerner* (2) has given extensive results of numerical integrations for $N \leqq 16$, but since then faster computers have become available. One can argue that these results cannot be applied to cases where N is large, say, $N > 1000$. The effects due to individual encounters will be much larger when N is small, and this cannot be smoothed out by doing many cases which only eliminates statistical fluctuations.

* The results of two cases with $N = 25$ integrated many relaxation times have been published in *Zs. f. Astrophys.*, **57**, 47, 1963.

Sverre Aarseth

DYNAMICAL EVOLUTION OF CLUSTERS OF GALAXIES, I

S. J. Aarseth

(Communicated by F. Hoyle)

(Received 1962 November 12)

Summary

Numerical integrations of the classical N-body problem have been carried out on a fast computer for a variety of clusters in the range $N = 25$ to $N = 100$. Newtonian forces are slightly modified to give convergence for collisions. The solutions are completely general and the results are applied to clusters of galaxies. It is found that the moment of inertia increases considerably even if bodies are not lost by ejection. At the same time there is an increase of mass in the central regions. The derived relaxation times are substantially longer than predicted by the theory of Chandrasekhar, but even so there is a deficiency of escapers for $N \gtrsim 50$. Some of the light cluster members are lost when the effect of cosmic expansion is included.

The dynamical formation rate of binaries is found to be small but this is compensated by long life-times for heavy doubles. Radially contracting clusters of irregular shapes are studied and a common feature is the formation of a compact sub-system of high stability. Field galaxies moving through a cluster do not affect the bound members significantly, but there is a likelihood of capture.

In some cases the integration time corresponds to a physical time $\sim 10^{10}$ yrs for a typical model cluster, but maximum errors in total energy may still be $\lesssim 0{\cdot}5$ per cent. The estimated computer time depends on the expression N^2t where t is the physical integration time.

---

1. *Introduction.*—Originally most clusters of galaxies were studied because they provide yard-sticks in the mapping of space. It is now realized that the clues to galaxy formation lie hidden in these island universes and more intensive studies of all their physical properties are being undertaken. Recent work by Abell (1) indicates that there are many different types of clusters, but the most numerous groups are found to contain around 50 visible bright galaxies. In the present paper we are interested in the dynamical behaviour of galaxies as they move about in a cluster and the effect this has on its large-scale evolution.

Given positions, velocities and masses for all cluster members and that the motions are governed by Newton's law, the future coordinates are in principle determined, provided the system is left to itself. Direct solutions of the N-body problem, however, have only been made possible by the introduction of high-speed computers. von Hoerner* (2) has given extensive results of numerical integrations for $N \leqq 16$, but since then faster computers have become available. One can argue that these results cannot be applied to cases where N is large, say, $N > 1000$. The effects due to individual encounters will be much larger when N is small, and this cannot be smoothed out by doing many cases which only eliminates statistical fluctuations.

* The results of two cases with $N = 25$ integrated many relaxation times have been published in *Zs. f. Astrophys.*, **57**, 47, 1963.

Sverre Aarseth

DYNAMICAL EVOLUTION OF CLUSTERS OF GALAXIES, I

S. J. Aarseth

(Communicated by F. Hoyle)

(Received 1962 November 12)

Summary

Numerical integrations of the classical N-body problem have been carried out on a fast computer for a variety of clusters in the range $N=25$ to $N=100$. Newtonian forces are slightly modified to give convergence for collisions. The solutions are completely general and the results are applied to clusters of galaxies. It is found that the moment of inertia increases considerably even if bodies are not lost by ejection. At the same time there is an increase of mass in the central regions. The derived relaxation times are substantially longer than predicted by the theory of Chandrasekhar, but even so there is a deficiency of escapers for $N \gtrsim 50$. Some of the light cluster members are lost when the effect of cosmic expansion is included.

The dynamical formation rate of binaries is found to be small but this is compensated by long life-times for heavy doubles. Radially contracting clusters of irregular shapes are studied and a common feature is the formation of a compact sub-system of high stability. Field galaxies moving through a cluster do not affect the bound members significantly, but there is a likelihood of capture.

In some cases the integration time corresponds to a physical time $\sim 10^{10}$ yrs for a typical model cluster, but maximum errors in total energy may still be $\leqslant 0{\cdot}5$ per cent. The estimated computer time depends on the

determined, provided the system is left to itself. Direct solutions of the N-body problem, however, have only been made possible by the introduction of high-speed computers. von Hoerner* (2) has given extensive results of numerical integra-

Abell (1) indicates that there are many different types of clusters, but the most numerous groups are found to contain around 50 visible bright galaxies. In the present paper we are interested in the dynamical behaviour of galaxies as they move about in a cluster and the effect this has on its large-scale evolution.

Given positions, velocities and masses for all cluster members and that the motions are governed by Newton's law, the future coordinates are in principle determined, provided the system is left to itself. Direct solutions of the N-body problem, however, have only been made possible by the introduction of high-speed computers. von Hoerner* (2) has given extensive results of numerical integrations for $N \leqq 16$, but since then faster computers have become available. One can argue that these results cannot be applied to cases where N is large, say, $N > 1000$. The effects due to individual encounters will be much larger when N is small, and this cannot be smoothed out by doing many cases which only eliminates statistical fluctuations.

* The results of two cases with $N=25$ integrated many relaxation times have been published in *Zs. f. Astrophys.*, **57**, 47, 1963.

N = 45 - 100

Sverre Aarseth

- the godfather of N-body codes?!
- groundworks for all tree codes...
- formation of sub-systems

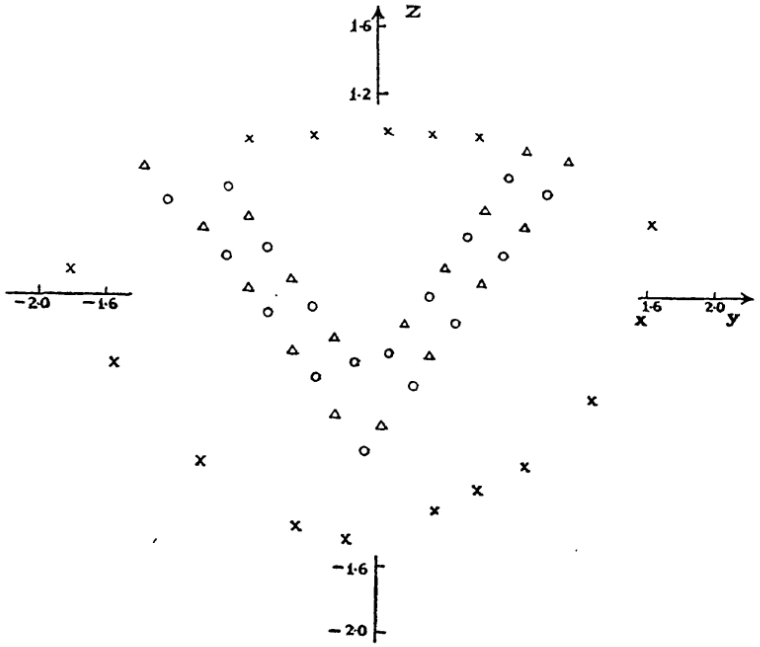

FIG. 5.—*Initial distribution in the yz-plane of V-shaped cluster with halo;* $N=50$, Δ: $m=1{\cdot}50$, o: $m=0{\cdot}50$, $\times$: *halo bodies.*

N = 45 - 100

Sverre Aarseth

- the godfather of N-body codes?!
- groundworks for all tree codes...
- formation of sub-systems

The large Hercules cluster is a particularly interesting irregular cluster. This system appears to have its main mass concentrated in a V-shape in space and consists of about 170 objects (**10**). It seems unlikely that such an irregular shape can be maintained for any long period of time or be the result of a chance configuration during a long life-time. One could therefore argue that the Hercules cluster is not very old and this would have cosmological implications.

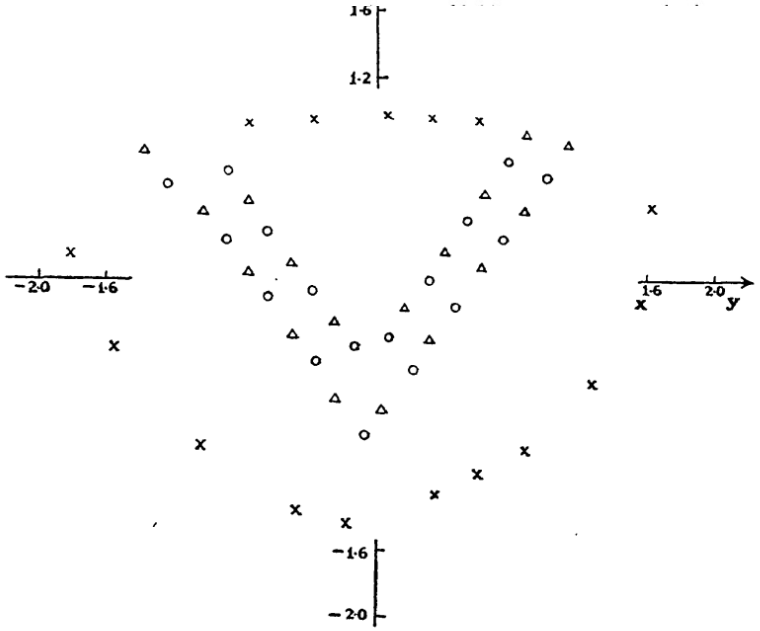

FIG. 5.—*Initial distribution in the yz-plane of V-shaped cluster with halo;* $N=50$, Δ: $m=1{\cdot}50$, o: $m=0{\cdot}50$, $\times$: *halo bodies.*

N = 45 - 100

Sverre Aarseth

- the godfather of N-body codes?!
- groundworks for all tree codes...
- formation of sub-systems

The large Hercules cluster is a particularly interesting irregular cluster. This system appears to have its main mass concentrated in a V-shape in space and consists of about 170 objects (**10**). It seems unlikely that such an irregular shape can be maintained for any long period of time or be the result of a chance configuration during a long life-time. One could therefore argue that the Hercules cluster is not very old and this would have cosmological implications.

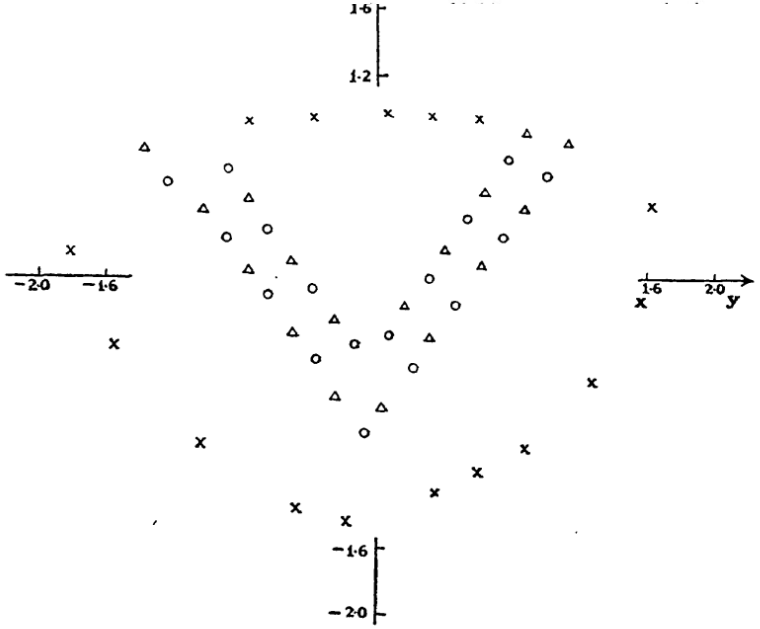

FIG. 5.—*Initial distribution in the yz-plane of V-shaped cluster with halo;* $N=50$, Δ: $m=1{\cdot}50$, o: $m=0{\cdot}50$, $\times$: *halo bodies.*

N = 45 - 100

Sverre Aarseth

- the godfather of N-body codes?!
- groundworks for all tree codes...
- formation of sub-systems

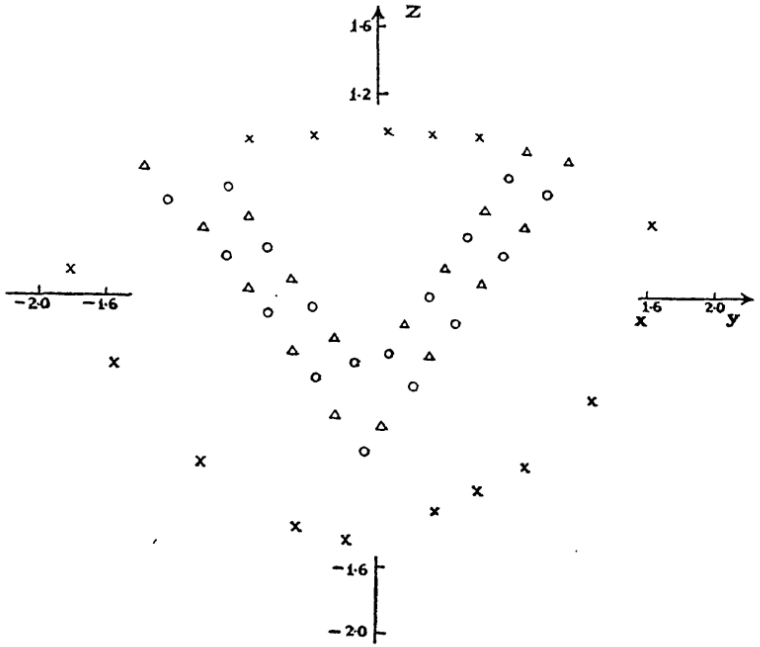

FIG. 5.—*Initial distribution in the yz-plane of V-shaped cluster with halo;* $N=50$, Δ: $m=1{\cdot}50$, o: $m=0{\cdot}50$, $\times$: *halo bodies.*

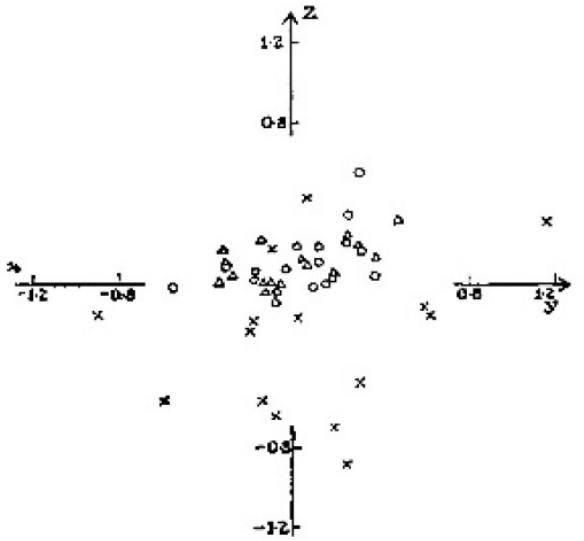

(*a*) $\tau=0{\cdot}28$ (*Near minimum contraction*).

N = 45 - 100

Sverre Aarseth

- the godfather of N-body codes?!
- groundworks for all tree codes...
- formation of sub-systems

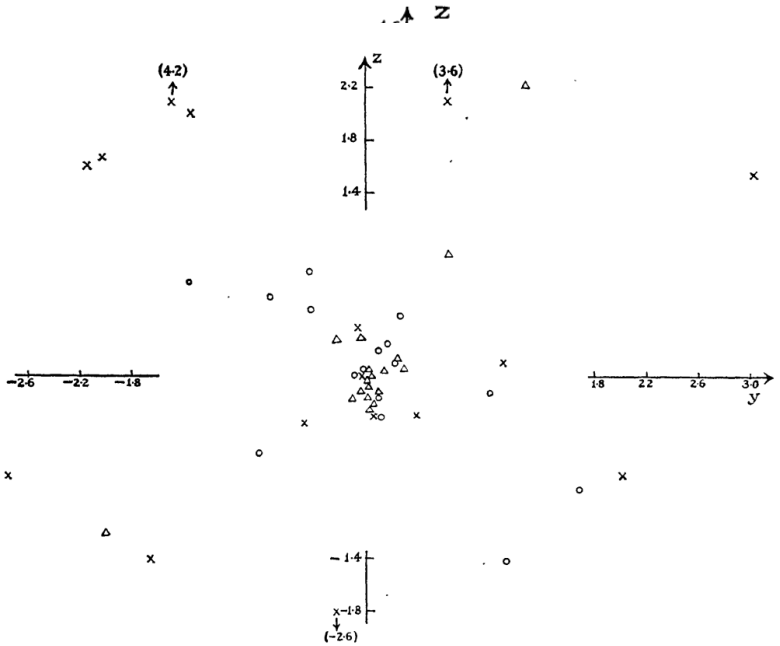

(c) $\tau = 0{\cdot}80$.

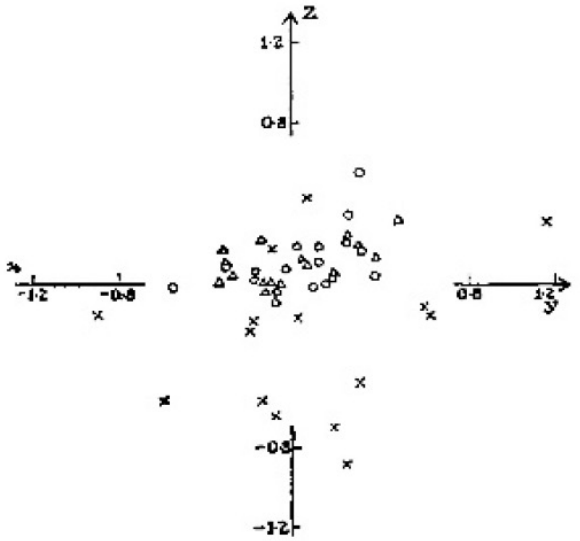

(a) $\tau = 0{\cdot}28$ (*Near minimum contraction*).

F =50,

FIG. 7.—*Structural developments in the yz-plane of V-shaped cluster with halo.*

The N-body Problem

- the equations

  - Newton's second law of motion

$$m\frac{d^2r}{dt^2} = F(r)$$

  - Newton's law of gravity

$$F = G\frac{Mm}{r^2}$$

- the two-body problem

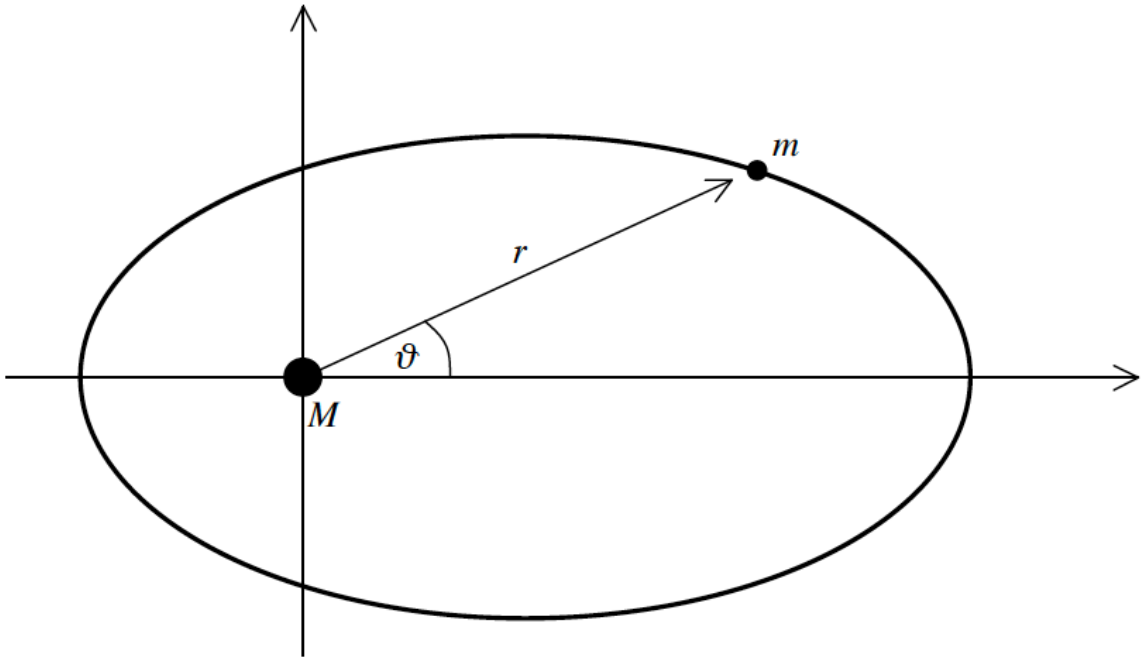

$$r(\vartheta) = \frac{k}{1 + \varepsilon \cos(\vartheta)}$$

- the three-body problem

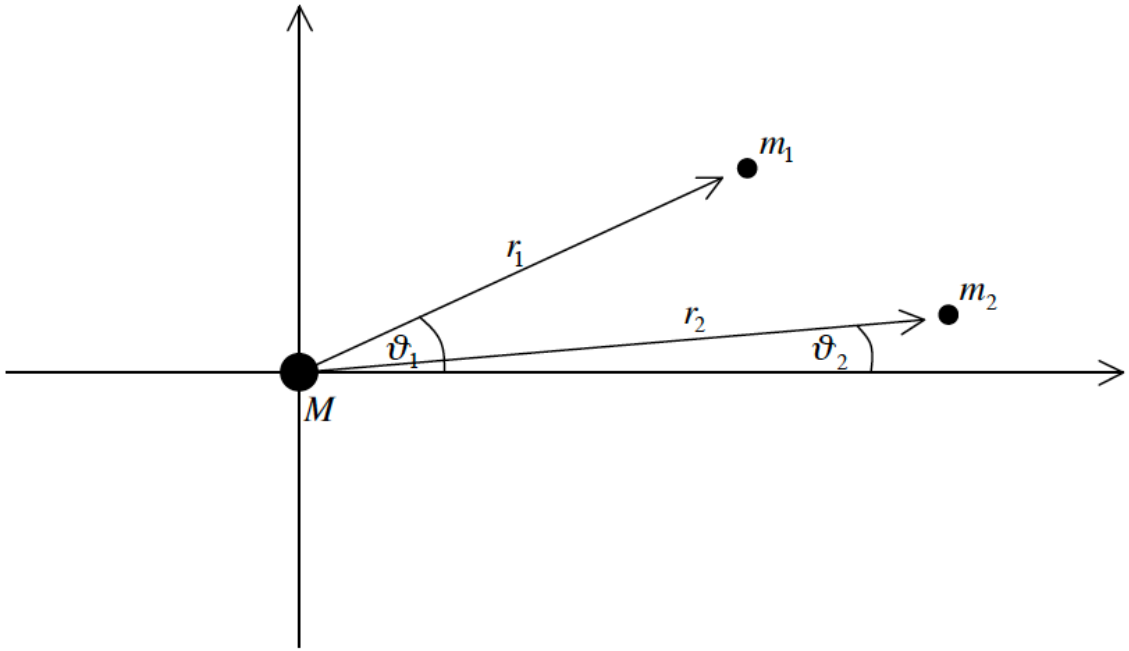

no analytical solution!

numerical integration required...

- the N-body problem

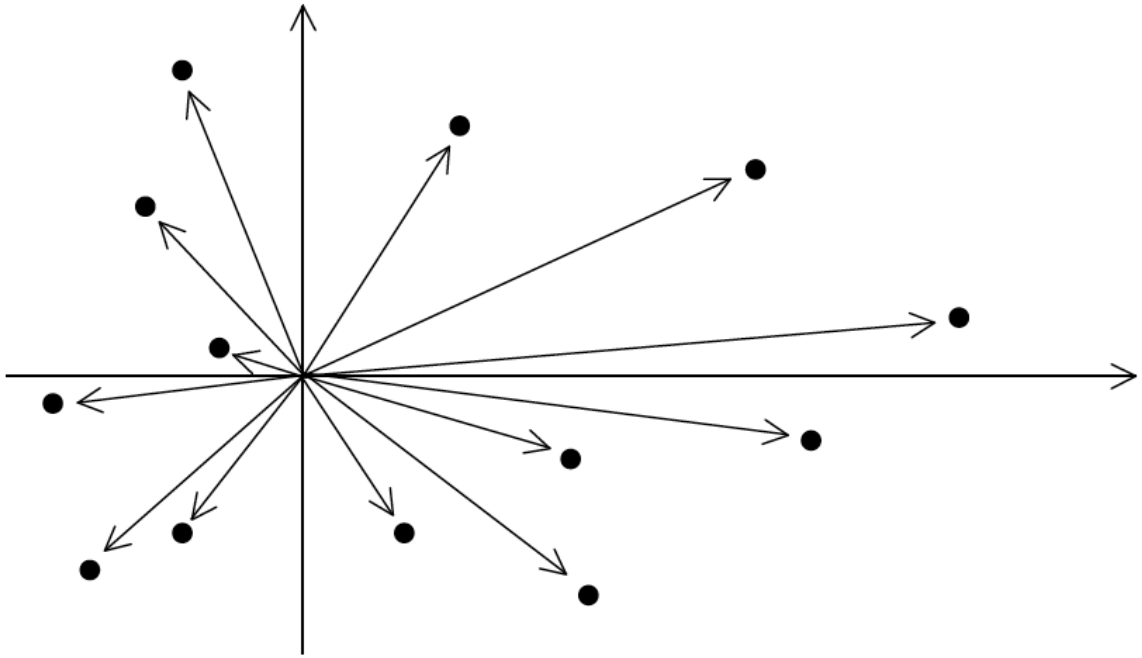

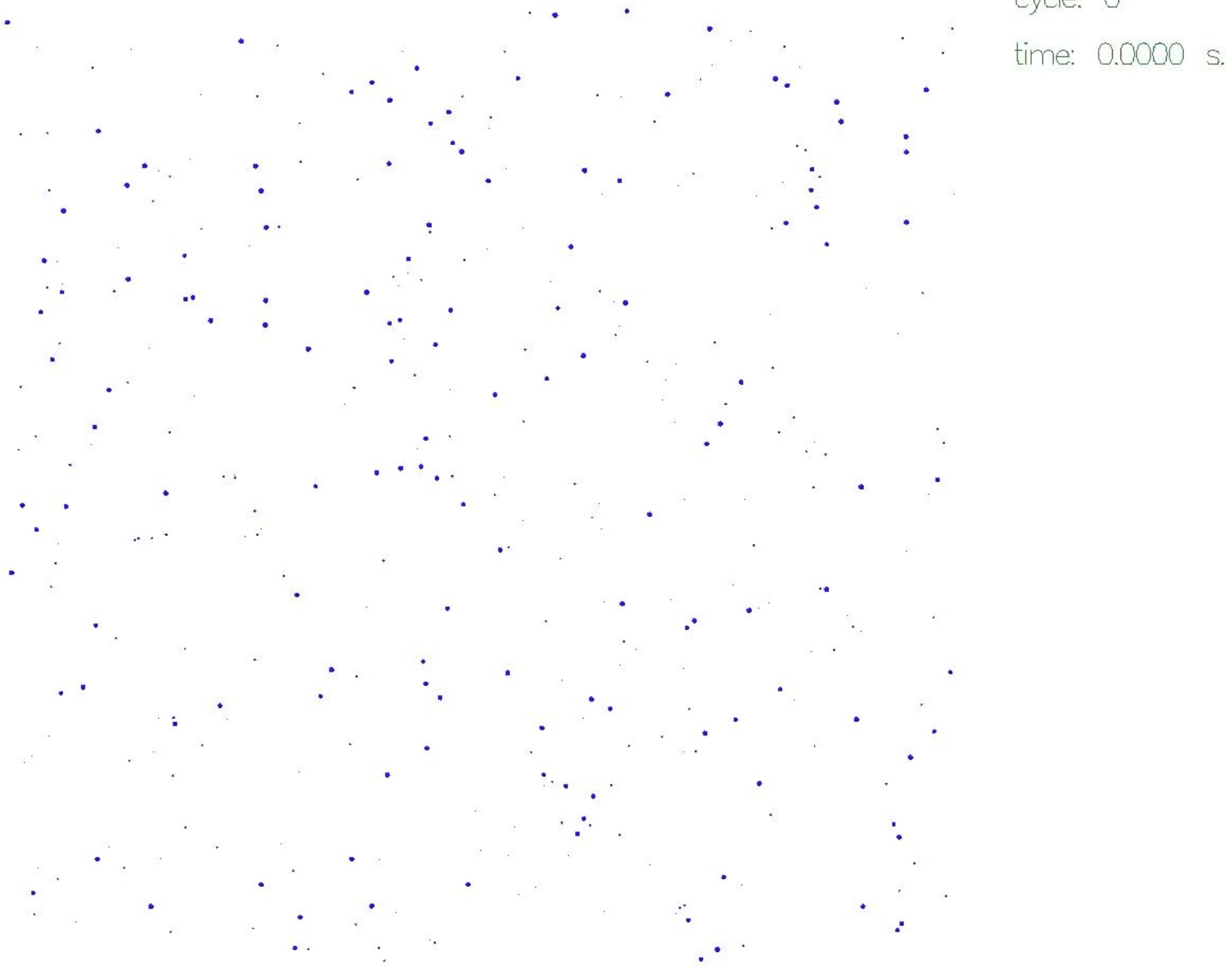
cycle: 0
time: 0.0000 s.

Numerical Integration of Ordinary Differential Equations

- ordinary differential equation

$$\frac{df}{dt} = G(f,t)$$

- ordinary differential equation

$$\frac{df}{dt} = G(f,t)$$

$$\Rightarrow \quad \frac{\Delta f}{\Delta t} = \frac{f(t_{i+1}) - f(t_i)}{t_{i+1} - t_i}$$

- ordinary differential equation

$$\frac{df}{dt} = G(f,t)$$

$$\Rightarrow \quad \frac{\Delta f}{\Delta t} = \frac{f(t_{i+1}) - f(t_i)}{t_{i+1} - t_i} = \frac{f_{i+1} - f_i}{t_{i+1} - t_i} = G(f_i, t_i)$$

- ordinary differential equation

$$\frac{df}{dt} = G(f,t)$$

$$\Rightarrow \quad \frac{\Delta f}{\Delta t} = \frac{f(t_{i+1}) - f(t_i)}{t_{i+1} - t_i} = \frac{f_{i+1} - f_i}{t_{i+1} - t_i} = G(f_i, t_i)$$

$$\Rightarrow \quad f_{i+1} = f_i + \Delta t \; G(f_i, t_i)$$

- ordinary differential equation
  - Euler scheme

$$f_{i+1} = f_i + \Delta t\, G(f_i, t_i)$$

$$\frac{df}{dt} = G(f,t)$$

first term in Taylor expansion of $f(t)$ about t_i !

- ordinary differential equation

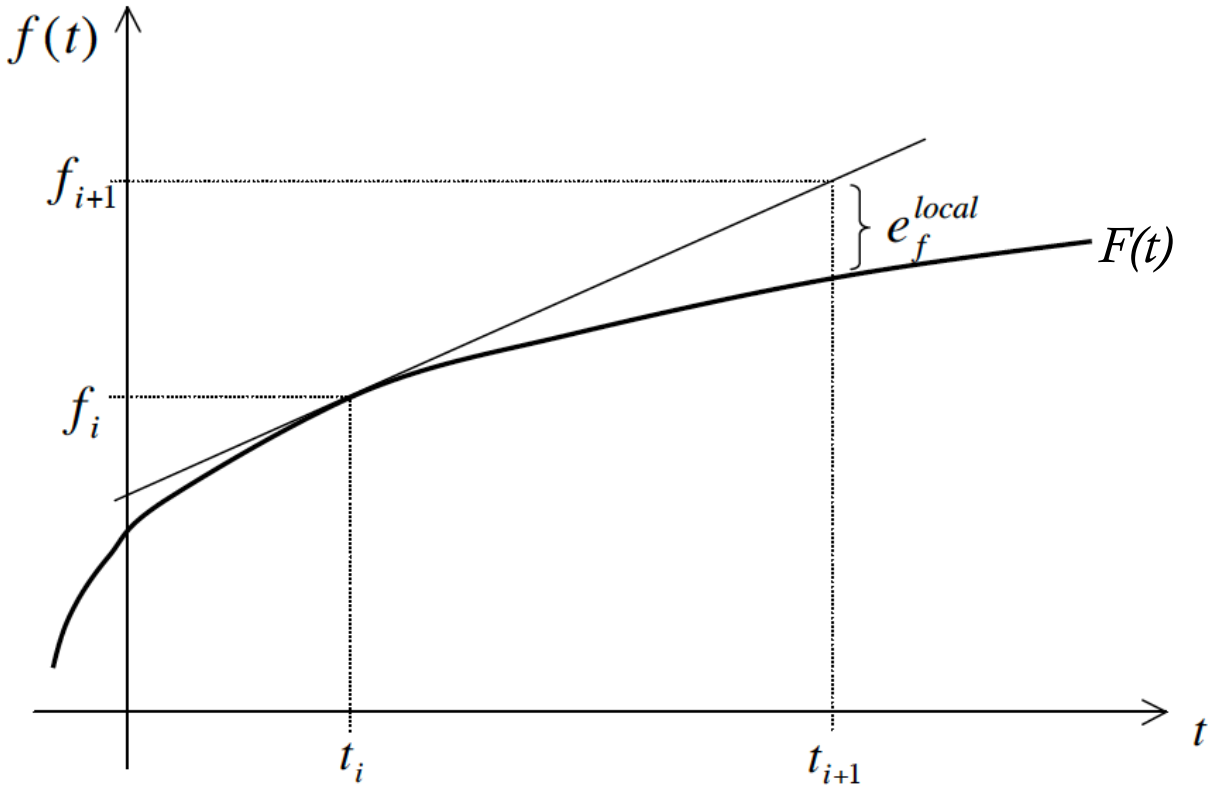

$$\Rightarrow \quad f_{i+1} = f_i + \Delta t \; G(f_i, t_i)$$

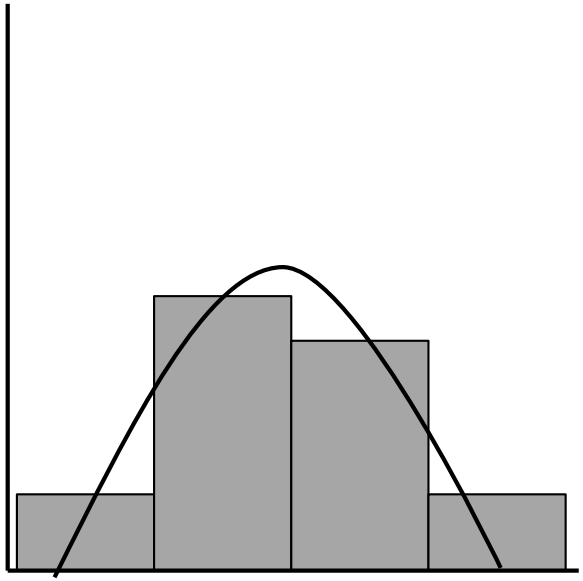

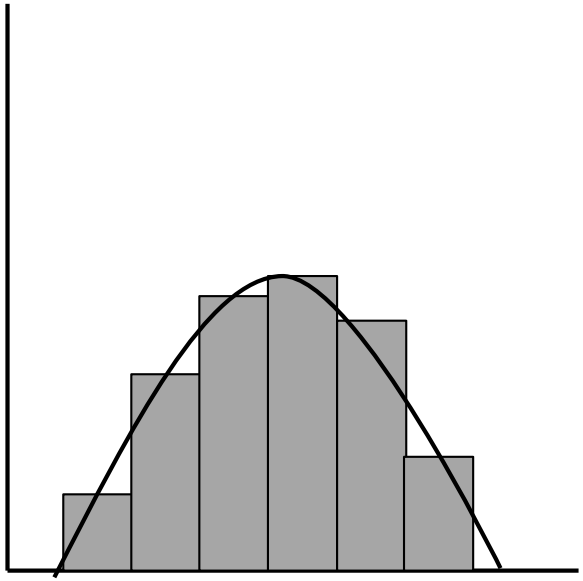

$$\int f(x)dx = \lim_{\Delta x \to 0} f(x)\Delta x$$

Error is thus a feature of numerical integration

- ordinary differential equation

  - Euler scheme

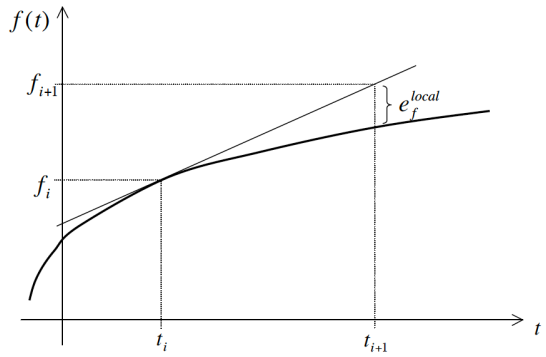

$$f_{i+1} = f_i + \Delta t \; G(f_i, t_i)$$

  - local error estimate

$$F(t_{i+1}) = F(t_i) + \Delta t \; \dot{F}(t_i) + \frac{(\Delta t)^2}{2} \ddot{F}(t_i) + \ldots$$

- ordinary differential equation

  - Euler scheme

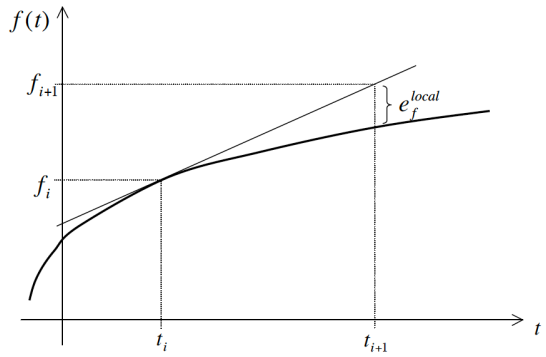

$$f_{i+1} = f_i + \Delta t \; G(f_i, t_i)$$

  - local error estimate

$$F(t_{i+1}) = F(t_i) + \Delta t \; \dot{F}(t_i) + \frac{(\Delta t)^2}{2} \ddot{F}(t_i) + \ldots$$

$$e_f^{local} = F(t_{i+1}) - f_{i+1} =$$

- ordinary differential equation

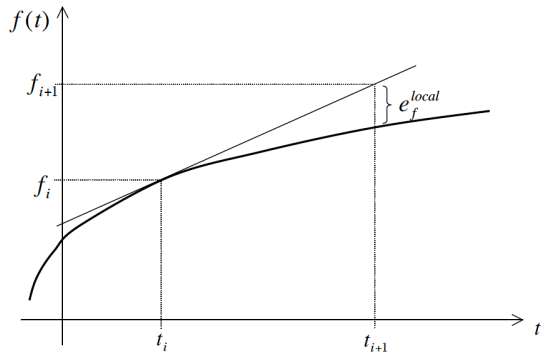

  - Euler scheme

$$f_{i+1} = f_i + \Delta t\, G(f_i, t_i)$$

  - local error estimate

$$F(t_{i+1}) = F(t_i) + \Delta t\, \dot{F}(t_i) + \frac{(\Delta t)^2}{2} \ddot{F}(t_i) + \ldots$$

$$e_f^{local} = F(t_{i+1}) - f_{i+1} = F(t_i) + \Delta t\, \dot{F}(t_i) + \frac{(\Delta t)^2}{2} \ddot{F}(t_i) + \ldots - \left(f_i + \Delta t\, G(f_i, t_i)\right)$$

- ordinary differential equation

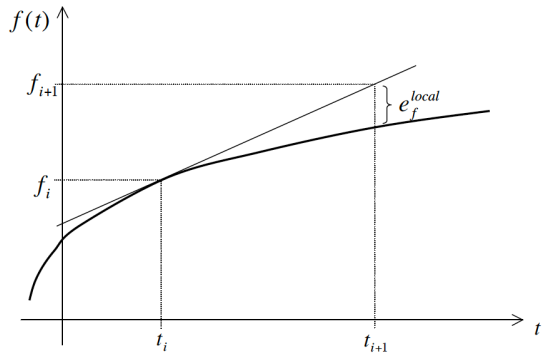

  - Euler scheme

$$f_{i+1} = f_i + \Delta t\, G(f_i, t_i)$$

  - local error estimate

$$F(t_{i+1}) = F(t_i) + \Delta t\, \dot{F}(t_i) + \frac{(\Delta t)^2}{2} \ddot{F}(t_i) + \ldots$$

$$e_f^{local} = F(t_{i+1}) - f_{i+1} = F(t_i) + \Delta t\, \dot{F}(t_i) + \frac{(\Delta t)^2}{2} \ddot{F}(t_i) + \ldots - \left(f_i + \Delta t\, G(f_i, t_i)\right)$$

$$\Rightarrow \qquad e_f^{local} \propto (\Delta t)^2$$

- ordinary differential equation
  - leap-frog scheme

The leapfrog scheme derives its name from the way it updates positions and velocities at staggered (or "leaping") time steps. Instead of updating both position and velocity at the same time, it updates them at alternating half-steps.

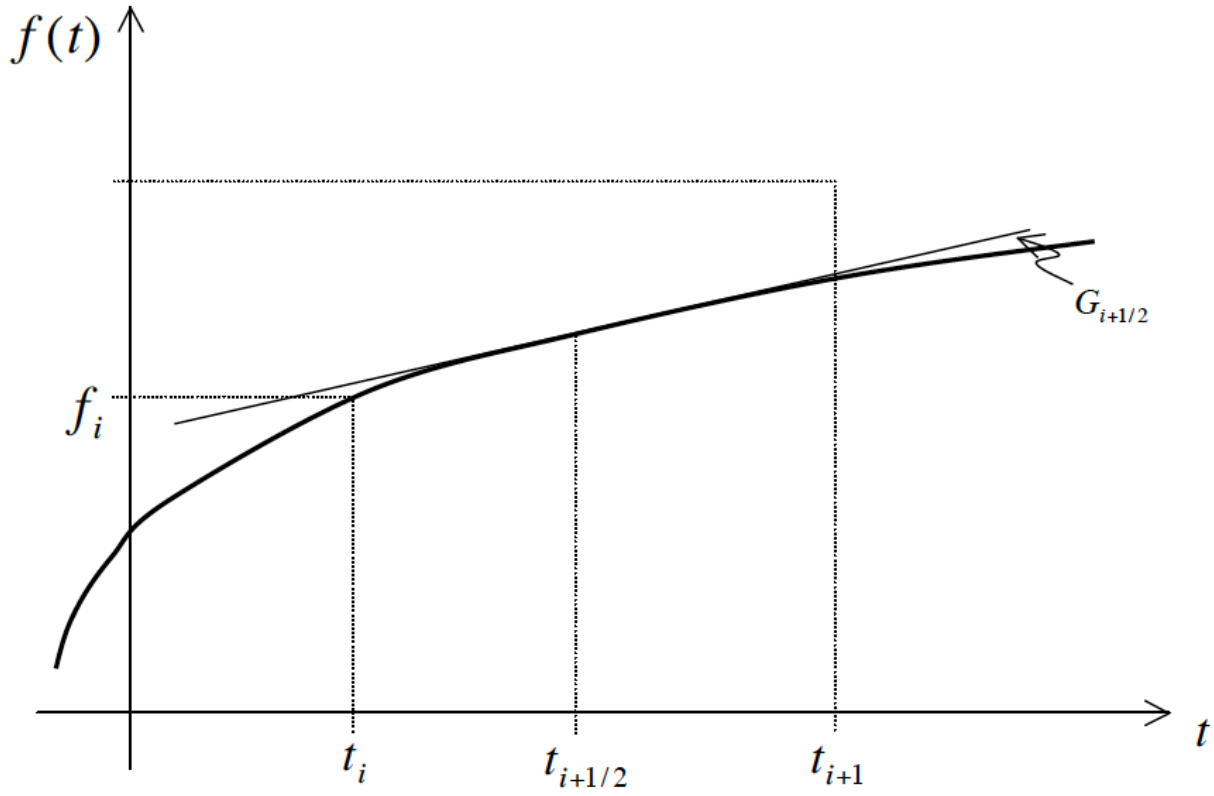

Position : dx/dt = v(t)
Velocity : dv/dt = a(x(t))
(acceleration is a function of gravitational force)

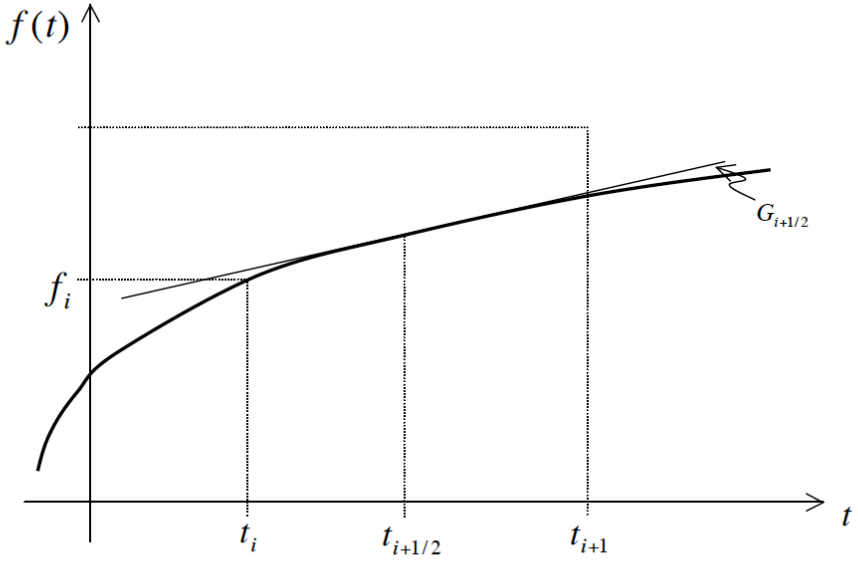

Approximate the solution at discrete time steps $t_n = n * dt$

Velocity Half-Step:

$v(t + dt/2) = v(t) + a(x(t)) * (dt/2)$

Updates the velocity to the midpoint of the next time interval.

Position : dx/dt = v(t)
Velocity : dv/dt = a(x(t))
(acceleration is a function of gravitational force)

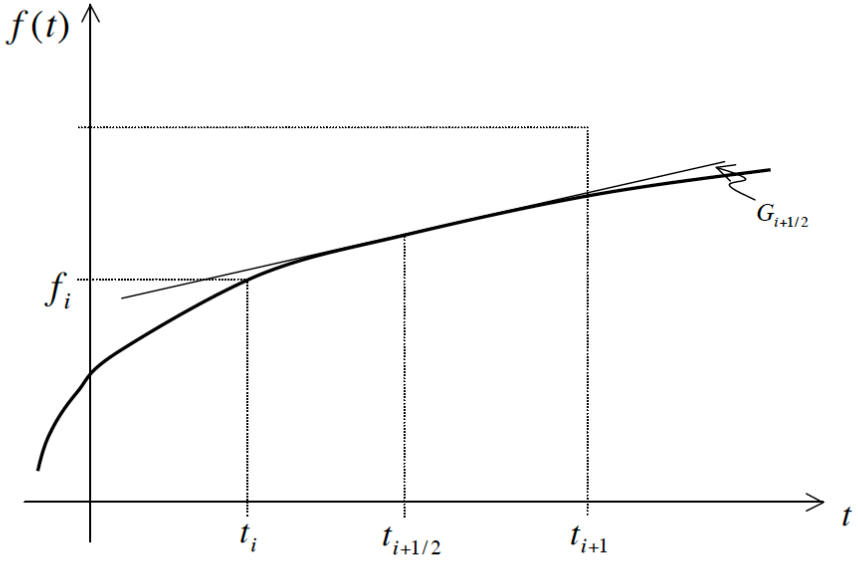

Approximate the solution at discrete time steps $t_n = n * dt$

Velocity Half-Step:

$v(t + dt/2) = v(t) + a(x(t)) * (dt/2)$

Updates the velocity to the midpoint of the next time interval.

Position Full-Step:

$x(t + dt) = x(t) + v(t + dt/2) * dt$

Updates the position using the velocity at the midpoint.

Position : dx/dt = v(t)
Velocity : dv/dt = a(x(t))
(acceleration is a function of gravitational force)

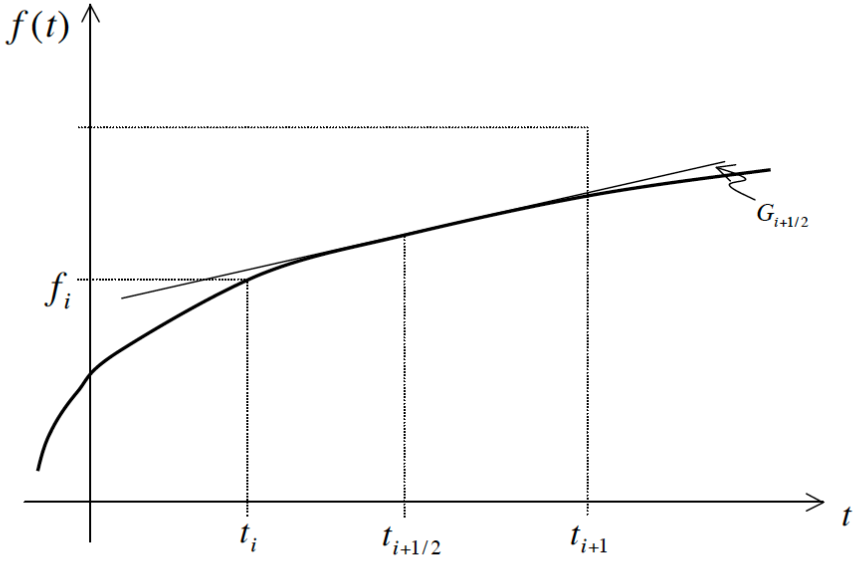

Approximate the solution at discrete time steps $t_n = n * dt$

Velocity Half-Step:

$v(t + dt/2) = v(t) + a(x(t)) * (dt/2)$

Updates the velocity to the midpoint of the next time interval.

Position Full-Step:

$x(t + dt) = x(t) + v(t + dt/2) * dt$

Updates the position using the velocity at the midpoint.

Velocity Half-Step (Completion):

$v(t + dt) = v(t + dt/2) + a(x(t + dt)) * (dt/2)$

Completes the velocity update to the end of the time interval.

- ordinary differential equation

  - leap-frog scheme

$$f_{i+1} = f_i + \Delta t \; G_{i+1/2}$$

+ second order accurate scheme

+ no additional calculations

+ symmetric and hence time reversible (energy conservation...)

+ very well suited for systems of type $\dfrac{d^2 f}{dt^2} = G(f)$

- ordinary differential equation
  - leap-frog scheme

$$\frac{d^2 f}{dt^2} = G(f)$$

- ordinary differential equation

  - leap-frog scheme

$$\frac{df}{dt} = h, \quad \frac{dh}{dt} = G(f)$$

$$f_{i+1} = f_i + \Delta t \, h_{i+1/2}$$

$$h_{i+3/2} = h_{i+1/2} + \Delta t \, G(f_{i+1})$$

- ordinary differential equation

  - leap-frog scheme

$$\frac{d^2 f}{dt^2} = G(f)$$

$$f_{i+1} = f_i + \Delta t\, h_{i+1/2}$$

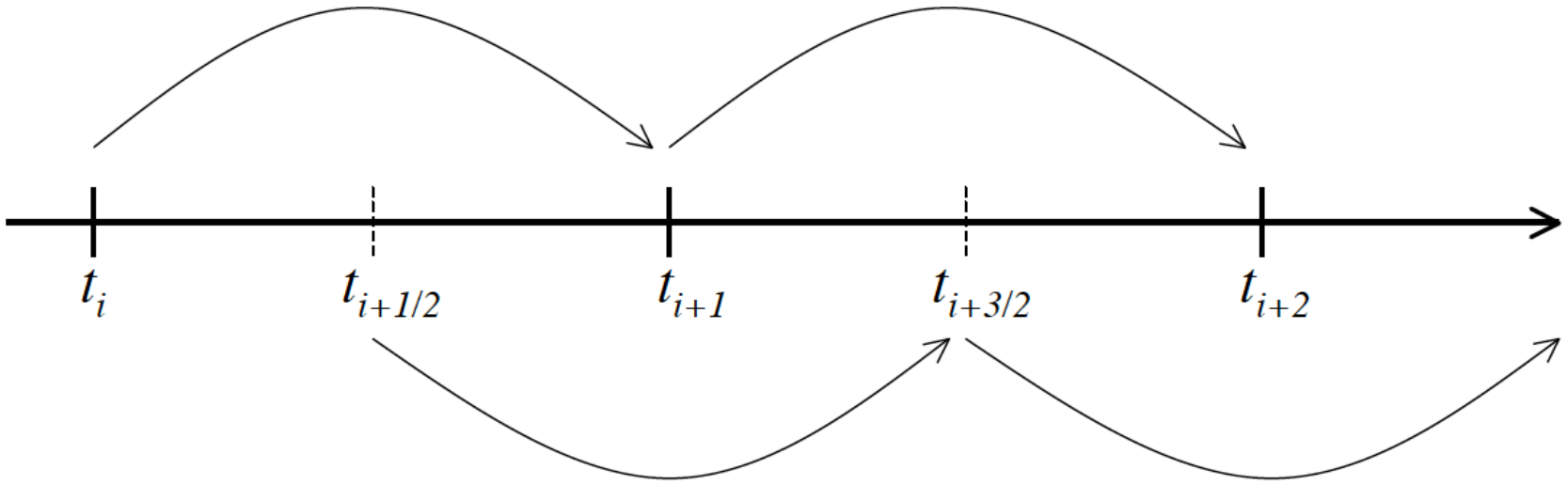

$$h_{i+3/2} = h_{i+1/2} + \Delta t\, G(f_{i+1})$$

- ordinary differential equation

  - leap-frog scheme - jumpstart

$$\frac{d^2 f}{dt^2} = G(f)$$

$$f_1 = f_0 + \Delta t \, h_{1/2}$$

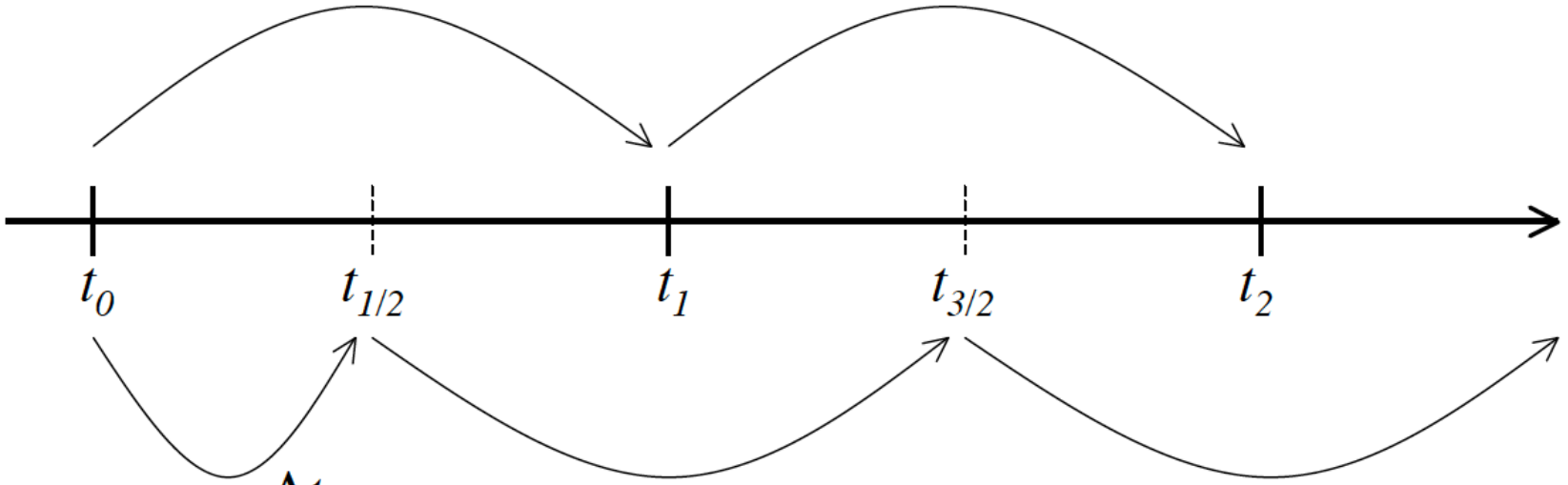

$$h_{1/2} = h_0 + \frac{\Delta t}{2} G(f_0)$$

- ordinary differential equation

  - leap-frog scheme - resync

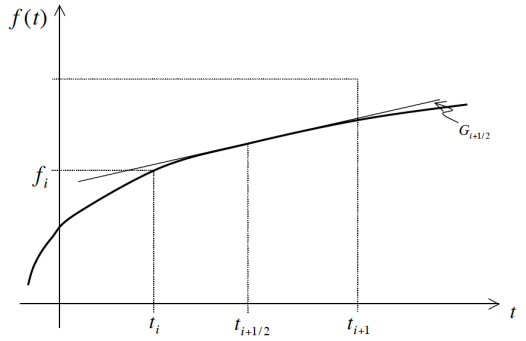

$$\frac{d^2 f}{dt^2} = G(f)$$

$$f_N = f_{N-1} + \Delta t\, h_{N-1/2}$$

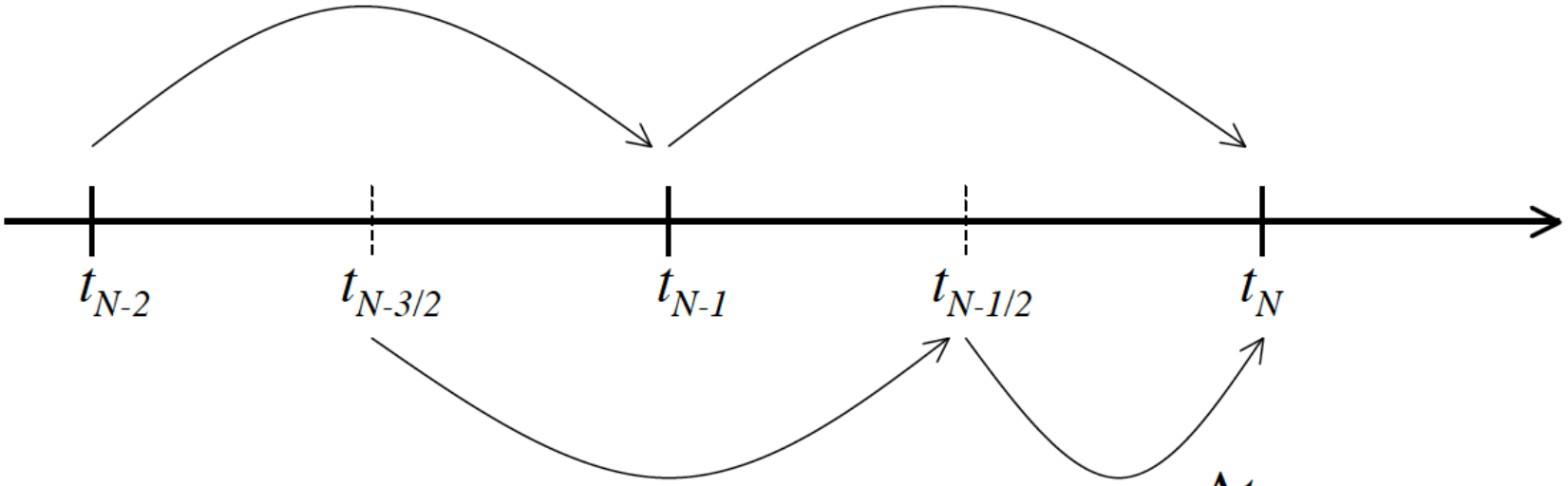

$$h_N = h_{N-1/2} + \frac{\Delta t}{2} G(f_N)$$

- ordinary differential equation

    - Runge-Kutta methods

gain even higher accuracy at the cost of...

+ even more calculations (i.e. trial steps)

+ additional memory requirements

- the equations

  - Newton's second law of motion

$$m\frac{d^2r}{dt^2} = F(r)$$

  - Newton's law of gravity

$$F = G\frac{Mm}{r^2}$$

- the equations

  - Newton's second law of motion

$$\frac{dr}{dt} = v, \quad \frac{dv}{dt} = f(r)$$

  - Newton's law of gravity

$$f(r) = G\frac{M}{r^2}$$

leap-frog integrator!

- leap-frog integration

$$m\frac{d^2r}{dt^2} = F(r)$$

$$F(r) = G\frac{Mm}{r^2}$$

$$\Longrightarrow$$

$$r_{i+1} = r_i + \Delta t\, v_{i+1/2}$$

$$v_{i+3/2} = v_{i+1/2} + \Delta t\, f(r_i)$$

$$f(r_i) = G\frac{M}{r_i^2}$$

dawn of N-body simulations

Galaxies are extended bodies but can generally be regarded as mass points. When two galaxies are involved in a collision, however, this is no longer a good approximation, because the forces are not convergent. To account for this, we take the potential due to the mass M at distance R to be

$$\Phi = \frac{GM}{[R^2+\xi^2]^{1/2}} \tag{1}$$

where ξ is a constant small distance, later to be associated with the effective size of a galaxy, and G is the gravitational constant.

12. *Method for numerical solution.*—The method for choosing the time-steps when integrating the equations of motion is a vital one, as it can easily lead to excessive demands on the machine time. In the method used by von Hoerner (**2**) the two closest bodies determine the time-step for the rest. The time to

$$\Delta\tau_i = \eta \min\left[\frac{1}{N}, \frac{F_i^2}{\dot{F}_i^2} + \delta^2\right]^{1/2}$$

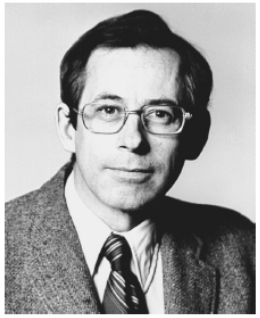

Jim Peebles

THE ASTRONOMICAL JOURNAL VOLUME 75, NUMBER 1 FEBRUARY 1970

Structure of the Coma Cluster of Galaxies*

P. J. E. PEEBLES†
Palmer Physical Laboratory, Princeton University, Princeton, New Jersey
(Received 7 October 1969)

In some cosmologies, a cluster of galaxies is imagined to be a gravitationally bound system which, in analogy with the formation of the Galaxy, originated as a collapsing protocluster. It is shown that a numerical model based on this picture is consistent with the observed features of the Coma Cluster of galaxies. The cluster mass derived from this model agrees with previous values; however, an analysis of the observational uncertainty within the framework of the model shows that the derived mass could be consistent with the estimated total mass provided by the galaxies in the cluster.

N = 300

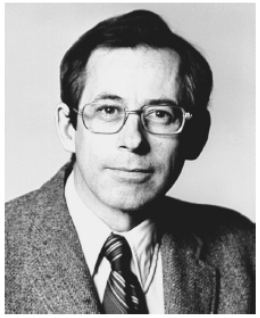

Jim Peebles

- same approach as Aarseth, just more particles..

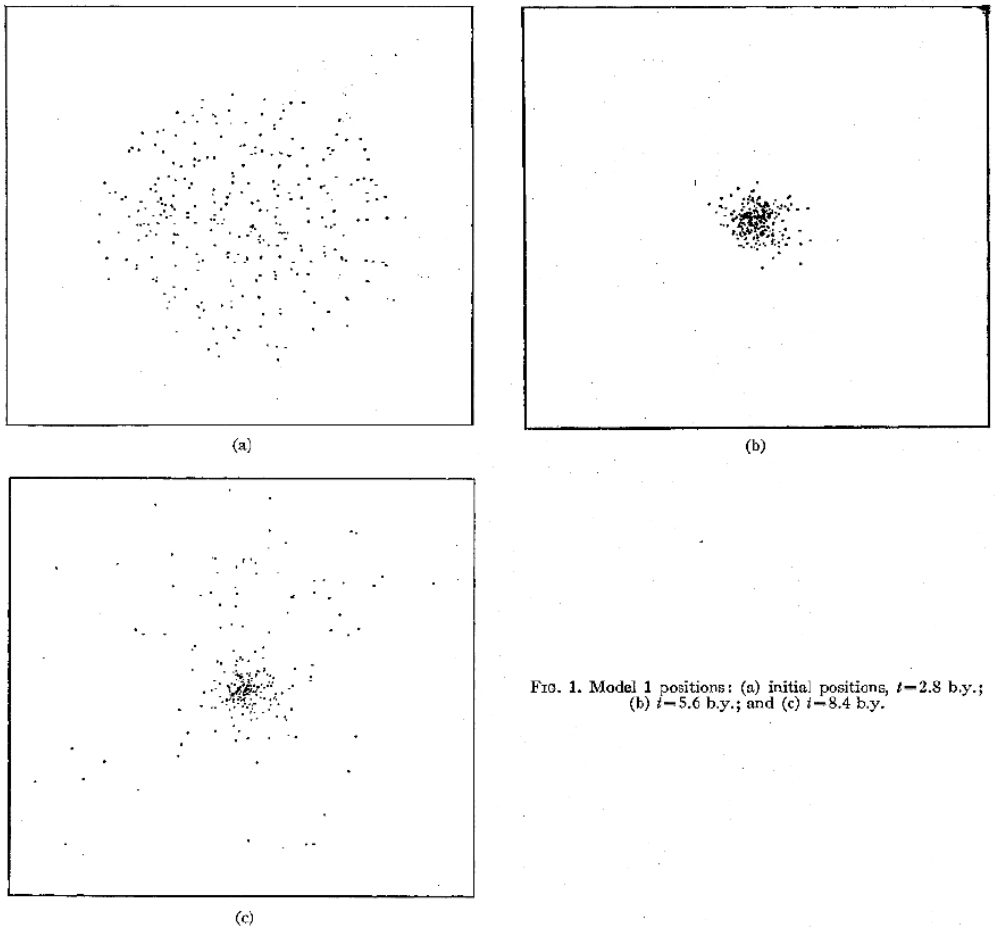

FIG. 1. Model 1 positions: (a) initial positions, $t=2.8$ b.y.; (b) $t=5.6$ b.y.; and (c) $t=8.4$ b.y.

N = 300

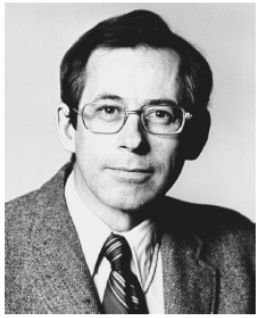

Jim Peebles

- same approach as Aarseth, just more particles..

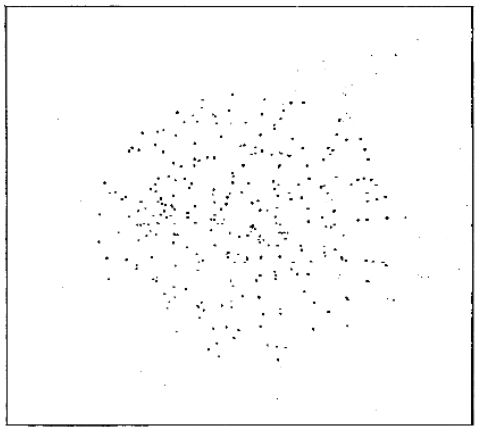

(a)

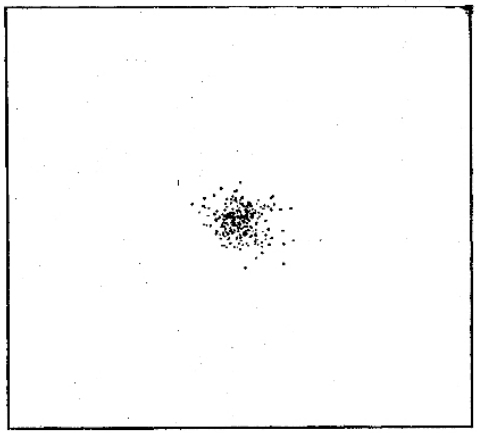

(b)

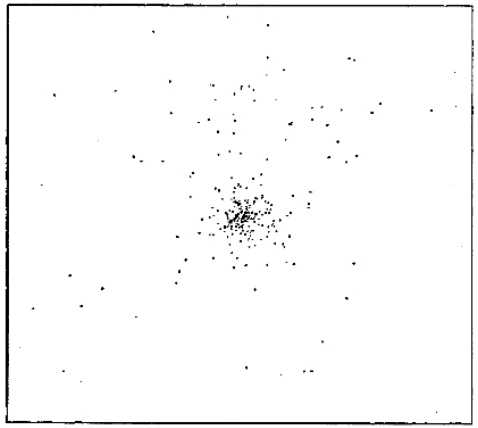

(c)

The adopted formula for the acceleration of the ith object is

$$\mathbf{a}_i = \sum (\mathbf{r}_j - \mathbf{r}_i)/[(\mathbf{r}_j - \mathbf{r}_i)^3 + c^3], \qquad (1)$$

where c is a characteristic size for the objects. Trials indicate that the model results are not sensitive to the assumed value of c (Table II below), although the required integration time increases markedly with decreasing c.

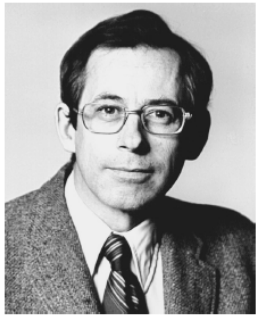

Jim Peebles

- same approach as Aarseth, just more particles..

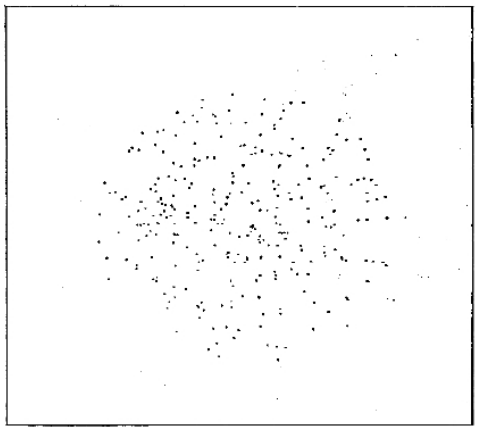

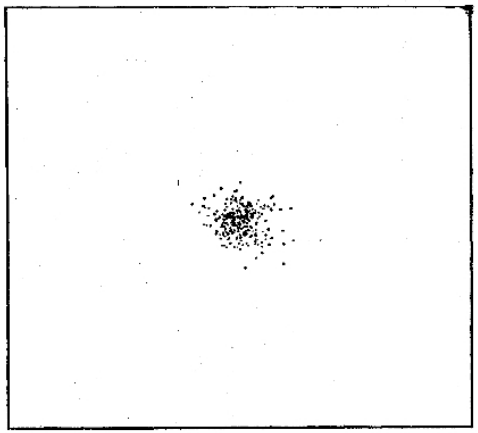

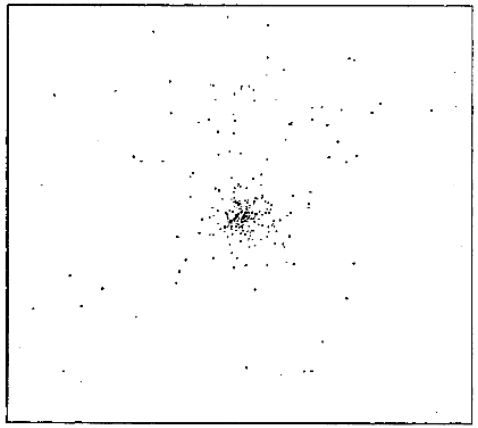

FIG. 5. Comparison of surface density runs in model 1 and observed in the Coma Cluster.

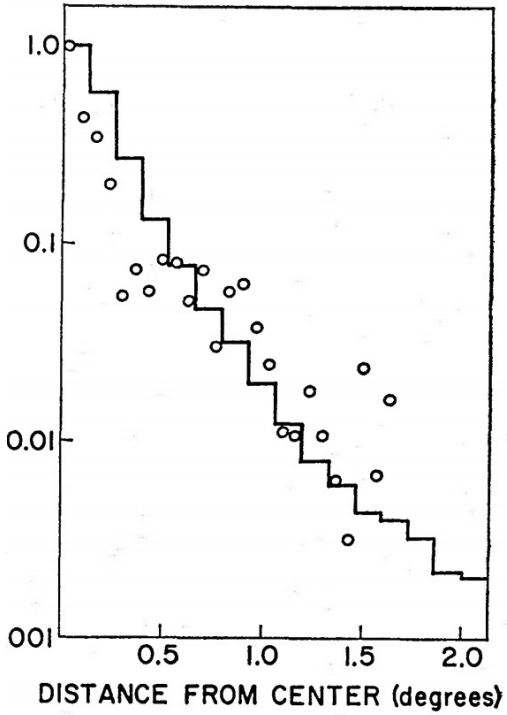

N = 300

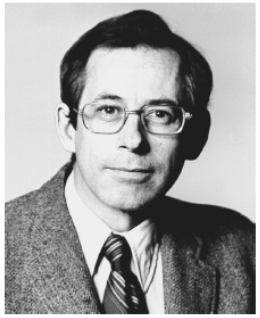

Jim Peebles

- same approach as Aarseth, just more particles..

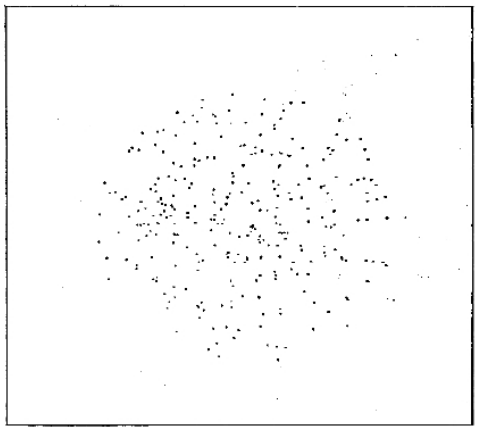

(a)

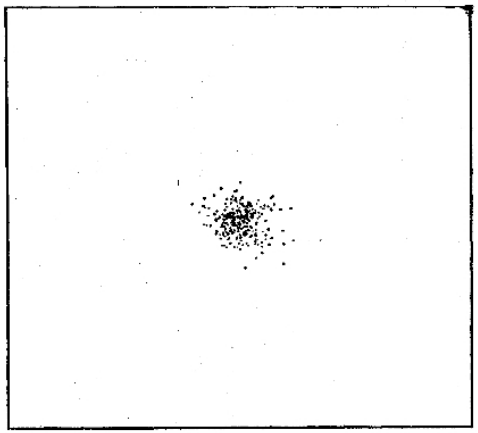

(b)

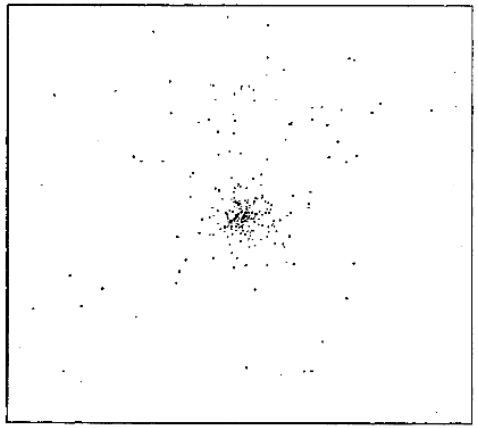

(c)

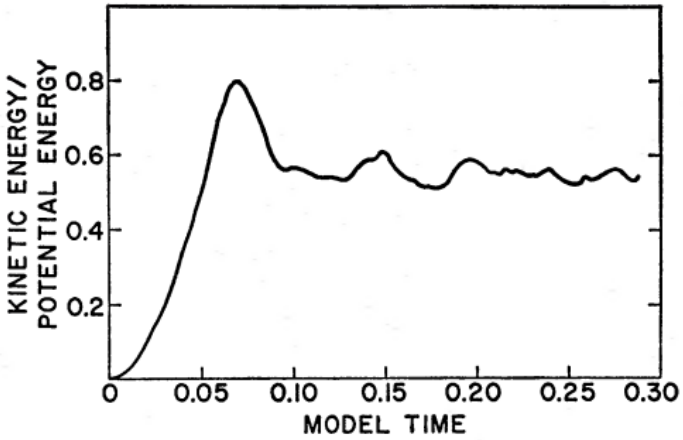

FIG 2. Ratio of kinetic to potential energy in model 1.

Simon White

Mon. Not. R. astr. Soc. (1976) **177**, 717–733.

THE DYNAMICS OF RICH CLUSTERS OF GALAXIES

Simon D. M. White

Institute of Astronomy, Madingley Road, Cambridge CB3 0HA

(Received 1976 March 26)

SUMMARY

An integration of the equations of motion of a 700-body system is presented. It provides a dynamical model for the growth and evolution of clustering in a bound system of galaxies with a realistic mass spectrum. Assuming that galaxy formation occurs during the initial Hubble expansion of the system, it is found that clustering grows in an extremely inhomogeneous fashion by the continual formation and amalgamation of sub-condensations. The early stages of the model may shed light on the formation of inhomogeneous clusters like Virgo, whilst the final state gives a good fit to the gross properties of the Coma cluster in spite of the strong mass segregation which is present. A dynamically consistent mass of $2{\cdot}4 \times 10^{15} M_{\odot}$ is derived for Coma.

1. INTRODUCTION

In an earlier paper (White 1976a, Paper I) the dynamical evolution of rich clusters of galaxies was investigated under the assumption that the visible galaxies contribute only a small fraction of the total cluster mass. It was found that appreciable mass segregation would result from relaxation effects under any reasonable assumption for the masses of the galaxies, and further that the amount of mass segregation in observed clusters could give a value for the mean mass-to-light ratio of the individual cluster galaxies. A naive application of the results of this paper appeared to show that the greater part of the cluster mass could not reside in the galaxies themselves, since this would give rise to more mass segregation than is consistent with observation. The basic assumptions underlying these results are not valid in such circumstances, however, and so it seemed wise to check the above conclusion by investigating the evolution of a model cluster in which the galaxies do contain all the mass.

The model presented in this paper is a numerical integration of the equations of motion of a system of 700 particles. It is an extension of the models of Aarseth (1963, 1966, 1969) and Peebles (1970), and it supersedes them in so far as it contains enough particles to model a rich galaxy cluster without any need for scaling the relative dynamical and relaxation times. The assumed mass distribution is sufficiently realistic to give a good representation of the evolution of a real cluster under the basic premises that the galaxies were formed significantly before the collapse of the cluster as a whole, and that they contain the major part of the cluster mass in amounts proportional to their luminosity.

The model shows that clusters form by the progressive amalgamation of an inhomogeneous system of subclusters. The early stages of the model thus provide a natural picture for the genesis of inhomogeneous clusters like Virgo or Hercules where there is some evidence that the merging process is still going on. The model

Simon White

Mon. Not. R. astr. Soc. (1976) **177**, 717–733.

THE DYNAMICS OF RICH CLUSTERS OF GALAXIES

Simon D. M. White

Institute of Astronomy, Madingley Road, Cambridge CB3 0HA

(Received 1976 March 26)

SUMMARY

An integration of the equations of motion of a 700-body system is presented. It provides a dynamical model for the growth and evolution of clustering in a bound system of galaxies with a realistic mass spectrum. Assuming that galaxy formation occurs during the initial Hubble expansion of the system, it is found that clustering grows in an extremely inhomogeneous fashion by the continual formation and amalgamation of sub-condensations. The early stages of the model may shed light on the formation of inhomogeneous clusters like Virgo, whilst the final state gives a good fit to the gross properties of the Coma cluster in spite of the strong mass segregation which is present. A dynamically consistent mass of $2{\cdot}4 \times 10^{15}\,M_{\odot}$ is derived for Coma.

1. INTRODUCTION

In an earlier paper (White 1976a, Paper I) the dynamical evolution of rich clusters of galaxies was investigated under the assumption that the visible galaxies contribute only a small fraction of the total cluster mass. It was found that appreciable mass segregation would result from relaxation effects under any reasonable assumption for the masses of the galaxies, and further that the amount of mass segregation in observed clusters could give a value for the mean mass-to-light ratio of the individual cluster galaxies. A naive application of the results of this paper appeared to show that the greater part of the cluster mass could not reside in the galaxies themselves, since this would give rise to more mass segregation than is consistent with observation. The basic assumptions underlying these results are not valid in such circumstances, however, and so it seemed wise to check the above conclusion by investigating the evolution of a model cluster in which the galaxies do contain all the mass.

The model presented in this paper is a numerical integration of the equations of motion of a system of 700 particles. It is an extension of the models of Aarseth (1963, 1966, 1969) and Peebles (1970), and it supersedes them in so far as it contains enough particles to model a rich galaxy cluster without any need for scaling the relative dynamical and relaxation times. The assumed mass distribution is sufficiently realistic to give a good representation of the evolution of a real cluster under the basic premises that the galaxies were formed significantly before the collapse of the cluster as a whole, and that they contain the major part of the cluster mass in amounts proportional to their luminosity.

The model shows that clusters form by the progressive amalgamation of an inhomogeneous system of subclusters. The early stages of the model thus provide a natural picture for the genesis of inhomogeneous clusters like Virgo or Hercules where there is some evidence that the merging process is still going on. The model

Simon White

Mon. Not. R. astr. Soc. (1976) **177**, 717–733.

THE DYNAMICS OF RICH CLUSTERS OF GALAXIES

Simon D. M. White

Institute of Astronomy, Madingley Road, Cambridge CB3 0HA

(Received 1976 March 26)

SUMMARY

An integration of the equations of motion of a 700-body system is presented. It provides a dynamical model for the growth and evolution of clustering in a bound system of galaxies with a realistic mass spectrum. Assuming that galaxy formation occurs during the initial Hubble expansion of the system, it is found that clustering grows in an extremely inhomogeneous fashion by the continual formation and amalgamation of sub-condensations. The early stages

Coma cluster in spite of the strong mass segregation which is present. A dynamically consistent mass of $2{\cdot}4 \times 10^{15} M_\odot$ is derived for Coma.

1. INTRODUCTION

In an earlier paper (White 1976a, Paper I) the dynamical evolution of rich clusters of galaxies was investigated under the assumption that the visible galaxies contribute only a small fraction of the total cluster mass. It was found that appreciable mass segregation would result from relaxation effects under any reasonable assumption for the masses of the galaxies, and further that the amount of mass segregation in observed clusters could give a value for the mean mass-to-light ratio of the individual cluster galaxies. A naive application of the results of this paper appeared to show that the greater part of the cluster mass could not reside in the galaxies themselves, since this would give rise to more mass segregation than is consistent with observation. The basic assumptions underlying these results are not valid in such circumstances, however, and so it seemed wise to check the above conclusion by investigating the evolution of a model cluster in which the galaxies do contain all the mass.

The model presented in this paper is a numerical integration of the equations of motion of a system of 700 particles. It is an extension of the models of Aarseth (1963, 1966, 1969) and Peebles (1970), and it supersedes them in so far as it contains enough particles to model a rich galaxy cluster without any need for scaling the relative dynamical and relaxation times. The assumed mass distribution is sufficiently realistic to give a good representation of the evolution of a real cluster under the basic premises that the galaxies were formed significantly before the collapse of the cluster as a whole, and that they contain the major part of the cluster mass in amounts proportional to their luminosity.

The model shows that clusters form by the progressive amalgamation of an inhomogeneous system of subclusters. The early stages of the model thus provide a natural picture for the genesis of inhomogeneous clusters like Virgo or Hercules where there is some evidence that the merging process is still going on. The model

Simon White

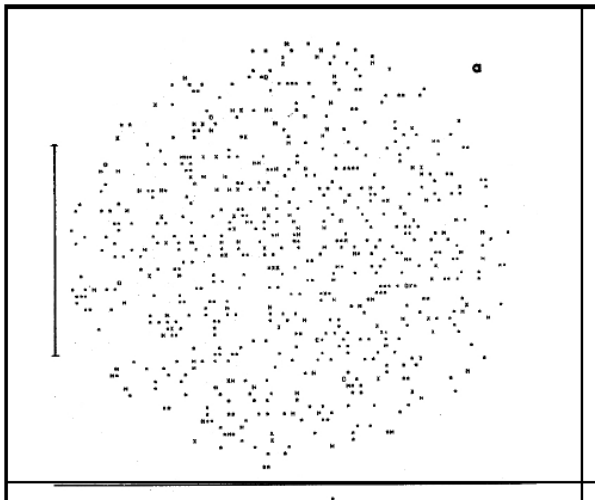

Simon White

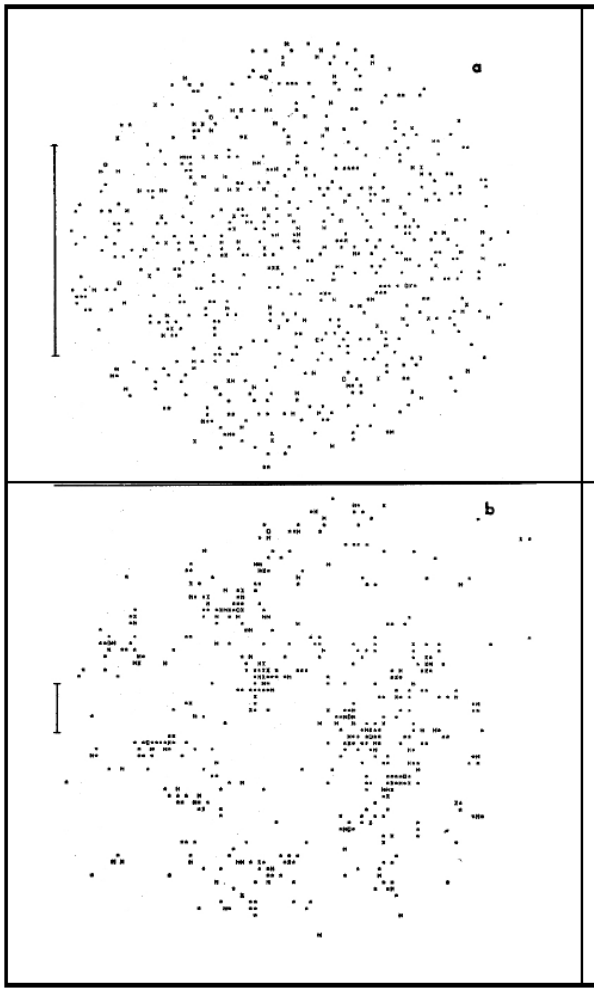

Simon White

N = 700

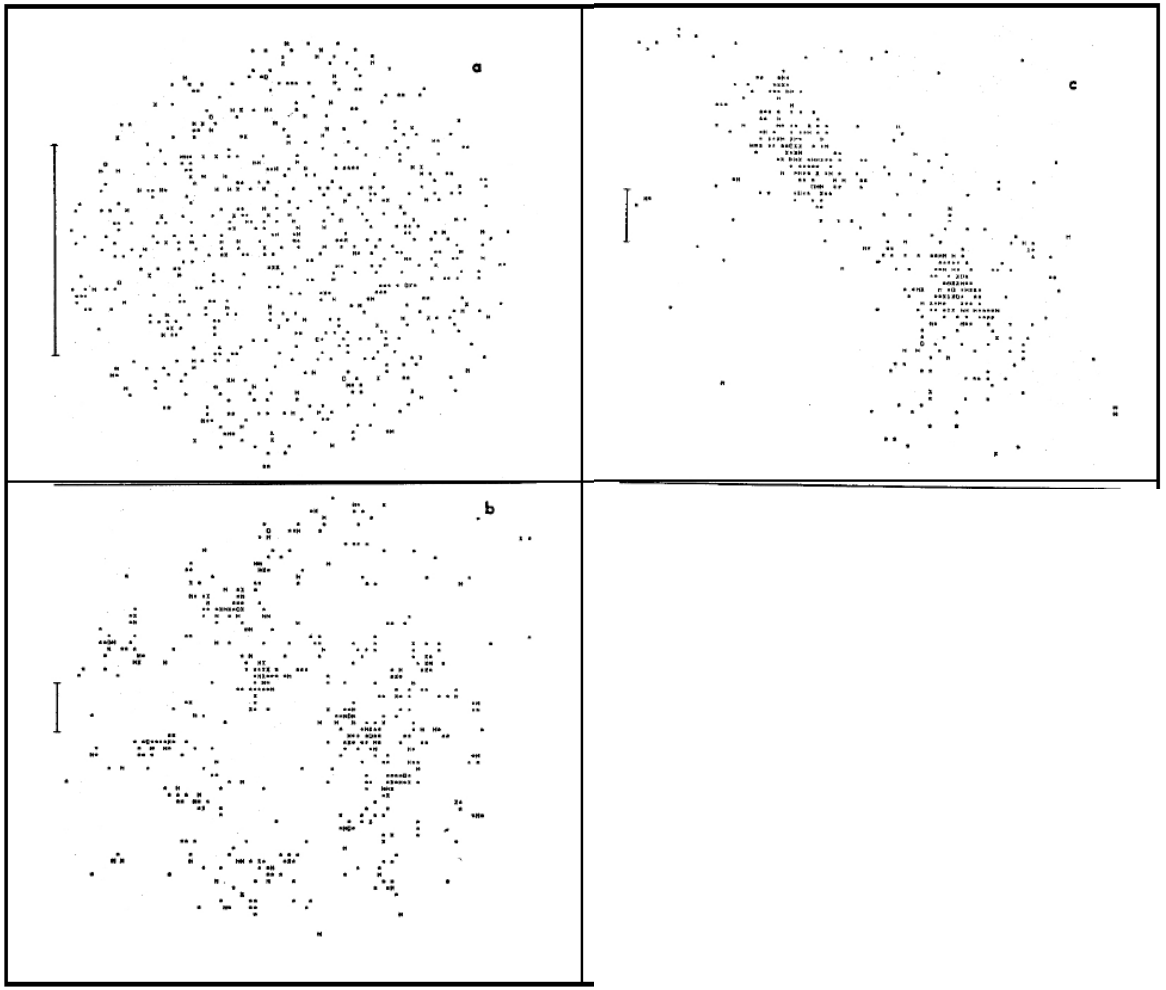

Simon White

N = 700

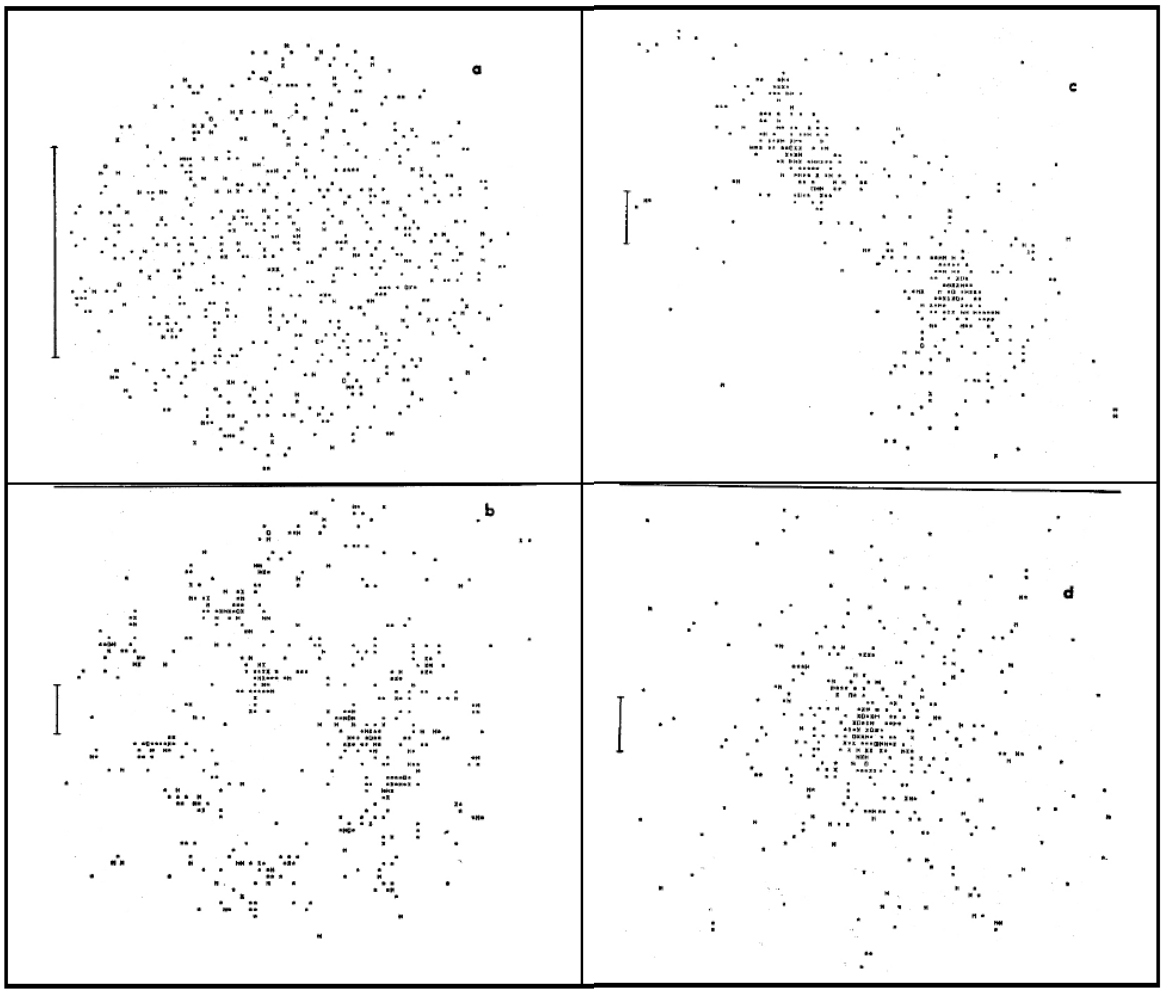

Simon White

"hierarchical structure formation"

N = 700

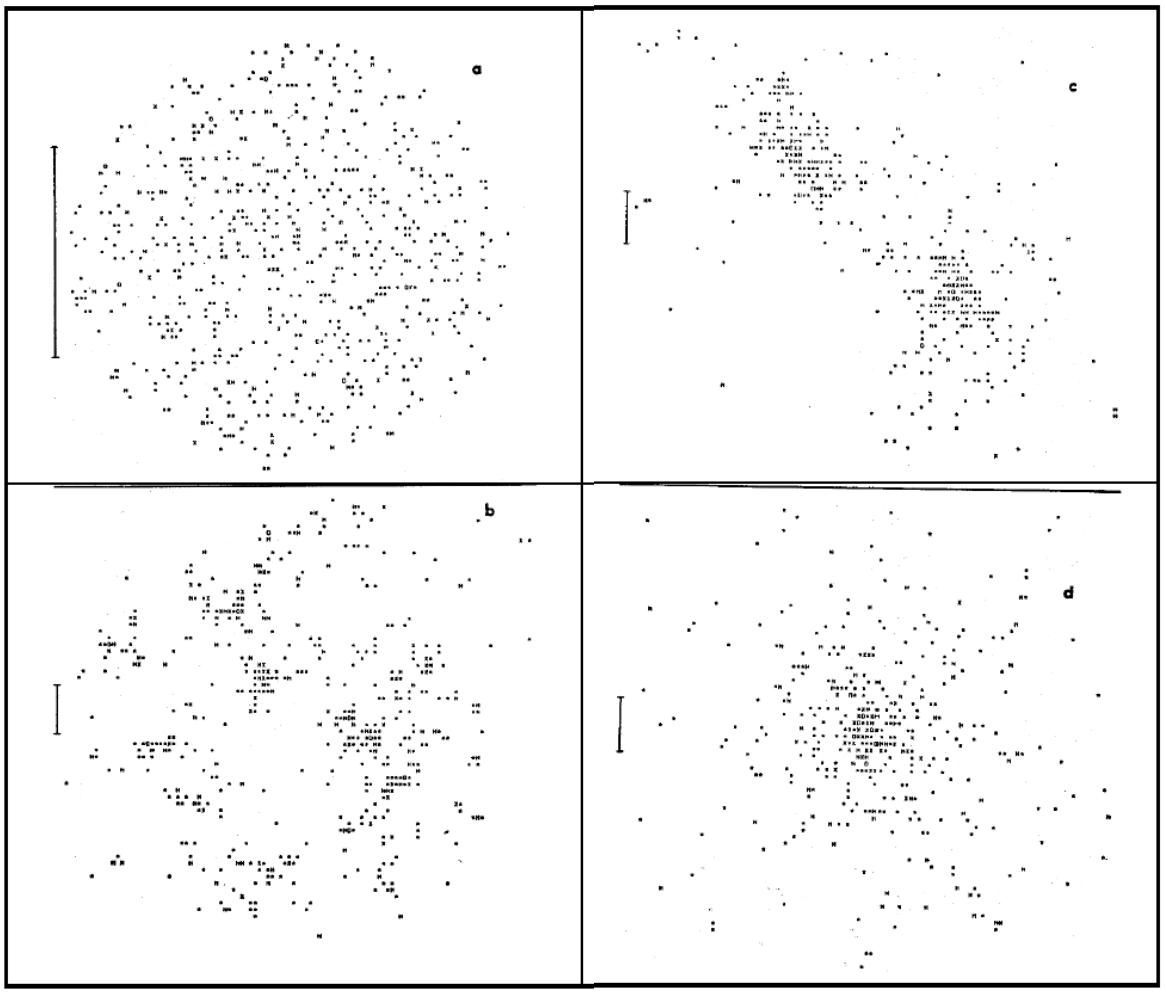

George Efstathiou

THE ASTROPHYSICAL JOURNAL SUPPLEMENT SERIES, 57:241–260, 1985 February

NUMERICAL TECHNIQUES FOR LARGE COSMOLOGICAL *N*-BODY SIMULATIONS

G. EFSTATHIOU,[1,2] M. DAVIS,[2,3] C. S. FRENK,[2,3,4] AND S. D. M. WHITE[2,3]
Received 1984 May 7, accepted 1984 July 24

ABSTRACT

We describe and compare techniques for carrying out large *N*-body simulations of the gravitational evolution of clustering in the fundamental cube of an infinite periodic universe. In particular, we consider both particle mesh (PM) codes and P^3M codes in which a higher resolution force is obtained by direct summation of contributions from neighboring particles. We discuss the mesh-induced anisotropies in the forces calculated by these schemes, and the extent to which they can model the desired $1/r^2$ particle-particle interaction. We also consider how transformation of the time variable can improve the efficiency with which the equations of motion are integrated. We present tests of the accuracy with which the resulting schemes conserve energy and are able to follow individual particle trajectories. We have implemented an algorithm which allows initial conditions to be set up to model any desired spectrum of linear growing mode density fluctuations. A number of tests demonstrate the power of this algorithm and delineate the conditions under which it is effective. We carry out several test simulations using a variety of techniques in order to show how the results are affected by dynamic range limitations in the force calculations, by boundary effects, by residual artificialities in the initial conditions, and by the number of particles employed. For most purposes cosmological simulations are limited by the resolution of their force calculation rather than by the number of particles they can employ. For this reason, while PM codes are quite adequate to study the evolution of structure on large scale, P^3M methods are to be preferred, in spite of their greater cost and complexity, whenever the evolution of small-scale structure is important. Thus, PM codes are adequate to study many aspects of the evolution of a neutrino-dominated universe, but P^3M codes are required to study hierarchical clustering such as may occur in a universe dominated by cold dark matter.

Subject headings: cosmology — galaxies: clustering — numerical methods

I. INTRODUCTION

The purpose of cosmological *N*-body codes is to calculate the nonlinear growth of structure in the universe by following individual particle trajectories under the action of gravity. By studying clustering from initial conditions of different types, it should be possible to isolate those aspects of the final (present) distribution which reflect conditions at early times and others which are mainly a result of nonlinear relaxation processes. Thus, while large-scale filamentary or cellular structure might plausibly result from a large coherence length in the initial field of density fluctuations, the density structure of individual clusters may contain little information about the initial conditions. Different hypotheses for the nature of the major constituents of the universe and for the origin of inhomogeneities lead to different and quite definite predictions for the density field at times when all fluctuations are linear. To test these predictions against the present matter distribution, it is necessary to extrapolate them forward in time. When such an extrapolation is carried out using an *N*-body code, two conditions must be met to obtain reliable results. First, the initial conditions must represent the predictions of linear theory faithfully in all aspects which significantly affect subsequent evolution. Second, the code must follow the evolution of structural properties of interest without undue distortion due to artificial softening of forces, or to effects resulting from the small number of particles and the finite size of the calculation. Both these requirements hinge on the effective resolution of the code.

The fundamental limit on the accessible dynamic range in mass comes from the number of particles employed, while the dynamic range in length is limited by the ratio of the size of the calculation to the softening scale. When an *N*-body system is used to represent the predictions of linear theory, all fluctuations on scales exceeding the mass of a single particle should be of small amplitude; as a result, the limit on dynamic range in mass initially corresponds to a length limit of order the mean interparticle separation. It is important to note that this is no longer true in the highly clustered distributions which occur at late times; the code can then represent the matter distribution accurately on scales smaller than the mean interparticle separation. The reliable dynamic range of a calculation is always less than the fundamental limits just discussed. It can be delineated only by careful testing of the results.

The combined requirements of a large dynamic range in mass and length, together with limitations imposed by the availability of computer time, inevitably lead to a compro-

[1] Institute of Astronomy, Cambridge, England.
[2] Institute for Theoretical Physics, University of California, Santa Barbara, California.
[3] Astronomy Department, University of California, Berkeley, California.
[4] Astronomy Centre, University of Sussex, Brighton, England.

George Efstathiou

THE ASTROPHYSICAL JOURNAL SUPPLEMENT SERIES, 57:241–260, 1985 February

NUMERICAL TECHNIQUES FOR LARGE COSMOLOGICAL *N*-BODY SIMULATIONS

G. EFSTATHIOU,[1,2] M. DAVIS,[2,3] C. S. FRENK,[2,3,4] AND S. D. M. WHITE[2,3]
Received 1984 May 7, accepted 1984 July 24

ABSTRACT

We describe and compare techniques for carrying out large *N*-body simulations of the gravitational evolution of clustering in the fundamental cube of an infinite periodic universe. In particular, we consider both particle mesh (PM) codes and P^3M codes in which a higher resolution force is obtained by direct summation of contributions from neighboring particles. We discuss the mesh-induced anisotropies in the forces calculated by these schemes, and the extent to which they can model the desired $1/r^2$ particle-particle interaction. We also consider how transformation of the time variable can improve the efficiency with which the equations of motion are integrated. We present tests of the accuracy with which the resulting schemes conserve energy and are able to follow individual particle trajectories. We have implemented an algorithm which allows initial conditions to be set up to model any desired spectrum of linear growing mode density fluctuations. A number of tests

We describe and compare techniques for carrying out large *N*-body simulations of the gravitational evolution of clustering in the fundamental cube of an infinite periodic universe. In particular, we consider both particle mesh (PM) codes and P^3M codes in which a higher resolution force is obtained by direct summation of contributions from neighboring particles. We discuss the mesh-induced anisotropies in the forces calculated by these schemes, and the extent to which they can model the desired $1/r^2$ particle-particle interaction. We also

I. INTRODUCTION

The purpose of cosmological *N*-body codes is to calculate the nonlinear growth of structure in the universe by following individual particle trajectories under the action of gravity. By studying clustering from initial conditions of different types, it should be possible to isolate those aspects of the final (present) distribution which reflect conditions at early times and others which are mainly a result of nonlinear relaxation processes. Thus, while large-scale filamentary or cellular structure might plausibly result from a large coherence length in the initial field of density fluctuations, the density structure of individual clusters may contain little information about the initial conditions. Different hypotheses for the nature of the major constituents of the universe and for the origin of inhomogeneities lead to different and quite definite predictions for the density field at times when all fluctuations are linear. To test these predictions against the present matter distribution, it is necessary to extrapolate them forward in time. When such an extrapolation is carried out using an *N*-body code, two conditions must be met to obtain reliable results. First, the initial conditions must represent the predictions of linear theory faithfully in all aspects which significantly affect subsequent evolution. Second, the code must follow the evolution of structural properties of interest without undue distortion due to artificial softening of forces, or to effects resulting from the small number of particles and the finite size of the calculation. Both these requirements hinge on the effective resolution of the code.

The fundamental limit on the accessible dynamic range in mass comes from the number of particles employed, while the dynamic range in length is limited by the ratio of the size of the calculation to the softening scale. When an *N*-body system is used to represent the predictions of linear theory, all fluctuations on scales exceeding the mass of a single particle should be of small amplitude; as a result, the limit on dynamic range in mass initially corresponds to a length limit of order the mean interparticle separation. It is important to note that this is no longer true in the highly clustered distributions which occur at late times; the code can then represent the matter distribution accurately on scales smaller than the mean interparticle separation. The reliable dynamic range of a calculation is always less than the fundamental limits just discussed. It can be delineated only by careful testing of the results.

The combined requirements of a large dynamic range in mass and length, together with limitations imposed by the availability of computer time, inevitably lead to a compro-

[1] Institute of Astronomy, Cambridge, England.
[2] Institute for Theoretical Physics, University of California, Santa Barbara, California.
[3] Astronomy Department, University of California, Berkeley, California.
[4] Astronomy Centre, University of Sussex, Brighton, England.

George Efstathiou

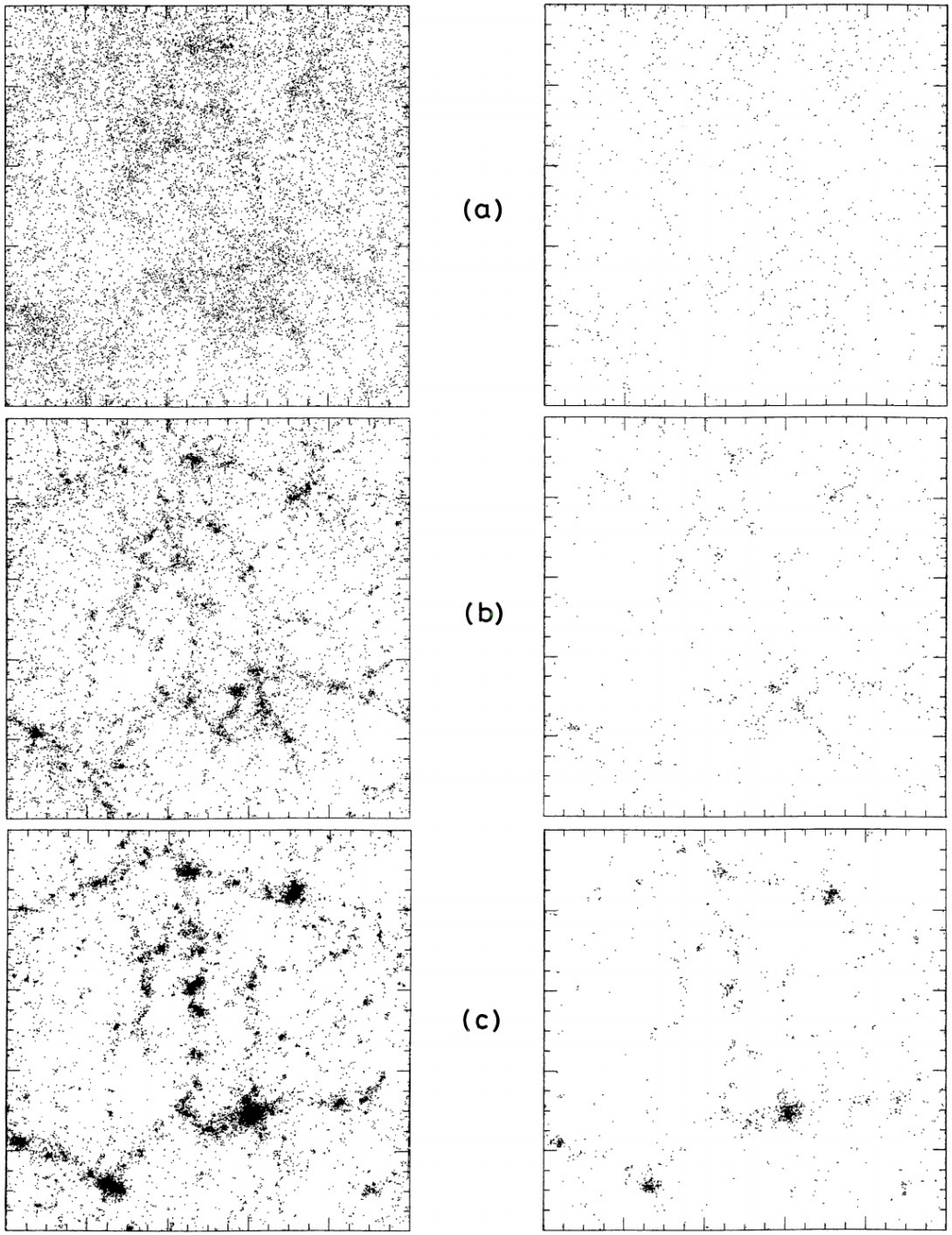

FIG. 9.—Evolution of two P^3M simulations with initial conditions generated using the algorithm described in § IV. The panel to the left shows a model with 32^3 particles perturbed from a grid: (*a*) shows the initial conditions, (*b*) shows the model after expansion by a factor $a = 1.6$, and (*c*) shows the model at $a = 3.0$. The same random numbers were used to generate the initial perturbations in the 20^3 particle model shown to the right. The initial conditions (*a*) have a slightly higher amplitude in this case, but the output times of (*b*) and (*c*) were chosen to match the corresponding pictures in the larger simulation.

On the clustering of particles in an expanding Universe

George Efstathiou

George Efstathiou* *Department of Physics, South Road, Durham DH1 3LE*
J. W. Eastwood *Culham Laboratory, Abingdon, Oxfordshire OX1 3BD*

Received 1980 June 23; in original form 1980 February 20

Summary. We investigate the clustering of particles in Friedmann models of the Universe using 1000- and 20 000-body numerical simulations. The results of these computations are analysed in terms of the two- and three-point correlation functions, the mean relative peculiar velocity between particle pairs $\langle v_{21} \rangle$, and the mean square peculiar velocity dispersion between pairs $\langle v_{21}^2 \rangle$. In the case of Einstein–de Sitter models we find that on scales corresponding to the transition region $\xi \sim 1$, $|\langle v_{21} \rangle| > Hr_{21}$ and this results in a non-power law form for $\xi(r)$, in rough agreement with simple analytic treatments based on the homogeneous spherical cluster models for the collapse of protoclusters. Our results are in conflict with the kinetic theory calculations of Davis & Peebles who studied the problem in the case of an Einstein–de Sitter Universe and found good agreement with observational data. These authors suggest that clusters develop substantial non-radial motions whilst they are still small density fluctuations, so that when a cluster fragments out of the general Hubble expansion, it is already virialized. This 'previrialization' effect does not appear to occur in the numerical models described here. We also examine the effects of particle discreteness and two-body relaxation, which are particularly important in the N-body models but neglected in the approach of Davis & Peebles. Because it is unclear as to whether these effects are important for galaxy clustering in the real Universe, it is difficult to assess the significance of our results. More observational and theoretical work is necessary in order to decide whether our approach is reasonable.

1 Introduction

The aim of this paper is to investigate whether gravitational instability can explain the observed forms of the low-order galaxy correlation functions (Peebles 1974a; Groth & Peebles 1977) under the assumption of some simple initial conditions.

On the clustering of particles in an expanding Universe

George Efstathi

George Efstathiou* *Department of Physics, South Road, Durham DH1 3LE*
J. W. Eastwood *Culham Laboratory, Abingdon, Oxfordshire OX1 3BD*

Summary. We investigate the clustering of particles in Friedmann models of the Universe using 1000- and 20 000-body numerical simulations. The results of these computations are analysed in terms of the two- and three-point correlation functions, the mean relative peculiar velocity between particle pairs $\langle v_{21} \rangle$, and the mean square peculiar velocity dispersion between pairs $\langle v_{21}^2 \rangle$. In the case of Einstein–de Sitter models we find that on scales corres-

treatments based on the homogeneous spherical cluster models for the collapse of protoclusters. Our results are in conflict with the kinetic theory calculations of Davis & Peebles who studied the problem in the case of an Einstein–de Sitter Universe and found good agreement with observational data. These authors suggest that clusters develop substantial non-radial motions whilst they are still small density fluctuations, so that when a cluster fragments out of the general Hubble expansion, it is already virialized. This 'previrialization' effect does not appear to occur in the numerical models described here. We also examine the effects of particle discreteness and two-body relaxation, which are particularly important in the *N*-body models but neglected in the approach of Davis & Peebles. Because it is unclear as to whether these effects are important for galaxy clustering in the real Universe, it is difficult to assess the significance of our results. More observational and theoretical work is necessary in order to decide whether our approach is

The aim of this paper is to investigate whether gravitational instability can explain the observed forms of the low-order galaxy correlation functions (Peebles 1974a; Groth & Peebles 1977) under the assumption of some simple initial conditions.

Peebles 1977) under the assumption of some simple initial conditions.

On the clustering of particles in an expanding Universe

George Efstathi

George Efstathiou* *Department of Physics, South Road, Durham DH1 3LE*
J. W. Eastwood *Culham Laboratory, Abingdon, Oxfordshire OX1 3BD*

Summary. We investigate the clustering of particles in Friedmann models of the Universe using 1000- and 20 000-body numerical simulations. The results of these computations are analysed in terms of the two- and three-point correlation functions, the mean relative peculiar velocity between particle pairs $\langle v_{21} \rangle$, and the mean square peculiar velocity dispersion between pairs $\langle v_{21}^2 \rangle$. In the case of Einstein–de Sitter models we find that on scales corres-

treatments based on the homogeneous spherical cluster models for the collapse of protoclusters. Our results are in conflict with the kinetic theory calculations of Davis & Peebles who studied the problem in the case of an Einstein–de Sitter Universe and found good agreement with observational data. These authors suggest that clusters develop substantial non-radial motions whilst they are still small density fluctuations, so that when a cluster fragments out of the general Hubble expansion, it is already virialized. This 'previrialization' effect does not appear to occur in the numerical models described here. We also examine the effects of particle discreteness and two-body relaxation, which are particularly important in the N-body models but neglected in the approach of Davis & Peebles. Because it is unclear as to whether these effects are important for galaxy clustering in the real Universe, it is difficult to assess the significance of our results. More observational and theoretical work is necessary in order to decide whether our approach is reasonable.

1 Introduction

The aim of this paper is to investigate whether gravitational instability can explain the observed forms of the low-order galaxy correlation functions (Peebles 1974a; Groth & Peebles 1977) under the assumption of some simple initial conditions.

George Efstathiou

Table 2. Number of particles in each of 32 × 32 X, Y cells for model 4 after expansion by a factor $a = 9.9$ (compare with Fig. 1).

Y/X	1	2	3	4	5	6	7	8	9	10	11	12	13	14	15	16	17	18	19	20	21	22	23	24	25	26	27	28	29	30	31	32
1	5	12	36	18	48	40	17	83	22	97	11	4	25	102	22	9	26	22	17	24	29	15	18	10	24	31	27	11	22	15	54	6
2	4	27	24	11	24	19	8	53	31	8	27	18	22	11	9	32	18	48	10	23	15	11	8	55	14	10	28	16	1	15	28	20
3	16	20	27	27	12	20	10	31	24	38	23	8	13	7	21	25	22	10	4	33	14	8	11	49	9	1	11	16	34	14	4	7
4	26	37	31	20	16	41	26	19	11	4	10	28	17	22	20	37	8	22	23	33	23	36	21	13	16	26	19	5	4	11	4	22
5	2	6	85	35	16	9	8	17	24	4	13	4	14	8	0	6	21	5	10	30	17	2	11	12	7	2	8	9	4	7	15	6
6	40	38	17	7	6	9	5	56	19	7	14	8	12	9	7	3	3	42	3	6	3	5	54	78	29	24	14	9	8	15	17	33
7	16	26	10	24	12	34	16	26	25	4	13	4	10	3	9	5	14	7	22	19	7	13	31	73	37	22	48	17	20	13	33	9
8	8	11	45	27	8	58	13	67	35	6	18	18	25	1	1	15	23	20	25	26	21	25	27	55	30	68	64	50	3	23	77	12
9	25	22	31	14	19	14	7	17	24	12	17	26	14	5	8	7	5	16	7	16	7	13	18	31	5	46	40	13	1	12	11	19
10	43	58	11	10	48	8	8	21	21	4	15	32	25	22	7	17	27	25	5	42	8	13	4	3	14	57	11	22	10	10	6	16
11	9	9	6	8	9	5	9	3	12	0	12	7	3	8	21	4	5	11	12	11	27	3	6	0	4	14	41	64	18	13	12	67
12	1	38	9	6	6	8	5	2	20	11	4	16	14	41	5	15	6	3	15	7	7	10	7	6	11	21	49	38	52	2	32	44
13	12	7	9	44	8	0	6	15	13	29	24	4	23	26	17	14	7	12	5	4	16	31	15	4	34	1	9	12	36	48	8	10
14	8	25	20	55	7	9	20	12	24	33	42	4	14	6	19	50	0	5	5	11	26	26	10	2	12	3	3	27	27	65	64	29
15	26	42	17	34	31	10	7	13	25	16	26	18	14	9	22	33	4	7	6	2	3	14	5	2	3	12	8	5	19	10	25	3
16	15	9	11	17	28	17	11	20	5	26	6	6	10	17	68	38	40	16	35	6	15	12	31	12	5	2	24	39	29	16	40	14
17	32	15	28	4	19	9	37	12	51	18	19	14	33	13	16	9	7	11	26	23	26	30	43	41	2	5	6	16	17	22	63	43
18	35	23	28	32	8	20	28	53	24	9	25	25	20	8	21	7	1	6	11	18	28	17	40	18	7	12	11	36	12	58	20	23
19	24	16	17	21	28	9	14	46	23	17	24	0	12	24	8	3	1	38	22	21	10	41	8	32	3	37	30	69	25	23	36	18
20	34	15	31	16	20	7	6	8	9	40	39	38	33	22	7	24	5	4	15	37	19	4	17	7	15	28	31	10	23	24	15	1
21	12	11	52	47	5	5	22	11	6	15	20	71	54	64	7	46	4	1	33	19	12	41	23	22	10	11	22	6	28	44	22	1
22	55	17	29	21	41	11	10	17	5	23	12	9	30	36	10	24	7	14	13	15	3	16	6	25	2	1	38	19	7	49	15	28
23	37	24	16	9	7	8	4	54	12	21	21	1	14	28	29	19	15	22	55	4	18	15	15	26	2	1	3	19	6	14	11	22
24	27	12	6	3	6	16	9	20	32	19	13	12	8	5	26	23	11	8	14	5	26	15	2	2	23	1	21	14	4	6	18	21
25	39	33	12	8	8	7	23	15	13	17	50	11	40	8	46	54	36	4	2	7	1	9	12	16	19	18	14	7	32	9	23	19
26	47	46	25	12	22	22	7	31	17	25	16	5	19	2	25	44	13	27	2	20	1	9	17	20	30	21	21	13	0	6	16	18
27	31	29	13	9	28	12	25	22	18	4	5	5	10	11	14	7	47	24	58	40	20	7	6	32	23	77	18	5	4	21	16	52
28	2	9	20	7	4	16	4	19	6	16	29	18	10	13	17	16	72	19	39	29	25	7	5	22	20	17	14	5	31	3	13	20
29	16	62	7	11	43	6	22	22	18	8	14	52	0	6	25	8	5	3	31	16	23	5	8	11	12	18	26	8	11	23	8	3
30	17	27	13	2	44	79	14	33	50	21	28	24	10	42	12	11	28	6	22	25	58	29	21	29	4	65	23	34	23	22	9	14
31	24	9	3	5	44	27	9	40	27	19	18	16	22	31	17	16	10	26	25	1	9	45	15	8	35	23	44	11	17	7	45	43
32	36	62	22	0	13	25	7	43	54	7	7	25	38	95	15	17	12	21	22	3	14	34	9	44	45	8	12	9	37	35	18	12

George Efstathiou

Table 2. Number of particles in each of 32 × 32 X, Y cells for model 4 after expansion by a factor $a = 9.9$ (compare with Fig. 1).

Y/X	1	2	3	4	5	6	7	8	9	10	11	12	13	14	15	16	17	18	19	20	21	22	23	24	25	26	27	28	29	30	31	32
1	5	12	36	18	48	40	17	83	22	97	11	4	25	102	22	9	26	22	17	24	29	15	18	10	24	31	27	11	22	15	54	6
2	4	27	24	11	24	19	8	53	31	8	27	18	22	11	9	32	18	48	10	23	15	11	8	55	14	10	28	16	1	15	28	20
3	16	20	27	27	12	20	10	31	24	38	23	8	13	7	21	25	22	10	4	33	14	8	11	49	9	1	11	16	34	14	4	7
4	26	37	31	20	16	41	26	19	11	4	10	28	17	22	20	37	8	22	23	33	23	36	21	13	16	26	19	5	4	11	4	22
5	2	6	85	35	16	9	8	17	24	4	13	4	14	8	0	6	21	5	10	30	17	2	11	12	7	2	8	9	4	7	15	6
6	40	38	17	7	6	9	5	56	19	7	14	8	12	9	7	3	3	42	3	6	3	5	54	78	29	24	14	9	8	15	17	33
7	16	26	10	24	12	34	16	26	25	4	13	4	10	3	9	5	14	7	22	19	7	13	31	73	37	22	48	17	20	13	33	9
8	8	11	45	27	8	58	13	67	35	6	18	18	25	1	1	15	23	20	25	26	21	25	27	55	30	68	64	50	3	23	77	12
9	25	22	31	14	19	14	7	17	24	12	17	26	14	5	8	7	5	16	7	16	7	13	18	31	5	46	40	13	1	12	11	19
10	43	58	11	10	48	8	8	21	21	4	15	32	25	22	7	17	27	25	5	42	8	13	4	3	14	57	11	22	10	10	6	16
11	9	9	6	8	9	5	9	3	12	0	12	7	3	8	21	4	5	11	12	11	27	3	6	0	4	14	41	64	18	13	12	67
12	1	38	9	6	6	8	5	2	20	11	4	16	14	41	5	15	6	3	15	7	7	10	7	6	11	21	49	38	52	2	32	44
13	12	7	9	44	8	0	6	15	13	29	24	4	23	26	17	14	7	12	5	4	16	31	15	4	34	1	9	12	36	48	8	10
14	8	25	20	55	7	9	20	12	24	33	42	4	14	6	19	50	0	5	5	11	26	26	10	2	12	3	3	27	27	65	64	29
15	26	42	17	34	31	10	7	13	25	16	26	18	14	9	22	33	4	7	6	2	3	14	5	2	3	12	8	5	19	10	25	3
16	15	9	11	17	28	17	11	20	5	26	6	6	10	17	68	38	40	16	35	6	15	12	31	12	5	2	24	39	29	16	40	14
17	32	15	28	4	19	9	37	12	51	18	19	14	33	13	16	9	7	11	26	23	26	30	43	41	2	5	6	16	17	22	63	43
18	35	23	28	32	8	20	28	53	24	9	25	25	20	8	21	7	1	6	11	18	28	17	40	18	7	12	11	36	12	58	20	23
19	24	16	17	21	28	9	14	46	23	17	24	0	12	24	8	3	1	38	22	21	10	41	8	32	3	37	30	69	25	23	36	18
20	34	15	31	16	20	7	6	8	9	40	39	38	33	22	7	24	5	4	15	37	19	4	17	7	15	28	31	10	23	24	15	1
21	12	11	52	47	5	5	22	11	6	15	20	71	54	64	7	46	4	1	33	19	12	41	23	22	10	11	22	6	28	44	22	1
22	55	17	29	21	41	11	10	17	5	23	12	9	30	36	10	24	7	14	13	15	3	16	6	25	2	1	38	19	7	49	15	28
23	37	24	16	9	7	8	4	54	12	21	21	1	14	28	29	19	15	22	55	4	18	15	15	26	2	1	3	19	6	14	11	22
24	27	12	6	3	6	16	9	20	32	19	13	12	8	5	26	23	11	8	14	5	26	15	2	2	23	1	21	14	4	6	18	21
25	39	33	12	8	8	7	23	15	13	17	50	11	40	8	46	54	36	4	2	7	1	9	12	16	19	18	14	7	32	9	23	19
26	47	46	25	12	22	22	7	31	17	25	16	5	19	2	25	44	13	27	2	20	1	9	17	20	30	21	21	13	0	6	16	18
27	31	29	13	9	28	12	25	22	18	4	5	5	10	11	14	7	47	24	58	40	20	7	6	32	23	77	18	5	4	21	16	52
28	2	9	20	7	4	16	4	19	6	16	29	18	10	13	17	16	72	19	39	29	25	7	5	22	20	17	14	5	31	3	13	20
29	16	62	7	11	43	6	22	22	18	8	14	52	0	6	25	8	5	3	31	16	23	5	8	11	12	18	26	8	11	23	8	3
30	17	27	13	2	44	79	14	33	50	21	28	24	10	42	12	11	28	6	22	25	58	29	21	29	4	65	23	34	23	22	9	14
31	24	9	3	5	44	27	9	40	27	19	18	16	22	31	17	16	10	26	25	1	9	45	15	8	35	23	44	11	17	7	45	43
32	36	62	22	0	13	25	7	43	54	7	7	25	38	95	15	17	12	21	22	3	14	34	9	44	45	8	12	9	37	35	18	12

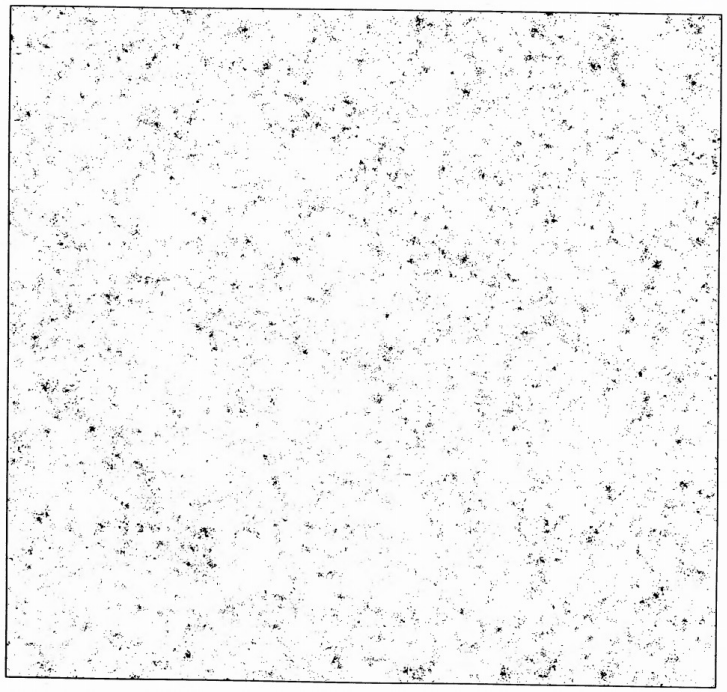

Figure 1. $X-Y$ projection of the particle positions for a 20 000-body numerical experiment after the system has expanded by a factor of 9.9. In this case the expansion follows that of an Einstein–de Sitter model, $\Omega_0 = 1.0$.

George Efstathiou

$32 X, Y$ cells for model 4 after expansion by a factor $a = 9.9$ (compare with Fig. 1).

9	10	11	12	13	14	15	16	17	18	19	20	21	22	23	24	25	26	27	28	29	30	31	32
22	97	11	4	25	102	22	9	26	22	17	24	29	15	18	10	24	31	27	11	22	15	54	6
31	8	27	18	22	11	9	32	18	48	10	23	15	11	8	55	14	10	28	16	1	15	28	20
24	38	23	8	13	7	21	25	22	10	4	33	14	8	11	49	9	1	11	16	34	14	4	7
11	4	10	28	17	22	20	37	8	22	23	33	23	36	21	13	16	26	19	5	4	11	4	22
24	4	13	4	14	8	0	6	21	5	10	30	17	2	11	12	7	2	8	9	4	7	15	6
19	7	14	8	12	9	7	3	3	42	3	6	3	5	54	78	29	24	14	9	8	15	17	33
25	4	13	4	10	3	9	5	14	7	22	19	7	13	31	73	37	22	48	17	20	13	33	9
35	6	18	18	25	1	1	15	23	20	25	26	21	25	27	55	30	68	64	50	3	23	77	12
24	12	17	26	14	5	8	7	5	16	7	16	7	13	18	31	5	46	40	13	1	12	11	19
21	4	15	32	25	22	7	17	27	25	5	42	8	13	4	3	14	57	11	22	10	10	6	16
12	0	12	7	3	8	21	4	5	11	12	11	27	3	6	0	4	14	41	64	18	13	12	67
20	11	4	16	14	41	5	15	6	3	15	7	7	10	7	6	11	21	49	38	52	2	32	44
13	29	24	4	23	26	17	14	7	12	5	4	16	31	15	4	34	1	9	12	36	48	8	10
24	33	42	4	14	6	19	50	0	5	5	11	26	26	10	2	12	3	3	27	27	65	64	29
25	16	26	18	14	9	22	33	4	7	6	2	3	14	5	2	3	12	8	5	19	10	25	3
5	26	6	6	10	17	68	38	40	16	35	6	15	12	31	12	5	2	24	39	29	16	40	14
51	18	19	14	33	13	16	9	7	11	26	23	26	30	43	41	2	5	6	16	17	22	63	43
24	9	25	25	20	8	21	7	1	6	11	18	28	17	40	18	7	12	11	36	12	58	20	23
23	17	24	0	12	24	8	3	1	38	22	21	10	41	8	32	3	37	30	69	25	23	36	18
9	40	39	38	33	22	7	24	5	4	15	37	19	4	17	7	15	28	31	10	23	24	15	1
6	15	20	71	54	64	7	46	4	1	33	19	12	41	23	22	10	11	22	6	28	44	22	1
5	23	12	9	30	36	10	24	7	14	13	15	3	16	6	25	2	1	38	19	7	49	15	28
12	21	21	1	14	28	29	19	15	22	55	4	18	15	26	2	23	1	3	19	6	14	11	22
32	19	13	12	8	5	26	23	11	8	14	5	26	15	2	2	16	19	14	4	6	18	21	
13	17	50	11	40	8	46	54	36	4	2	7	1	9	12	16	19	18	14	7	32	9	23	19
17	25	16	5	19	2	25	44	13	27	2	20	1	9	17	20	30	21	21	13	0	6	16	18
18	4	5	5	10	11	14	7	47	24	58	40	20	7	6	32	23	77	18	5	4	21	16	52
6	16	29	18	10	13	17	16	72	19	39	29	25	7	5	22	20	17	14	5	31	3	13	20
18	8	14	52	0	6	25	8	5	3	31	16	23	5	8	11	12	18	26	8	11	23	8	3
50	21	28	24	10	42	12	11	28	6	22	25	58	29	21	29	4	65	23	34	23	22	9	14
27	19	18	16	22	31	17	16	10	26	25	1	9	45	15	8	35	23	44	11	17	7	45	43
54	7	7	25	38	95	15	17	12	21	22	3	14	34	9	44	45	8	12	9	37	35	18	12

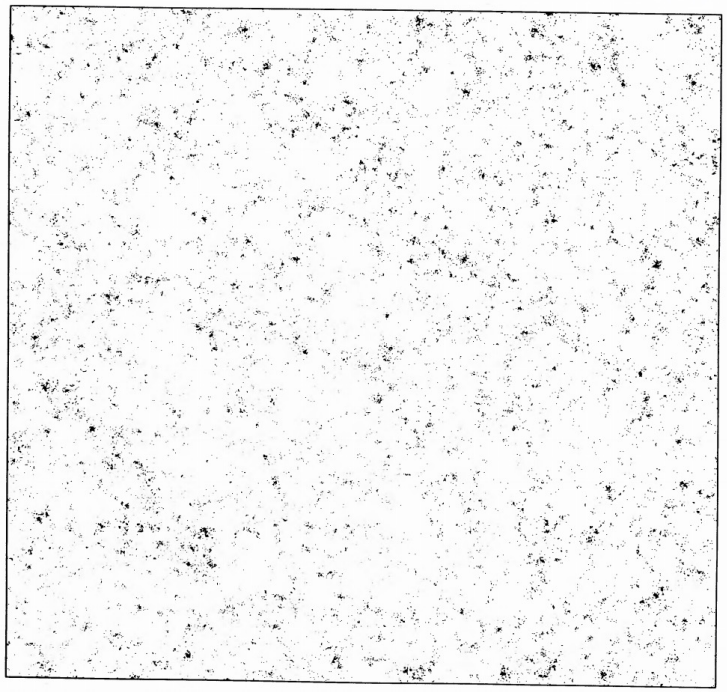

Figure 1. $X-Y$ projection of the particle positions for a 20 000-body numerical experiment after the system has expanded by a factor of 9.9. In this case the expansion follows that of an Einstein–de Sitter model, $\Omega_0 = 1.0$.

The number of clustered galaxies within a radius $r_0 = 5h^{-1}$ Mpc (corresponding to $\xi(r_0) = 1$) is $\langle N \rangle \approx 30$ (taking the mean space density of bright galaxies as $0.02\,h^{-3}$ Mpc). This number is comparable to the mean number of clustered particles within radius x_0 $[\xi(x_0) = 1]$ of the particle distributions analysed in Section 4. Hence if we are justified in assuming the existence of some epoch z_* when galaxies were weakly clustered and act thereafter as the fundamental point particles, our approach may be applicable. We now explore the consequences of this hypothesis.

N = 32768

George Efstathiou

- Zel'dovich approximation for generating realistic initial conditions
- in-depth study of numerical effects

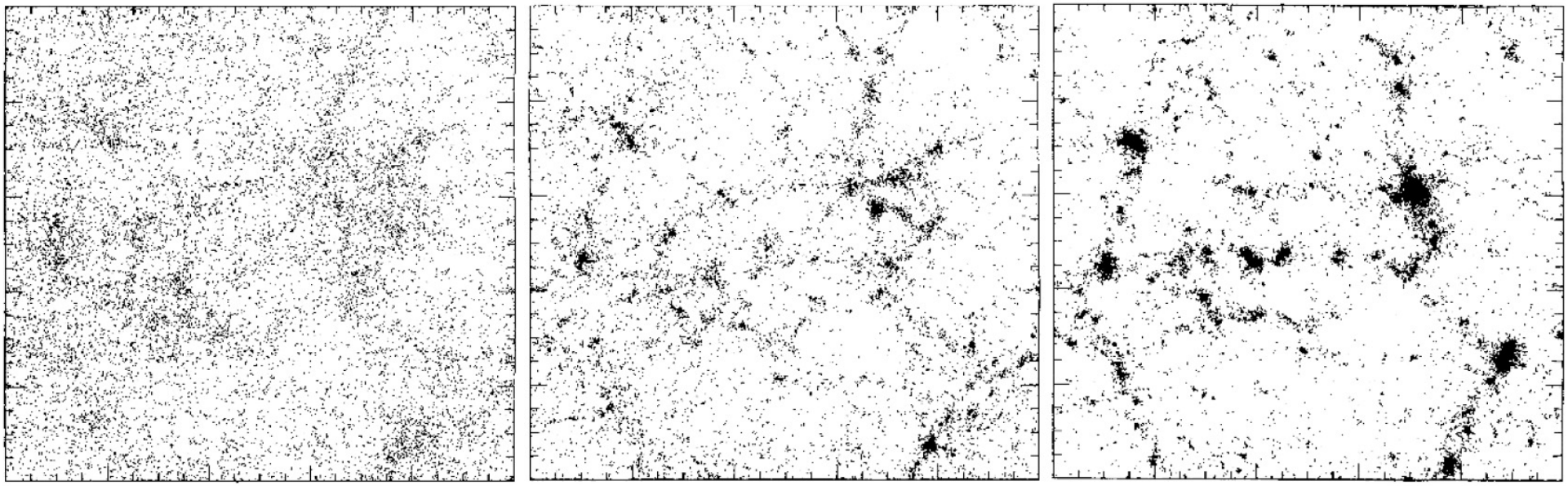

Marc Davis

THE ASTROPHYSICAL JOURNAL, 292:371–394, 1985 May 15

THE EVOLUTION OF LARGE-SCALE STRUCTURE IN A UNIVERSE DOMINATED BY COLD DARK MATTER

MARC DAVIS,[1,2] GEORGE EFSTATHIOU,[1,3] CARLOS S. FRENK,[1,4] AND SIMON D. M. WHITE[2,5]
Received 1984 August 20; accepted 1984 November 30

ABSTRACT

We present the results of numerical simulations of nonlinear gravitational clustering in universes dominated by weakly interacting, "cold" dark matter (e.g., axions or photinos). These studies employ a high resolution N-body code with periodic boundary conditions and 32,768 particles; they can accurately represent the theoretical initial conditions over a factor of 16 in length scale. We have followed the evolution of ensembles of models with $\Omega = 1$ and $\Omega < 1$ from the initial conditions predicted for a "constant curvature" primordial fluctuation spectrum. We also ran one model of a flat universe with a positive cosmological constant. Large filamentary structures, superclusters of clumps, and large low-density regions appear at certain times in all our simulations; however, we do not find large regions as extreme as the apparent void in Boötes. The evolution of the two-point correlation function, $\xi(r)$, is not self-similar; its effective power-law index becomes more negative with time. Models with $\Omega = 1$ are inconsistent with observation if galaxies are assumed to be unbiased tracers of the underlying mass distribution. The peculiar velocities of galaxies are predicted to be much too large. In addition, at times when the shape of $\xi(r)$ matches that observed, the amplitude of clustering is inferred to be too small for any acceptable value of the Hubble constant. Better agreement is obtained for $\Omega = 0.2$, but in both cases the rms relative peculiar velocity of particle pairs decreases markedly with pair separation, whereas the corresponding quantity for galaxies is observed to increase slowly. In all models the three-point correlation function ζ is found to fit the observed form, $\zeta \propto Q\xi^2$, but with Q depending weakly on scale. On small scales Q substantially exceeds its observed value. Consistent with this, the mass distribution of clusters is very broad, showing the presence of clumps with a very wide range in mass at any given time. The model with a positive cosmological constant closely resembles an open model with the same value of Ω. If galaxies are a random sampling of the mass distribution, none of our models is fully consistent with observation. An alternative hypothesis is that galaxies formed only at high peaks of the initial density field. The clustering properties of such "galaxies" are biased; they appear preferentially in high-density regions and so are more correlated than the overall mass distribution. Their two- and three-point correlation functions and their relative peculiar velocity distribution may be consistent with observation even in a universe with $\Omega = 1$. If this is an appropriate model for galaxy formation, it may be possible to reconcile a flat universe with most aspects of the observed galaxy distribution.

Subject headings: galaxies: clustering — galaxies: formation — numerical methods

I. INTRODUCTION

The fundamental problem of understanding the structure of our universe can be approached by phenomenological study of its present configuration or by analytical study of its origins. In recent years considerable progress has been made on both these fronts, but it has become clear that a major difficulty lies in bridging the gap between them. Large-scale surveys of galaxy redshifts have revealed many aspects of the three-dimensional morphology of the galaxy distribution. (See the recent reviews Oort 1983; Davis 1984.) At the same time there has been widespread enthusiasm in the cosmological community over new ideas injected both by Grand Unified Theories and by the possibility of an early inflationary epoch. The present ratio of photons to baryons may be explained by non-equilibrium particle interactions at grand unification energies (Weinberg 1979), while inflation can account for the homogeneity and flatness of the universe and for the low abundance of magnetic monopoles (Guth 1981). Thus some of the most fundamental parameters of our universe may be explained in a natural fashion. Inflationary models make a specific prediction for the form of the density perturbation spectrum from which observed structure must grow (Guth and Pi 1982; Hawking 1982; Starobinskii 1982; Bardeen, Steinhardt, and Turner 1983). Perturbations in curvature arise from quantum fluctuations during inflation. The time invariance of de Sitter space ensures that their amplitude as they are swept across the event horizon during the inflationary epoch, and consequently as they return across it in the present Friedmann universe, is independent of scale. Their distribution thus has the Harrison-Zel'dovich "constant curvature" form. Perturbations generated in this way are adiabatic, with no fluctuation in photon-to-baryon ratio. So far inflationary models have been able to predict the correct fluctuation amplitude only for very specific and finely tuned theories for the underlying particle physics. The prediction of an adiabatic scale-invariant spectrum is not, however, restricted to such models (see, e.g., Harrison 1970; Zel'dovich 1972; Kibble 1976; Turner and Schramm 1978; Press 1980).

If any inflationary model is valid, the present value of the cosmological density parameter Ω is expected to be very close to unity. Constraints from Big Bang nucleosynthesis suggest, however, that the density of baryonic material is an order of

[1] Institute for Theoretical Physics, University of California, Santa Barbara.
[2] Astronomy and Physics Departments, University of California, Berkeley.
[3] Institute of Astronomy, University of Cambridge.
[4] Astronomy Centre, University of Sussex.
[5] Steward Observatory, University of Arizona.

Marc Davis

THE ASTROPHYSICAL JOURNAL, 292:371–394, 1985 May 15

THE EVOLUTION OF LARGE-SCALE STRUCTURE IN A UNIVERSE DOMINATED BY COLD DARK MATTER

MARC DAVIS,[1,2] GEORGE EFSTATHIOU,[1,3] CARLOS S. FRENK,[1,4] AND SIMON D. M. WHITE[2,5]
Received 1984 August 20; accepted 1984 November 30

ABSTRACT

We present the results of numerical simulations of nonlinear gravitational clustering in universes dominated by weakly interacting, "cold" dark matter (e.g., axions or photinos). These studies employ a high resolution N-body code with periodic boundary conditions and 32,768 particles; they can accurately represent the theoretical initial conditions over a factor of 16 in length scale. We have followed the evolution of ensembles of models with $\Omega = 1$ and $\Omega < 1$ from the initial conditions predicted for a "constant curvature" primordial fluctuation spectrum. We also ran one model of a flat universe with a positive cosmological constant. Large filamentary structures, superclusters of clumps, and large low-density regions appear at certain times in all our simulations; however, we do not find large regions as extreme as the apparent void in Boötes. The evolution of the two-point correlation function, $\xi(r)$, is not self-similar; its effective power-law index becomes more negative with time. Models with $\Omega = 1$ are inconsistent with observation if galaxies are assumed to be unbiased tracers of the underlying mass distribution. The peculiar velocities of galaxies are predicted to be much too large. In addition, at times when the shape of $\xi(r)$ matches that observed, the amplitude of clustering is inferred to be too small for any acceptable value of the Hubble constant. Better agreement is obtained for $\Omega = 0.2$, but in both cases the rms relative peculiar velocity of particle pairs decreases markedly with pair separation, whereas the corresponding quantity for galaxies is observed to increase slowly. In all models the three-point correlation function ζ is found to fit the observed form, $\zeta \propto Q\xi^2$, but with Q depending weakly on scale. On small scales Q substantially exceeds its observed value. Consistent with this, the mass distribution of more correlated than the overall mass distribution. Their two- and three-point correlation functions and their relative peculiar velocity distribution may be consistent with observation even in a universe with $\Omega = 1$. If this is an appropriate model for galaxy formation, it may be possible to reconcile a flat universe with most aspects of the observed galaxy distribution.

Subject headings: galaxies: clustering — galaxies: formation — numerical methods

tive with time. Models with $\Omega = 1$ are inconsistent with observation if galaxies are assumed to be unbiased tracers of the underlying mass distribution. The peculiar velocities of galaxies are predicted to be much too

I. INTRODUCTION

The fundamental problem of understanding the structure of our universe can be approached by phenomenological study of its present configuration or by analytical study of its origins. In recent years considerable progress has been made on both these fronts, but it has become clear that a major difficulty lies in bridging the gap between them. Large-scale surveys of galaxy redshifts have revealed many aspects of the three-dimensional morphology of the galaxy distribution. (See the recent reviews Oort 1983; Davis 1984.) At the same time there has been widespread enthusiasm in the cosmological community over new ideas injected both by Grand Unified Theories and by the possibility of an early inflationary epoch. The present ratio of photons to baryons may be explained by non-equilibrium particle interactions at grand unification energies (Weinberg 1979), while inflation can account for the homogeneity and flatness of the universe and for the low abundance of magnetic monopoles (Guth 1981). Thus some of the most fundamental parameters of our universe may be explained in a natural fashion. Inflationary models make a specific prediction for the form of the density perturbation spectrum from which observed structure must grow (Guth and Pi 1982; Hawking 1982; Starobinskii 1982; Bardeen, Steinhardt, and Turner 1983). Perturbations in curvature arise from quantum fluctuations during inflation. The time invariance of de Sitter space ensures that their amplitude as they are swept across the event horizon during the inflationary epoch, and consequently as they return across it in the present Friedmann universe, is independent of scale. Their distribution thus has the Harrison-Zel'dovich "constant curvature" form. Perturbations generated in this way are adiabatic, with no fluctuation in photon-to-baryon ratio. So far inflationary models have been able to predict the correct fluctuation amplitude only for very specific and finely tuned theories for the underlying particle physics. The prediction of an adiabatic scale-invariant spectrum is not, however, restricted to such models (see, e.g., Harrison 1970; Zel'dovich 1972; Kibble 1976; Turner and Schramm 1978; Press 1980).

If any inflationary model is valid, the present value of the cosmological density parameter Ω is expected to be very close to unity. Constraints from Big Bang nucleosynthesis suggest, however, that the density of baryonic material is an order of

[1] Institute for Theoretical Physics, University of California, Santa Barbara.
[2] Astronomy and Physics Departments, University of California, Berkeley.
[3] Institute of Astronomy, University of Cambridge.
[4] Astronomy Centre, University of Sussex.
[5] Steward Observatory, University of Arizona.

N = 32768

Marc Davis

- invention of friends-of-friends (FOF) halo finding algorithm
- biased galaxy formation

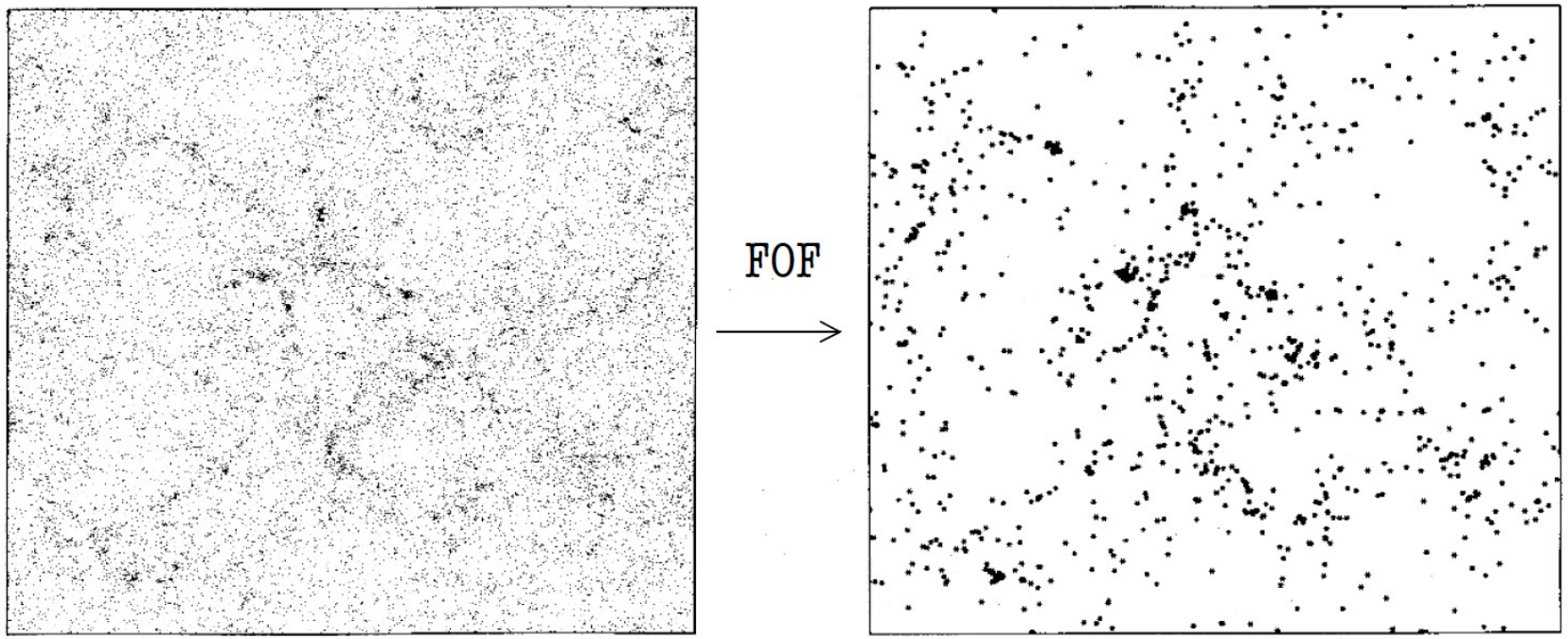

FIG. 16.—The projected distribution of all particles (*left*) and of the "galaxies" (*right*) in EdS1 at $a = 1.4$. The side of the box is $32.5h^{-1}$ Mpc. "Galaxies" are assumed to form only at the 2.5 σ peaks of the linear density distribution.

- mode of operation

  - group all particles together whose distances obey:

$$\boxed{\left|\vec{r}_i - \vec{r}_j\right| \le b\bar{d}} \qquad \bar{d} = \frac{B}{\sqrt[3]{N}}$$

  - typical "linking-length values:

$$b \approx 0.1 - 0.2$$

$\Rightarrow$intrinsically difficult to find sub-halos:

hierarchical FOF (HFOF), minimal-spanning-tree (MST), ...

N = 32768

Marc Davis

- invention of friends-of-friends (FOF) halo finding algorithm
- biased galaxy formation

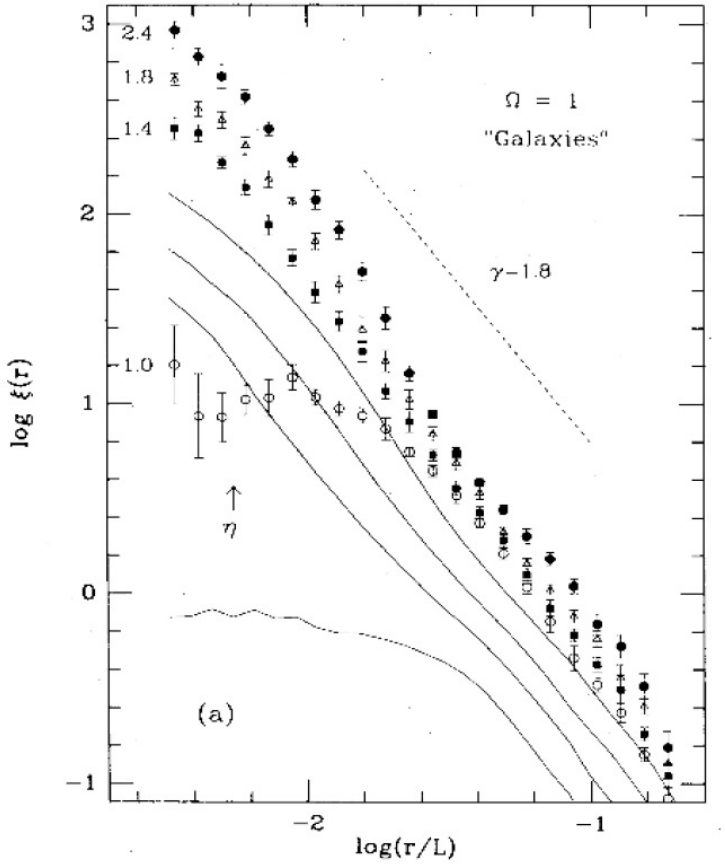

Marc Davis

386

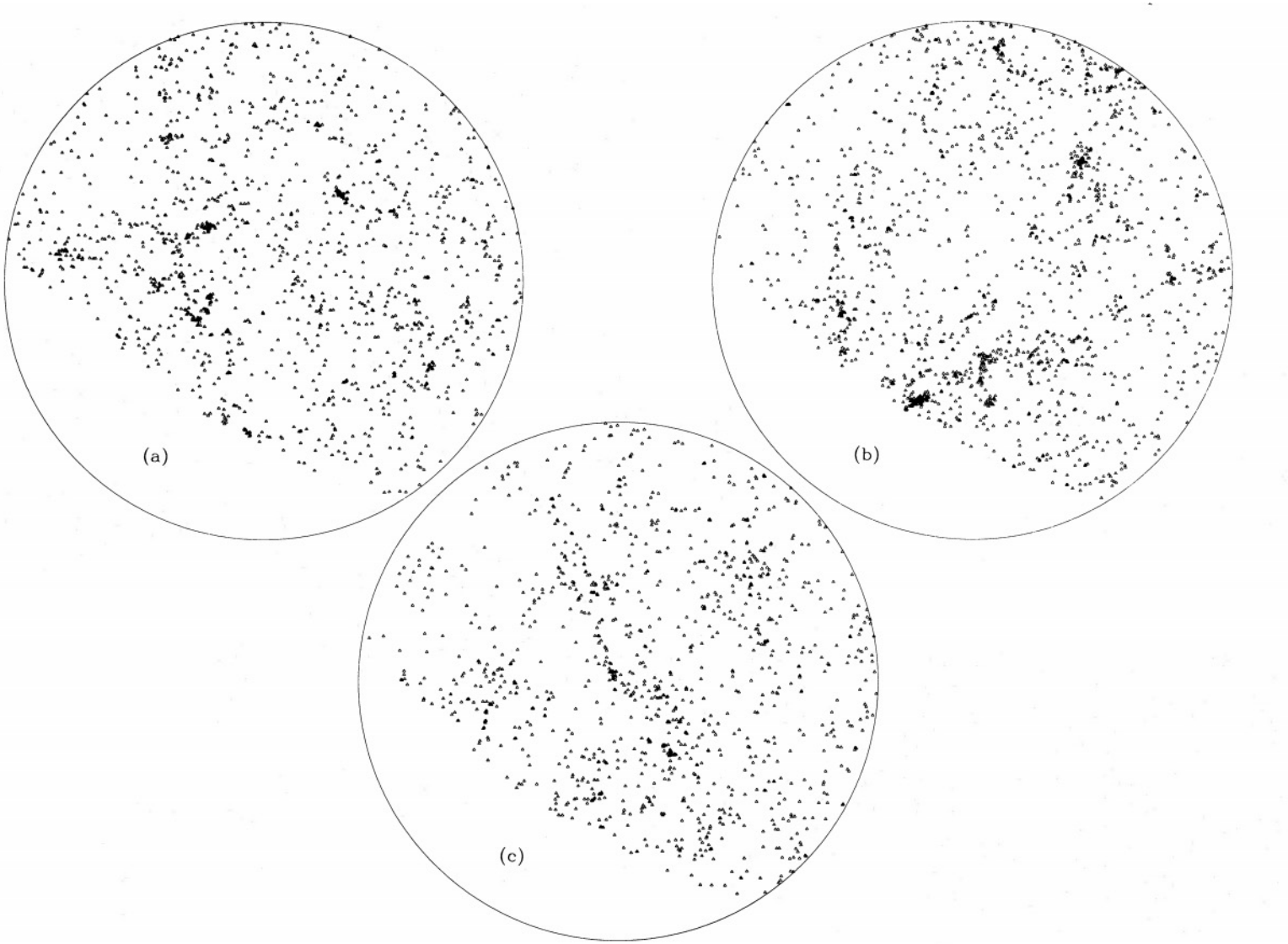

FIG. 12.—Redshift catalogs constructed from two open models (O2 and O3) are shown in (*a*) and (*b*) as projections onto the "sky." Particles were selected for inclusion in these catalogs in such a way as to mimic the northern CfA survey. The real data are shown in the same format in (*c*). These are equal area plots of the sky; the outer circle corresponds to Galactic latitude $+40°$, while the empty regions correspond to declinations below 0°. In constructing the catalog from O3 shown in (*b*), the "observer" was purposely sited near a prominent cluster.

Julio Navarro

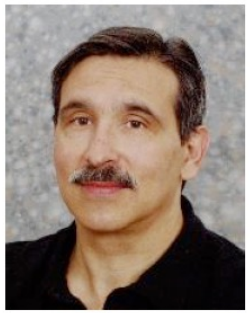

Carlos Frenk

Simon White

THE ASTROPHYSICAL JOURNAL, 490:493–508, 1997 December 1

A UNIVERSAL DENSITY PROFILE FROM HIERARCHICAL CLUSTERING

JULIO F. NAVARRO[1]
Steward Observatory, 933 North Cherry Avenue, University of Arizona, Tucson, AZ 85721-0065; jnavarro@as.arizona.edu.
CARLOS S. FRENK
Department of Physics, University of Durham, South Road, Durham DH1 3LE, England; c.s.frenk@uk.ac.durham
AND
SIMON D. M. WHITE
Max-Planck-Institut für Astrophysik, Karl-Schwarzschild-Strasse 1, 85740, Garching bei München, Germany;
swhite@mpa-garching.mpg.de
Received 1996 November 13; accepted 1997 July 15

ABSTRACT

We use high-resolution N-body simulations to study the equilibrium density profiles of dark matter halos in hierarchically clustering universes. We find that all such profiles have the same shape, independent of the halo mass, the initial density fluctuation spectrum, and the values of the cosmological parameters. Spherically averaged equilibrium profiles are well fitted over two decades in radius by a simple formula originally proposed to describe the structure of galaxy clusters in a cold dark matter universe. In any particular cosmology, the two scale parameters of the fit, the halo mass and its characteristic density, are strongly correlated. Low-mass halos are significantly denser than more massive systems, a correlation that reflects the higher collapse redshift of small halos. The characteristic density of an equilibrium halo is proportional to the density of the universe at the time it was assembled. A suitable definition of this assembly time allows the same proportionality constant to be used for all the cosmologies that we have tested. We compare our results with previous work on halo density profiles and show that there is good agreement. We also provide a step-by-step analytic procedure, based on the Press-Schechter formalism, that allows accurate equilibrium profiles to be calculated as a function of mass in any hierarchical model.

Subject headings: cosmology: theory — dark matter — galaxies: halos — methods: numerical

1. INTRODUCTION

It has been 25 years since the discovery that galaxies are surrounded by extended massive halos of dark matter. A variety of observational probes—disk rotation curves, stellar kinematics, gas rings, motions of globular clusters, planetary nebulae and satellite galaxies, hot gaseous atmospheres, gravitational lensing effects—are now making it possible to map halo mass distributions in some detail. These distributions are intimately linked to the nature of the dark matter, to the way halos formed, and to the cosmological context of halo formation.

Insight into these links came first from analytic studies. Building on the early work of Gunn & Gott (1972), similarity solutions were obtained by Fillmore & Goldreich (1984) and Bertschinger (1985) for the self-similar collapse of spherical perturbations in an Einstein–de Sitter universe. Such solutions necessarily resemble power laws in the virialized regions. Hoffman & Shaham (1985) and Hoffman (1988) extended this analysis by considering open universes, and by modeling as scale-free spherical perturbations the objects that form by hierarchical clustering from power-law initial density perturbation spectra [$P(k) \propto k^n$]. They argued that isothermal structure ($\rho \propto r^{-2}$) should be expected in an Einstein–de Sitter universe if $n \leq -2$, and that steeper profiles should be expected for larger n and in open universes.

Despite the schematic nature of these arguments, their general predictions were verified as numerical data became available from N-body simulations of hierarchical cosmologies. Power-law fits to halo density profiles in a variety of simulations all show a clear steepening as n increases or the density of the universe decreases (Frenk et al. 1985, 1988; Quinn, Salmon, & Zurek 1986; Efstathiou et al. 1988; Zurek, Quinn, & Salmon 1988; Warren et al. 1992; Crone, Evrard, & Richstone 1994). An apparent exception was the work of West, Dekel, & Oemler (1987), who found that *galaxy cluster* density profiles show no clear dependence on n.

Significant departures from power-law behavior were first reported by Frenk et al. (1988), who noted that halo profiles in cold dark matter (CDM) simulations steepen progressively with increasing radius. Efstathiou et al. (1988) found similar departures—at odds with the analytic predictions—in their simulations of scale-free hierarchical clustering. They also noted that these departures were most obvious in their best resolved halos. Similar effects were noted by Dubinski & Carlberg (1991) in a high-resolution simulation of a galaxy-sized CDM halo. These authors found their halo to be well described by a density profile with a gently changing logarithmic slope, specifically the one proposed by Hernquist (1990).

In earlier papers of this series, we used high-resolution simulations to study the formation of CDM halos with masses spanning about 4 orders of magnitude, ranging from dwarf galaxy halos to those of rich galaxy clusters (Navarro, Frenk, & White 1995, 1996). This work showed that the equilibrium density profiles of CDM halos of all masses can be accurately fitted over two decades in radius by the simple formula

$$\frac{\rho(r)}{\rho_{\rm crit}} = \frac{\delta_c}{(r/r_s)(1 + r/r_s)^2}, \qquad (1)$$

[1] Bart J. Bok Fellow.

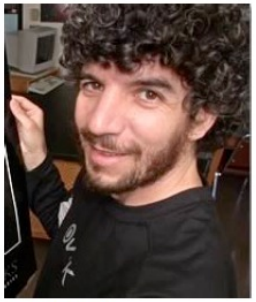

Julio Navarro

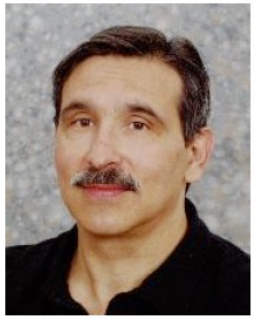

Carlos Frenk

Simon White

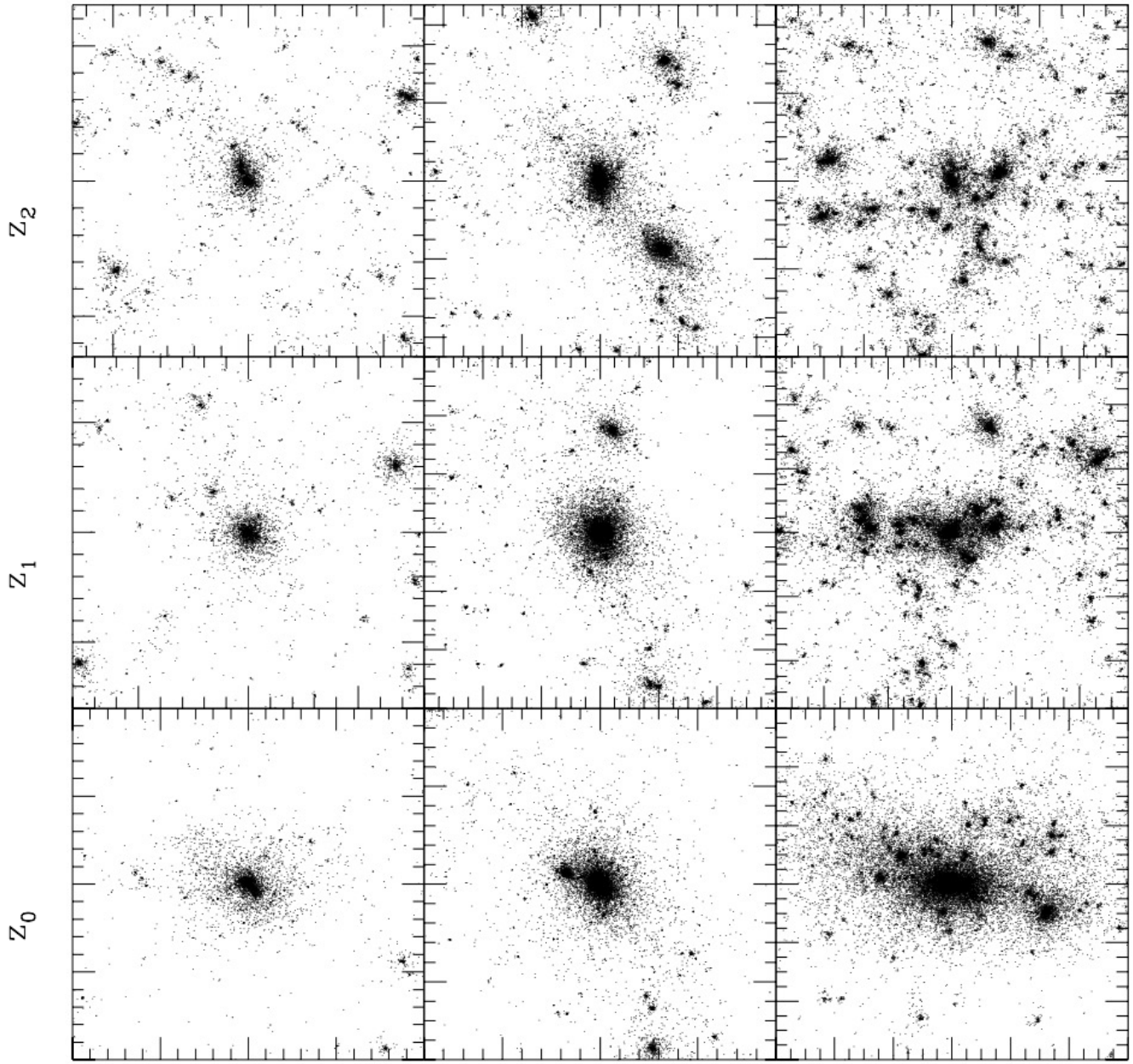

Julio Navarro

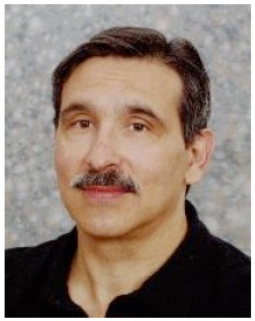

Carlos Frenk

Simon White

- invented the re-simulation technique...
  → about 5000 - 10000 particles per halo in cosmological box!

- ...and the infamous NFW profile:

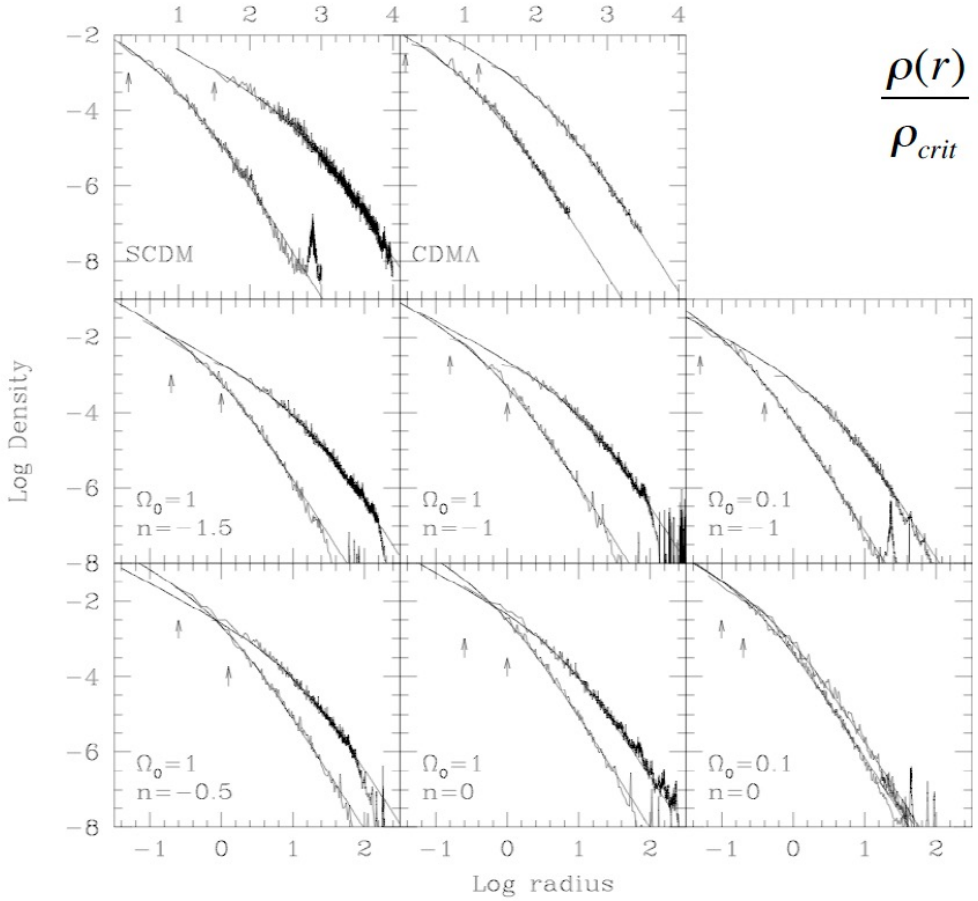

$$\frac{\rho(r)}{\rho_{crit}} = \frac{\delta_c}{\frac{r}{r_s}\left(1+\frac{r}{r_s}\right)^2}$$

Julio Navarro

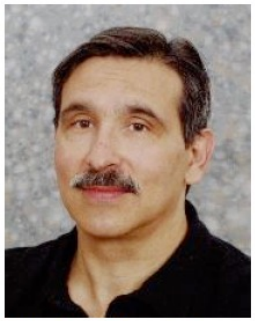

Carlos Frenk

Simon White

$$\frac{\rho(r)}{\rho_{crit}} = \frac{\delta_c}{\frac{r}{r_s}\left(1+\frac{r}{r_s}\right)^2}$$

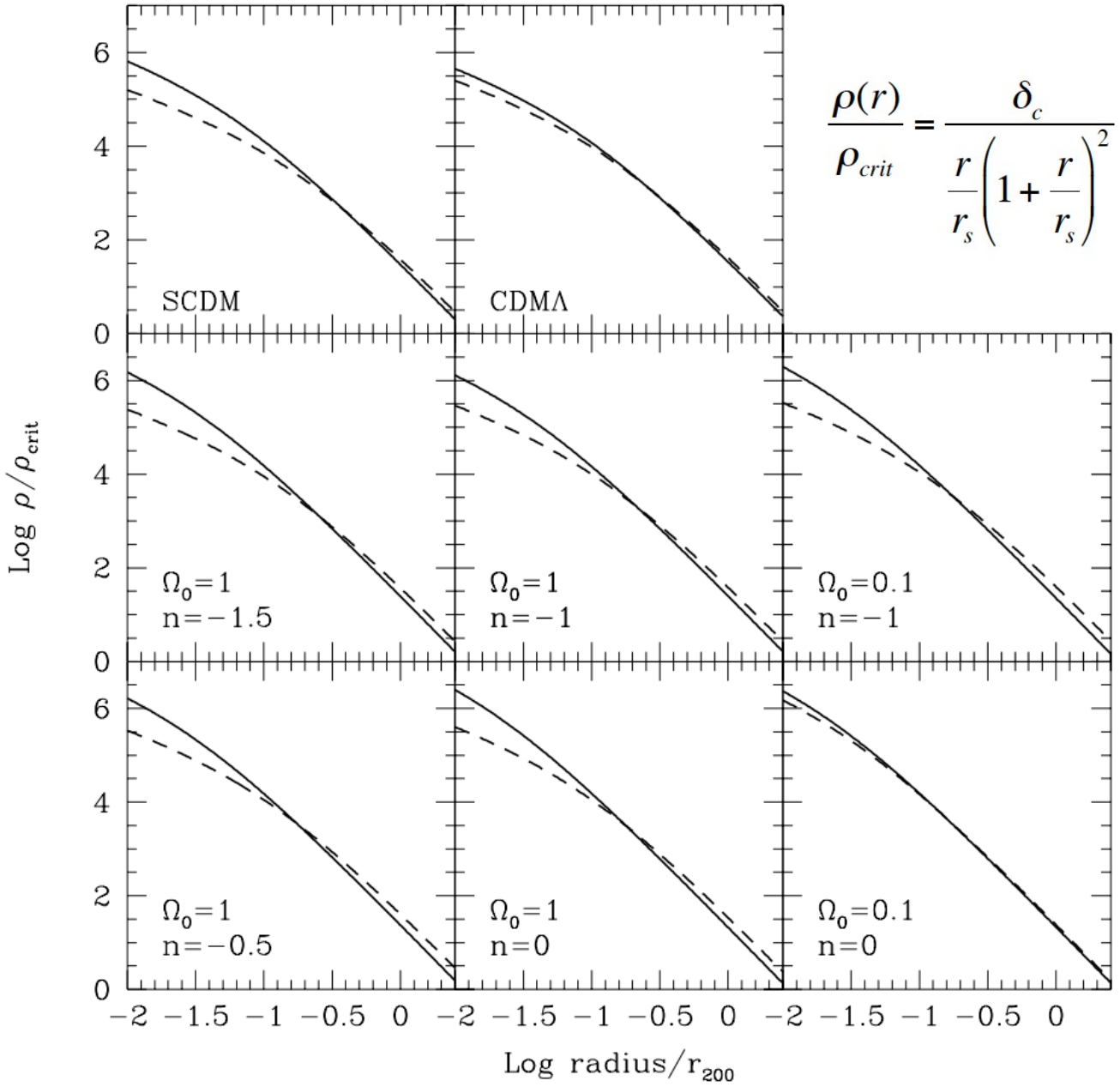

Anatoly Klypin

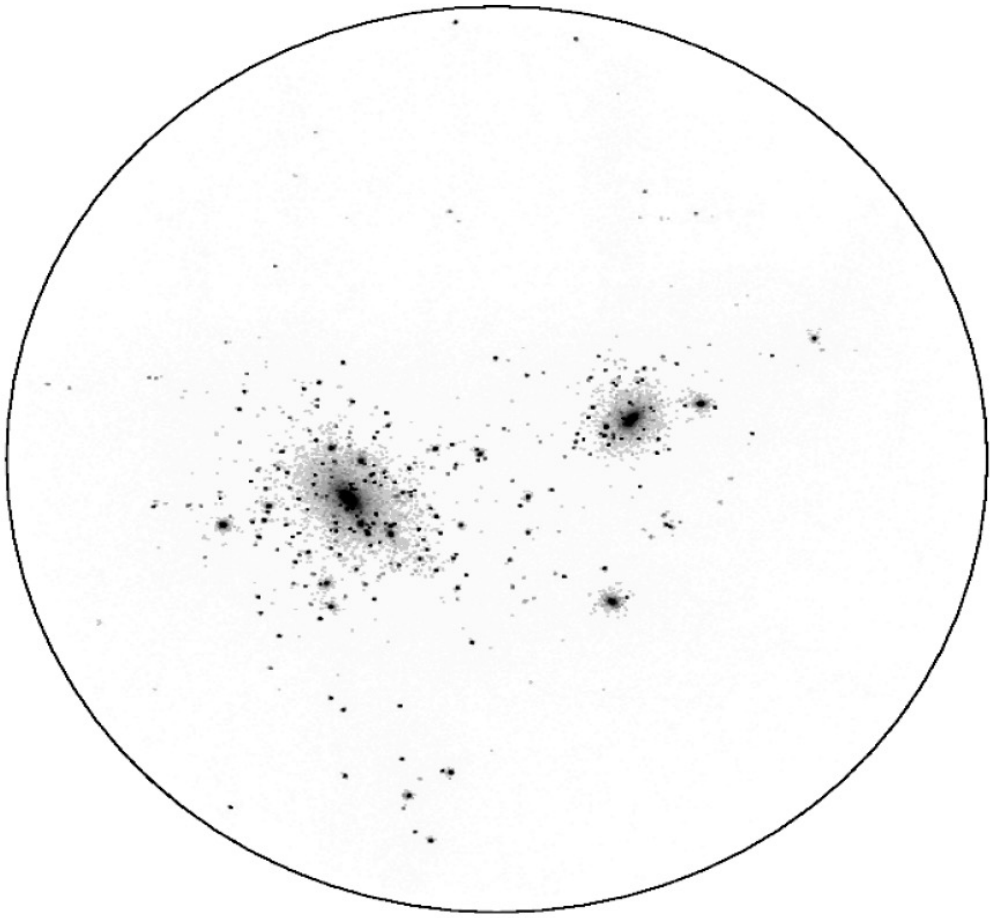

simulation of the Local Group

Anatoly Klypin

THE ASTROPHYSICAL JOURNAL, 522:82–92, 1999 September 1

WHERE ARE THE MISSING GALACTIC SATELLITES?

ANATOLY KLYPIN, ANDREY V. KRAVTSOV, AND OCTAVIO VALENZUELA
Astronomy Department, New Mexico State University, Box 30001, Department 4500, Las Cruces, NM 88003-0001
AND
FRANCISCO PRADA
Instituto de Astronomia, Apartado Postal 877, 22900 Ensenada, Mexico
Received 1999 January 18; accepted 1999 April 15

ABSTRACT

According to the hierarchical clustering scenario, galaxies are assembled by merging and accretion of numerous satellites of different sizes and masses. This ongoing process is not 100% efficient in destroying all of the accreted satellites, as evidenced by the satellites of our Galaxy and of M31. Using published data, we have compiled the circular velocity (V_{circ}) distribution function (VDF) of galaxy satellites in the Local Group. We find that within the volumes of radius of 570 kpc (400 h^{-1} kpc assuming the Hubble constant[1] $h = 0.7$) centered on the Milky Way and Andromeda, the average VDF is roughly approximated as $n(> V_{circ}) \approx 55 \pm 11(V_{circ}/10 \text{ km s}^{-1})^{-1.4\pm0.4}\ h^3\ \text{Mpc}^{-3}$ for V_{circ} in the range $\approx$10–70 km s^{-1}. The observed VDF is compared with results of high-resolution cosmological simulations. We find that the VDF in models is very different from the observed one: $n(> V_{circ}) \approx 1200(V_{circ}/10 \text{ km s}^{-1})^{-2.75}\ h^3$ Mpc^{-3}. Cosmological models thus predict that a halo the size of our Galaxy should have about 50 dark matter satellites with circular velocity greater than 20 km s^{-1} and mass greater than $3 \times 10^8\ M_\odot$ within a 570 kpc radius. This number is significantly higher than the approximately dozen satellites actually observed around our Galaxy. The difference is even larger if we consider the abundance of satellites in simulated galaxy groups similar to the Local Group. The models predict $\sim$300 satellites inside a 1.5 Mpc radius, while only $\sim$40 satellites are observed in the Local Group. The observed and predicted VDFs cross at $\approx$50 km s^{-1}, indicating that the predicted abundance of satellites with $V_{circ} \gtrsim 50$ km s^{-1} is in reasonably good agreement with observations. We conclude, therefore, that unless a large fraction of the Local Group satellites has been missed in observations, there is a dramatic discrepancy between observations and hierarchical models, regardless of the model parameters. We discuss several possible explanations for this discrepancy including identification of some satellites with the high-velocity clouds observed in the Local Group and the existence of dark satellites that failed to accrete gas and form stars either because of the expulsion of gas in the supernovae-driven winds or because of gas heating by the intergalactic ionizing background.

Subject headings: cosmology: theory — galaxies: clusters: general — galaxies: interactions — Galaxy: formation — Local Group — methods: numerical

1. INTRODUCTION

Satellites of galaxies are important probes of the dynamics and masses of galaxies. Currently, analysis of satellite dynamics is one of the best methods of estimating the masses within large radii of our Galaxy and of the Local Group (e.g., Einasto & Lynden-Bell 1982; Lynden-Bell, Cannon, & Godwin 1983; Zaritsky et al. 1989; Fich & Tremaine 1991), as well as the masses of other galaxies (Zaritsky & White 1994; Zaritsky et al. 1997). Although the satellites of the Milky Way and Andromeda galaxy have been studied for a long period of time, their number is still uncertain. More and more satellites are being discovered (Irwin et al. 1990; Whiting, Irwin, & Hau 1997; Armandroff, Davies, & Jacoby 1998; Karachentseva & Karachentsev 1998) with a wide range of properties; some of them are relatively large and luminous and have appreciable star formation rates (e.g., M33 and the Large Magellanic Cloud [LMC]). Exempting the strange case of IC 10, which exhibits a high star formation rate (0.7 $M_\odot$ yr^{-1}; Mateo 1998), most of the satellites are dwarf spheroidals and dwarf ellipticals with signs of only mild star formation of 10^{-3} $M_\odot$ yr^{-1}. The star formation history of the satellites shows remarkable diversity: almost every galaxy is a special case (Grebel 1998; Mateo 1998). This diversity makes it very difficult to come up with a simple general model for formation of satellites in the Local Group. Because of the generally low star formation rates, it is not unexpected that the metallicities of the satellites are low: from $\approx 10^{-2}$ for Draco and And III to $\approx 10^{-1}$ for NGC 205 and Pegasus (Mateo 1998). There are indications that properties of the satellites correlate with their distance to the Milky Way (MW) or Andromeda, with dwarf spheroidals and dwarf ellipticals being closer to the central galaxy (Grebel 1997). Overall, about 40 satellites in the Local Group have been found.

Formation and evolution of galaxy satellites is still an open problem. According to the hierarchical scenario, small dark matter (DM) halos should on average collapse earlier than larger ones. To some degree, this is supported by observations of rotation curves of DM-dominated dwarfs and low surface brightness galaxies. The curves indicate that the smaller the maximum circular velocity, the higher the central density of these galaxies. This is expected from the hierarchical models in which the smaller galaxies collapse earlier when the density of the universe was higher (Kravtsov et al. 1998; Kormendy & Freeman 1998). Thus, it is likely that the satellites of the MW galaxy were formed before the main body of the MW was assembled. Some of

[1] Assuming $H_0 = 100\,h$ km s^{-1} Mpc^{-1}.

Anatoly Klypin

THE ASTROPHYSICAL JOURNAL, 522:82–92, 1999 September 1

WHERE ARE THE MISSING GALACTIC SATELLITES?

— — Astronomy Department, New Mexico State University, Box 30001, Department 4500, Las Cruces, NM 88003-0001 — —

AND

FRANCISCO PRADA
Instituto de Astronomia, Apartado Postal 877, 22900 Ensenada, Mexico
Received 1999 January 18; accepted 1999 April 15

ABSTRACT

According to the hierarchical clustering scenario, galaxies are assembled by merging and accretion of numerous satellites of different sizes and masses. This ongoing process is not 100% efficient in destroying all of the accreted satellites, as evidenced by the satellites of our Galaxy and of M31. Using published data, we have compiled the circular velocity (V_{circ}) distribution function (VDF) of galaxy satellites in the Local Group. We find that within the volumes of radius of 570 kpc (400 h^{-1} kpc assuming the Hubble constant[1] $h = 0.7$) centered on the Milky Way and Andromeda, the average VDF is roughly approximated as $n(> V_{circ}) \approx 55 \pm 11(V_{circ}/10 \text{ km s}^{-1})^{-1.4\pm0.4}\ h^3 \text{ Mpc}^{-3}$ for V_{circ} in the range $\approx$10–70 km s^{-1}. The observed VDF is compared with results of high-resolution cosmological simulations. We find that the VDF in models is very different from the observed one: $n(> V_{circ}) \approx 1200(V_{circ}/10 \text{ km s}^{-1})^{-2.75}\ h^3$ Mpc^{-3}. Cosmological models thus predict that a halo the size of our Galaxy should have about 50 dark matter satellites with circular velocity greater than 20 km s^{-1} and mass greater than $3 \times 10^8\ M_\odot$ within a 570 kpc radius. This number is significantly higher than the approximately dozen satellites actually observed around our Galaxy. The difference is even larger if we consider the abundance of satellites in simulated galaxy groups similar to the Local Group. The models predict $\sim$300 satellites inside a 1.5 Mpc radius, while only $\sim$40 satellites are observed in the Local Group. The observed and predicted VDFs cross at $\approx$50 km s^{-1}, indicating that the predicted abundance of satellites with $V_{circ} \gtrsim 50$ km s^{-1} is in reasonably good agreement with observations. We conclude, therefore, that unless a large fraction of the Local Group satellites has been missed in observations, there is a dramatic discrepancy between observations and hierarchical models, regardless of the model parameters. We discuss several possible explanations for this discrepancy including identification of some satellites with the high-velocity clouds observed in the Local Group and the existence of dark satellites that failed to accrete gas and form stars either because of the expulsion of gas in the supernovae-driven winds or because of gas heating by the intergalactic ionizing background.

Subject headings: cosmology: theory — galaxies: clusters: general — galaxies: interactions — Galaxy: formation — Local Group — methods: numerical

1. INTRODUCTION

Satellites of galaxies are important probes of the dynamics and masses of galaxies. Currently, analysis of satellite dynamics is one of the best methods of estimating the masses within large radii of our Galaxy and of the Local Group (e.g., Einasto & Lynden-Bell 1982; Lynden-Bell, Cannon, & Godwin 1983; Zaritsky et al. 1989; Fich & Tremaine 1991), as well as the masses of other galaxies (Zaritsky & White 1994; Zaritsky et al. 1997). Although the satellites of the Milky Way and Andromeda galaxy have been studied for a long period of time, their number is still uncertain. More and more satellites are being discovered (Irwin et al. 1990; Whiting, Irwin, & Hau 1997; Armandroff, Davies, & Jacoby 1998; Karachentseva & Karachentsev 1998) with a wide range of properties; some of them are relatively large and luminous and have appreciable star formation rates (e.g., M33 and the Large Magellanic Cloud [LMC]). Exempting the strange case of IC 10, which exhibits a high star formation rate (0.7 $M_\odot$ yr^{-1}; Mateo 1998), most of the satellites are dwarf spheroidals and dwarf ellipticals with signs of only mild star formation of 10^{-3} $M_\odot$ yr^{-1}. The star formation history of the satellites shows remarkable diversity: almost every galaxy is a special case (Grebel 1998; Mateo 1998). This diversity makes it very difficult to come up with a simple general model for formation of satellites in the Local Group. Because of the generally low star formation rates, it is not unexpected that the metallicities of the satellites are low: from $\approx 10^{-2}$ for Draco and And III to $\approx 10^{-1}$ for NGC 205 and Pegasus (Mateo 1998). There are indications that properties of the satellites correlate with their distance to the Milky Way (MW) or Andromeda, with dwarf spheroidals and dwarf ellipticals being closer to the central galaxy (Grebel 1997). Overall, about 40 satellites in the Local Group have been found.

Formation and evolution of galaxy satellites is still an open problem. According to the hierarchical scenario, small dark matter (DM) halos should on average collapse earlier than larger ones. To some degree, this is supported by observations of rotation curves of DM-dominated dwarfs and low surface brightness galaxies. The curves indicate that the smaller the maximum circular velocity, the higher the central density of these galaxies. This is expected from the hierarchical models in which the smaller galaxies collapse earlier when the density of the universe was higher (Kravtsov et al. 1998; Kormendy & Freeman 1998). Thus, it is likely that the satellites of the MW galaxy were formed before the main body of the MW was assembled. Some of

[1] Assuming $H_0 = 100\ h$ km s^{-1} Mpc^{-1}.

Ben Moore

THE ASTROPHYSICAL JOURNAL, 524:L19–L22, 1999 October 10

DARK MATTER SUBSTRUCTURE WITHIN GALACTIC HALOS

BEN MOORE, SEBASTIANO GHIGNA, AND FABIO GOVERNATO
Department of Physics, Science Laboratories, South Road, University of Durham, Durham, England, DH1 3LE, UK;
ben.moore@durham.ac.uk, ssg@durham.ac.uk, fabio@antares.merate.mi.astro.it
GEORGE LAKE, THOMAS QUINN, AND JOACHIM STADEL
Department of Astronomy, Box 351580, University of Washington, Seattle, WA 98195-1580;
lake@hermes.astro.washington.edu, trq@hermes.astro.washington.edu, stadel@hermes.astro.washington.edu
AND
PAOLO TOZZI
Osservatorio Astronomico di Roma, Via Frascati, 33, Monteporzio Catone, Rome, I-00040, Italy; paolo@pha.jhu.edu
Received 1999 April 16; accepted 1999 August 2; published 1999 September 13

ABSTRACT

We use numerical simulations to examine the substructure within galactic and cluster mass halos that form within a hierarchical universe. Clusters are easily reproduced with a steep mass spectrum of thousands of substructure clumps that closely matches the observations. However, the survival of dark matter substructure also occurs on galactic scales, leading to the remarkable result that galaxy halos appear as scaled versions of galaxy clusters. The model predicts that the virialized extent of the Milky Way's halo should contain about 500 satellites with circular velocities larger than the Draco and Ursa Minor systems, i.e., bound masses $\gtrsim 10^8\ M_\odot$ and tidally limited sizes $\gtrsim 1$ kpc. The substructure clumps are on orbits that take a large fraction of them through the stellar disk, leading to significant resonant and impulsive heating. Their abundance and singular density profiles have important implications for the existence of old thin disks, cold stellar streams, gravitational lensing, and indirect/direct detection experiments.

Subject headings: cosmology: observations — cosmology: theory — dark matter — galaxies: clusters: general — galaxies: formation

1. INTRODUCTION

The growth of structure in the universe by the hierarchical accretion and merging of dark matter halos is an attractive and well-motivated cosmological model (White & Rees 1978; Davis et al. 1985). The gravitational clustering process is governed by the dark matter component, and the baryons play only a minor role. The idea that galaxies are defined as those objects where gas can quickly cool predates the current hierarchical model (Hoyle 1953), and it has been invoked to set the scale for survival versus disruption (Rees & Ostriker 1977; White & Rees 1978).

Comparing the predictions of this model with nonlinear structures, such as the internal properties of galaxy clusters, has proved to be difficult. Numerical simulations had ubiquitously failed to find surviving substructure or "halos orbiting within halos" (e.g., Katz & White 1993; Summers, Davis, & Evrard 1995). It was generally thought that the so-called "overmerging" problem could be overcome by the inclusion of a baryonic component to increase the potential depth of galactic halos.

Analytic work suggested that overmerging was due entirely to poor spatial and mass resolution (Moore, Katz, & Lake 1996a). This has been verified by higher resolution simulations of clusters in which galactic halos survive without any inclusion of gasdynamics (Moore et al. 1998; Ghigna et al. 1998; Klypin et al. 1998). When a galaxy and its dark matter halo enter a larger structure, the outer regions are stripped away by the global tides and mutual interactions. The central region survives intact so that a galaxy may continue to be observed as a distinct structure within a cluster, with its own truncated dark matter halo (Natarajan et al. 1998).

In a hierarchical universe, galaxies form by a similar merging and accretion process as clusters (Klypin et al. 1999). Overmerging on galactic scales is a necessary requirement, otherwise previous generations of the hierarchy would preclude the formation of disks. Observations suggest that overmerging has been nearly complete on galactic scales. The Milky Way contains just 11 satellites within its virial radius with $\sigma_{\rm satellite}/\sigma_{\rm halo} \gtrsim 0.07$, which is equivalent to $\sigma_{\rm satellite} = 10$ km s^{-1} (cf. Mateo 1998 and references within). The same velocity-dispersion ratio in a cluster corresponds to counting galaxies more massive than the Large Magellanic Clouds ($\sigma_{\rm LMC} \sim 50$ km s^{-1}); there are 500–1000 such systems in a rich cluster (Binggeli, Sandage, & Tammann 1985; Driver, Couch, & Phillipps 1999). The same discrepancy exists at higher masses. The Coma Cluster contains $\gtrsim 30$ galaxies brighter than the characteristic break in the luminosity function, L_* ($\equiv \sigma > 200$ km s^{-1} (Lucey et al. 1991). By scaling this limit to a galaxy halo, we find just two satellites in the Milky Way or three near Andromeda.

Why should substructure be destroyed in galactic halos but not in clusters? Analytic calculations suggested that galaxies should contain more satellites than are observed (Kauffmann, White, & Guilderdoni 1993). The shape of the power spectrum varies over these scales in a way such that galaxies form several billions of years before the clusters, and as a result, the mass function of their progenitor clumps may differ. Furthermore, as the power spectrum asymptotically approaches a slope of -3, clumps of all masses will be collapsing simultaneously, and the timescale between collapse and subsequent merging becomes shorter. These effects may conspire to preferentially smooth out the mass distribution within galactic halos. In this Letter, we use numerical simulations to study the formation of galactic halos that have sufficient force and mass resolution to resolve satellite galaxies as small as Draco. This allows us to

Ben Moore

THE ASTROPHYSICAL JOURNAL, 524:L19–L22, 1999 October 10

DARK MATTER SUBSTRUCTURE WITHIN GALACTIC HALOS

BEN MOORE, SEBASTIANO GHIGNA, AND FABIO GOVERNATO
Department of Physics, Science Laboratories, South Road, University of Durham, Durham, England, DH1 3LE, UK;
ben.moore@durham.ac.uk, ssg@durham.ac.uk, fabio@antares.merate.mi.astro.it
GEORGE LAKE, THOMAS QUINN, AND JOACHIM STADEL
Department of Astronomy, Box 351580, University of Washington, Seattle, WA 98195-1580;
lake@hermes.astro.washington.edu, trq@hermes.astro.washington.edu, stadel@hermes.astro.washington.edu
AND
PAOLO TOZZI
Osservatorio Astronomico di Roma, Via Frascati, 33, Monteporzio Catone, Rome, I-00040, Italy; paolo@pha.jhu.edu
Received 1999 April 16; accepted 1999 August 2; published 1999 September 13

ABSTRACT

We use numerical simulations to examine the substructure within galactic and cluster mass halos that form within a hierarchical universe. Clusters are easily reproduced with a steep mass spectrum of thousands of substructure clumps that closely matches the observations. However, the survival of dark matter substructure also occurs on galactic scales, leading to the remarkable result that galaxy halos appear as scaled versions of galaxy clusters. The model predicts that the virialized extent of the Milky Way's halo should contain about 500 satellites with circular velocities larger than the Draco and Ursa Minor systems, i.e., bound masses $\gtrsim 10^8\ M_\odot$ and tidally limited sizes $\gtrsim 1$ kpc. The substructure clumps are on orbits that take a large fraction of them through the stellar disk, leading to significant resonant and impulsive heating. Their abundance and singular density profiles have important implications for the existence of old thin disks, cold stellar streams, gravitational lensing, and indirect/direct detection experiments.

The model predicts that the virialized extent of the Milky Way's halo should contain about 500 satellites with circular velocities larger than the Draco and Ursa Minor systems, i.e., bound masses $\gtrsim 10^8\ M_\odot$ and tidally limited sizes $\gtrsim 1$ kpc.

erned by the dark matter component, and the baryons play only a minor role. The idea that galaxies are defined as those objects where gas can quickly cool predates the current hierarchical model (Hoyle 1953), and it has been invoked to set the scale for survival versus disruption (Rees & Ostriker 1977; White & Rees 1978).

Comparing the predictions of this model with nonlinear structures, such as the internal properties of galaxy clusters, has proved to be difficult. Numerical simulations had ubiquitously failed to find surviving substructure or "halos orbiting within halos" (e.g., Katz & White 1993; Summers, Davis, & Evrard 1995). It was generally thought that the so-called "overmerging" problem could be overcome by the inclusion of a baryonic component to increase the potential depth of galactic halos.

Analytic work suggested that overmerging was due entirely to poor spatial and mass resolution (Moore, Katz, & Lake 1996a). This has been verified by higher resolution simulations of clusters in which galactic halos survive without any inclusion of gasdynamics (Moore et al. 1998; Ghigna et al. 1998; Klypin et al. 1998). When a galaxy and its dark matter halo enter a larger structure, the outer regions are stripped away by the global tides and mutual interactions. The central region survives intact so that a galaxy may continue to be observed as a distinct structure within a cluster, with its own truncated dark matter halo (Natarajan et al. 1998).

In a hierarchical universe, galaxies form by a similar merging and accretion process as clusters (Klypin et al. 1999). Over-

$\sigma_{\rm satellite}/\sigma_{\rm halo} \gtrsim 0.07$, which is equivalent to $\sigma_{\rm satellite} = 10$ km s^{-1} (cf. Mateo 1998 and references within). The same velocity-dispersion ratio in a cluster corresponds to counting galaxies more massive than the Large Magellanic Clouds ($\sigma_{\rm LMC} \sim 50$ km s^{-1}); there are 500–1000 such systems in a rich cluster (Binggeli, Sandage, & Tammann 1985; Driver, Couch, & Phillipps 1999). The same discrepancy exists at higher masses. The Coma Cluster contains $\gtrsim 30$ galaxies brighter than the characteristic break in the luminosity function, $L_* \equiv \sigma > 200$ km s^{-1} (Lucey et al. 1991). By scaling this limit to a galaxy halo, we find just two satellites in the Milky Way or three near Andromeda.

Why should substructure be destroyed in galactic halos but not in clusters? Analytic calculations suggested that galaxies should contain more satellites than are observed (Kauffmann, White, & Guilderdoni 1993). The shape of the power spectrum varies over these scales in a way such that galaxies form several billions of years before the clusters, and as a result, the mass function of their progenitor clumps may differ. Furthermore, as the power spectrum asymptotically approaches a slope of -3, clumps of all masses will be collapsing simultaneously, and the timescale between collapse and subsequent merging becomes shorter. These effects may conspire to preferentially smooth out the mass distribution within galactic halos. In this Letter, we use numerical simulations to study the formation of galactic halos that have sufficient force and mass resolution to resolve satellite galaxies as small as Draco. This allows us to

Ben Moore

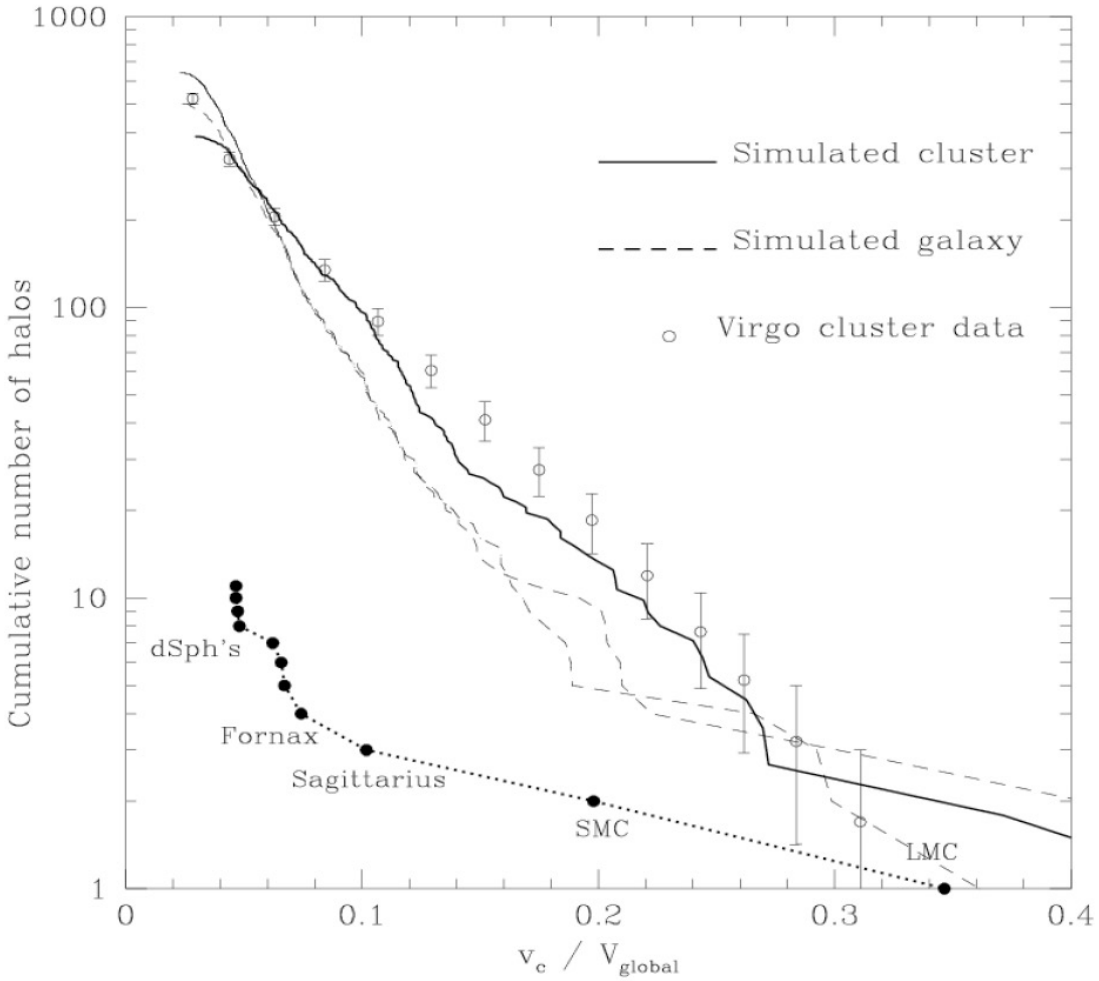
1000
100
10
1
0
0.1
0.2
0.3
0.4
Cumulative number of halos
v_c / V_{global}
Simulated cluster
Simulated galaxy
Virgo cluster data
dSph's
Fornax
Sagittarius
SMC
LMC

The “missing satellite problem”

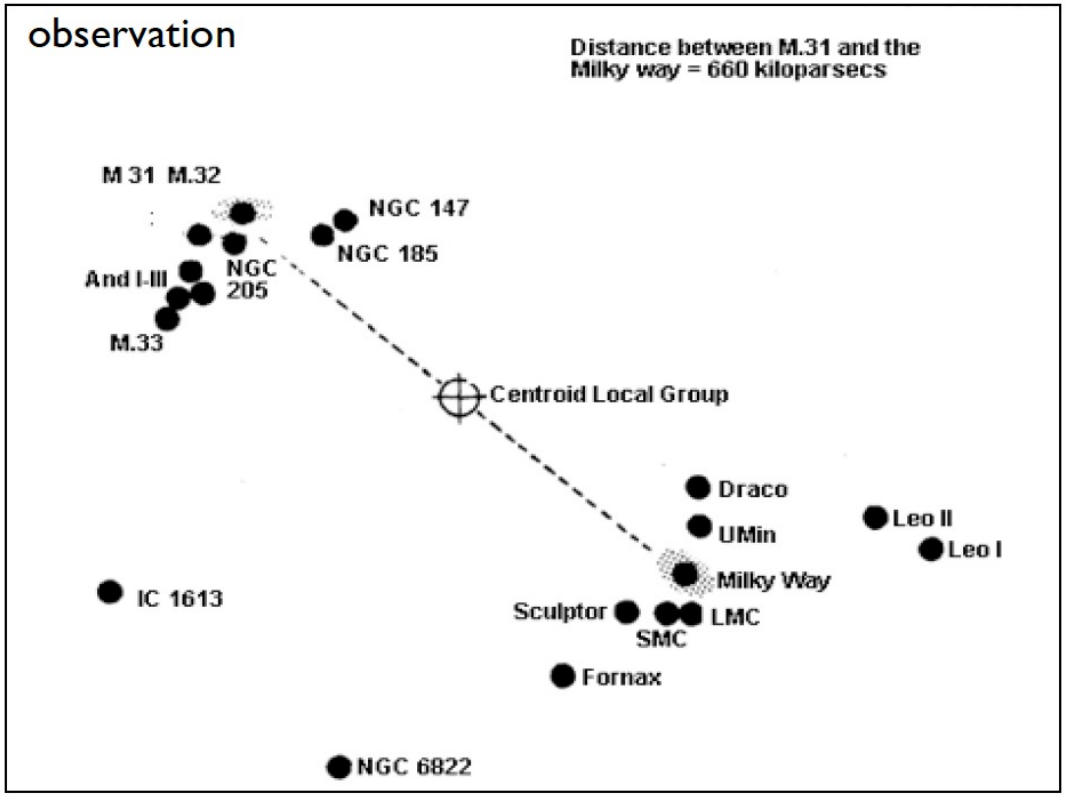

➢ super-galactic scales:

✓ perfect match

➢ sub-galactic scales:

observations		**simulations**
• shallow density cores	<–>	• steep density profiles
• only a few satellite galaxies	<–>	• hundreds of satellite galaxies

- <u>possible solutions:</u>
  - the simulations are wrong
  - the observations are wrong
  - the cosmological model is wrong
  - the law of gravity is wrong
  - who knows what else can be wrong...

➢ possible solutions:

- the simulations are wrong: a lot of physics is still missing
- the observations are wrong: better telescopes, please
- the cosmological model is wrong: maybe, but just a little bit...
- the law of gravity is wrong: unlikely!?
- who knows what else can be wrong...

Numerical (Astro-)Physics:

solving differential equations
of the physics under investigation
using computers

- **N-body**

  - plasma physics
  - molecular dynamics
  - stellar systems, e.g. globular clusters
  - individual galaxies
  - the whole Universe

- **Fluid Dynamics**

  - solar and stellar physics
  - magneto-hydrodynamics
  - aero-plane design
  - meteorology
  - oceanography

- **N-body**

  - plasma physics
  - molecular dynamics
  - stellar systems, e.g. globular clusters
  - individual galaxies
  - the whole Universe

- **Fluid Dynamics**

  - solar and stellar physics
  - magneto-hydrodynamics
  - aero-plane design
  - meteorology
  - oceanography

How do we set up the initial conditions?

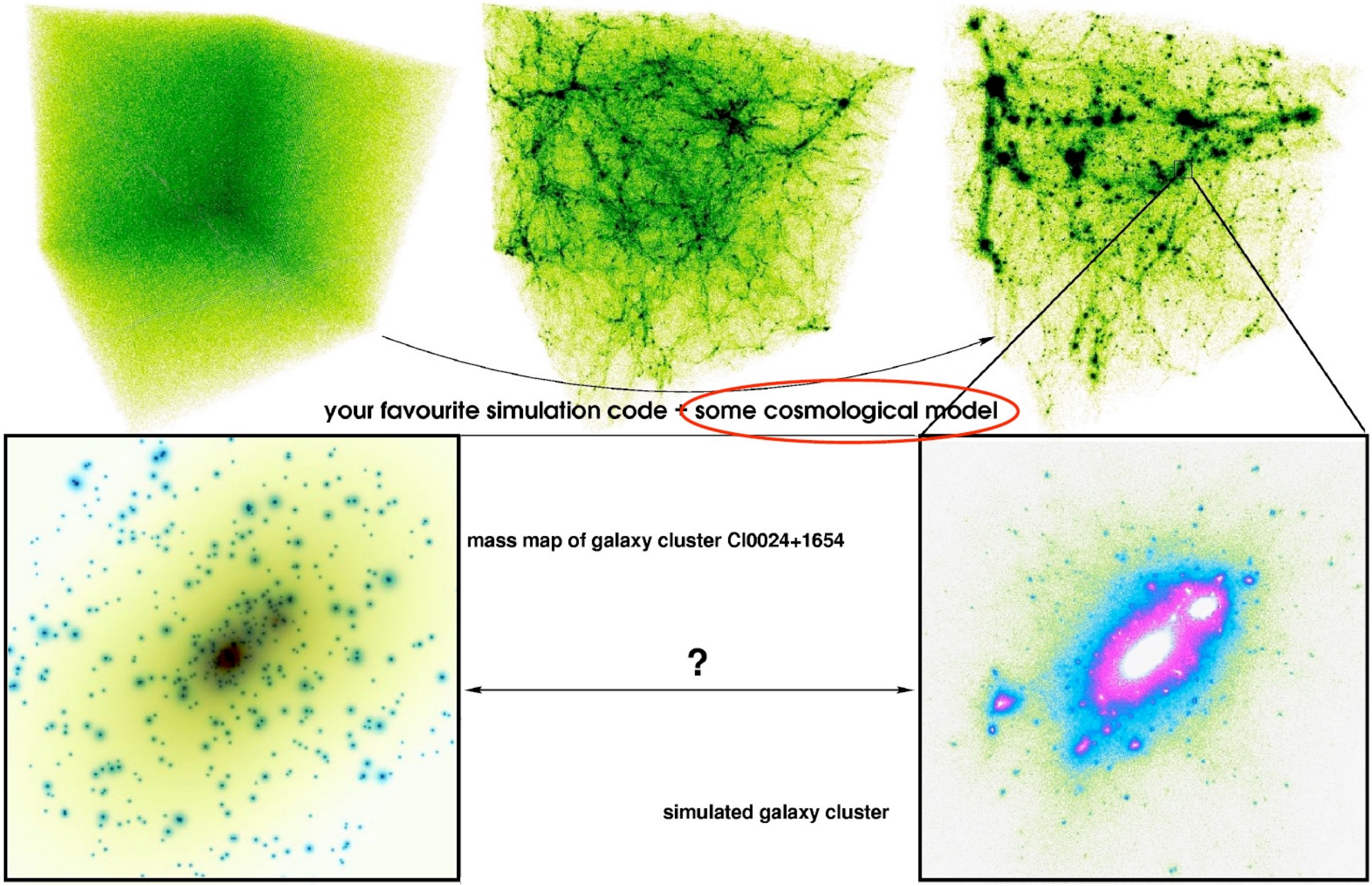
your favourite simulation code + some cosmological model
mass map of galaxy cluster Cl0024+1654
?
simulated galaxy cluster

- evolution of the Universe:

  - Friedmann equations

$$H^2(t) = H_0^2 \left(\Omega_{m,0}\, a^{-3}(t) + \Omega_{\Lambda,0}\right)$$

$$q(t) = \frac{1}{2}\Omega_m(t) - \Omega_\Lambda(t)$$

  - comoving coordinates

$$\vec{r} = a(t)\vec{x}$$

$$\dot{\vec{r}} = a\dot{\vec{x}} + H\vec{r}$$

$$H = \frac{\dot{a}}{a}, \quad q = \frac{\ddot{a}a}{\dot{a}^2}$$

- <u>ΛCDM model:</u>

  - matter content of Universe: $\Omega_{m,0} \sim 0.3 = 0.26_{DM} + 0.04_{stars+gas}$
  - cosmological constant: $\Omega_{\Lambda,0} \sim 0.7$
  - expansion rate of the Universe: $H_0 \sim 70$ km/s/Mpc
  - nature of matter: cold !?
  - amplitude of initial density perturbations: $\sigma_8 \sim 0.92$

determining the overall expansion of the Universe and

influencing initial density perturbations (i.e. initial conditions)...

why N-bodies?

dark matter particles are collisionless!

or in other words...

the evolution of the Universe is driven by the mean potential
rather than two-body interactions of dark matter particles

- mean free path of dark matter particles

$$\sigma \approx 10^{-42} cm^2$$
$$m_{DM} \approx 10^2 GeV \approx 10^{-22} g$$
$$\rho_{crit} \approx 10^{-30} \frac{g}{cm^3}$$

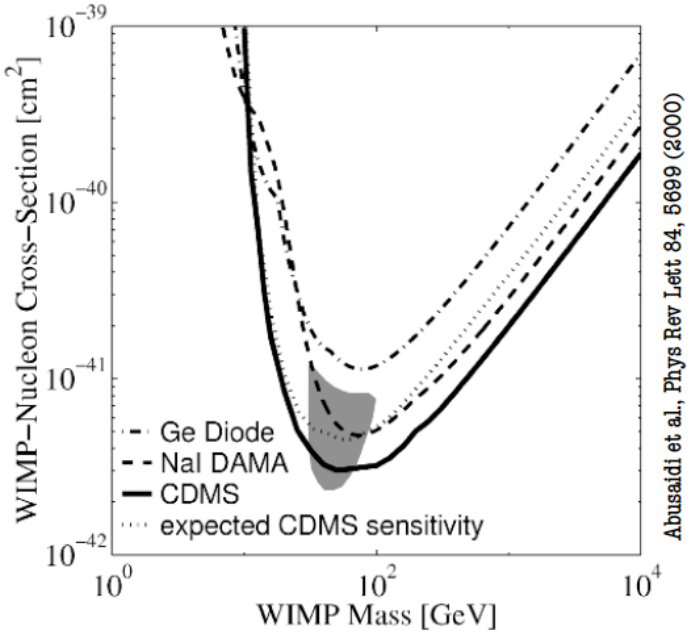

$$\rho_{crit} = \frac{N m_{DM}}{V} = n\, m_{DM}$$
$$n \approx 10^{-8} \frac{1}{cm^3}$$

$$\lambda = \frac{1}{n\sigma} \approx \frac{1}{10^{-8} 10^{-42}} cm = 10^{50} cm \approx 10^{30} Mpc$$

how to describe a collisionless system?

- phase-space distribution function

$$f(\vec{r},\vec{v},t)\ d^3r\ d^3v$$

probability* of finding a dark matter particle in the interval:

$$[\vec{r}-\frac{d\vec{r}}{2},\ \vec{r}+\frac{\vec{d}r}{2}]$$
$$[\vec{v}-\frac{d\vec{v}}{2},\ \vec{v}+\frac{d\vec{v}}{2}]$$

e.g., particle with velocity v_1 and coordinate r_1: $f(\vec{r},\vec{v}) = \delta(\vec{r}-\vec{r}_1)\delta(\vec{v}-\vec{v}_1)$

* $\int f(\vec{r},\vec{v},t)\ d^3r\ d^3v = 1$

continuity, self-gravity and no collisions =>

- collisionless Boltzmann equation (CBE)

$$\frac{\partial f}{\partial t} + \sum_{i=1}^{3} \left(v_i \frac{\partial f}{\partial r_i} - \frac{\partial \Phi}{\partial r_i} \frac{\partial f}{\partial v_i} \right) = 0$$ ⇒ **impossible to solve numerically!**

- coupled with Poisson's equation

$$\Delta \Phi(\vec{r}) = 4\pi G \rho(\vec{r})$$ ⇒ **we'll deal with it later...**

- initial value problem

the initial values

$$f(\vec{r}(t_0),\vec{v}(t_0))$$

Hamiltonian of the system

$$H = \frac{1}{2}v^2 + \Phi(\vec{r})$$

the equations of motion

$$\{\vec{r},H\} = \frac{\partial H}{\partial \vec{v}}$$

$$\{\vec{v},H\} = -\frac{\partial H}{\partial \vec{r}}$$

- initial value problem

the initial values

$$f(\vec{r}(t_0),\vec{v}(t_0))$$

Hamiltonian of the system

$$H = \frac{1}{2}v^2 + \Phi(\vec{r})$$

the equations of motion

$$\{\vec{r},H\} = \frac{\partial H}{\partial \vec{v}}$$

$$\{\vec{v},H\} = -\frac{\partial H}{\partial \vec{r}}$$

- N-body approach

1. sample $f(r_i(t_0),v_i(t_0))$ with $i=1, \ldots, N$ points $[r_i(t_0),v_i(t_0)]$

2. those $[r_i(t),v_i(t)]$ obeying the equations-of-motion sample $f(r_i(t),v_i(t))$

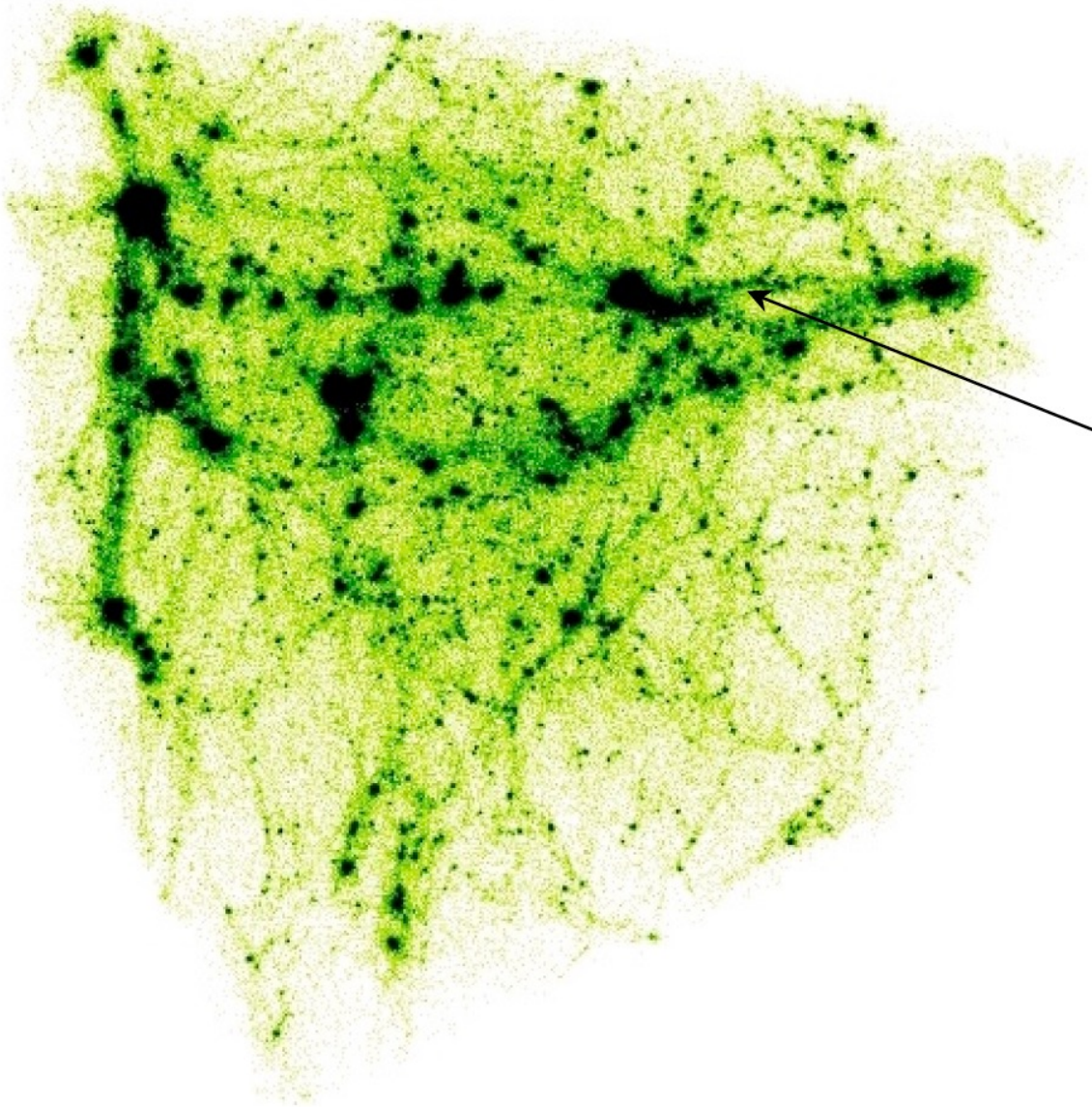

N bodies are used to sample the evolution of the Universe

one "simulation particle" represents *billions* of dark matter particles:

$m_{\mathrm{simu}} \sim 10^{7} M_{\odot}$ vs $m_{\mathrm{DM}} << 10^{-27} M_{\odot}$

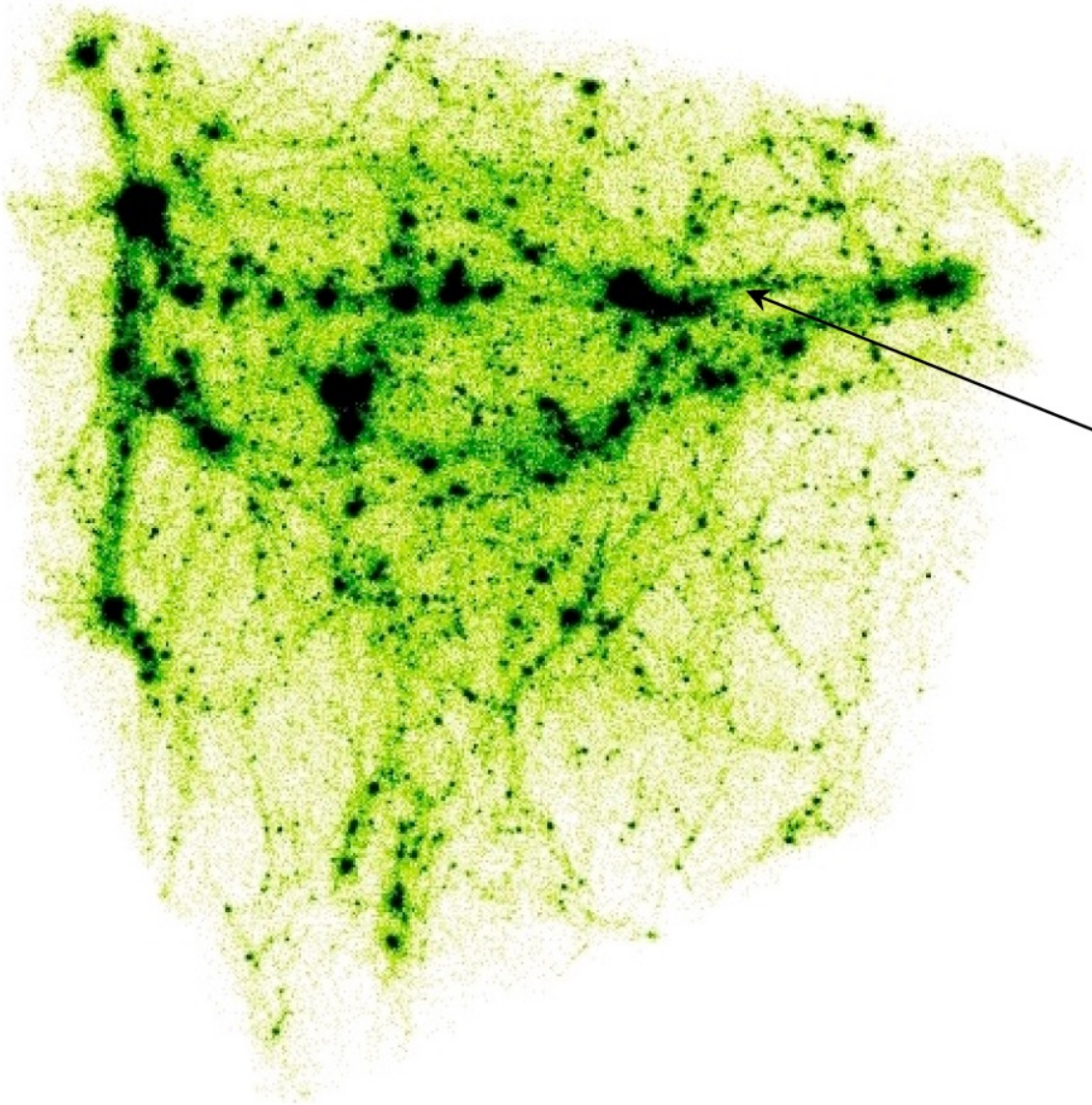

N bodies are used to sample the evolution of the Universe

one "simulation particle" represents *billions* of dark matter particles:

$m_{\text{simu}} \sim 10^{7} M_{\odot}$ vs $m_{\text{DM}} << 10^{-27} M_{\odot}$

(non-baryonic) dark matter candidates

axion:	10^{-5} eV	
neutrino:	10eV	
WIMP:	1-10^{3} GeV	
monopoles:	10^{16} GeV	
Planck relics:	10^{19} GeV	<< 1g

???

$0.5 MeV \approx 9 \cdot 10^{-28} g$

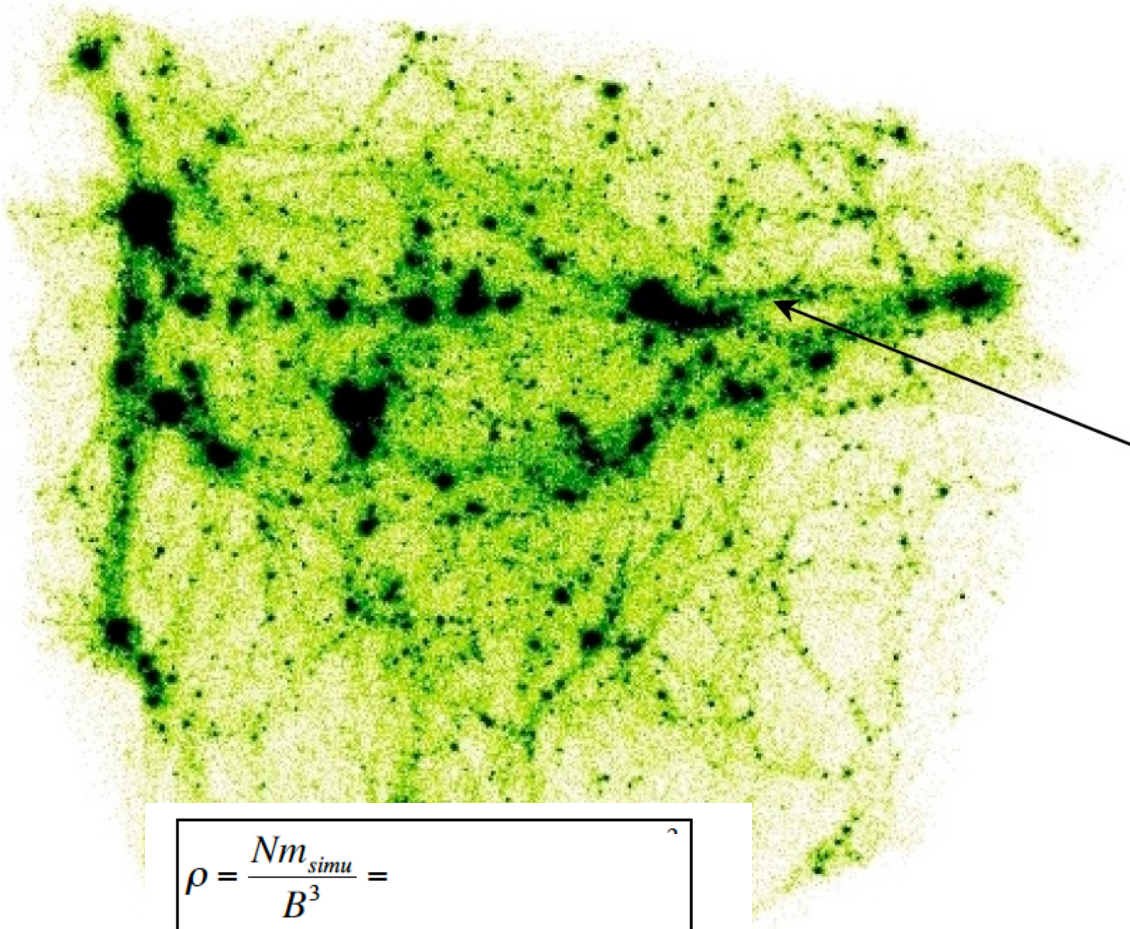

N bodies are used to sample the evolution of the Universe

one "simulation particle" represents *billions* of dark matter particles:

$m_{\text{simu}} \sim 10^{7} M_{\odot}$ vs $m_{\text{DM}} << 10^{-27} M_{\odot}$

$$\rho = \frac{N m_{simu}}{B^3} =$$

(non-baryonic) dark matter candidates

axion:	10^{-5} eV	
neutrino:	10eV	
WIMP:	1-10^{3} GeV	
monopoles:	10^{16} GeV	
Planck relics:	10^{19} GeV	<< 1g

???

$0.5 MeV \approx 9 \cdot 10^{-28} g$

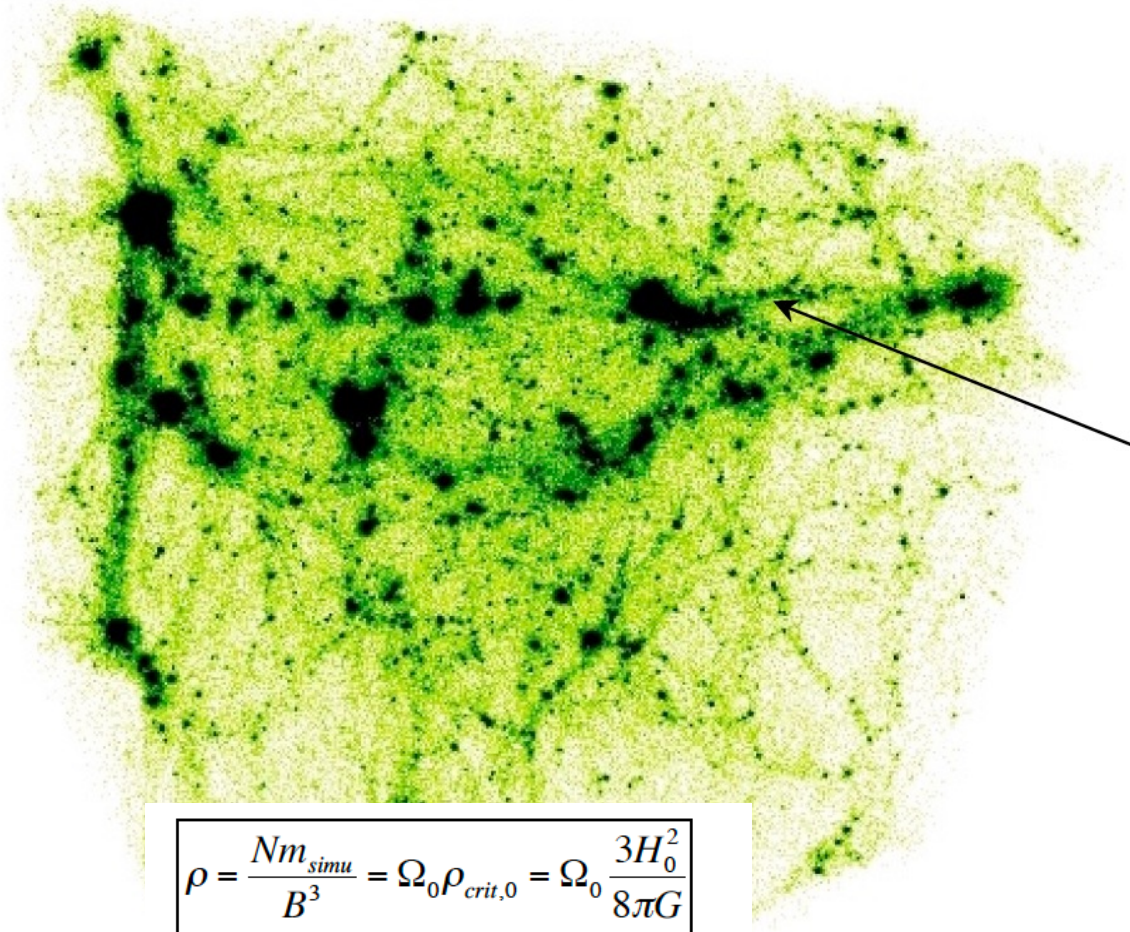

N bodies are used to sample the evolution of the Universe

one "simulation particle" represents *billions* of dark matter particles:

$m_{\mathrm{simu}} \sim 10^{7} M_{\odot}$ vs $m_{\mathrm{DM}} << 10^{-27} M_{\odot}$

$$\rho = \frac{N m_{simu}}{B^3} = \Omega_0 \rho_{crit,0} = \Omega_0 \frac{3H_0^2}{8\pi G}$$

(non-baryonic) dark matter candidates

axion:	10^{-5} eV	
neutrino:	10eV	
WIMP:	1-10^{3} GeV	
monopoles:	10^{16} GeV	
Planck relics:	10^{19} GeV	<< 1g

???

$0.5 MeV \approx 9 \cdot 10^{-28} g$

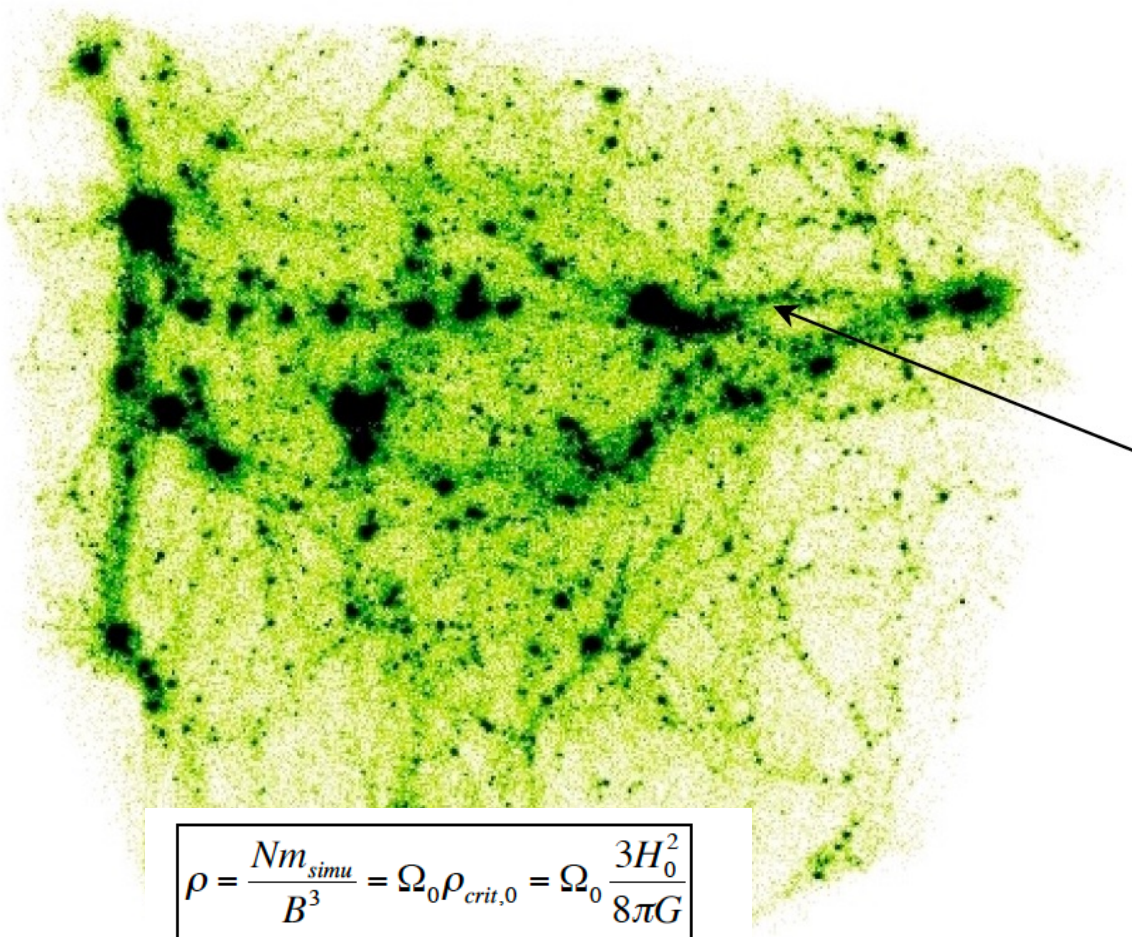

N bodies are used to sample the evolution of the Universe

one "simulation particle" represents *billions* of dark matter particles:

$m_{\mathrm{simu}} \sim 10^{7} M_{\odot}$ vs $m_{\mathrm{DM}} << 10^{-27} M_{\odot}$

$$\rho = \frac{N m_{simu}}{B^3} = \Omega_0 \rho_{crit,0} = \Omega_0 \frac{3H_0^2}{8\pi G}$$

$$\Rightarrow \quad m_{simu} = \Omega_0 \frac{3H_0^2}{8\pi G} \frac{B^3}{N}$$

(non-baryonic) dark matter candidates

axion:	10^{-5} eV	
neutrino:	10eV	
WIMP:	1-10^{3} GeV	
monopoles:	10^{16} GeV	
Planck relics:	10^{19} GeV	<< 1g

???

$0.5 MeV \approx 9 \cdot 10^{-28} g$

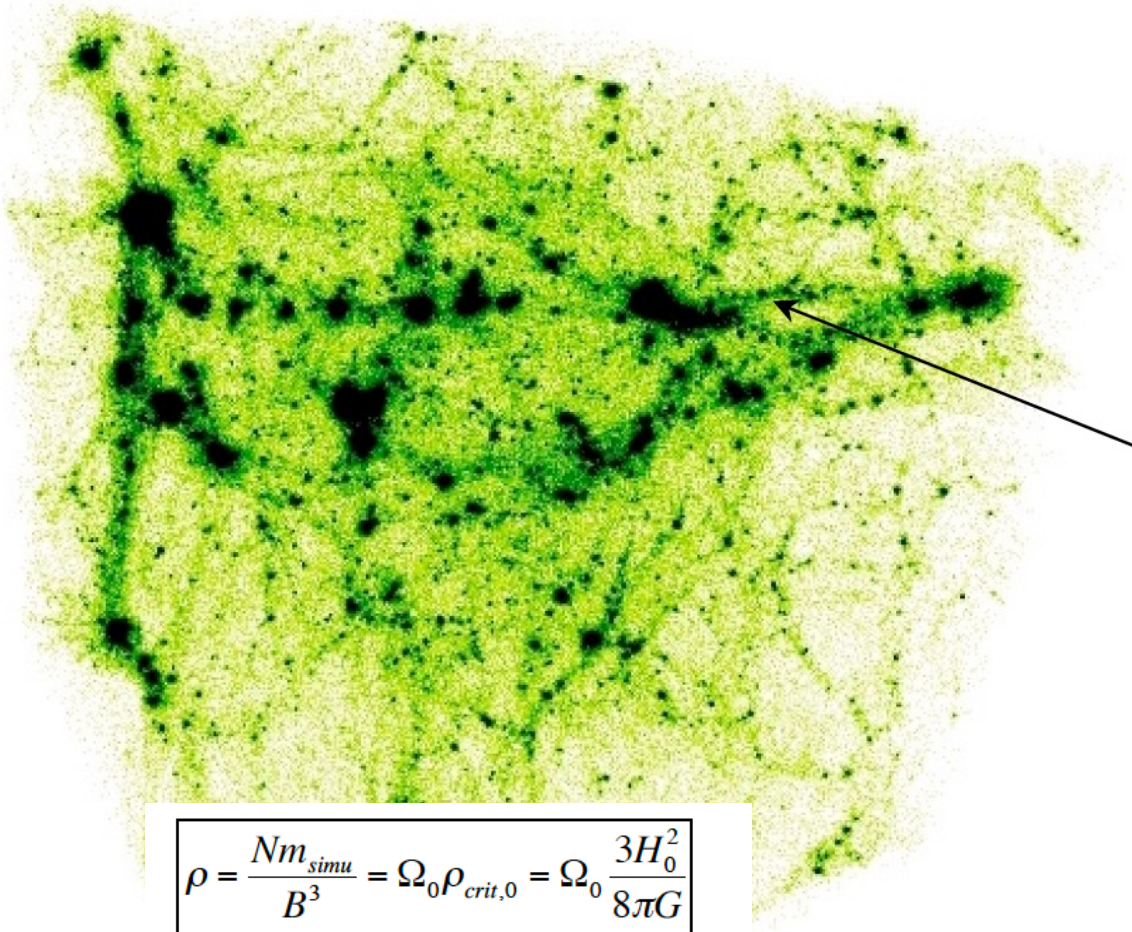

N bodies are used to sample the evolution of the Universe

one "simulation particle" represents *billions* of dark matter particles:

$m_{\text{simu}} \sim 10^{7} M_{\odot}$ vs $m_{\text{DM}} << 10^{-27} M_{\odot}$

$$\rho = \frac{N m_{simu}}{B^3} = \Omega_0 \rho_{crit,0} = \Omega_0 \frac{3H_0^2}{8\pi G}$$

$$\Rightarrow \quad m_{simu} = \Omega_0 \frac{3H_0^2}{8\pi G} \frac{B^3}{N}$$

$$B \approx 50 Mpc\,, \quad N \approx 1024^3$$

$$\Rightarrow \quad m_{simu} \approx 10^7 M_{\odot}$$

(non-baryonic) dark matter candidates

axion:	10^{-5} eV	
neutrino:	10eV	
WIMP:	1-10^3 GeV	
monopoles:	10^{16} GeV	
Planck relics:	10^{19} GeV	<< 1g

???

$0.5 MeV \approx 9 \cdot 10^{-28} g$

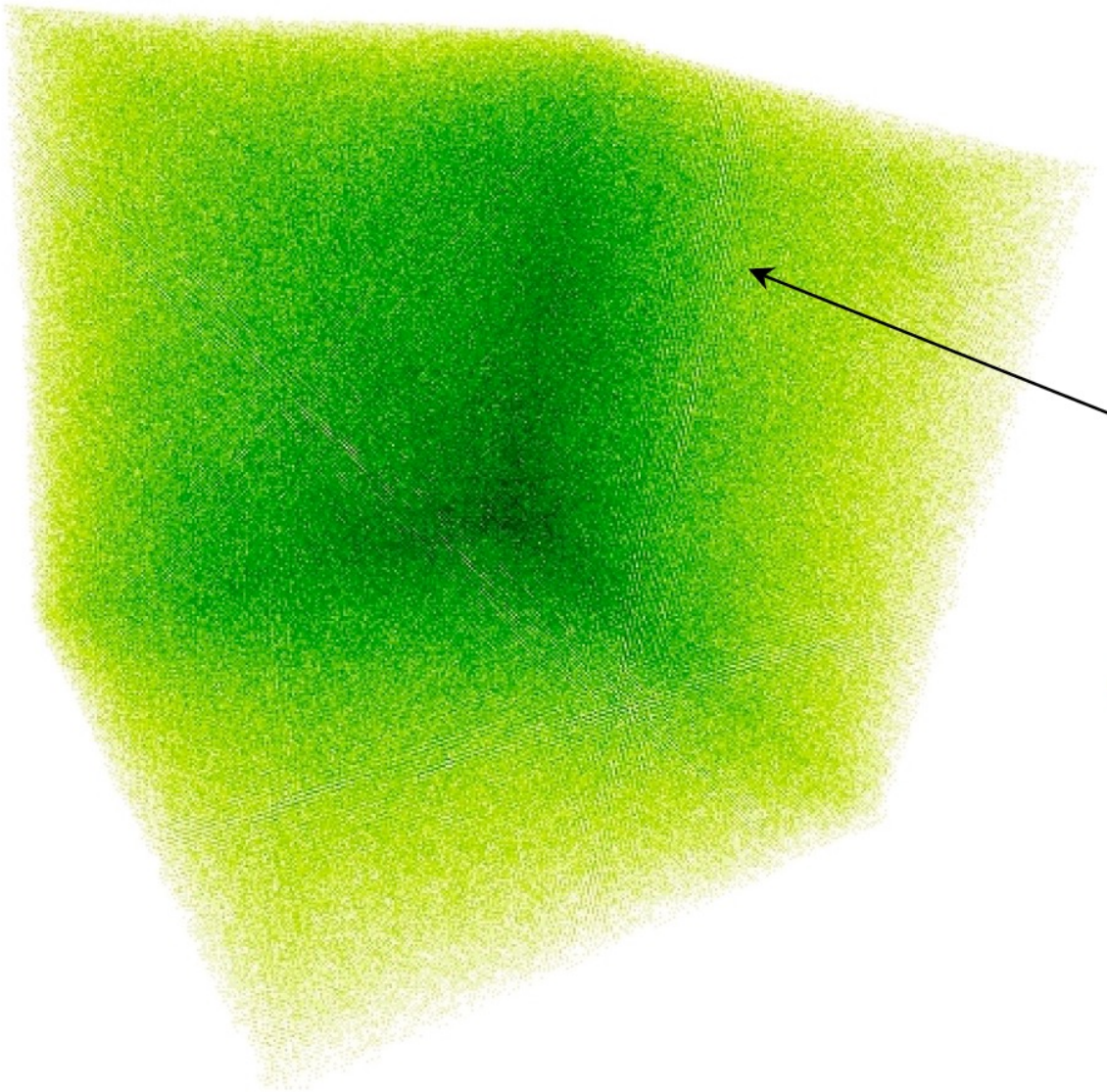

N bodies are used to sample

the evolution of the Universe

one “simulation particle”

represents

billions of dark matter particles:

$m_{\mathrm{simu}} \sim 10^{7} M_{\odot}$ vs $m_{\mathrm{DM}} << 10^{-27} M_{\odot}$

how to obtain $\vec{r}(t_0)\,, \vec{v}(t_0)$?

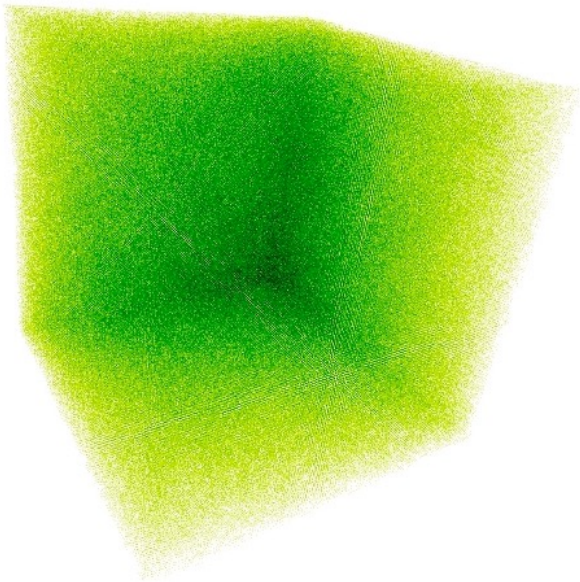

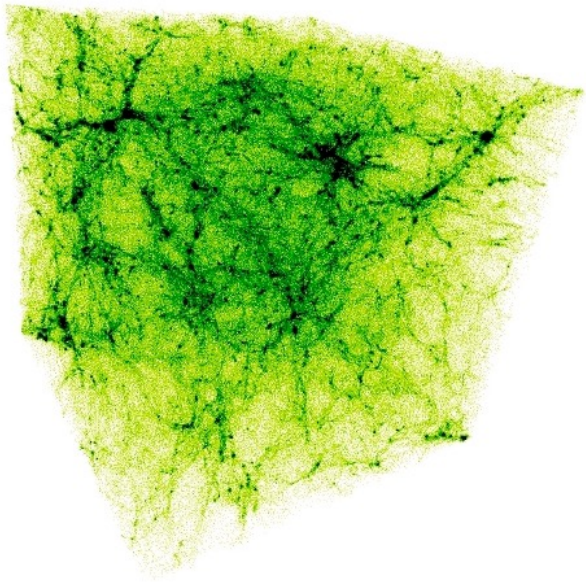

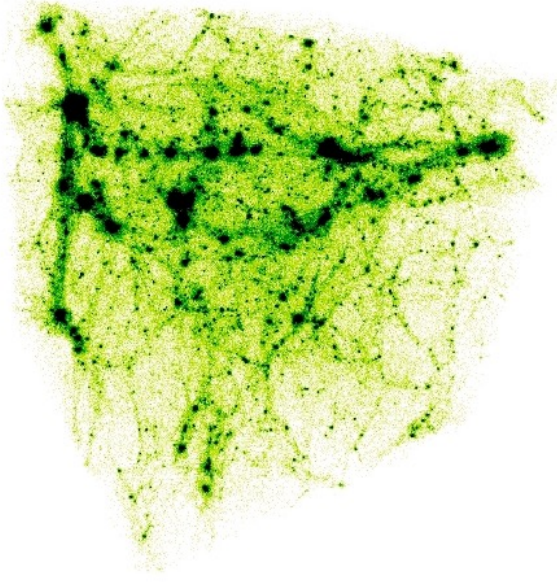

?

1. create an infinite homogenous and isotropic Universe

2. superimpose cosmological density perturbations

cosmological initial conditions

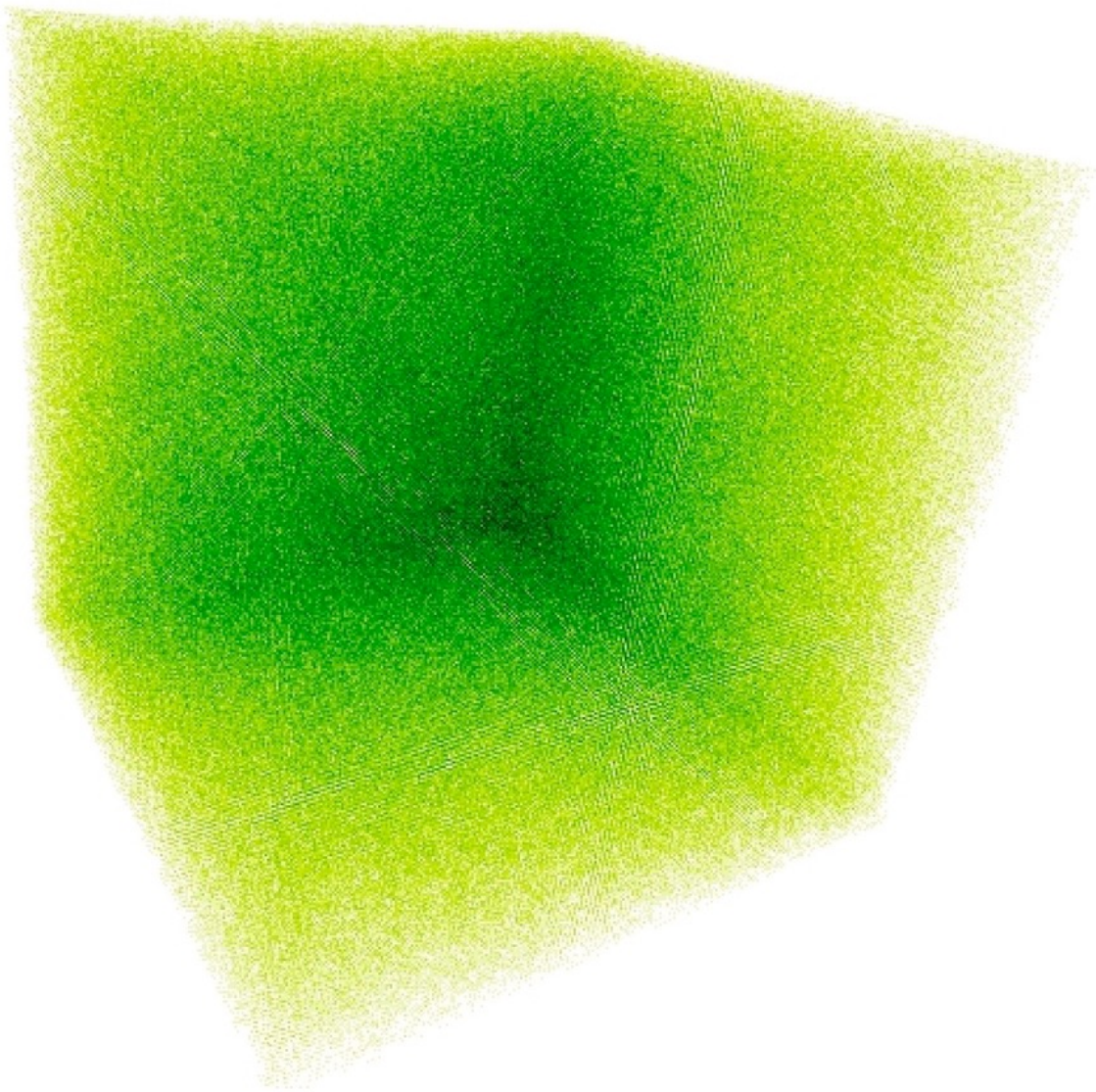

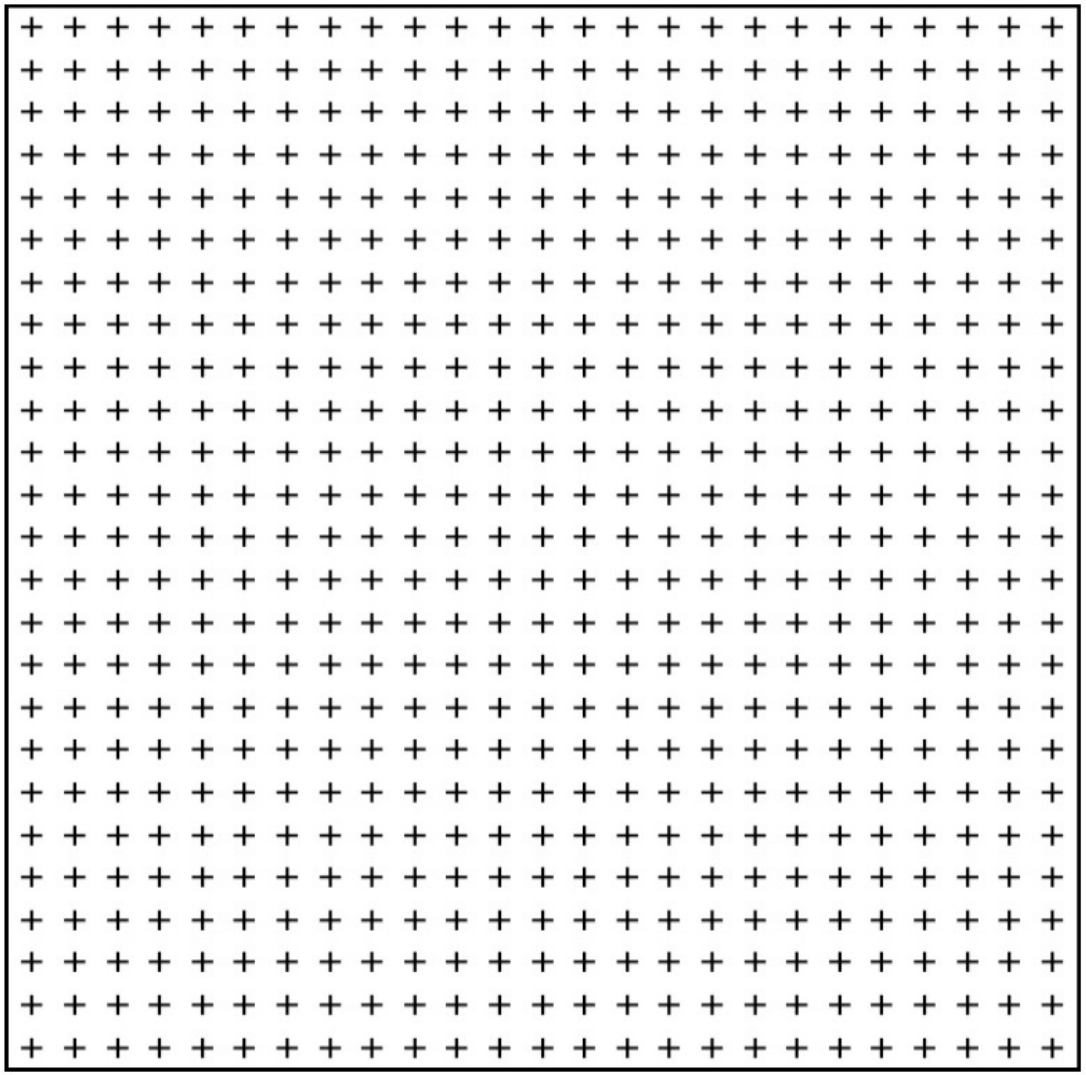

homogeneous
&
isotropic

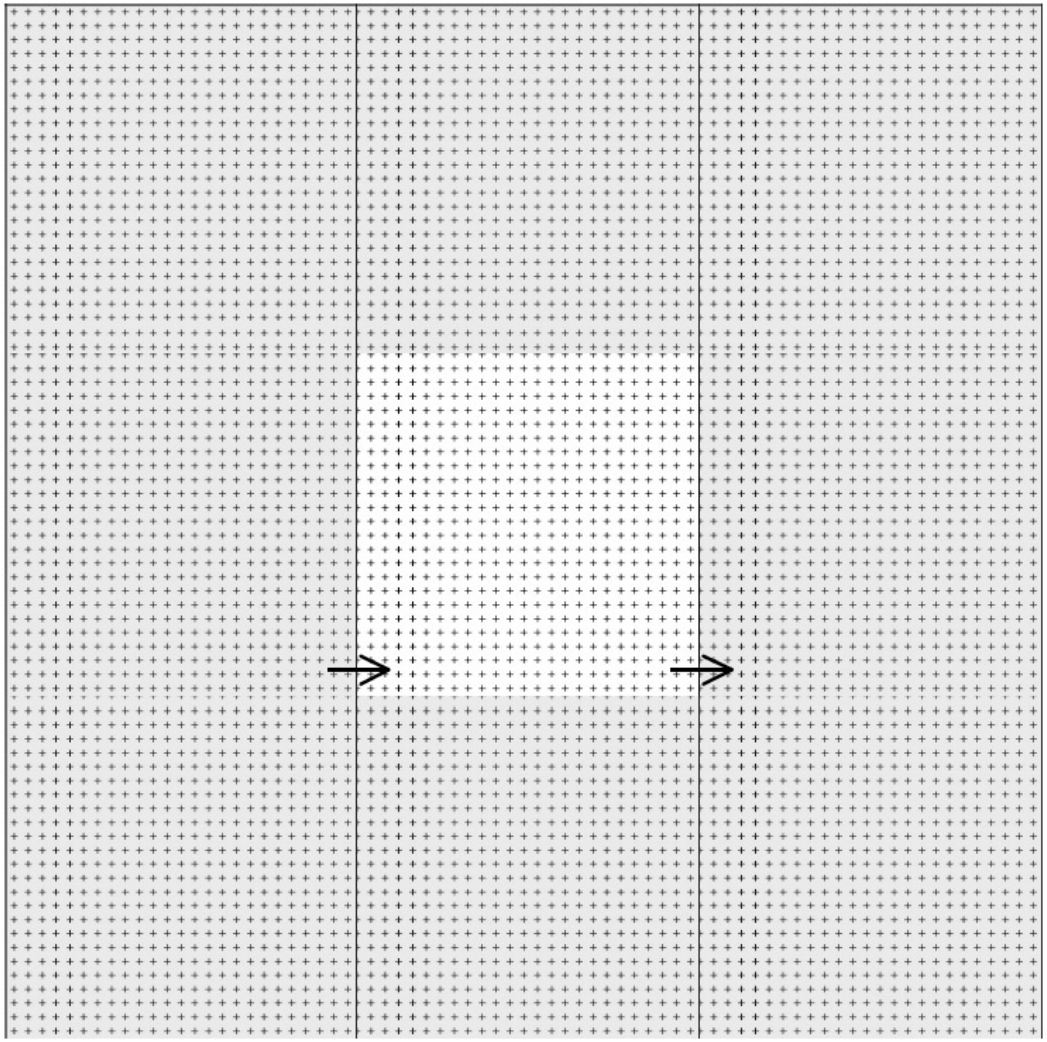

infinite

(periodic boundary conditions)

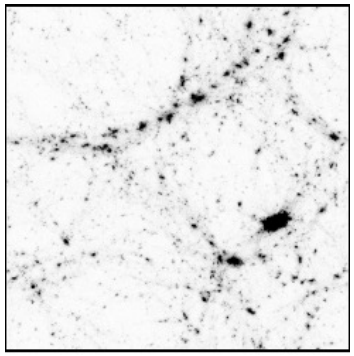

infinite

(periodic boundary conditions)

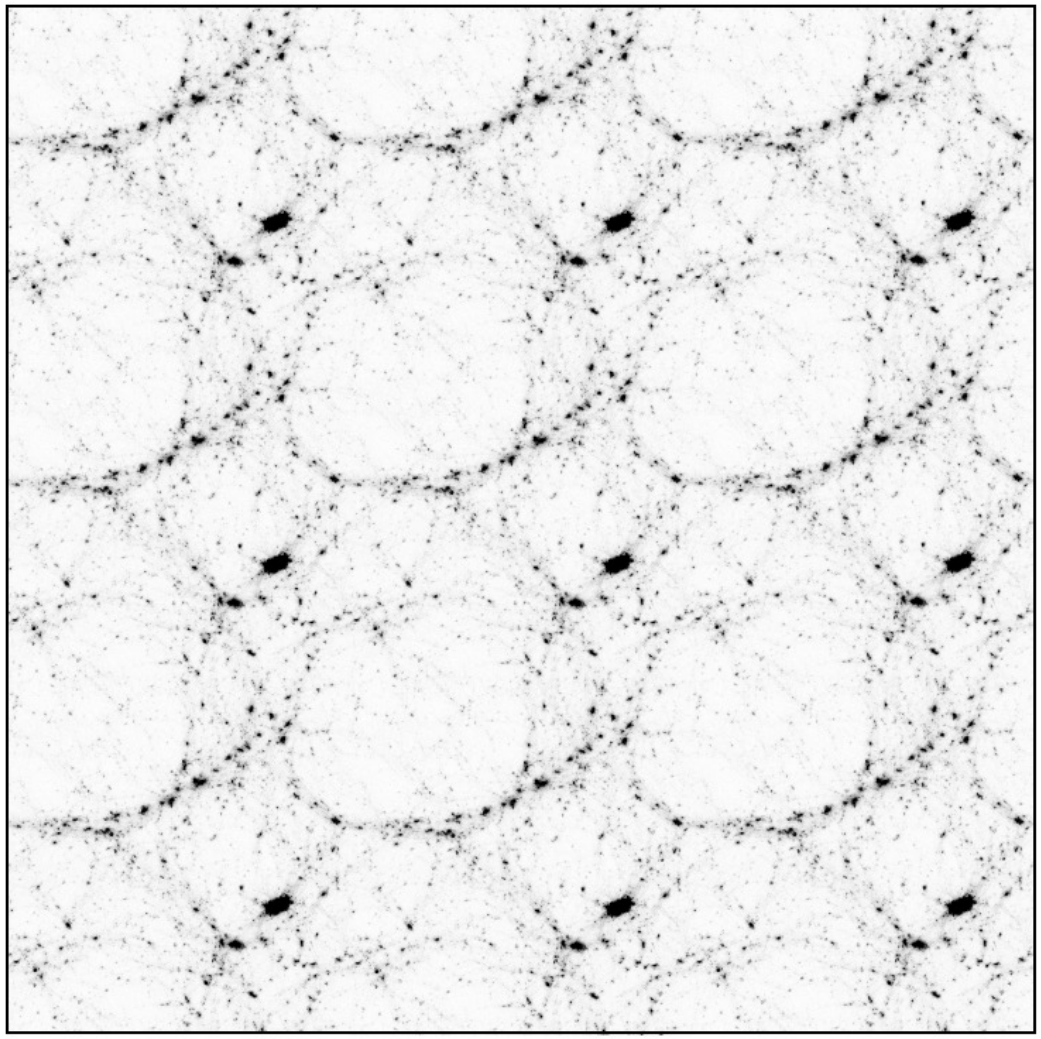

infinite

(periodic boundary conditions)

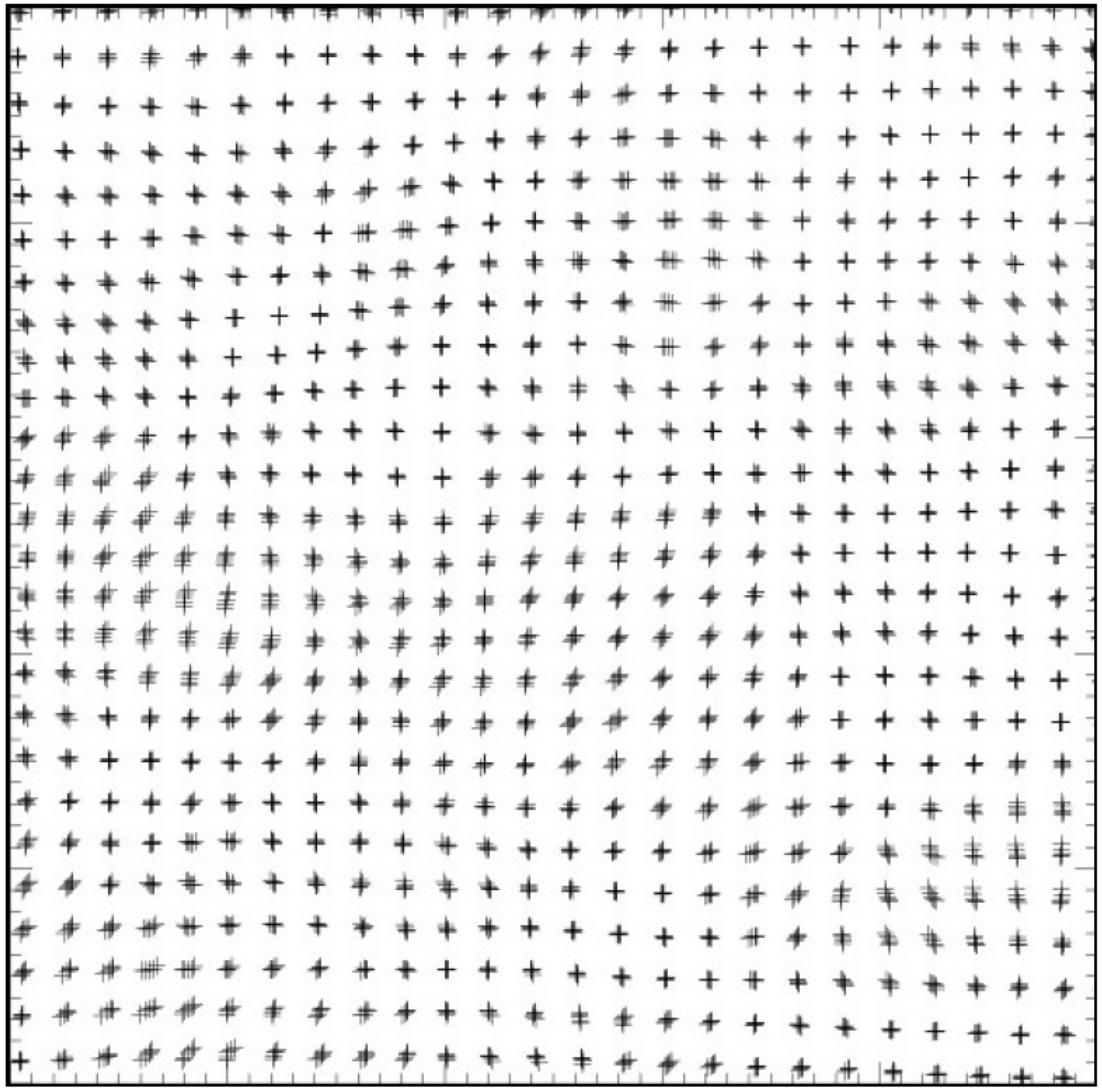

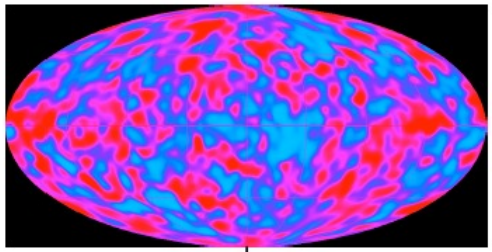

temperature fluctuations
converted into density perturbations

- density contrast:

$$\delta(\vec{x},t) = \frac{\rho(\vec{x},t) - \overline{\rho}(t)}{\overline{\rho}(t)}$$

$\Rightarrow$ decomposition of $\delta(x)$ into waves

$$\hat{\delta}(\vec{k}) = \sum \delta(\vec{x}) e^{-i\vec{k}\cdot\vec{x}} \qquad P(k) = \left\langle \left| \hat{\delta}(\vec{k}) \right|^2 \right\rangle_{|\vec{k}|=k}$$

Fourier transformation of density contrast

$$\hat{\delta}(\vec{k}) = \sum \delta(\vec{x}) e^{-i\vec{k}\cdot\vec{x}} \qquad P(k) = \left\langle \left| \hat{\delta}(\vec{k}) \right|^2 \right\rangle_{|\vec{k}|=k}$$

long wavelength

short wavelength,
large amplitude

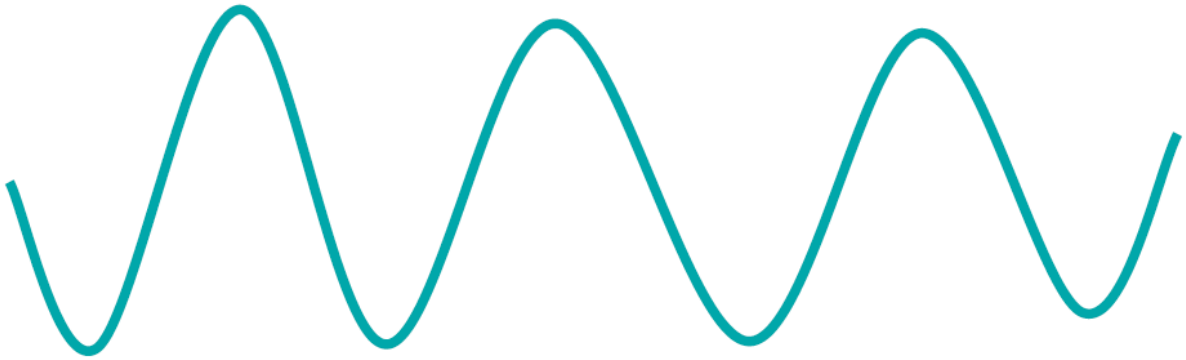

short wavelength,
small amplitude

$$\hat{\delta}(\vec{k}) = \sum \delta(\vec{x}) e^{-i\vec{k}\cdot\vec{x}}$$

$$P(k) = \left\langle \left| \hat{\delta}(\vec{k}) \right|^2 \right\rangle_{|\vec{k}|=k}$$

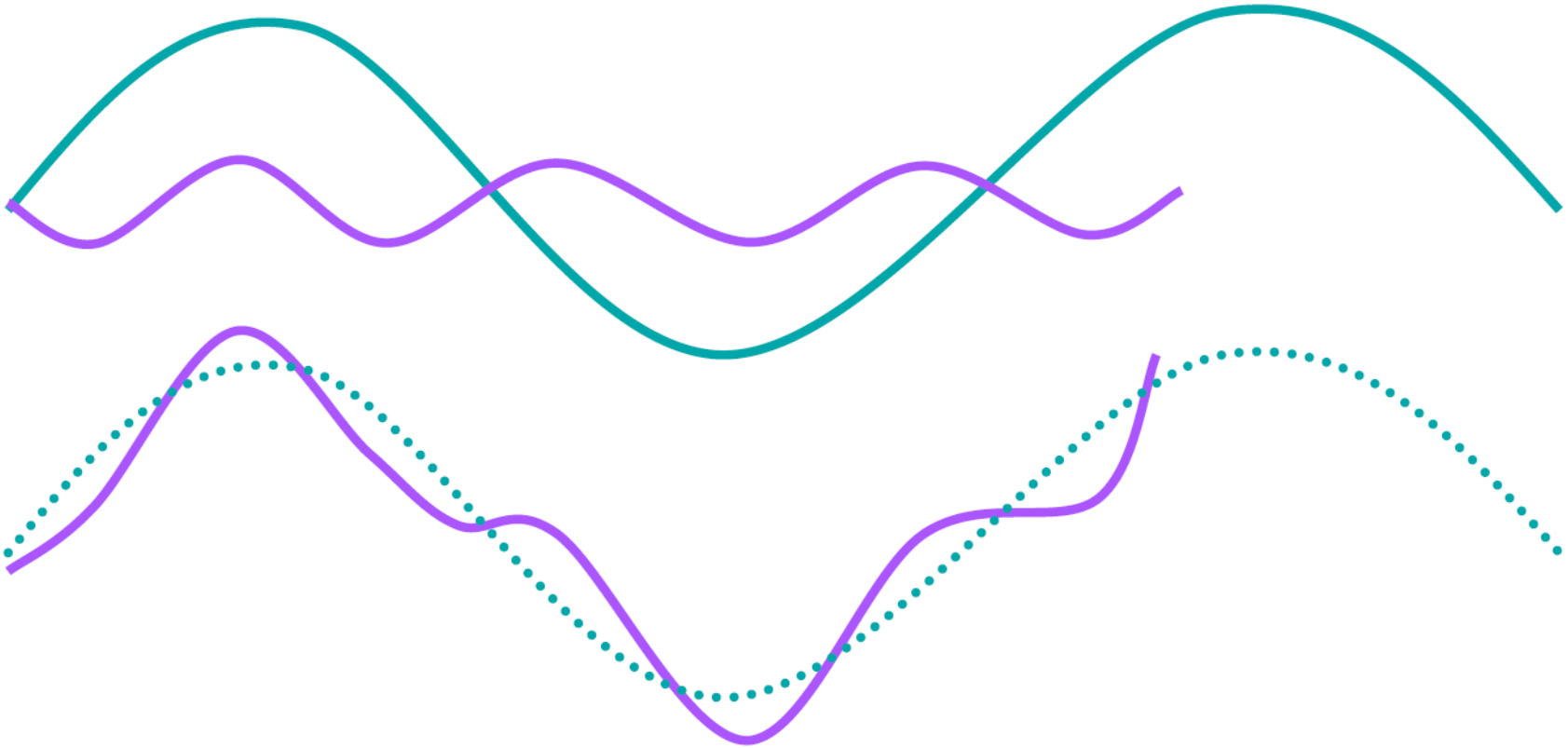

$$\hat{\delta}(\vec{k}) = \sum \delta(\vec{x}) e^{-i\vec{k}\cdot\vec{x}} \qquad P(k) = \left\langle \left| \hat{\delta}(\vec{k}) \right|^2 \right\rangle_{|\vec{k}|=k}$$

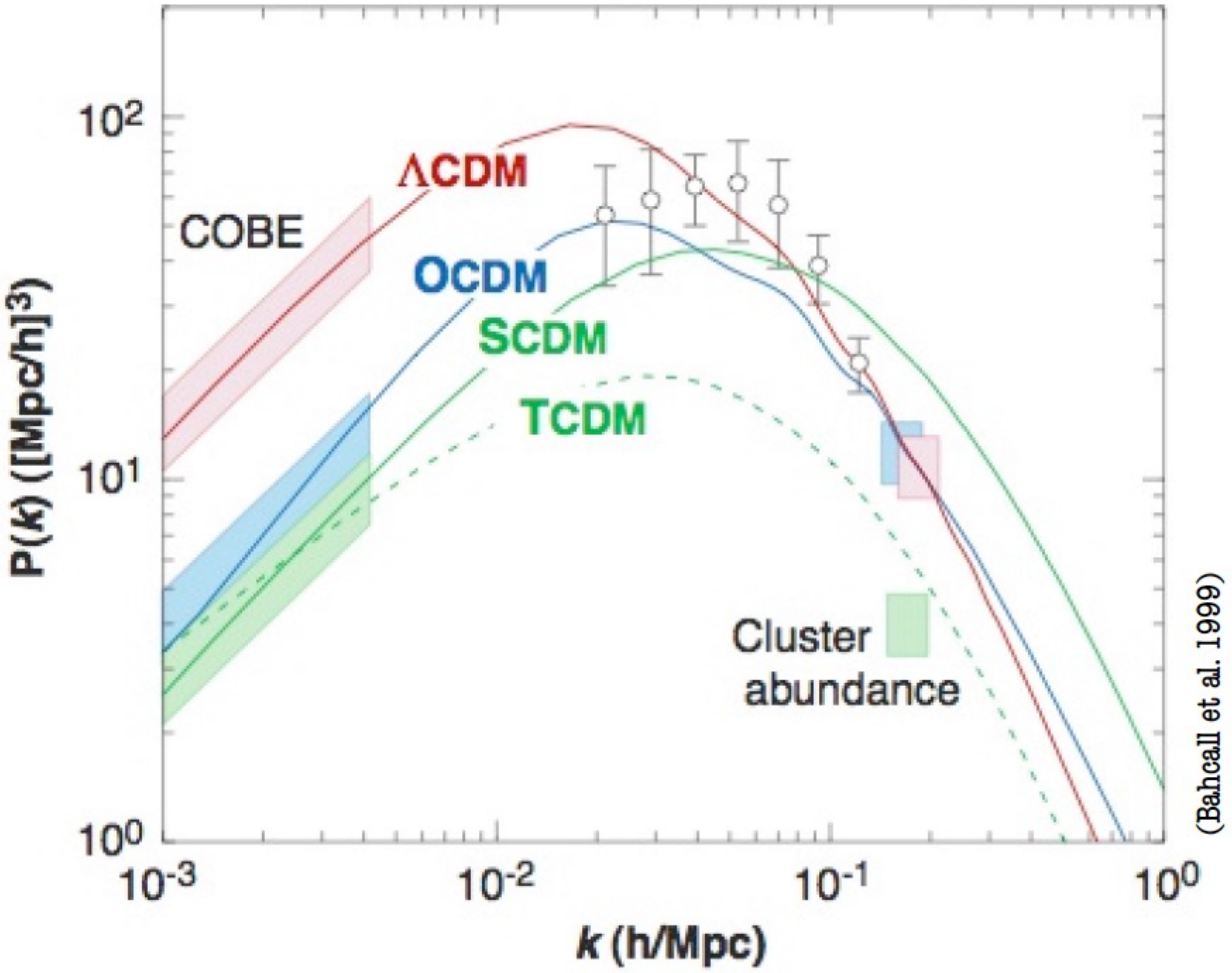

$$\hat{\delta}(\vec{k}) = \sum \delta(\vec{x}) e^{-i\vec{k}\cdot\vec{x}} \qquad P(k) = \left\langle \left| \hat{\delta}(\vec{k}) \right|^2 \right\rangle_{|\vec{k}|=k}$$

- inflation theory

$$P_i(k) = Ak^n \qquad \text{with } n = 1 \text{ (Harrision - Zeldovich spectrum)}$$

- transferring $P(k)$ across recombination

$$P(k) = T^2(k) P_i(k)$$

$$\hat{\delta}(\vec{k}) = \sum \delta(\vec{x}) e^{-i\vec{k}\cdot\vec{x}}$$

$$P(k) = \left\langle \left| \hat{\delta}(\vec{k}) \right|^2 \right\rangle_{|\vec{k}|=k}$$

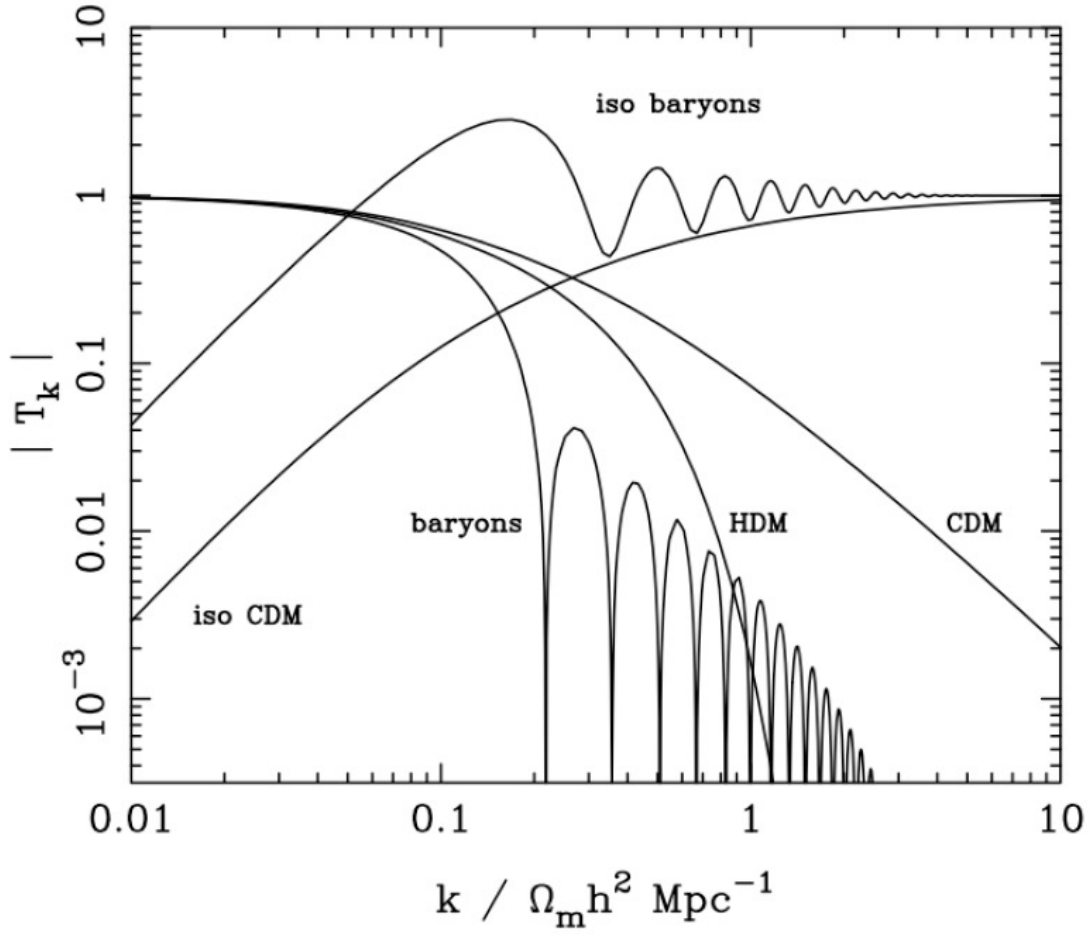

$$P(k) = T^2(k) P_i(k)$$

$$\hat{\delta}(\vec{k}) = \sum \delta(\vec{x}) e^{-i\vec{k}\cdot\vec{x}}$$

$$P(k) = \left\langle \left| \hat{\delta}(\vec{k}) \right|^2 \right\rangle_{|\vec{k}|=k}$$

homogeneous & isotropic

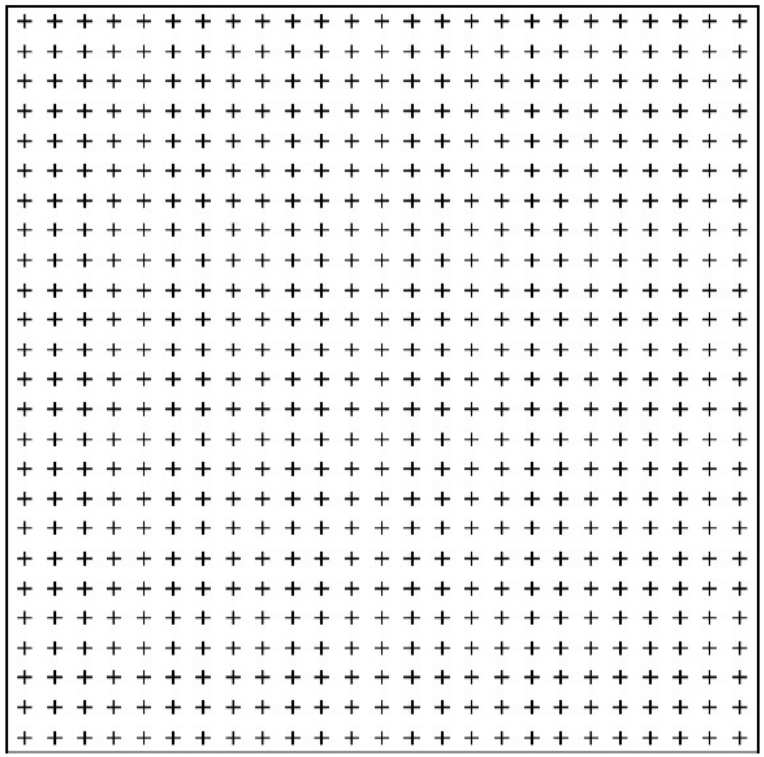

?

initial conditions

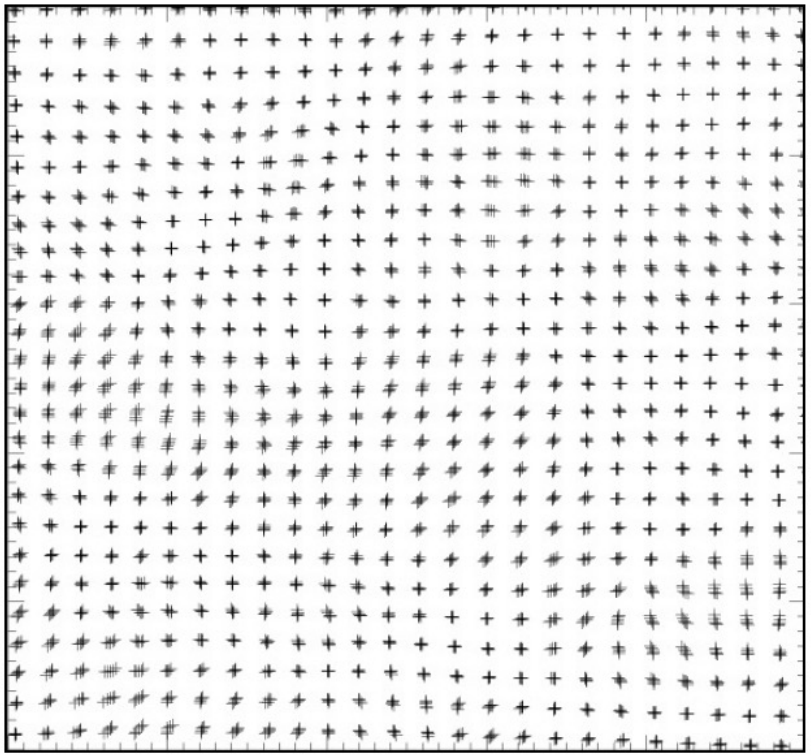

$$\hat{\delta}(\vec{k}) = \sum \delta(\vec{x}) e^{-i\vec{k}\cdot\vec{x}}$$

$$P(k) = \left\langle \left| \hat{\delta}(\vec{k}) \right|^2 \right\rangle_{|\vec{k}|=k}$$

homogeneous & isotropic

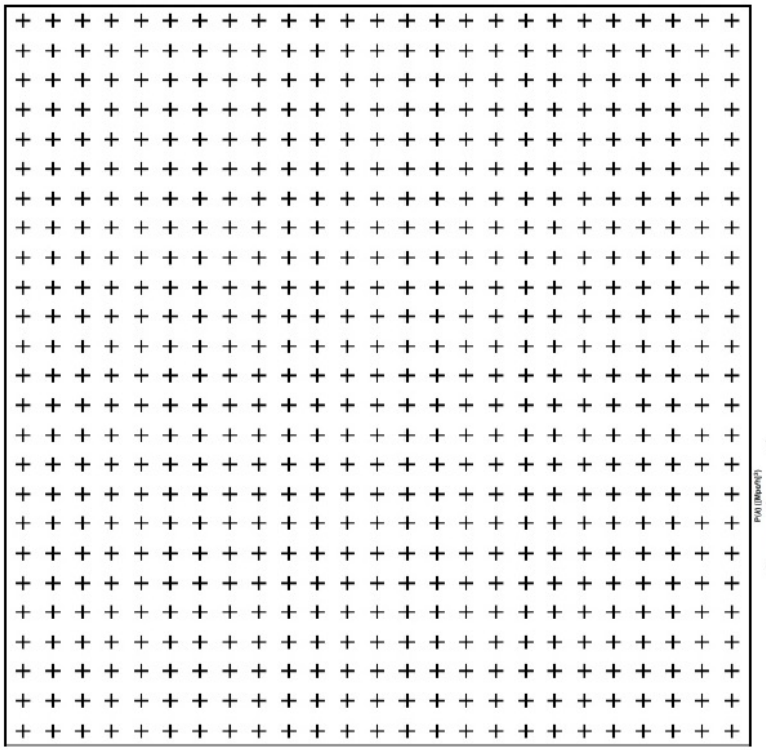

$P(k)$

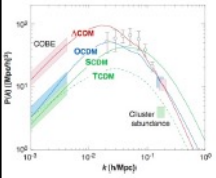

initial conditions

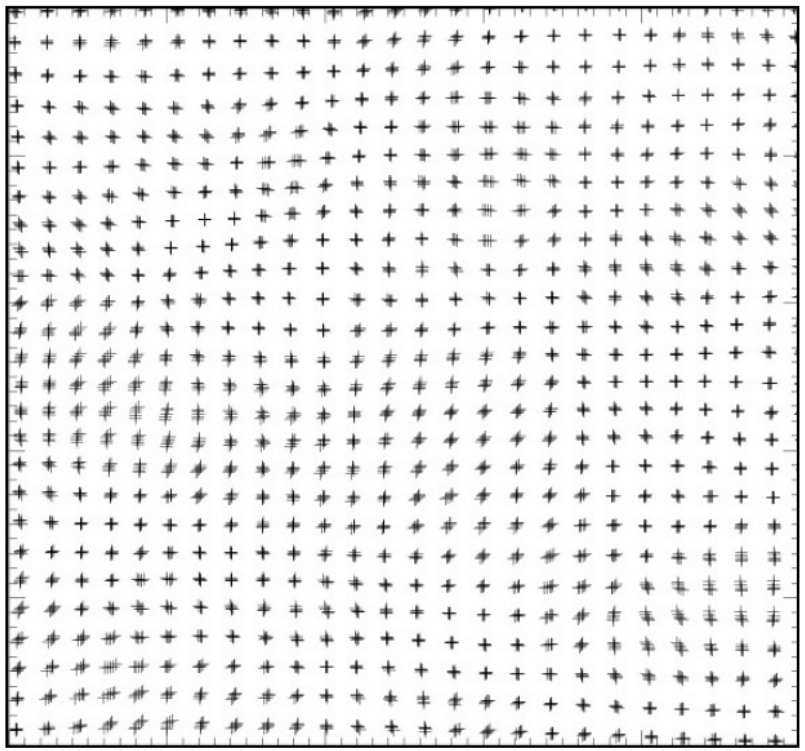

$$\hat{\delta}(\vec{k}) = \sum \delta(\vec{x}) e^{-i\vec{k}\cdot\vec{x}}$$

$$P(k) = \left\langle \left| \hat{\delta}(\vec{k}) \right|^2 \right\rangle_{|\vec{k}|=k}$$

homogeneous & isotropic

initial conditions

imposing a spectrum of fluctuations on a particle distribution

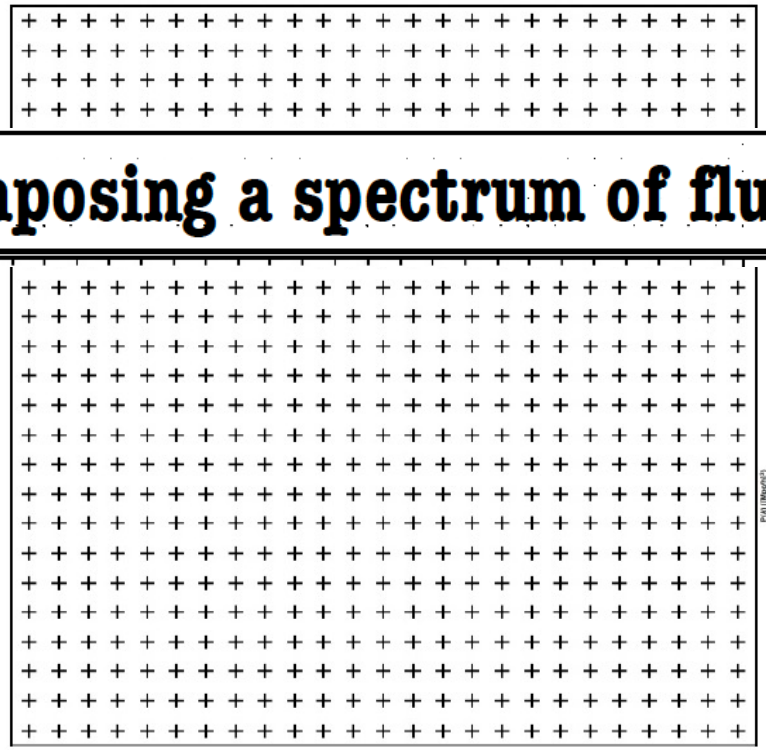

$P(k)$

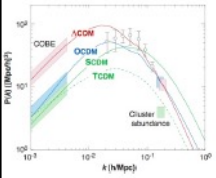

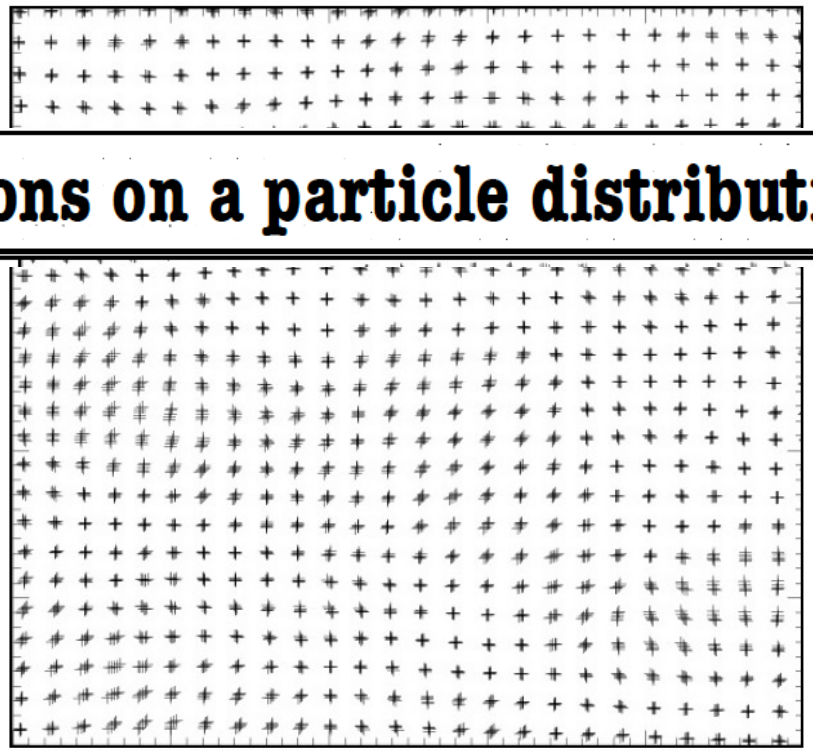

evolution dominated by dark matter
(at least since z~7000)

⇓

the evolution of a collisionless fluid in an expanding Universe

- generating IC's in practice

  - choose cosmological model — ΛCDM?!
  - choose box size — B
  - choose number of particles — N
  - choose starting redshift — z_i

these choices are not free but interwoven...

- generating IC's in practice
  - wavenumber limitation

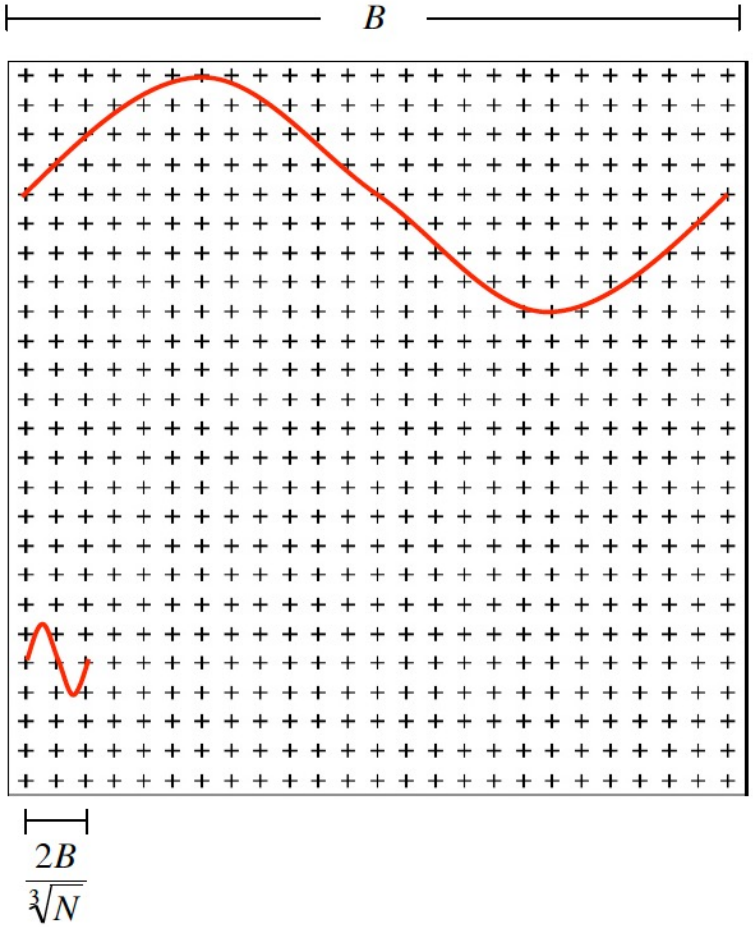

ΛCDM vs. ΛWDM
B=100 h^{-1}Mpc
N=256^3

- generating IC's in practice
  - wavenumber limitation

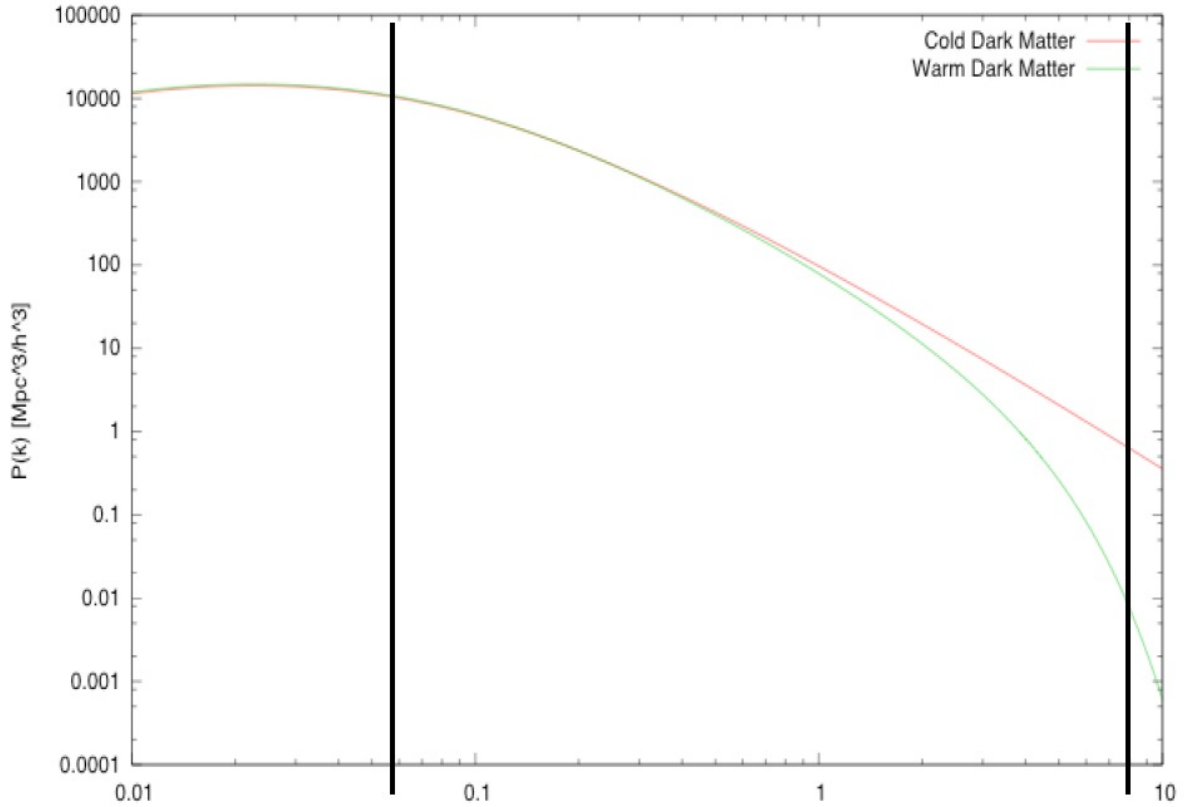

$\frac{2\pi}{B}$ $\frac{\pi}{B/\sqrt[3]{N}}$

ΛCDM vs. ΛWDM
B=100 h^{-1}Mpc
$N=32^3$

- generating IC's in practice
  - wavenumber limitation

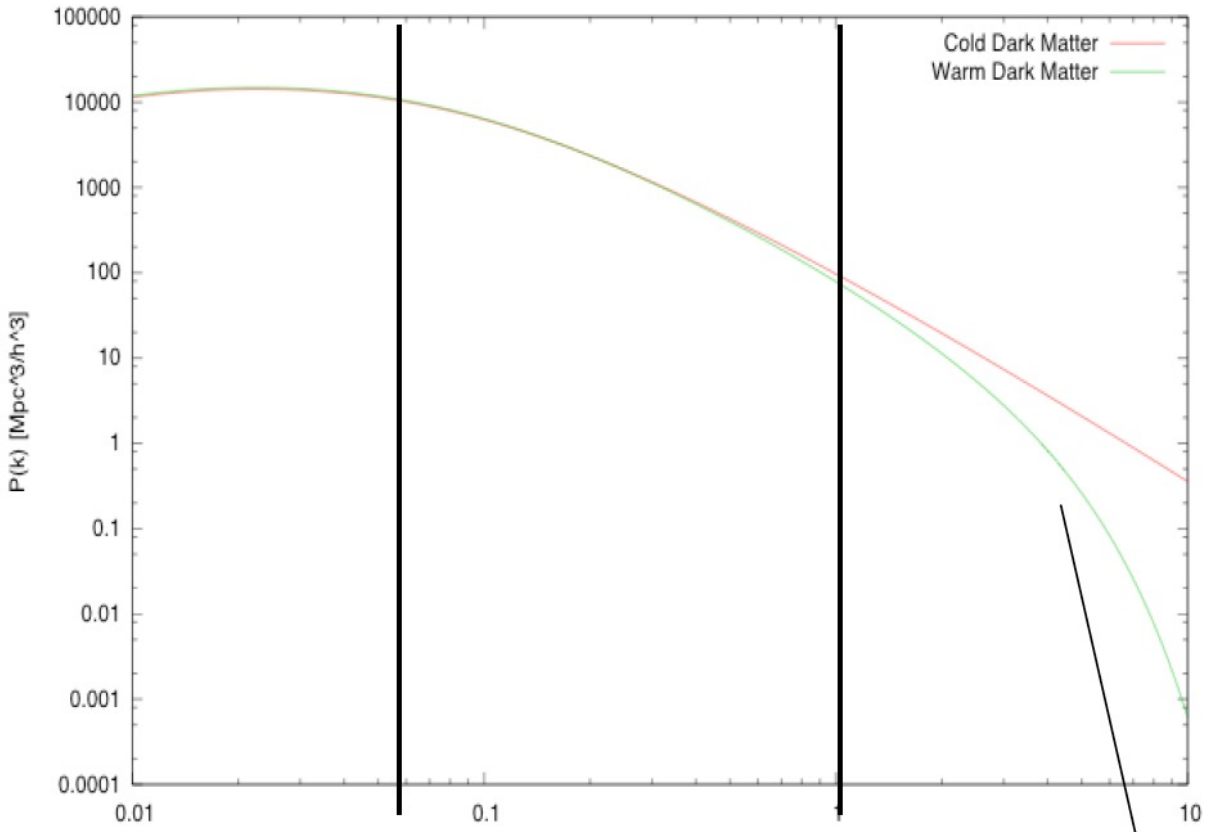

$\frac{2\pi}{B}$ $\frac{\pi}{B/\sqrt[3]{N}}$

interesting features not modeled...

- generating IC's in practice
  - wavenumber limitation

ΛCDM vs. ΛWDM
B=100 h^{-1}Mpc
N=32^3
?

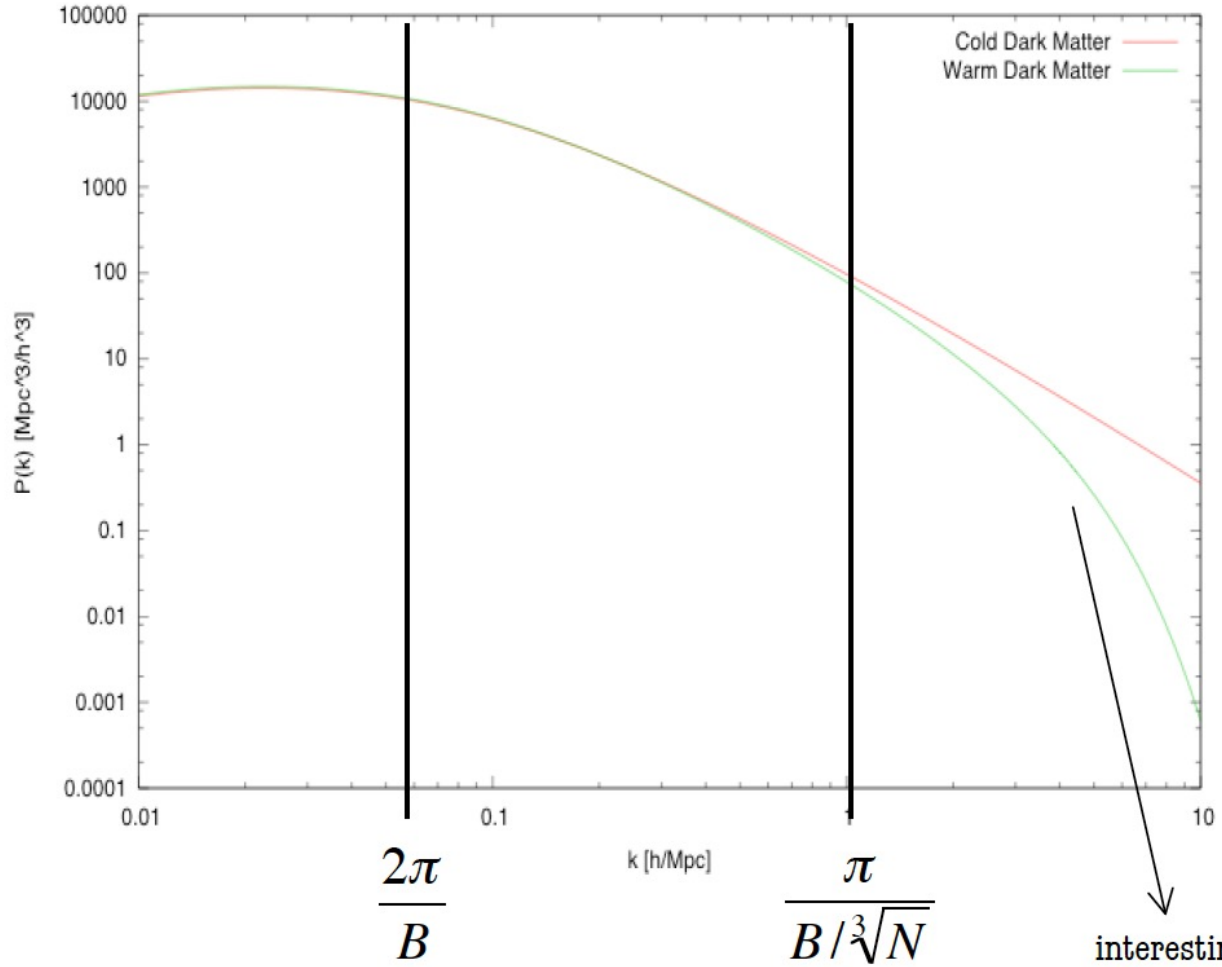

$\frac{2\pi}{B}$ $\frac{\pi}{B/\sqrt[3]{N}}$

interesting features not modeled...

ΛCDM vs. ΛWDM
B=100 h^{-1}Mpc
N=32^3
?

- why h^{-1}Mpc ?

$$\rho = \frac{N m_{simu}}{B^3} = \Omega_0 \rho_{crit,0} = \Omega_0 \frac{3H_0^2}{8\pi G} = \Omega_0 \frac{3 \cdot (100h^2)}{8\pi G}$$

$$\Rightarrow \quad m_{simu} = \Omega_0 \frac{300h^2}{8\pi G} \frac{B^3}{N}$$

$$\Rightarrow \quad h m_{simu} = \Omega_0 \frac{300}{8\pi G} \frac{(hB)^3}{N}$$

$$\Rightarrow \quad \tilde{m}_{simu} = \Omega_0 \frac{300}{8\pi G} \frac{\tilde{B}^3}{N}$$

distances and masses have to be divided by h to get physical values...

- alternative - Glass IC's

"Grid" IC's

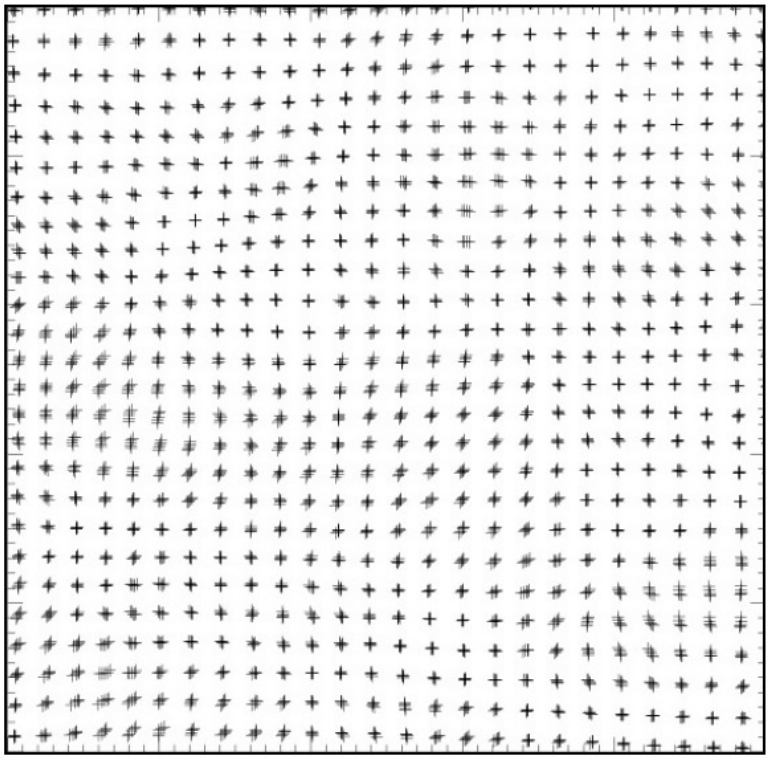

"Glass" IC's

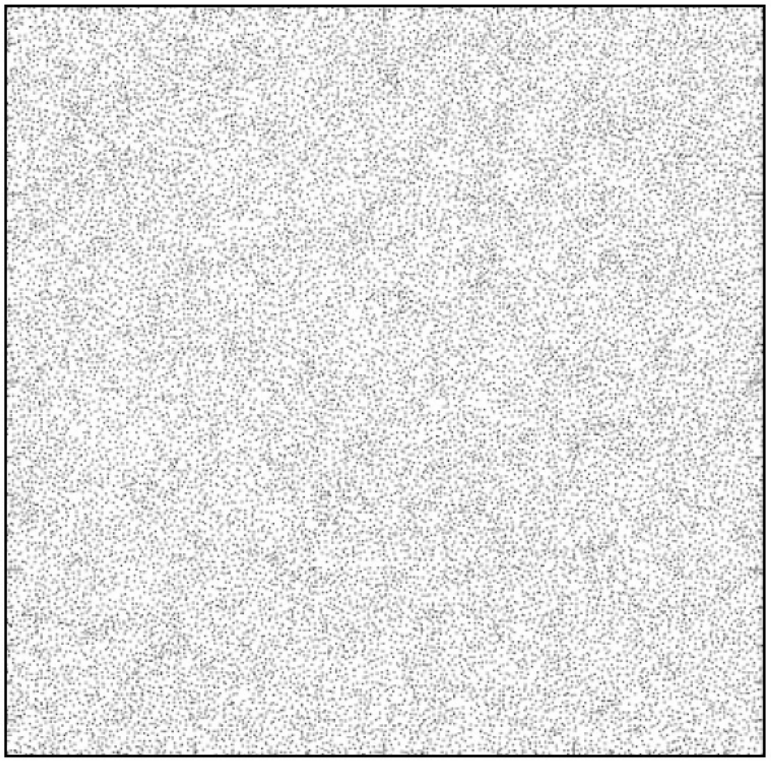

- alternative - Glass IC's

  - random positions for N particles

  - evolve them forward in time under their mutual gravity (i.e. N-body code), but:

    reverse the sign of gravity!

  - use this "Glass" as Lagrangian positions q for Zel'dovich approximation

- alternative - Glass IC's

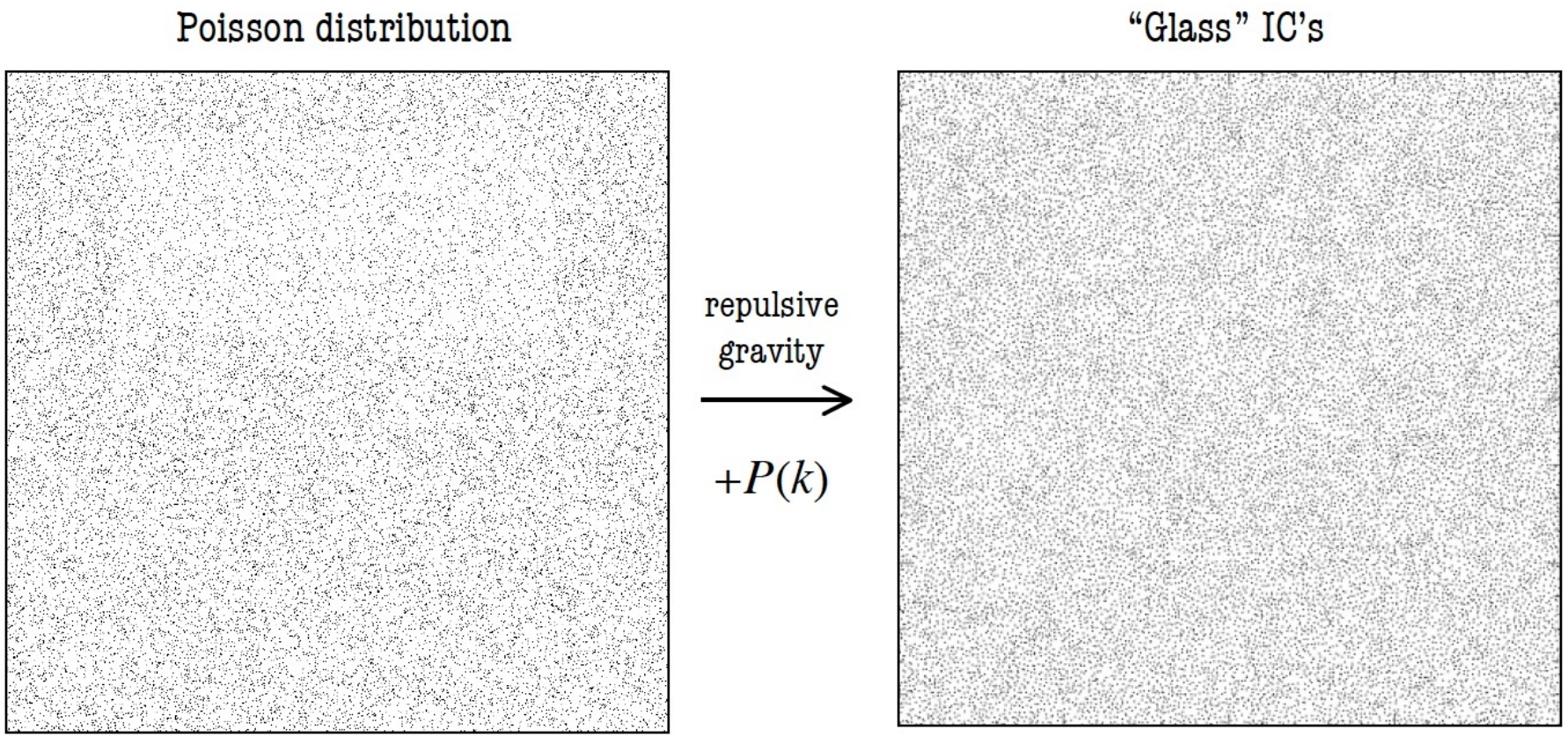

- alternative - Glass IC's

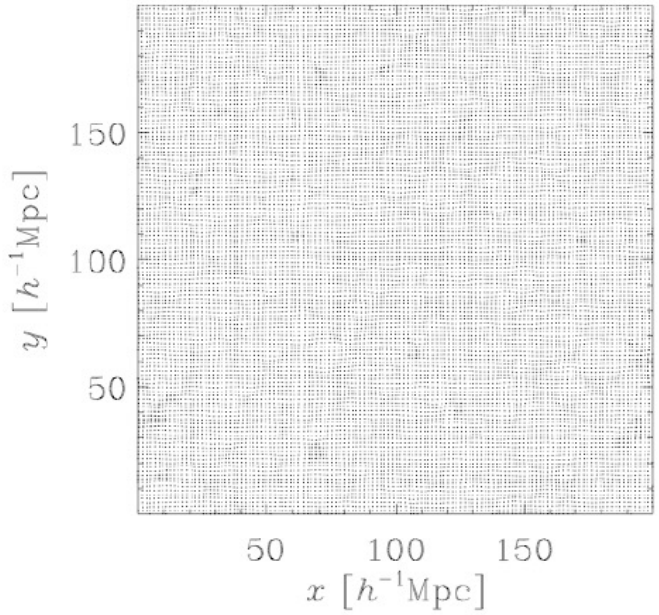

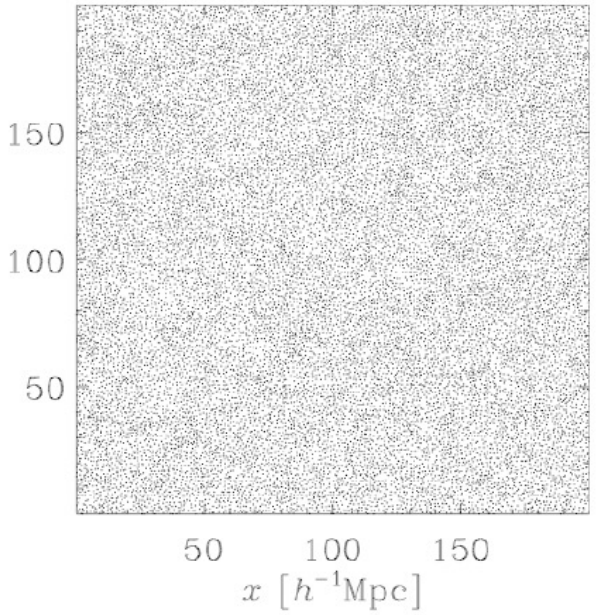

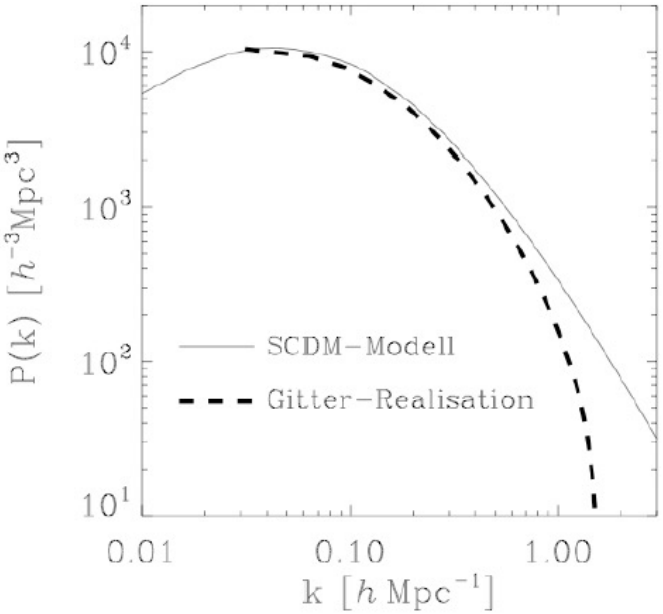

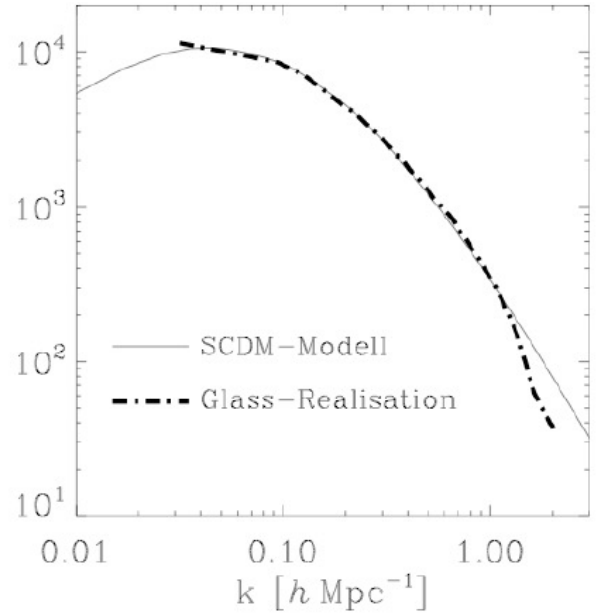

- alternative - Glass IC's

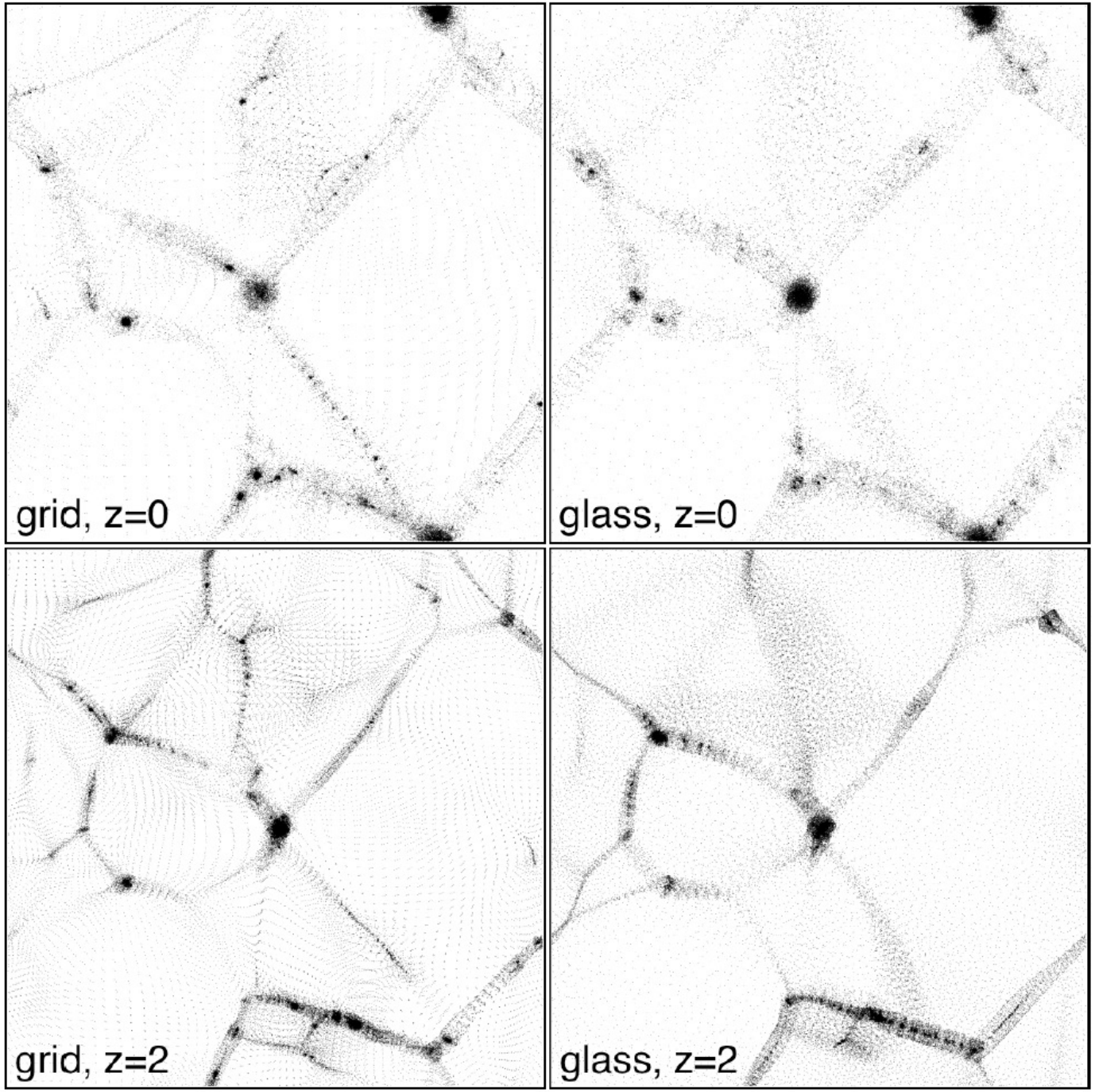

Goetz & Sommer-Larson (2003)

- choose cosmological model ΛCDM?!

  => cosmological power spectrum of density perturbations $P(k)$

- choose box size B
- choose number of particles N^3

  => put them down on regular NxNxN grid

- choose starting redshift z_i

  => use Zel'dovich approximation to displace particles according to $P(k)$

There are different types of cosmological simulations

There are different types of cosmological simulations

Stand alone

Cosmological

Zoom-in

There are different types of cosmological simulations

Stand alone

“ideal”

+ Box is finite, not periodic

+ different types of particles (*N*-body, gas, starts, Black holes)

+ used for simulating mergers, interactions, secular evolution

+ usually only few objects with high resolution

Cosmological

Zoom-in

There are different types of cosmological simulations

Stand alone

"ideal"

+ Box is finite, not periodic

+ different types of particles (*N*-body, gas, starts, Black holes)

+ used for simulating mergers, interactions, secular evolution

+ usually only few objects with high resolution

Cosmological

Zoom-in

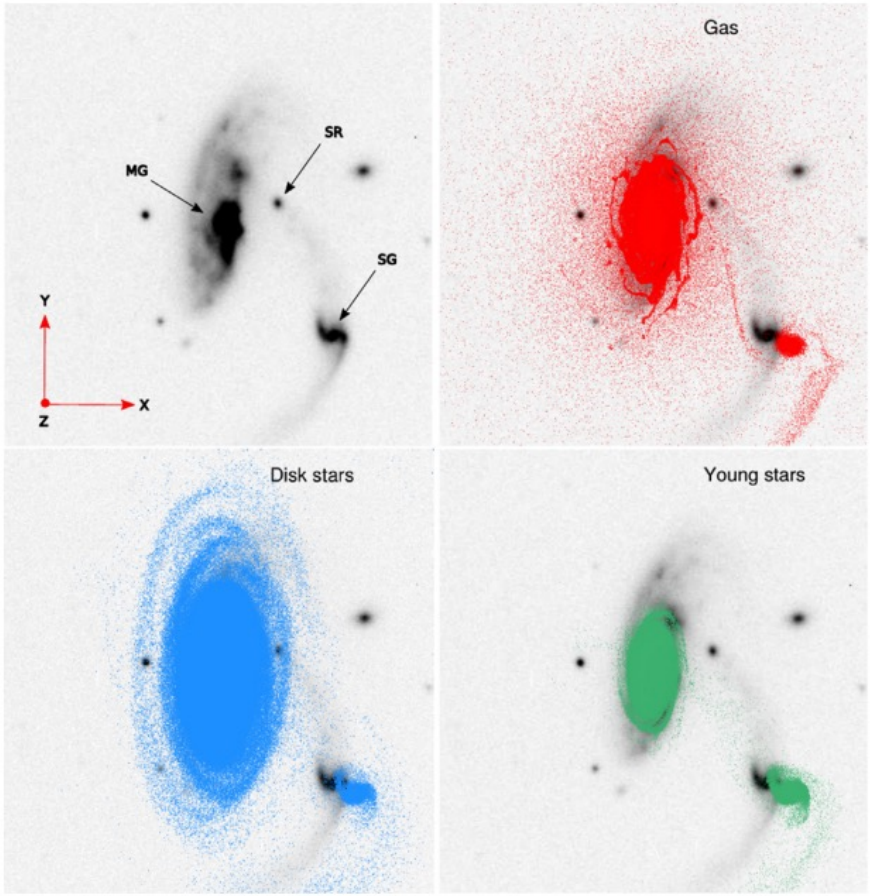

There are different types of cosmological simulations

Stand alone	Cosmological	Zoom-in
“ideal”	N body and/or fluid	
+ Box is finite, not periodic	+ Box is periodic	
+ different types of particles (*N*-body, gas, starts, Black holes)	+ different types of particles (*N*-body, gas, starts, Black holes)	
+ used for simulating mergers, interactions, secular evolution	+ used for simulating the formation of the large scale structure	
+ usually only few objects with high resolution	+ used to simulate large statistical samples of objects	

There are different types of cosmological simulations

Stand alone	Cosmological	Zoom-in
"ideal"	N body and/or fluid	N body and/or fluid
+ Box is finite, not periodic	+ Box is periodic	+box is periodic
+ different types of particles (*N*-body, gas, starts, Black holes)	+ different types of particles (*N*-body, gas, starts, Black holes)	+ different types of particles (*N*-body, gas, starts, Black holes)
+ used for simulating mergers, interactions, secular evolution	+ used for simulating the formation of the large scale structure	+ used for simulating one or two objects at HIGH RES *within* the large scale structure
+ usually only few objects with high resolution	+ used to simulate large statistical samples of objects	

There are different types of cosmological simulations

Zoom-in

N body and/or fluid

+box is periodic

+ different types of particles (*N*-body, gas, starts, Black holes)

+ used for simulating one or two objects at HIGH RES *within* the large scale structure

+ used for simulating mergers, interactions, secular evolution

+ usually only few objects with high resolution

+ used for simulating the formation of the large scale structure

+ used to simulate large statistical samples of objects

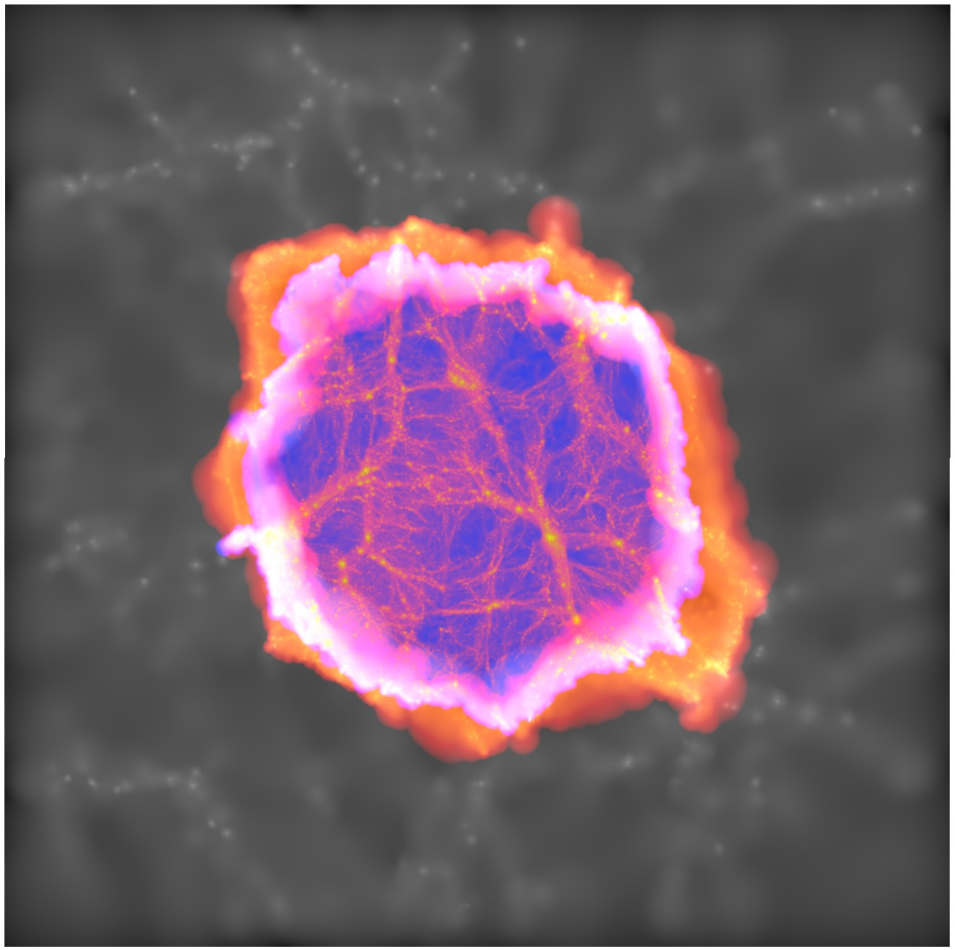

"zoom" initial conditions for high Resolution simulations

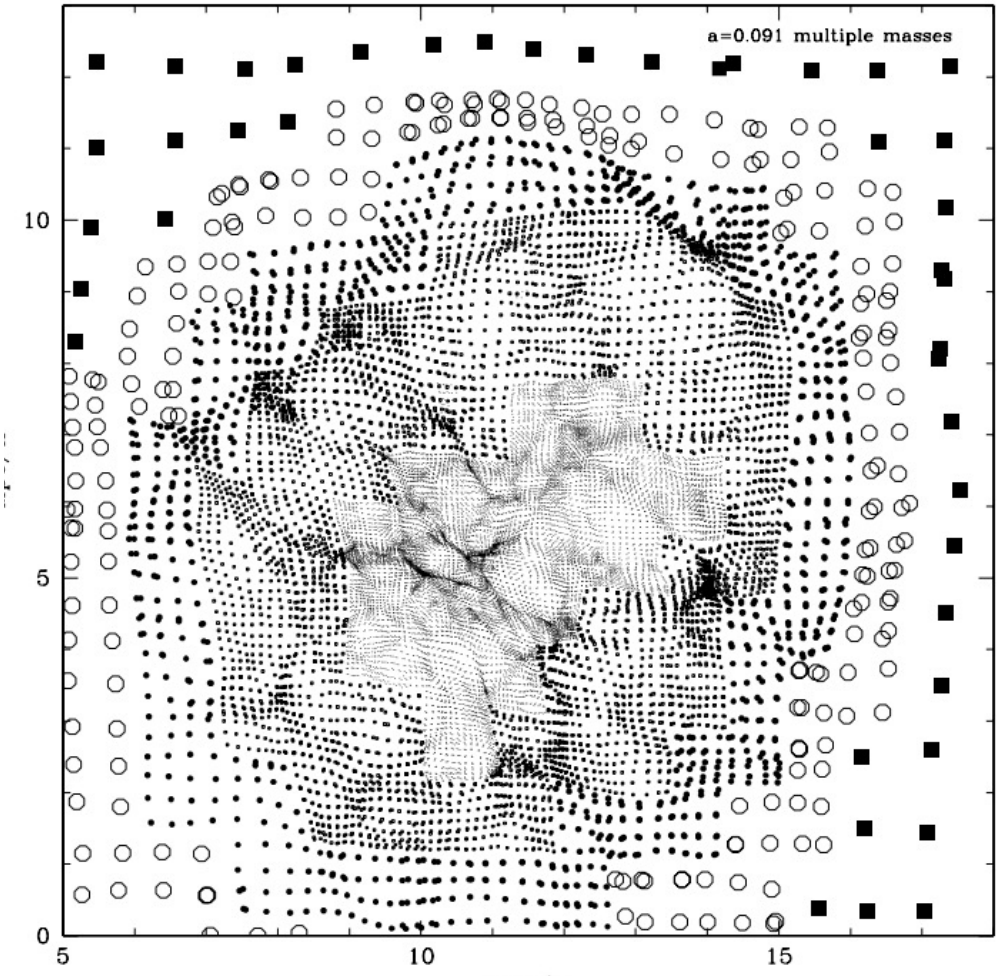

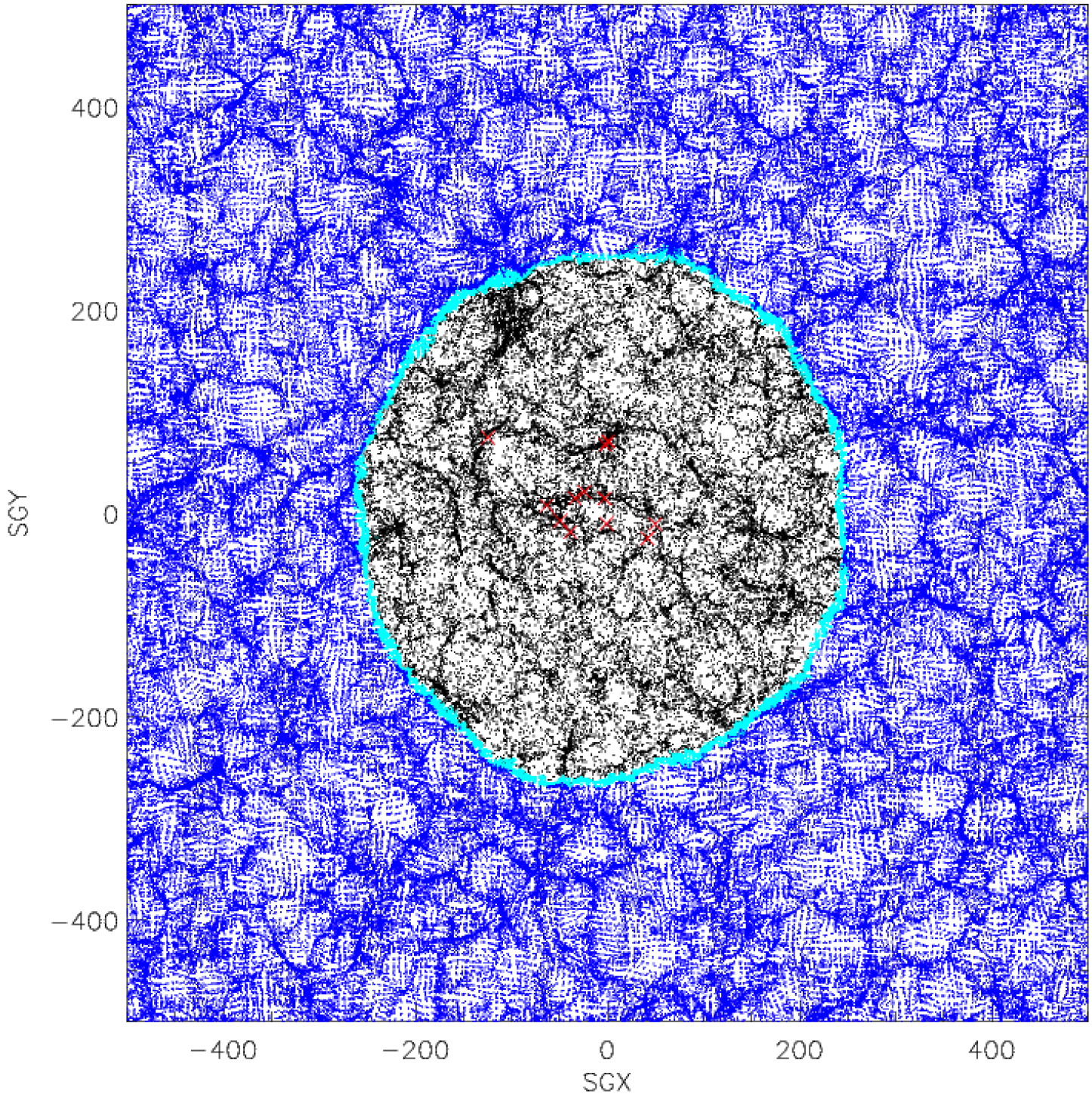
400
200
0
−200
−400
SGY
−400
−200
0
200
400
SGX

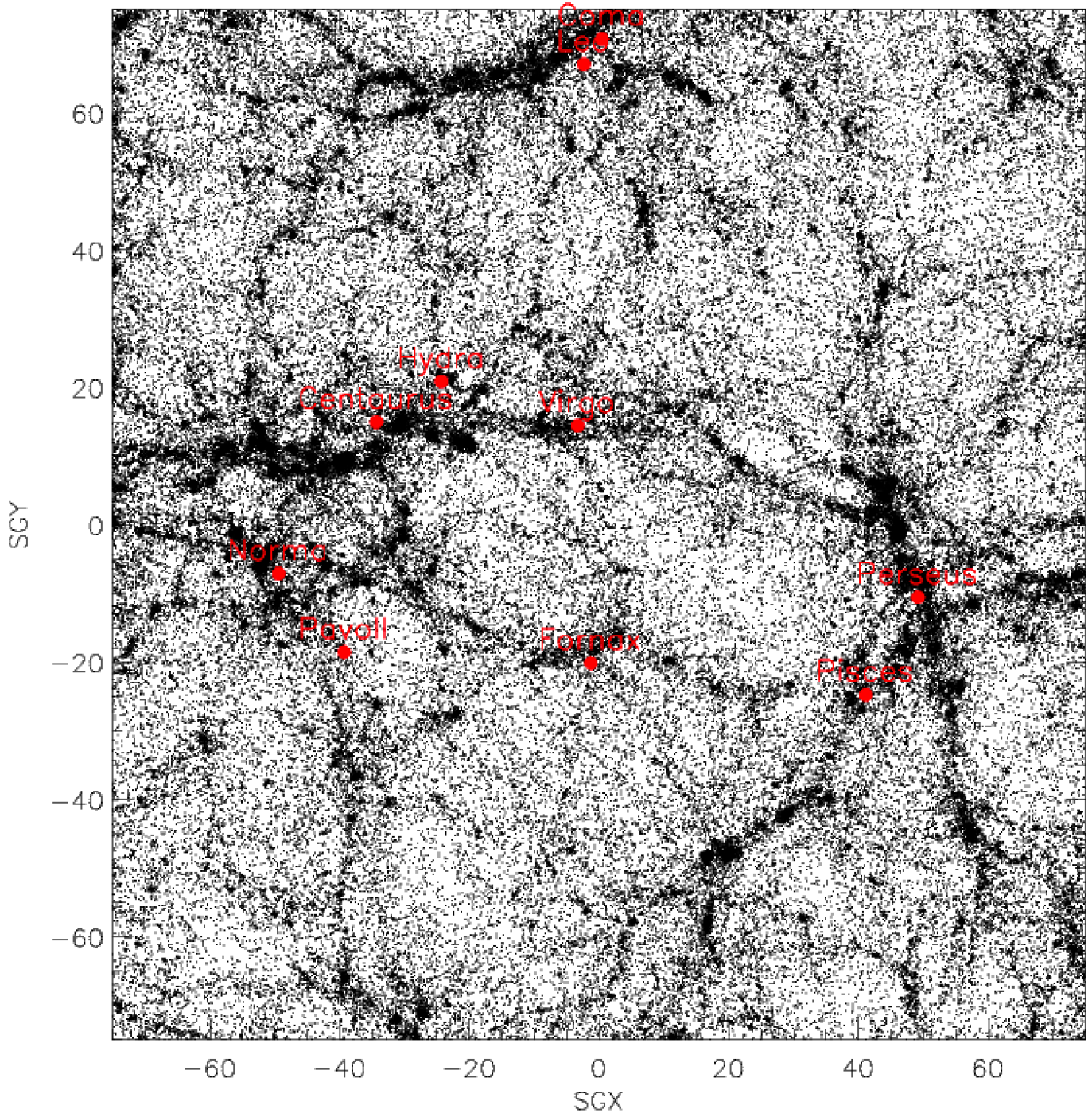
Coma
Leo
Hydra
Centaurus
Virgo
Norma
Perseus
Pavoll
Fornax
Pisces
60
40
20
0
−20
−40
−60
SGY
−60
−40
−20
0
20
40
60
SGX

Tree Codes

- obtaining the forces
  - Poisson's equation

$$\Delta\Phi(\vec{r}) = 4\pi G\rho(\vec{r})$$

$$\vec{F}(\vec{r}) = -m\nabla\Phi(\vec{r})$$

heart and soul of every *N*-body code

- obtaining the forces
  - Poisson's equation

$$\Delta\Phi(\vec{r}) = 4\pi G\rho(\vec{r})$$

$$\vec{F}(\vec{r}) = -m\nabla\Phi(\vec{r})$$

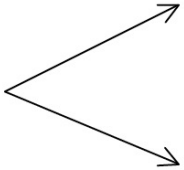

particle approach ($\vec{x}_i$ = comoving position of ith particle)

$$\vec{F}(\vec{x}_i) = -\sum_{i\neq j} \frac{Gm_i m_j}{(x_i - x_j)^3}(\vec{x}_i - \vec{x}_j)$$

grid approach ($\vec{r}_{i,j,k}$ = position of centre of grid cell (i,j,k))

$$\Delta\Phi(\vec{r}_{i,j,k}) = 4\pi G\rho(\vec{r}_{i,j,k})$$

$$\vec{F}(\vec{r}_{i,j,k}) = -m\nabla\Phi(\vec{r}_{i,j,k})$$

heart and soul of every *N*-body code

the particle approach

- direct particle-particle summation (PP)

$$\rho(\vec{r}) = \sum_{i=1}^{N} m_i \delta_{\text{Dirac}}(\vec{r} - \vec{r}_i)$$

analytical solution to Poisson's equation

$$\vec{F}_i(\vec{r}_i) = -\sum_{i \neq j} \frac{G m_i m_j}{(r_i - r_j)^3} (\vec{r}_i - \vec{r}_j) \quad \forall i \in N$$

- direct particle-particle summation (PP)

$$\rho(\vec{r}) = \sum_{i=1}^{N} m_i \delta_{\text{Dirac}}(\vec{r} - \vec{r}_i)$$

analytical solution to Poisson's equation

$$\vec{F}_i(\vec{r}_i) = -\sum_{i \neq j} \frac{G m_i m_j}{(r_i - r_j)^3} (\vec{r}_i - \vec{r}_j) \quad \forall i \in N$$

✓	advantage:	easy to code
↯	drawback:	extremely time consuming (N^2 operations)

- direct particle-particle summation (PP)

$$\rho(\vec{r}) = \sum_{i=1}^{N} m_i \delta_{\text{Dirac}}(\vec{r} - \vec{r}_i)$$

analytical solution to Poisson's equation

$$\vec{F}_i(\vec{r}_i) = -\sum_{i \neq j} \frac{G m_i m_j}{(r_i - r_j)^3} (\vec{r}_i - \vec{r}_j) \quad \forall i \in N$$

overcoming the "N^2" issue?!

✓	advantage:	easy to code
↯	drawback:	extremely time consuming (N^2 operations)

- direct particle-particle summation (PP)

$$\vec{F}_i(\vec{r}_i) = -\sum_{i \neq j} \frac{G m_i m_j}{(r_i - r_j)^3} (\vec{r}_i - \vec{r}_j) \quad \forall i \in N$$

organizing particles into a “tree structure” will give $N \log(N)$ operations

Solving for Gravity

- direct particle-particle summation (PP)

$$\vec{F}_i(\vec{r}_i) = -\sum_{i \neq j} \frac{G m_i m_j}{(r_i - r_j)^3} (\vec{r}_i - \vec{r}_j) \quad \forall i \in N$$

- generating the tree:

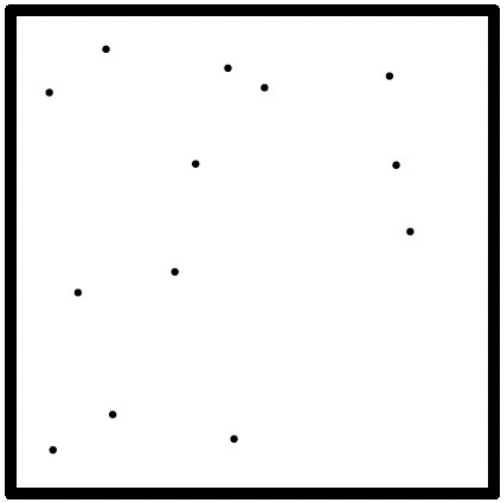

Solving for Gravity

- direct particle-particle summation (PP)

$$\vec{F}_i(\vec{r}_i) = -\sum_{i \neq j} \frac{G m_i m_j}{(r_i - r_j)^3} (\vec{r}_i - \vec{r}_j) \quad \forall i \in N$$

- generating the tree:

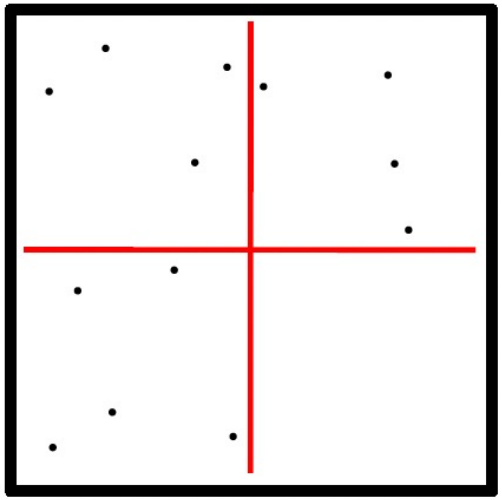

Solving for Gravity

- direct particle-particle summation (PP)

$$\vec{F}_i(\vec{r}_i) = -\sum_{i \neq j} \frac{G m_i m_j}{(r_i - r_j)^3} (\vec{r}_i - \vec{r}_j) \quad \forall i \in N$$

- generating the tree:

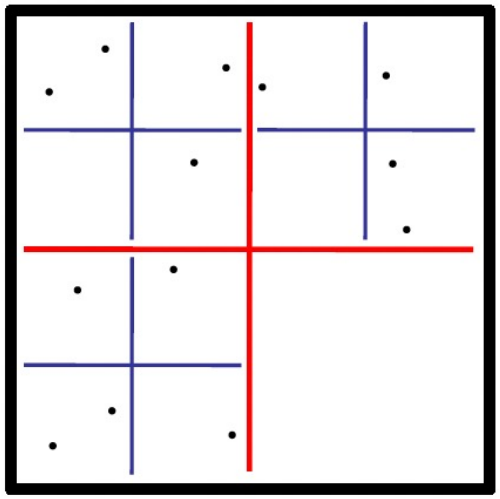

Solving for Gravity

- direct particle-particle summation (PP)

$$\vec{F}_i(\vec{r}_i) = -\sum_{i \neq j} \frac{G m_i m_j}{(r_i - r_j)^3} (\vec{r}_i - \vec{r}_j) \quad \forall i \in N$$

- generating the tree:

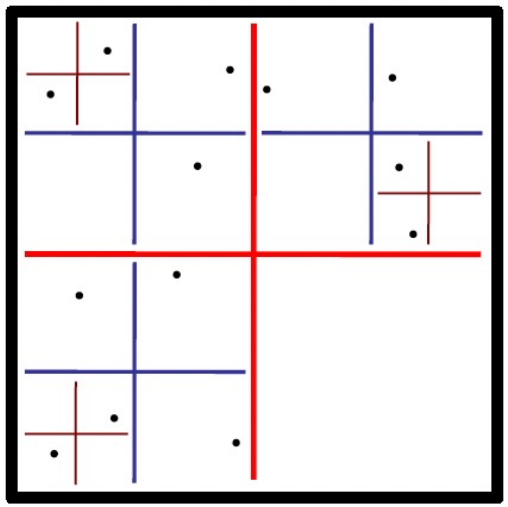

Solving for Gravity

- direct particle-particle summation (PP)

$$\vec{F}_i(\vec{r}_i) = -\sum_{i \neq j} \frac{G m_i m_j}{(r_i - r_j)^3} (\vec{r}_i - \vec{r}_j) \quad \forall i \in N$$

- generating the tree:

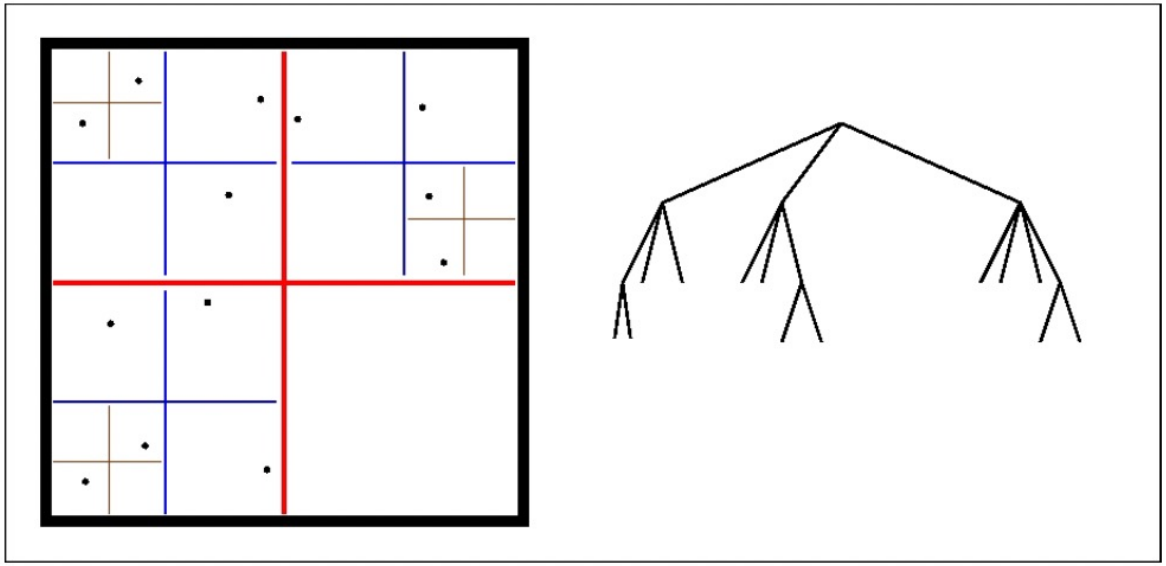

- direct particle-particle summation (PP)

$$\vec{F}_i(\vec{r}_i) = -\sum_{i \neq j} \frac{G m_i m_j}{(r_i - r_j)^3} (\vec{r}_i - \vec{r}_j) \quad \forall i \in N$$

- generating the tree:

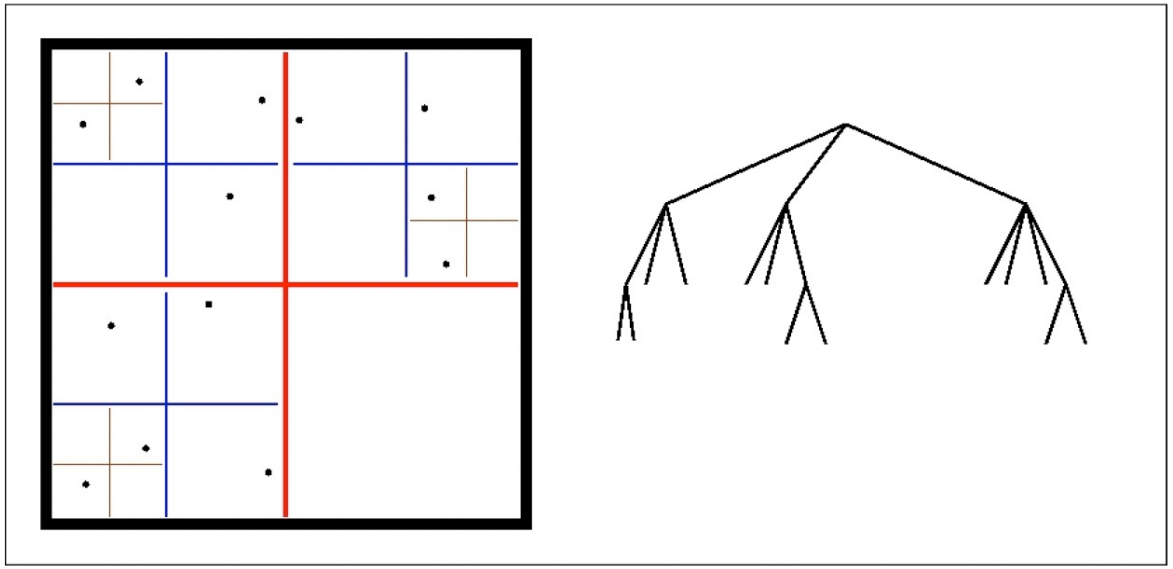

- direct particle-particle summation (PP)

$$\vec{F}_i(\vec{r}_i) = -\sum_{i \neq j} \frac{G m_i m_j}{(r_i - r_j)^3}(\vec{r}_i - \vec{r}_j) \quad \forall i \in N$$

- generating the tree:

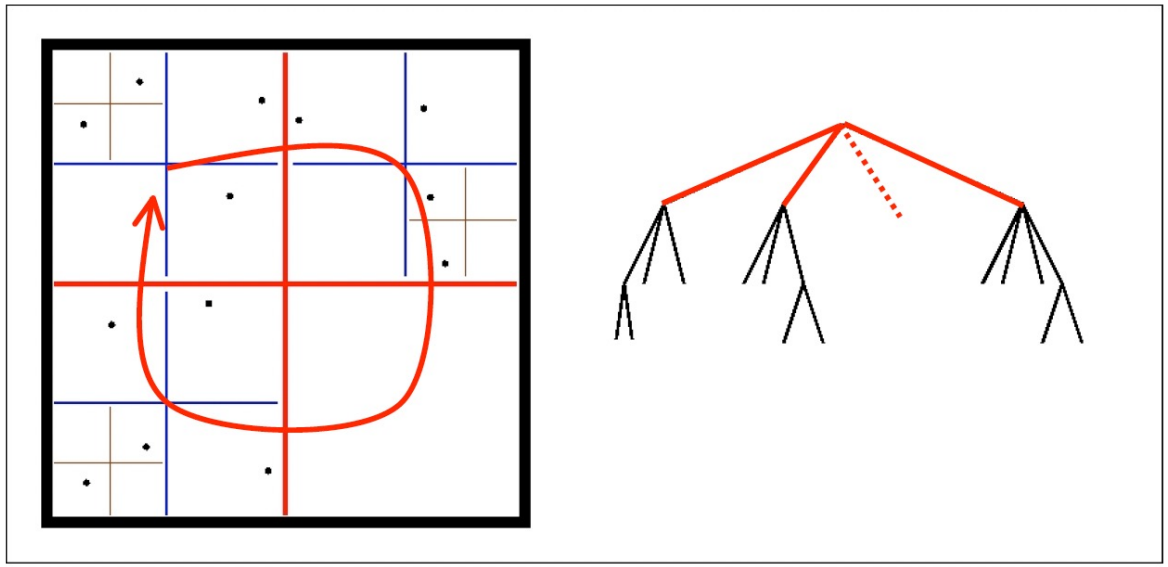

- direct particle-particle summation (PP)

$$\vec{F}_i(\vec{r}_i) = -\sum_{i \neq j} \frac{G m_i m_j}{(r_i - r_j)^3} (\vec{r}_i - \vec{r}_j) \quad \forall i \in N$$

- generating the tree:

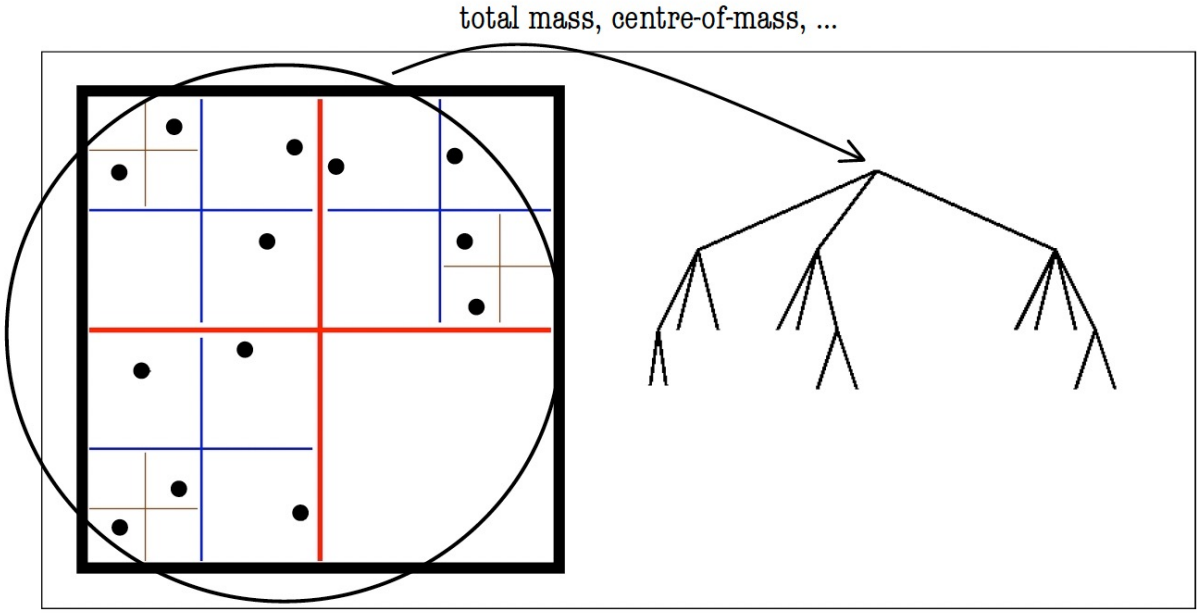

- direct particle-particle summation (PP)

$$\vec{F}_i(\vec{r}_i) = -\sum_{i \neq j} \frac{G m_i m_j}{(r_i - r_j)^3} (\vec{r}_i - \vec{r}_j) \quad \forall i \in N$$

- generating the tree:

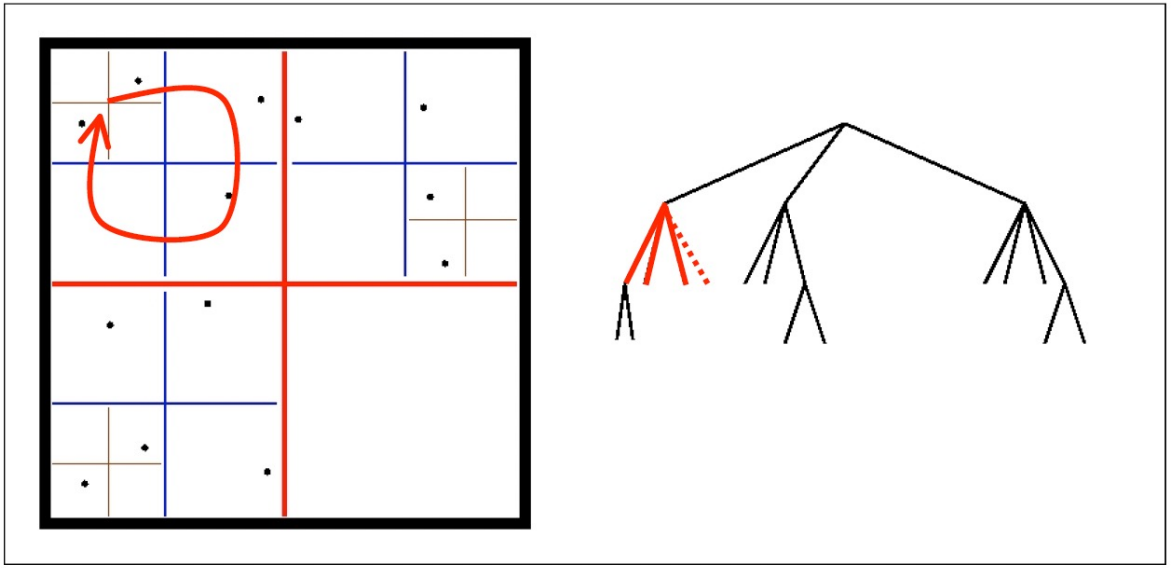

- direct particle-particle summation (PP)

$$\vec{F}_i(\vec{r}_i) = -\sum_{i \neq j} \frac{G m_i m_j}{(r_i - r_j)^3} (\vec{r}_i - \vec{r}_j) \quad \forall i \in N$$

- generating the tree:

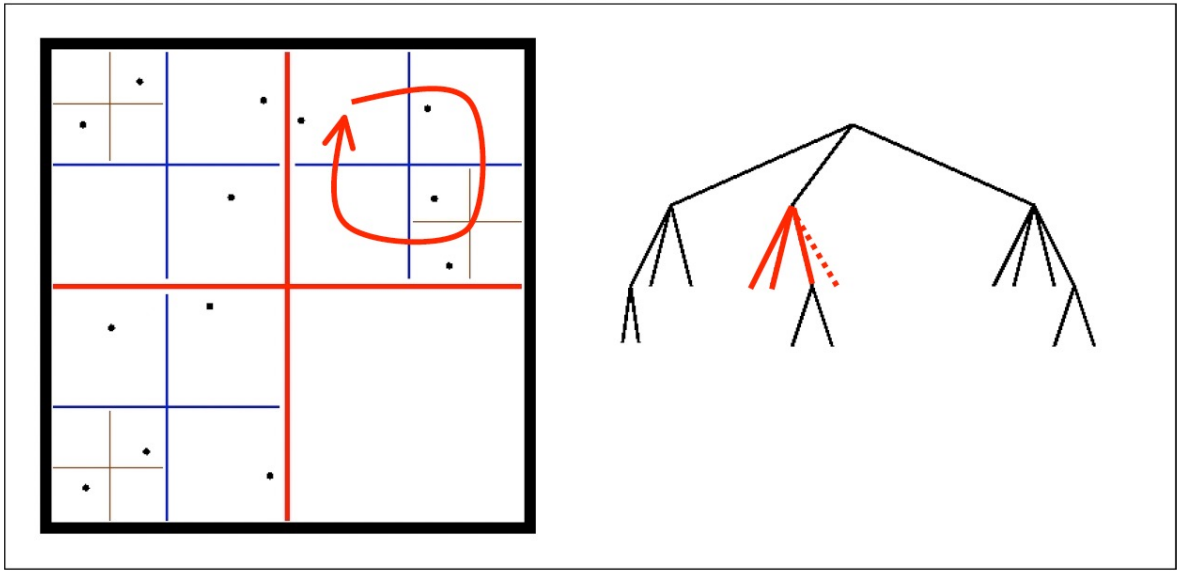

- direct particle-particle summation (PP)

$$\vec{F}_i(\vec{r}_i) = -\sum_{i \neq j} \frac{G m_i m_j}{(r_i - r_j)^3} (\vec{r}_i - \vec{r}_j) \quad \forall i \in N$$

- generating the tree:

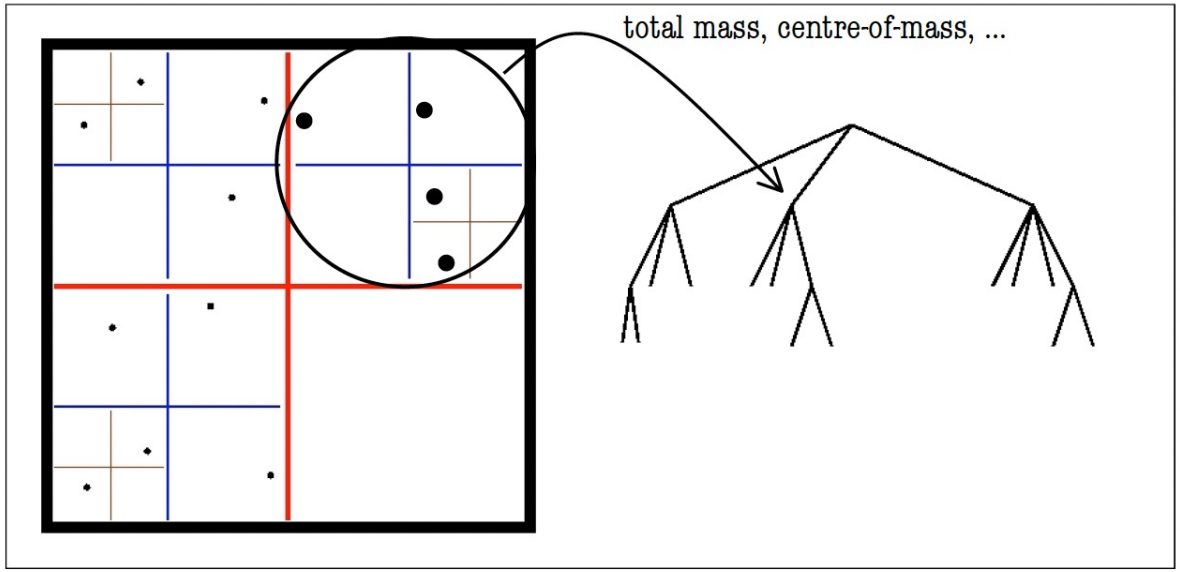

- direct particle-particle summation (PP)

$$\vec{F}_i(\vec{r}_i) = -\sum_{i \neq j} \frac{G m_i m_j}{(r_i - r_j)^3} (\vec{r}_i - \vec{r}_j) \quad \forall i \in N$$

- generating the tree:

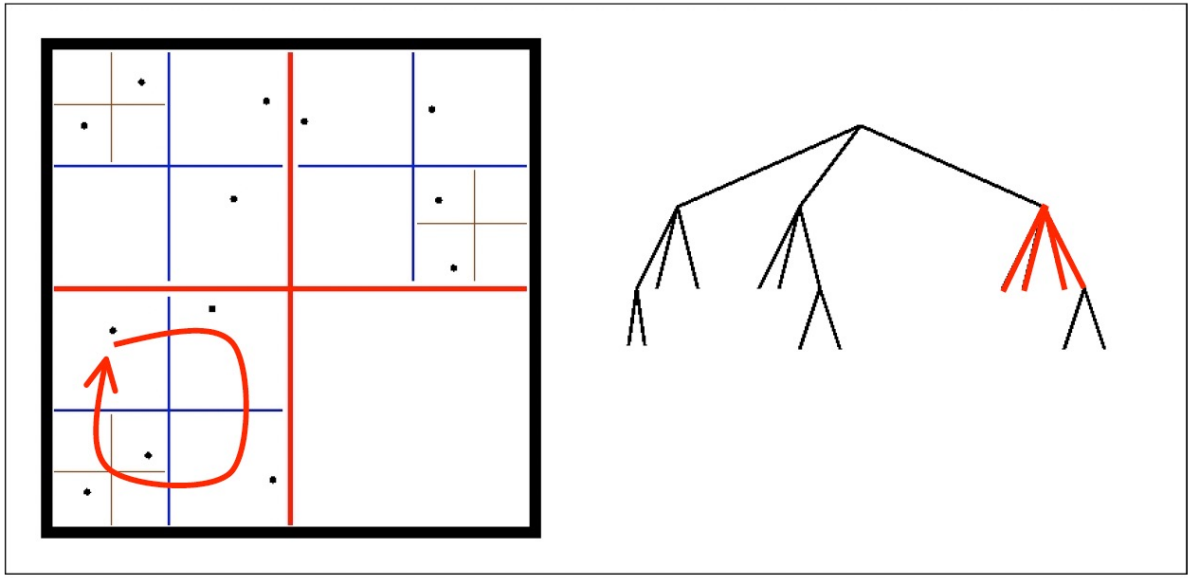

- direct particle-particle summation (PP)

$$\vec{F}_i(\vec{r}_i) = -\sum_{i \neq j} \frac{G m_i m_j}{(r_i - r_j)^3} (\vec{r}_i - \vec{r}_j) \quad \forall i \in N$$

- generating the tree:

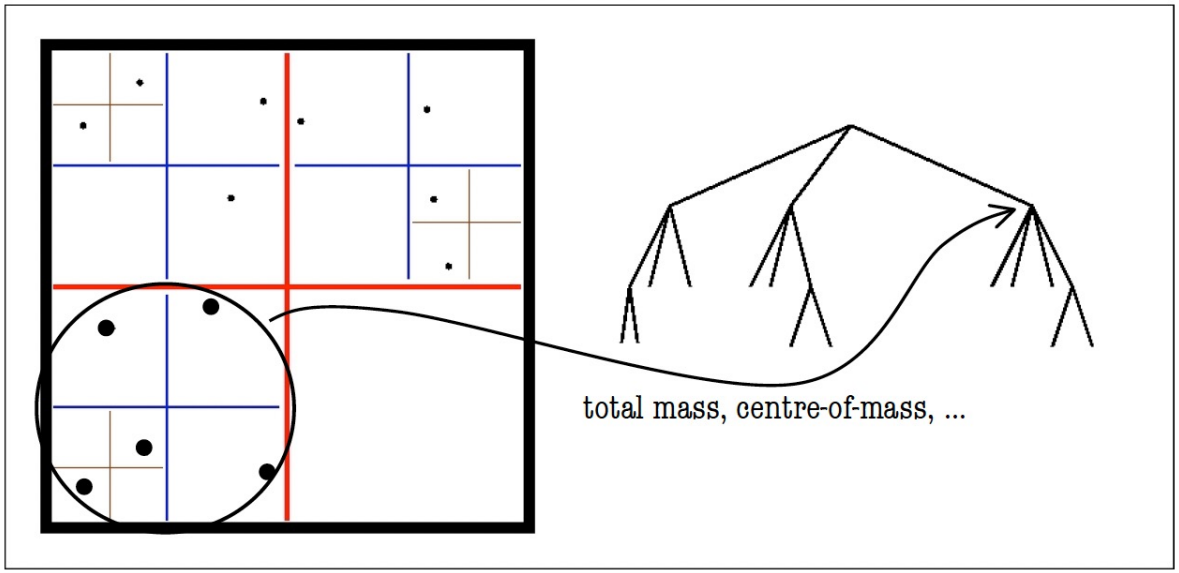

- direct particle-particle summation (PP)

$$\vec{F}_i(\vec{r}_i) = -\sum_{i \neq j} \frac{G m_i m_j}{(r_i - r_j)^3} (\vec{r}_i - \vec{r}_j) \quad \forall i \in N$$

- generating the tree:

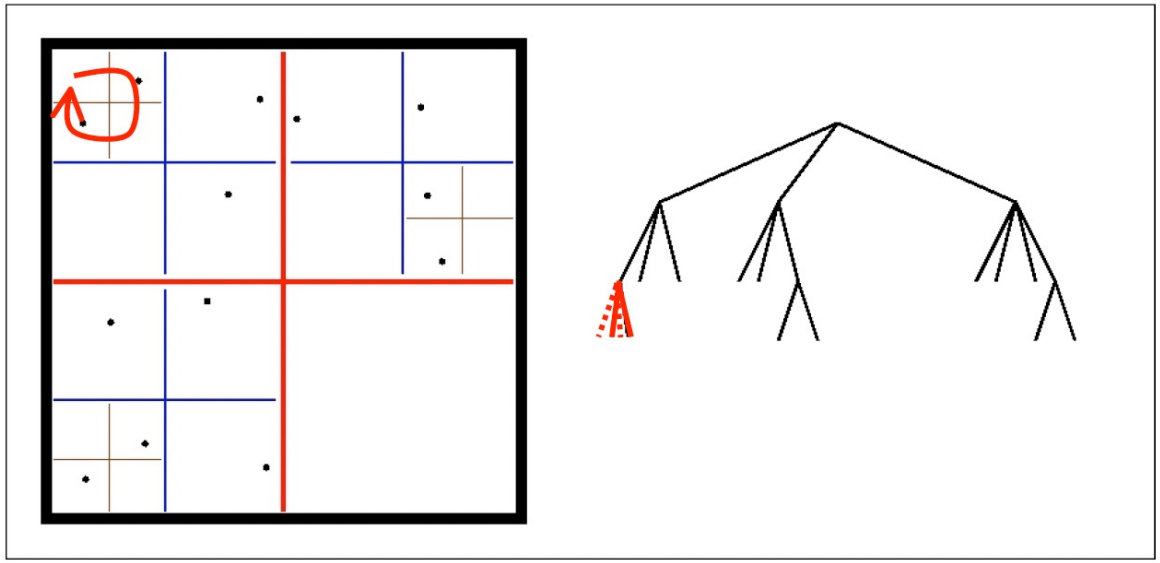

- direct particle-particle summation (PP)

$$\vec{F}_i(\vec{r}_i) = -\sum_{i \neq j} \frac{G m_i m_j}{(r_i - r_j)^3} (\vec{r}_i - \vec{r}_j) \quad \forall i \in N$$

- generating the tree:

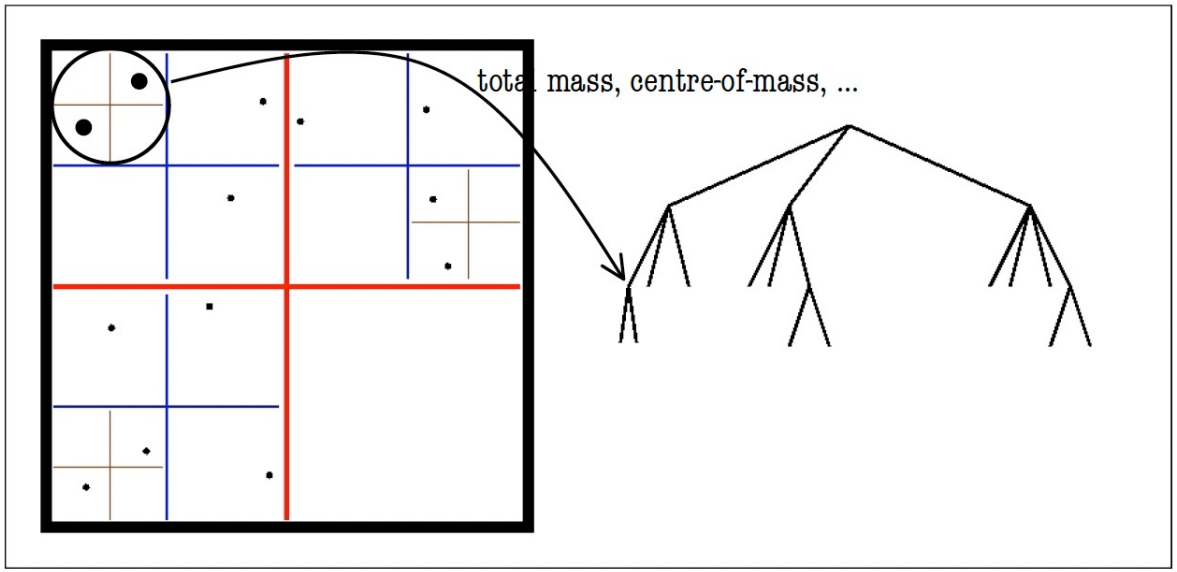

- direct particle-particle summation (PP)

$$\vec{F}_i(\vec{r}_i) = -\sum_{i \neq j} \frac{G m_i m_j}{(r_i - r_j)^3} (\vec{r}_i - \vec{r}_j) \quad \forall i \in N$$

- generating the tree:

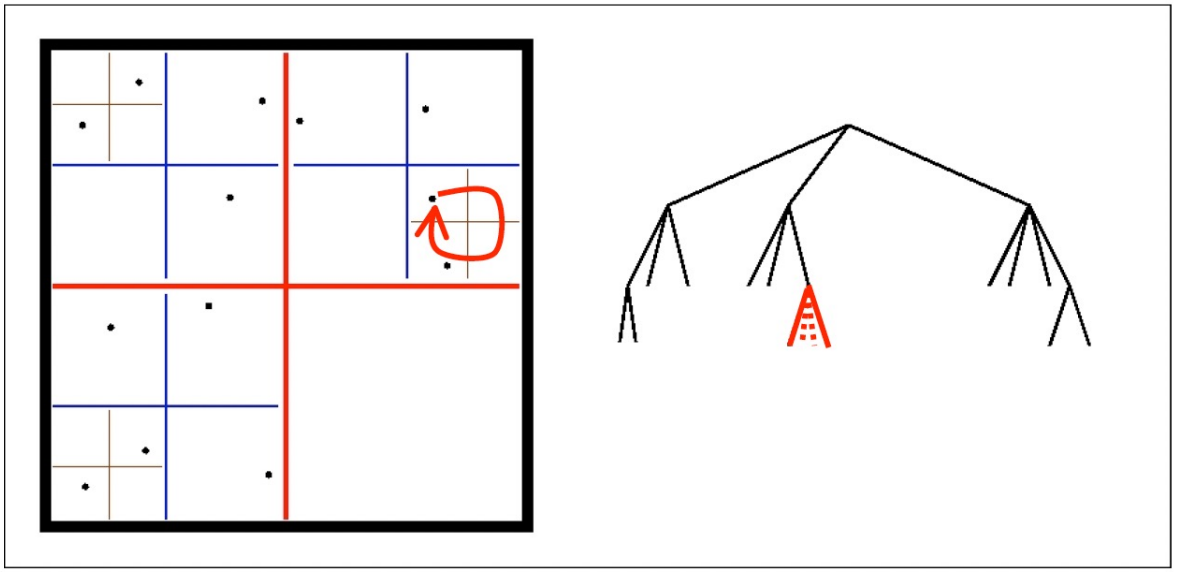

- direct particle-particle summation (PP)

$$\vec{F}_i(\vec{r}_i) = -\sum_{i \neq j} \frac{G m_i m_j}{(r_i - r_j)^3} (\vec{r}_i - \vec{r}_j) \quad \forall i \in N$$

- generating the tree:

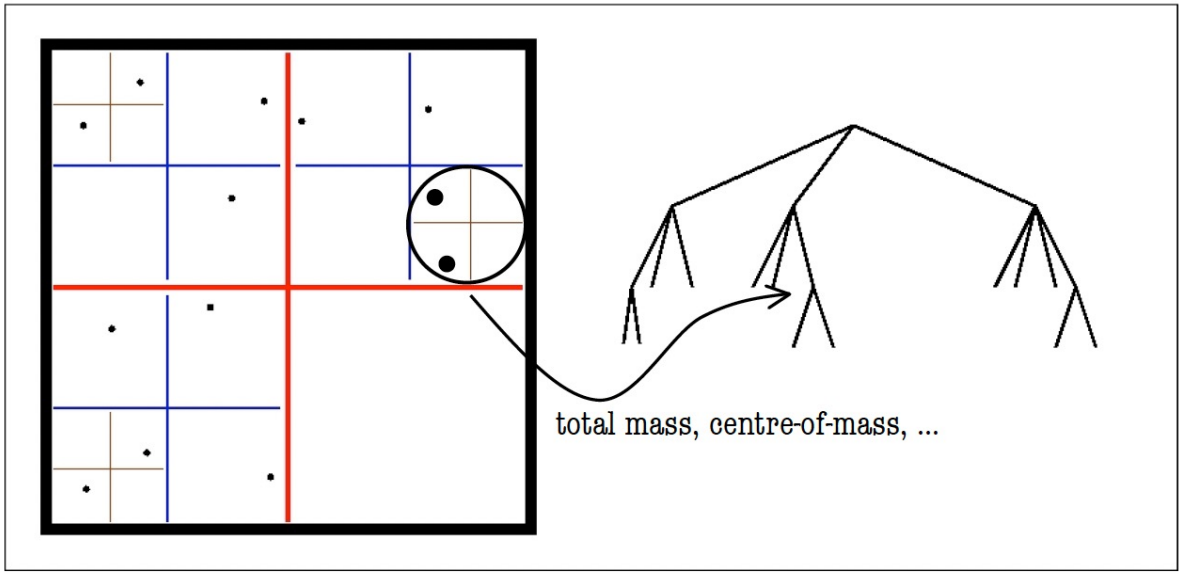

- direct particle-particle summation (PP)

$$\vec{F}_i(\vec{r}_i) = -\sum_{i \neq j} \frac{G m_i m_j}{(r_i - r_j)^3} (\vec{r}_i - \vec{r}_j) \quad \forall i \in N$$

- generating the tree:

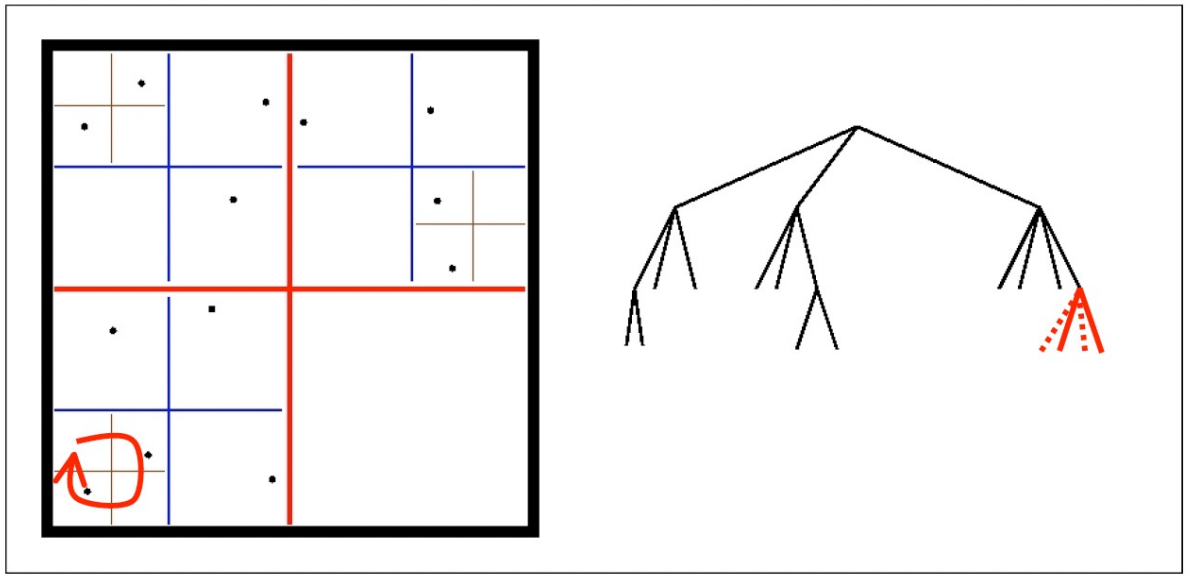

- direct particle-particle summation (PP)

$$\vec{F}_i(\vec{r}_i) = -\sum_{i \neq j} \frac{G m_i m_j}{(r_i - r_j)^3} (\vec{r}_i - \vec{r}_j) \quad \forall i \in N$$

- generating the tree:

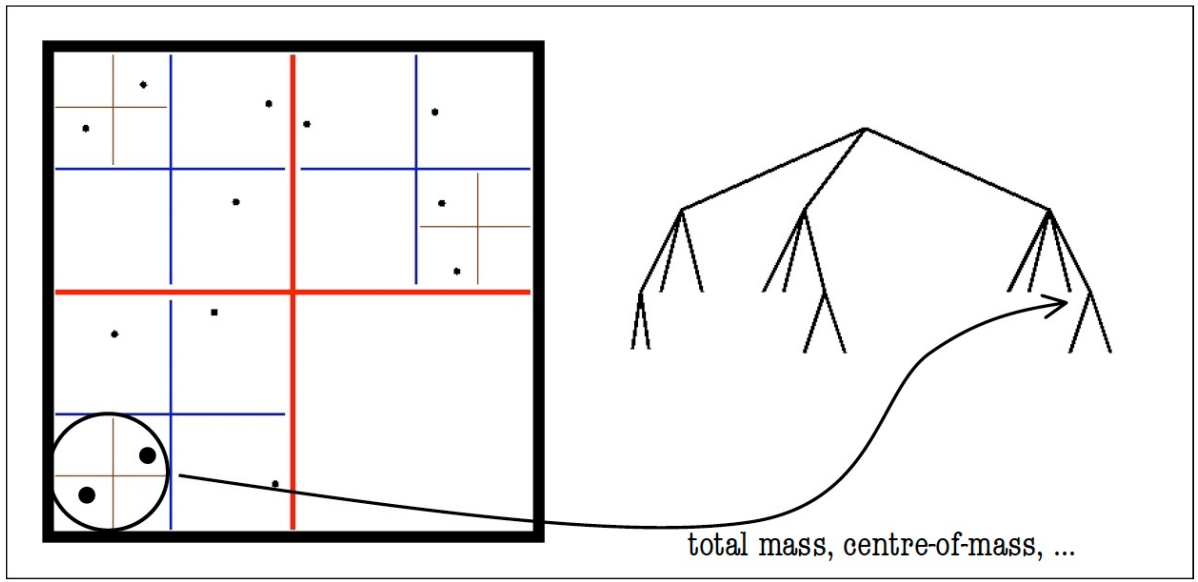

- direct particle-particle summation (PP)

$$\vec{F}_i(\vec{r}_i) = -\sum_{i \neq j} \frac{G m_i m_j}{(r_i - r_j)^3} (\vec{r}_i - \vec{r}_j) \quad \forall i \in N$$

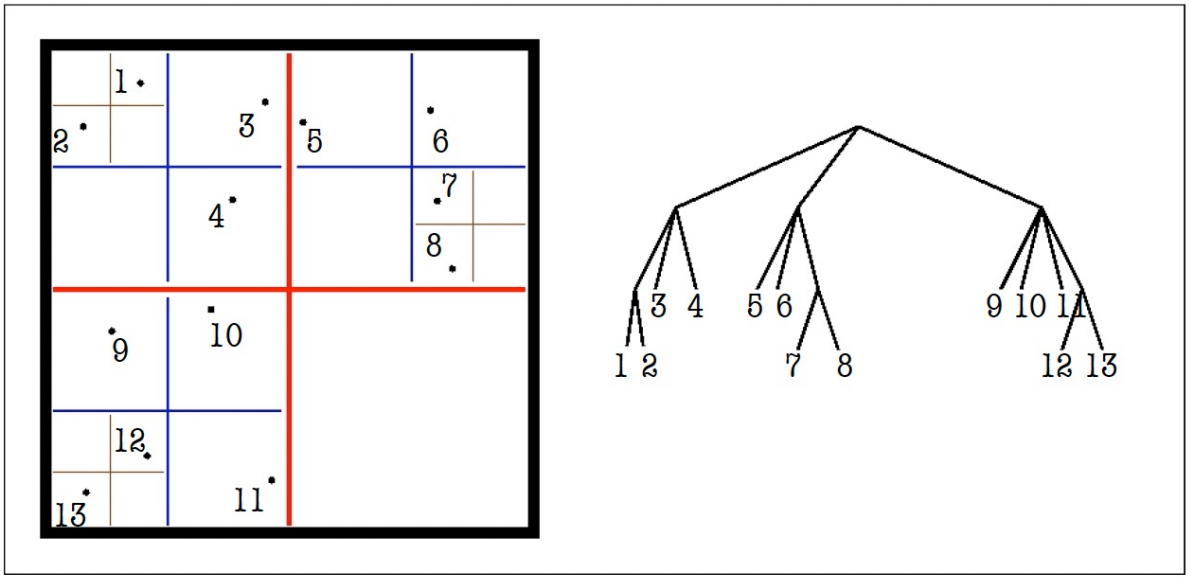

- direct particle-particle summation (PP)

$$\vec{F}_i(\vec{r}_i) = -\sum_{i \neq j} \frac{G m_i m_j}{(r_i - r_j)^3} (\vec{r}_i - \vec{r}_j) \quad \forall i \in N$$

- walking the tree ($\forall i \in N$):

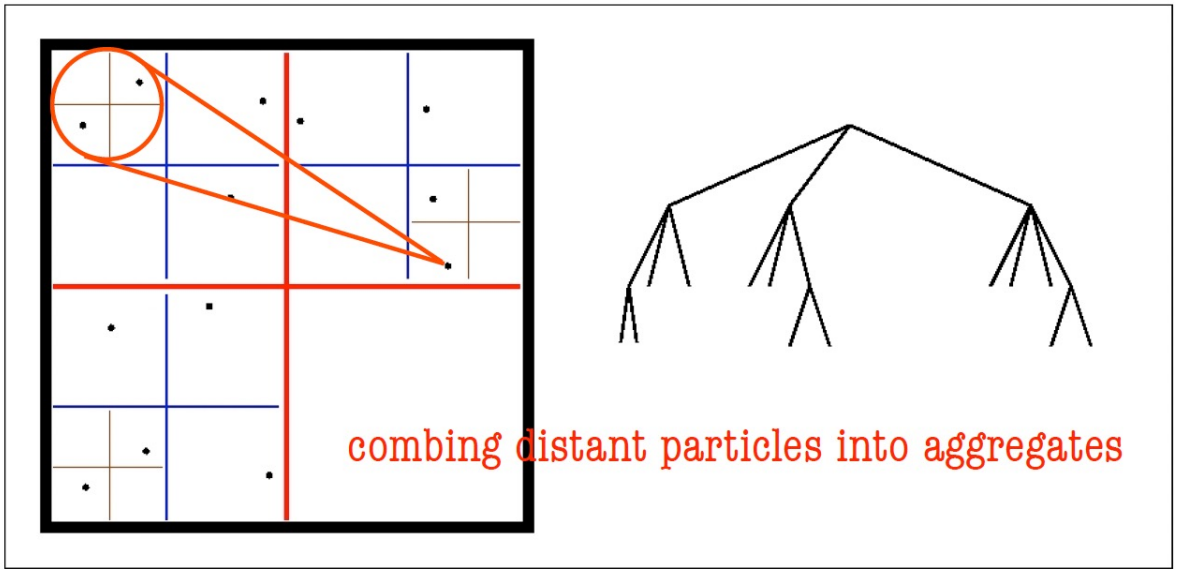

- direct particle-particle summation (PP)

$$\vec{F}_i(\vec{r}_i) = -\sum_{i \neq j} \frac{G m_i m_j}{(r_i - r_j)^3} (\vec{r}_i - \vec{r}_j) \quad \forall i \in N$$

- walking the tree ($\forall i \in N$):

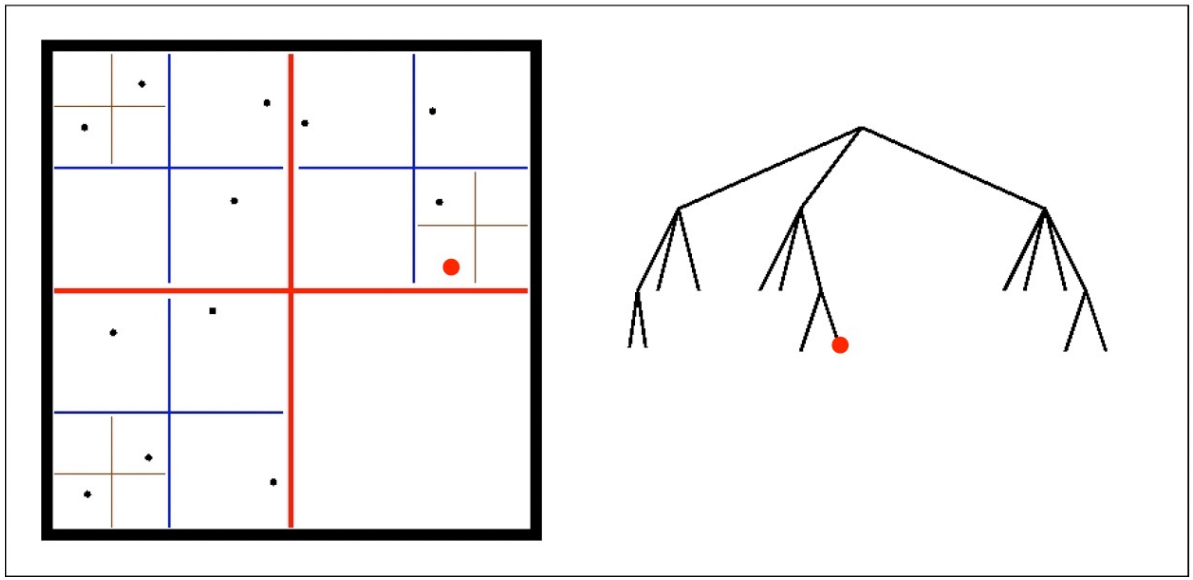

- direct particle-particle summation (PP)

$$\vec{F}_i(\vec{r}_i) = -\sum_{i \neq j} \frac{G m_i m_j}{(r_i - r_j)^3} (\vec{r}_i - \vec{r}_j) \quad \forall i \in N$$

- walking the tree ($\forall i \in N$):

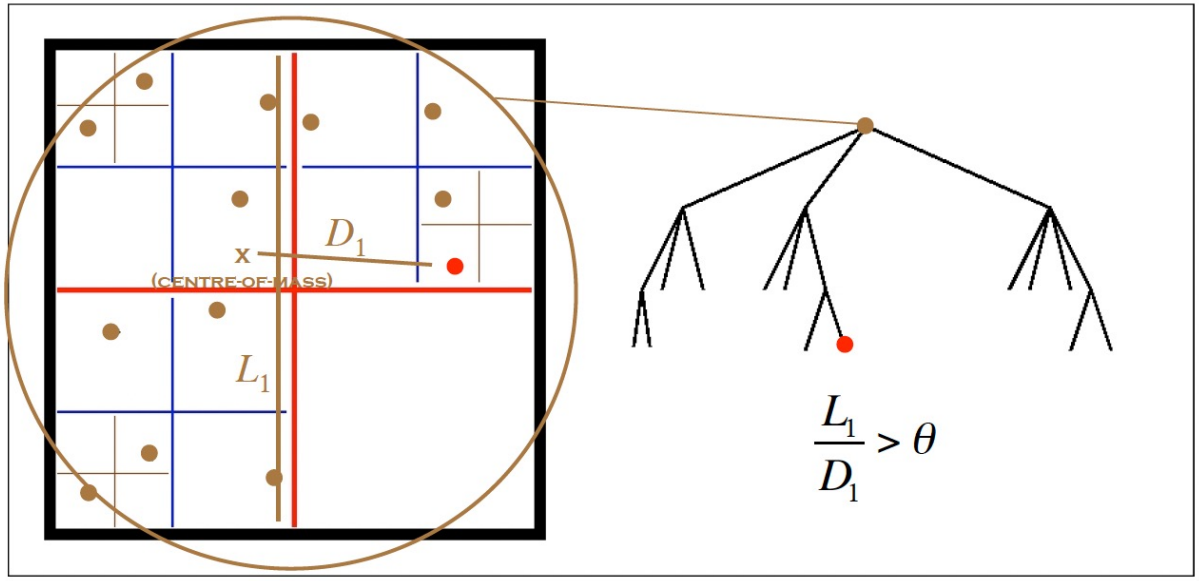

- direct particle-particle summation (PP)

$$\vec{F}_i(\vec{r}_i) = -\sum_{i \neq j} \frac{G m_i m_j}{(r_i - r_j)^3} (\vec{r}_i - \vec{r}_j) \quad \forall i \in N$$

- walking the tree ($\forall i \in N$):

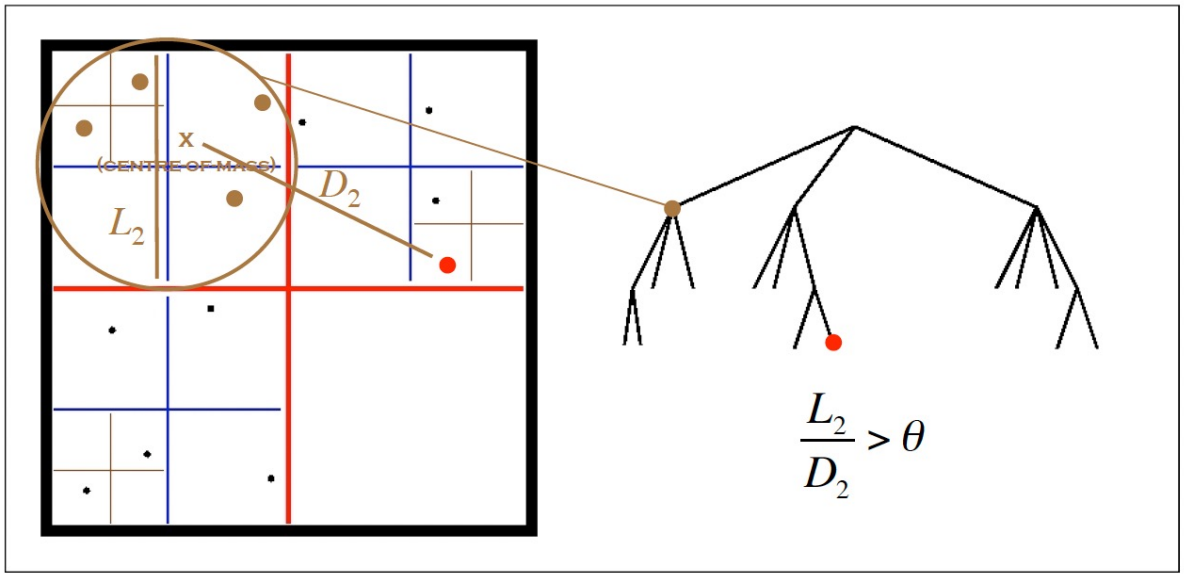

- direct particle-particle summation (PP)

$$\vec{F}_i(\vec{r}_i) = -\sum_{i \neq j} \frac{G m_i m_j}{(r_i - r_j)^3}(\vec{r}_i - \vec{r}_j) \quad \forall i \in N$$

- walking the tree ($\forall i \in N$):

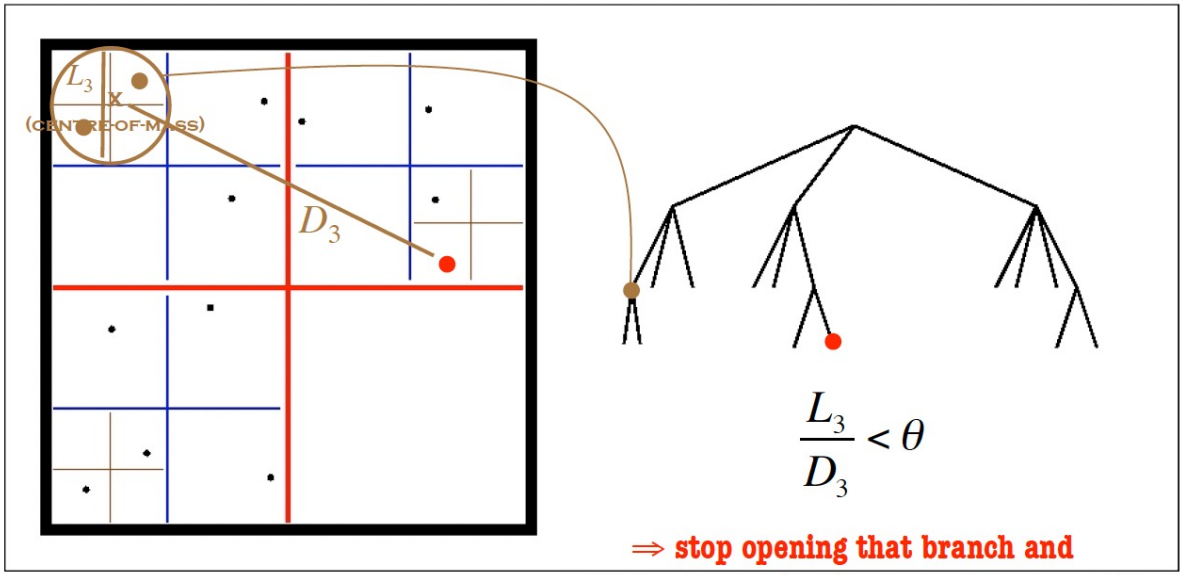

- direct particle-particle summation (PP)

$$\vec{F}_i(\vec{r}_i) = -\sum_{i \neq j} \frac{G m_i m_j}{(r_i - r_j)^3} (\vec{r}_i - \vec{r}_j) \quad \forall i \in N$$

- walking the tree ($\forall i \in N$):

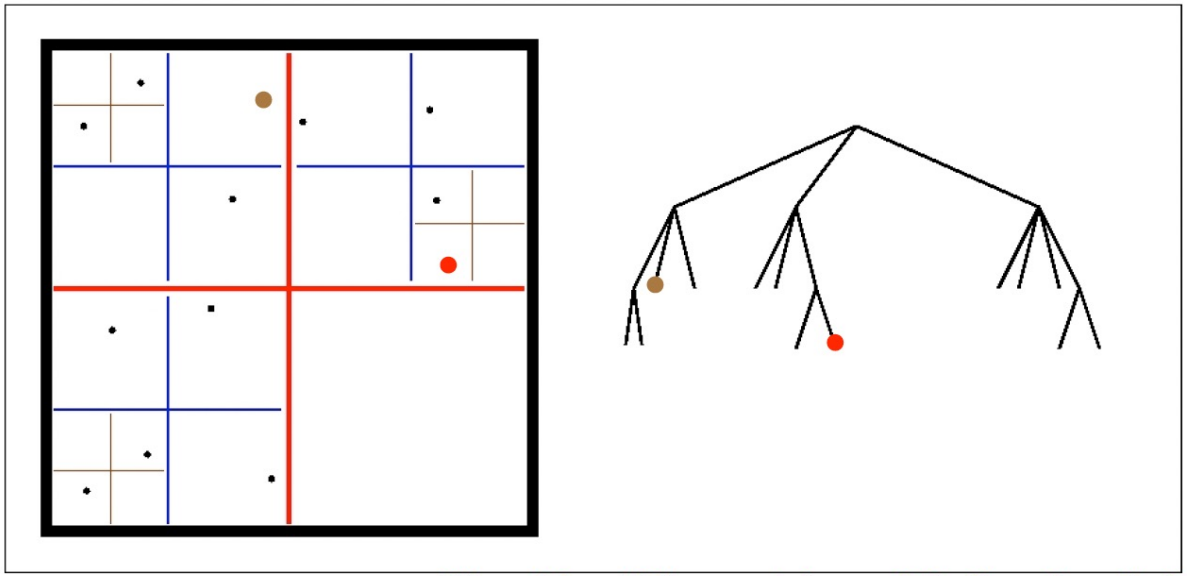

we still need to add the remaining contributions from that branch...

- direct particle-particle summation (PP)

$$\vec{F}_i(\vec{r}_i) = -\sum_{i \neq j} \frac{G m_i m_j}{(r_i - r_j)^3} (\vec{r}_i - \vec{r}_j) \quad \forall i \in N$$

- walking the tree ($\forall i \in N$):

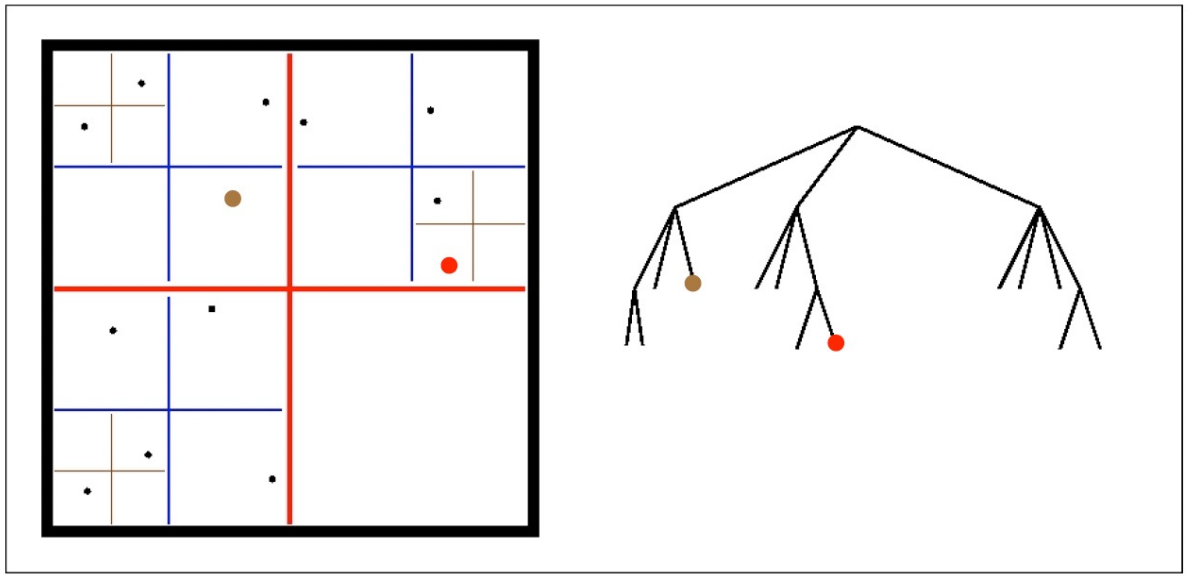

we still need to add the remaining contributions from that branch...

the grid approach

a.k.a.

the particle-mesh (PM) method

- numerically integrate Poisson's equation

$$\Delta\Phi(\vec{g}_{k,l,m}) = 4\pi G\left(\rho(\vec{g}_{k,l,m}) - \overline{\rho}\right)$$

$$\vec{F}(\vec{g}_{k,l,m}) = -m\nabla\Phi(\vec{g}_{k,l,m})$$

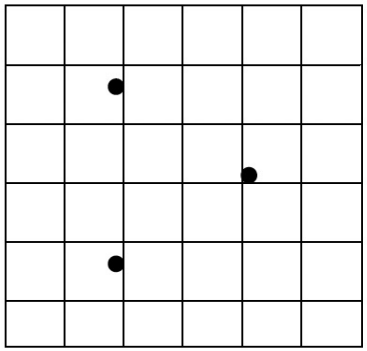

1. calculate mass density on grid $\quad \vec{x}_i \rightarrow \rho(\vec{g}_{k,l,m})$
2. solve Poisson's equation on grid $\quad \Phi(\vec{g}_{k,l,m})$
3. differentiate potential to get forces $\quad \vec{F}(\vec{g}_{k,l,m})$
4. interpolate forces back to particles $\quad \vec{F}(\vec{g}_{k,l,m}) \rightarrow \vec{F}(\vec{x}_i)$

- numerically integrate Poisson's equation

$$\Delta\Phi(\vec{g}_{k,l,m}) = 4\pi G\left(\rho(\vec{g}_{k,l,m}) - \overline{\rho}\right)$$

$$\vec{F}(\vec{g}_{k,l,m}) = -m\nabla\Phi(\vec{g}_{k,l,m})$$

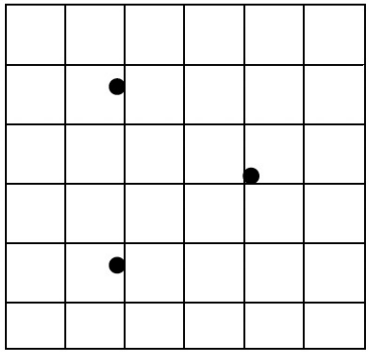

1. calculate mass density on grid $\quad \vec{x}_i \rightarrow \rho(\vec{g}_{k,l,m})$
2. solve Poisson's equation on grid $\quad \Phi(\vec{g}_{k,l,m})$
3. differentiate potential to get forces $\quad \vec{F}(\vec{g}_{k,l,m})$
4. interpolate forces back to particles $\quad \vec{F}(\vec{g}_{k,l,m}) \rightarrow \vec{F}(\vec{x}_i)$

sounds like a waste of time and computer resources,
but **exceptionally fast** in practice

- numerically integrate Poisson's equation

$$\Delta\Phi(\vec{g}_{k,l,m}) = 4\pi G\left(\rho(\vec{g}_{k,l,m}) - \overline{\rho}\right)$$

$$\vec{F}(\vec{g}_{k,l,m}) = -m\nabla\Phi(\vec{g}_{k,l,m})$$

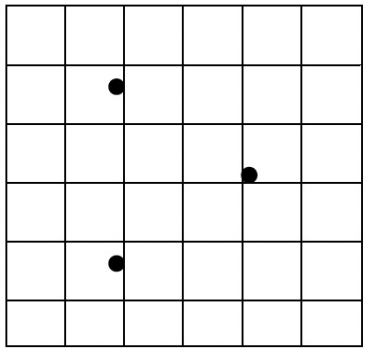

1. calculate mass density on grid $\quad \vec{x}_i \rightarrow \rho(\vec{g}_{k,l,m})$?
2. solve Poisson's equation on grid $\quad \Phi(\vec{g}_{k,l,m})$
3. differentiate potential to get forces $\quad \vec{F}(\vec{g}_{k,l,m})$
4. interpolate forces back to particles $\quad \vec{F}(\vec{g}_{k,l,m}) \rightarrow \vec{F}(\vec{x}_i)$

- density assignment schemes

$$\vec{x}_i \rightarrow \rho(\vec{g}_{k,l,m})$$

example: 1 particle on 1 dimensional grid

$$M(g_k) = mW(d) \qquad d = |x - g_k|$$

mass assignment function

$$\rho(g_k) = \frac{M(g_k)}{H}$$

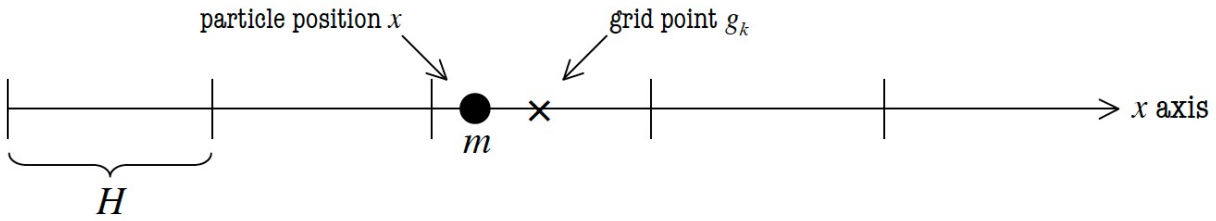

- density assignment schemes

$$\vec{x}_i \rightarrow \rho(\vec{g}_{k,l,m})$$

example: 1 particle on 1 dimensional grid

- hierarchy of mass assignment schemes:
  - Nearest-Grid-Point NGP
  - Could-In-Cell CIC
  - Triangular-Shaped Cloud TSC
  - ...

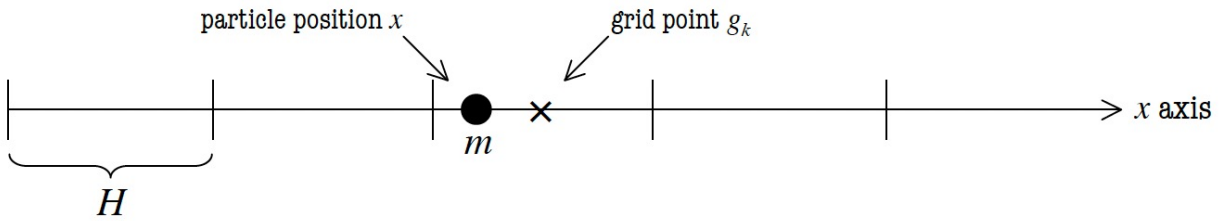

- density assignment schemes

$$\vec{x}_i \rightarrow \rho(\vec{g}_{k,l,m})$$

Nearest-Grid-Point (NGP):

mass assignment function:

$$W(d) = \begin{cases} 1 & d \le H/2 \\ 0 & \text{otherwise} \end{cases}$$

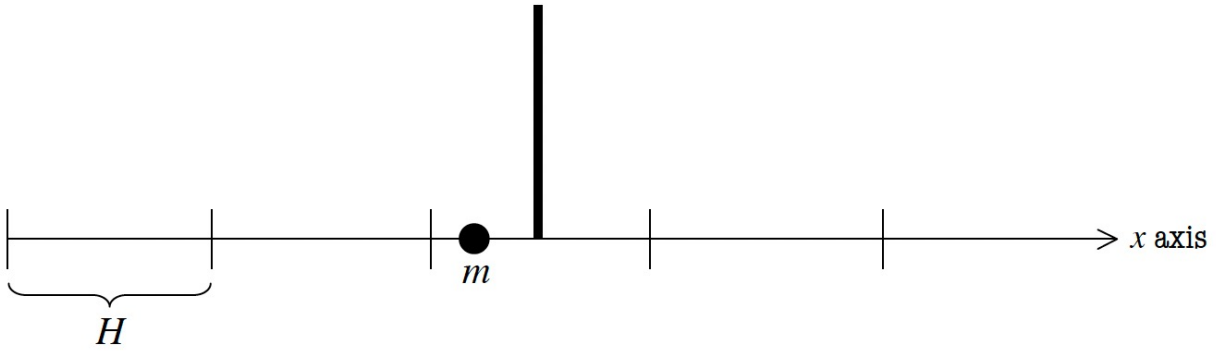

- density assignment schemes

$$\vec{x}_i \rightarrow \rho(\vec{g}_{k,l,m})$$

Nearest-Grid-Point (NGP):

particle shape:

$$S(x) = \delta(x)$$

mass assignment function:

$$W(d) = \begin{cases} 1 & d \le H/2 \\ 0 & \text{otherwise} \end{cases}$$

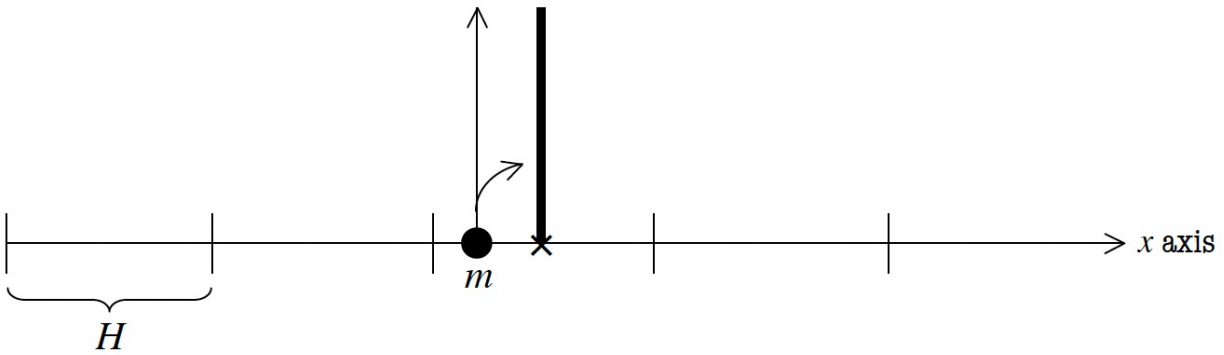

- density assignment schemes

$$\vec{x}_i \rightarrow \rho(\vec{g}_{k,l,m})$$

Cloud-In-Cell (CIC):

mass assignment function:

$$W(d) = \begin{cases} 1 - \dfrac{d}{H} & d \le H \\ 0 & \text{otherwise} \end{cases}$$

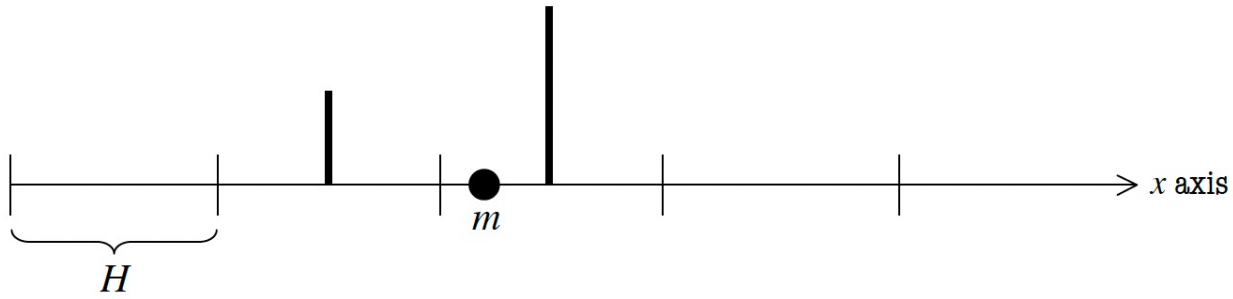

- density assignment schemes

$$\vec{x}_i \rightarrow \rho(\vec{g}_{k,l,m})$$

Cloud-In-Cell (CIC):

particle shape:

$$S(x) = \begin{cases} 1 & |x| \le H/2 \\ 0 & \text{otherwise} \end{cases}$$

mass assignment function:

$$W(d) = \begin{cases} 1 - \dfrac{d}{H} & d \le H \\ 0 & \text{otherwise} \end{cases}$$

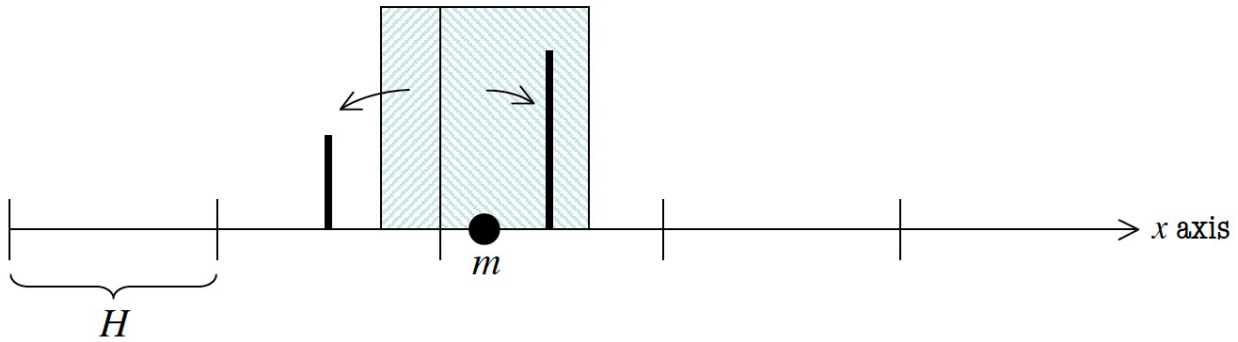

- density assignment schemes

$$\vec{x}_i \rightarrow \rho(\vec{g}_{k,l,m})$$

Triangular-Shaped-Cloud (TSC):

mass assignment function:

$$W(d) = \begin{cases} \frac{3}{4} - \left(\frac{d}{H}\right)^2 & d \le \frac{H}{2} \\ \frac{1}{2}\left(\frac{3}{2} - \frac{d}{H}\right)^2 & \frac{H}{2} \le d \le \frac{3H}{2} \\ 0 & \text{otherwise} \end{cases}$$

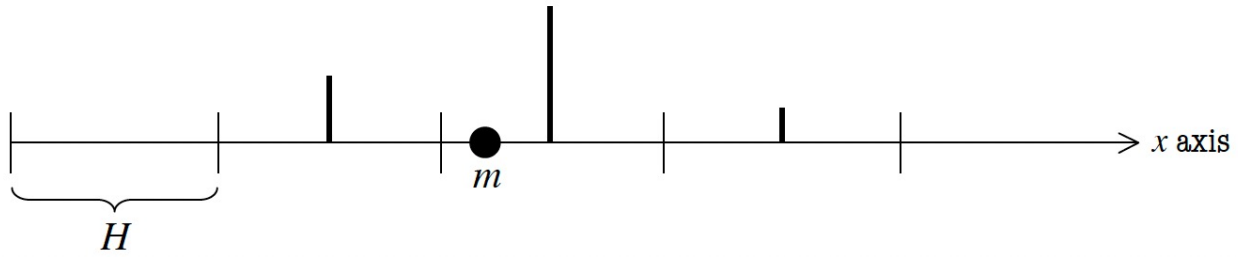

- density assignment schemes

$$\vec{x}_i \rightarrow \rho(\vec{g}_{k,l,m})$$

Triangular-Shaped-Cloud (TSC):

particle shape:

$$S(x) = \begin{cases} 1 - \dfrac{|x|}{H} & |x| \le H \\ 0 & \text{otherwise} \end{cases}$$

mass assignment function:

$$W(d) = \begin{cases} \dfrac{3}{4} - \left(\dfrac{d}{H}\right)^2 & d \le \dfrac{H}{2} \\ \dfrac{1}{2}\left(\dfrac{3}{2} - \dfrac{d}{H}\right)^2 & \dfrac{H}{2} \le d \le \dfrac{3H}{2} \\ 0 & \text{otherwise} \end{cases}$$

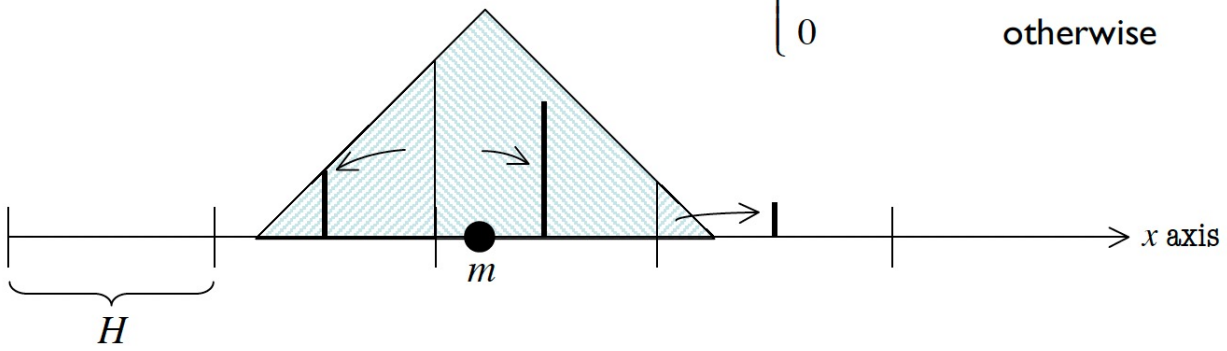

- density assignment schemes

$$\vec{x}_i \rightarrow \rho(\vec{g}_{k,l,m})$$

N particles on 3 dimensional grid

$$\vec{d} = \vec{x}_i - \vec{g}_{k,l,m}$$

$$M(\vec{g}_{k,l,m}) = \sum_{i=1}^{N} m_i W(|d_x|) W(|d_y|) W(|d_z|)$$

$$\rho(\vec{g}_{k,l,m}) = \frac{M(\vec{g}_{k,l,m})}{H^3}$$

- density assignment schemes

$$\vec{x}_i \rightarrow \rho(\vec{g}_{k,l,m})$$

N particles on 3 dimensional grid

$$\vec{d} = \vec{x}_i - \vec{g}_{k,l,m}$$

$$M(\vec{g}_{k,l,m}) = \sum_{i=1}^{N} m_i W(|d_x|) W(|d_y|) W(|d_z|)$$

for every grid point we need to loop over all *N* particles...

$$\rho(\vec{g}_{k,l,m}) = \frac{M(\vec{g}_{k,l,m})}{H^3}$$

- density assignment schemes - in practice

$$\vec{x}_i \rightarrow \rho(\vec{g}_{k,l,m})$$

- example for CIC assignment in 2D:

$\vec{x}_i$ contributes its mass m_i to the 4 closest grid points :

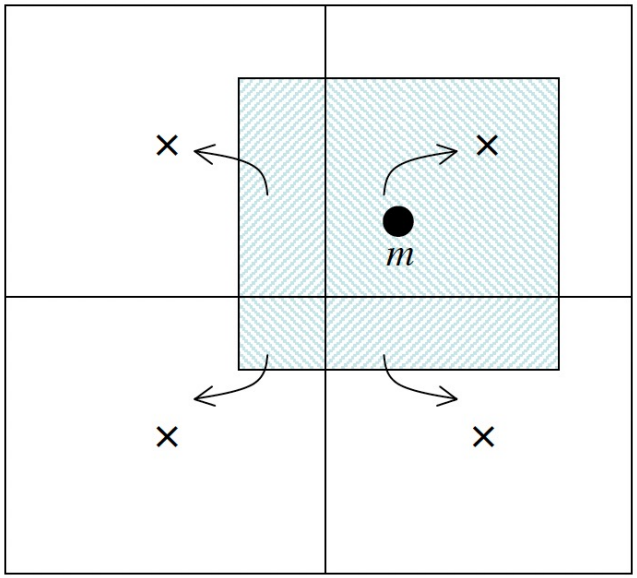

- density assignment schemes - in practice

$$\vec{x}_i \rightarrow \rho(\vec{g}_{k,l,m})$$

- example for CIC assignment in 3D:

$\vec{x}_i$ contributes its mass m_i to the 8 closest grid points :

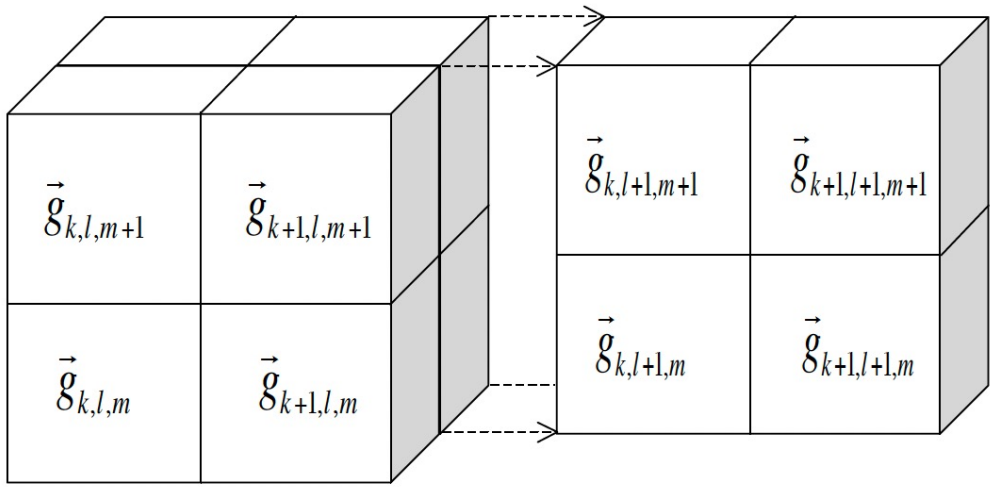

- density assignment schemes
  - which scheme to choose?

NGP = stepwise force	(1 grid point)
CIC = continuous piecewise linear force	(8 grid points)
TSC = continuous force and first derivative	(27 grid points)

- density assignment schemes
  - which scheme to choose?

NGP = too crude

CIC = common choice

TSC = pretty smooth

increased smoothing of density field

smoothing the density field will lead to a “bias” in the forces
but at the same time decrease the “variance”! (more later...)

- density assignment schemes
  - which scheme to choose?

NGP = too crude

CIC = common choice

TSC = pretty smooth

increased smoothing of density field

smoothing the density field will lead to a “bias” in the forces
but at the same time decrease the “variance”! (more later...)

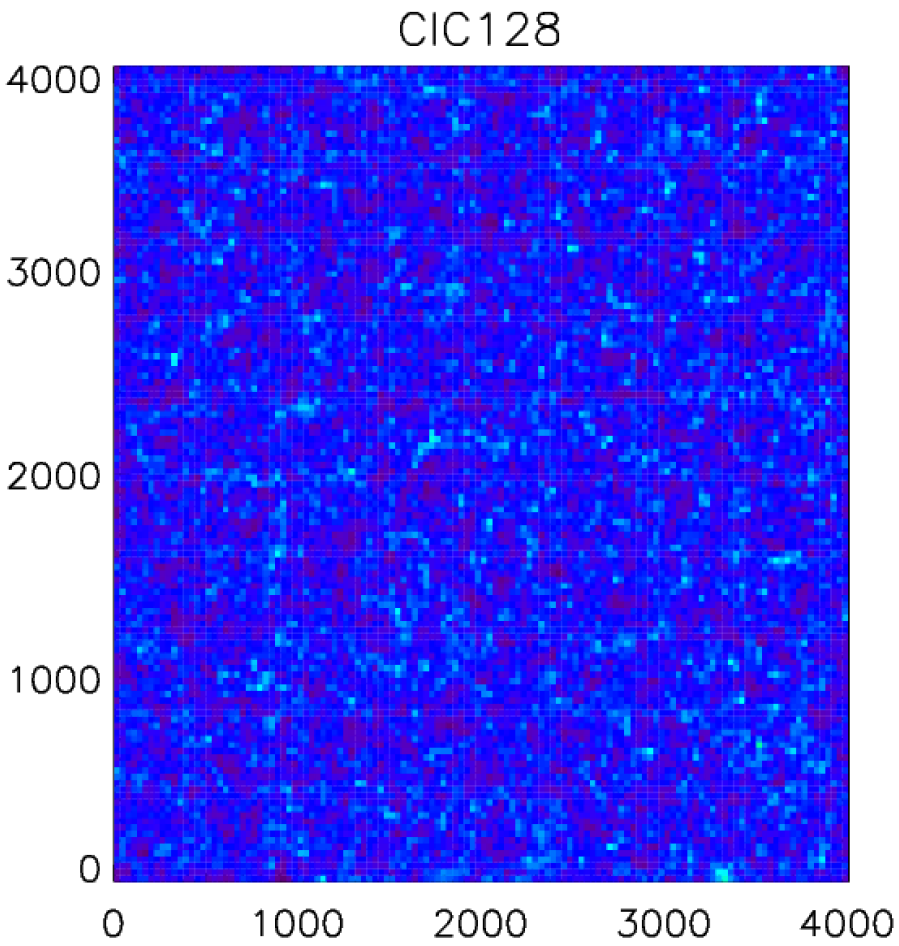
CIC128
4000
3000
2000
1000
0
0
1000
2000
3000
4000

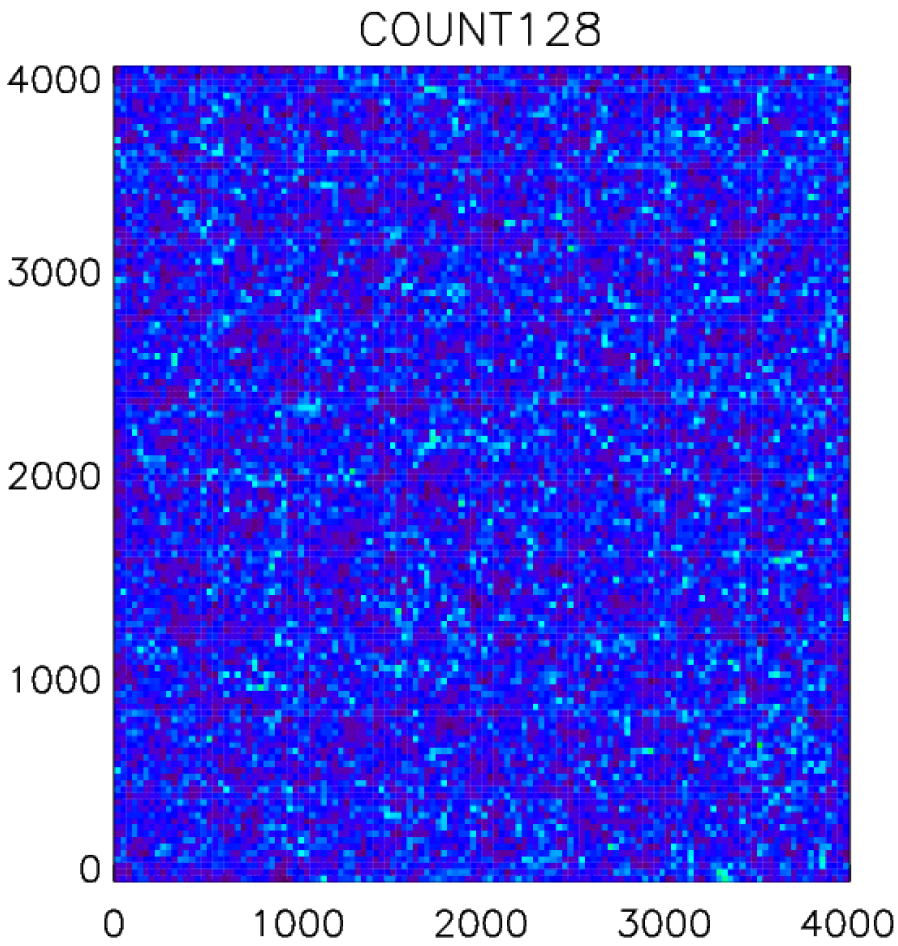
COUNT128
4000
3000
2000
1000
0
0
1000
2000
3000
4000

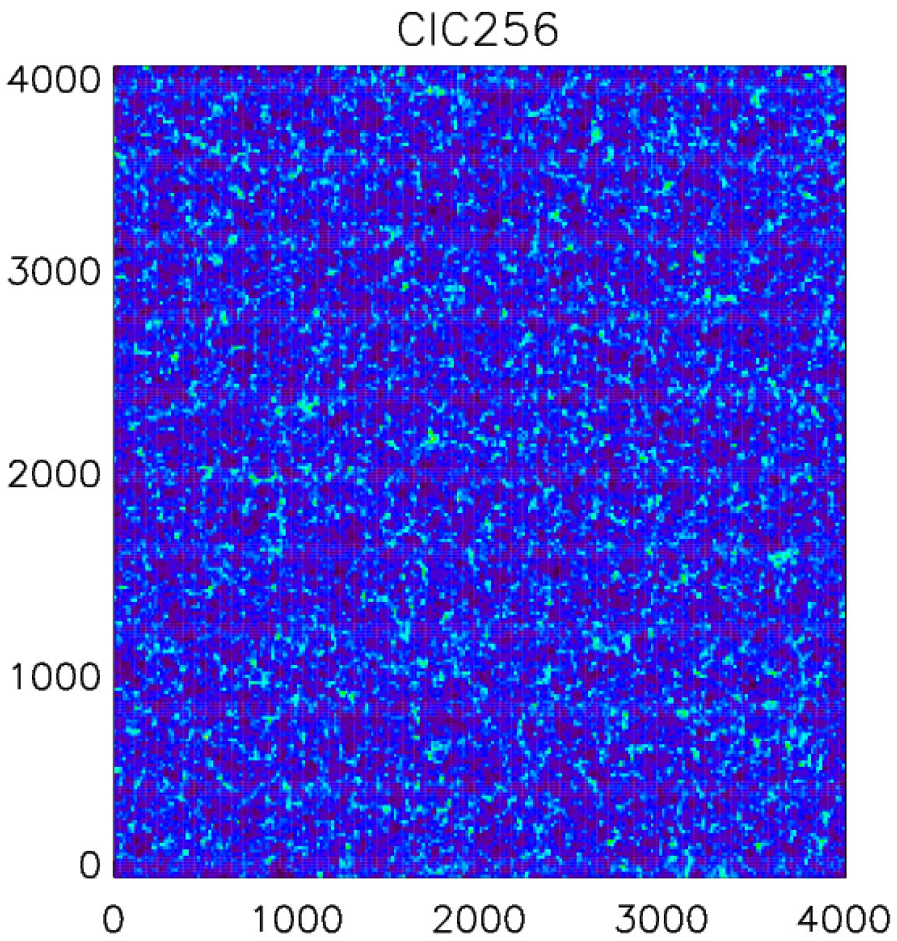
CIC256
4000
3000
2000
1000
0
0
1000
2000
3000
4000

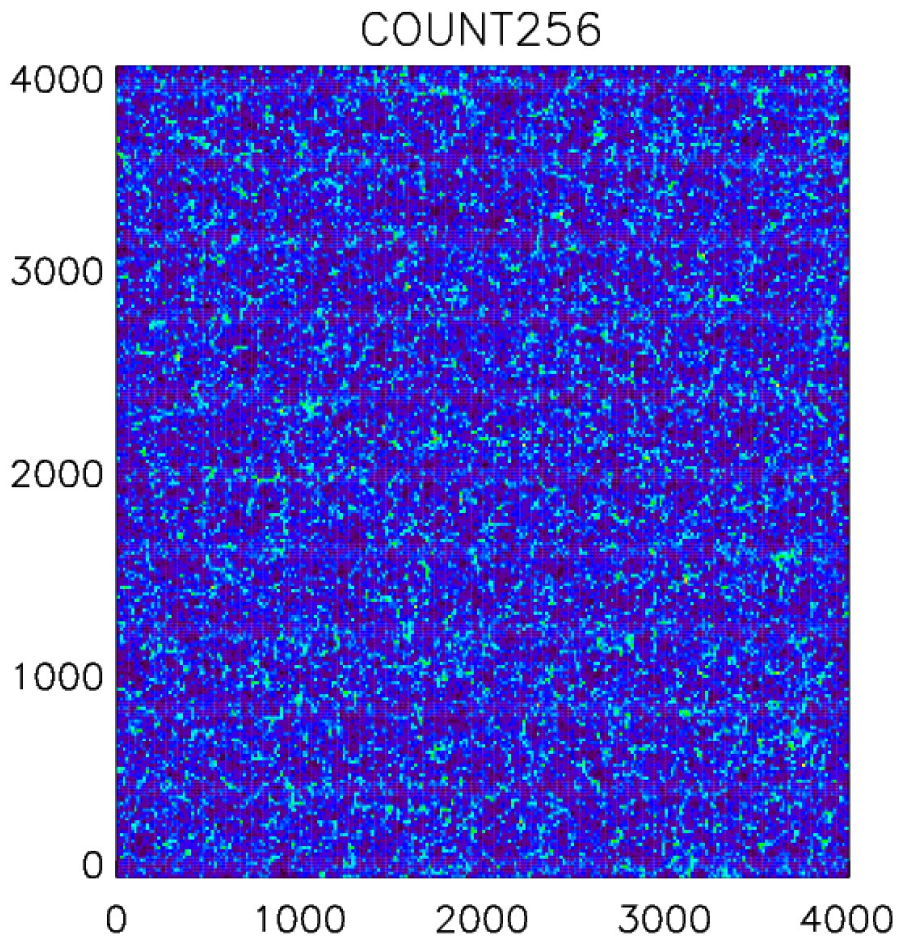
COUNT256
4000
3000
2000
1000
0
0
1000
2000
3000
4000

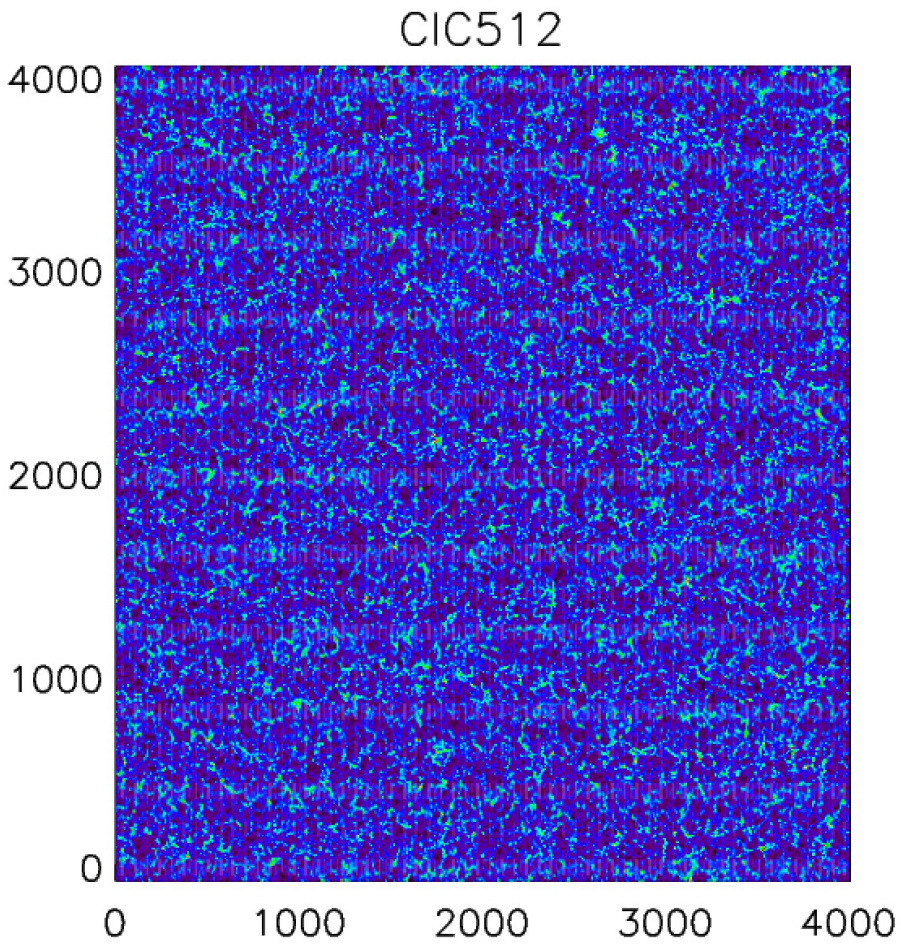
CIC512
4000
3000
2000
1000
0
0
1000
2000
3000
4000

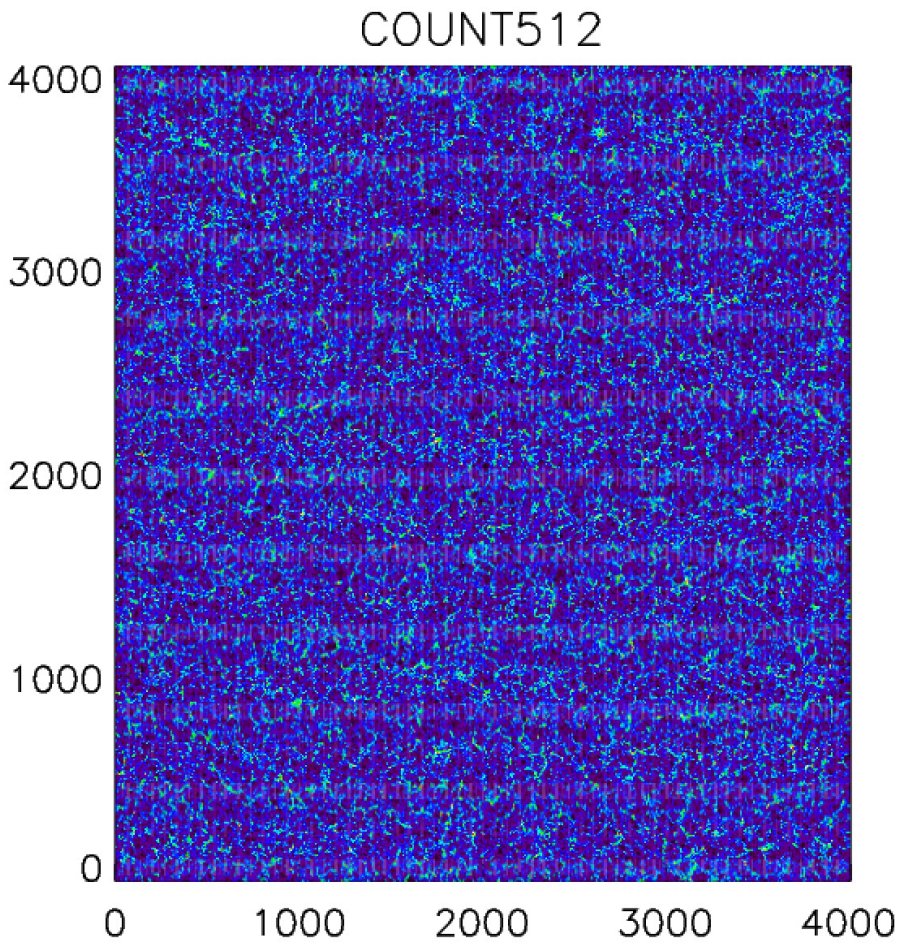
COUNT512
4000
3000
2000
1000
0
0
1000
2000
3000
4000

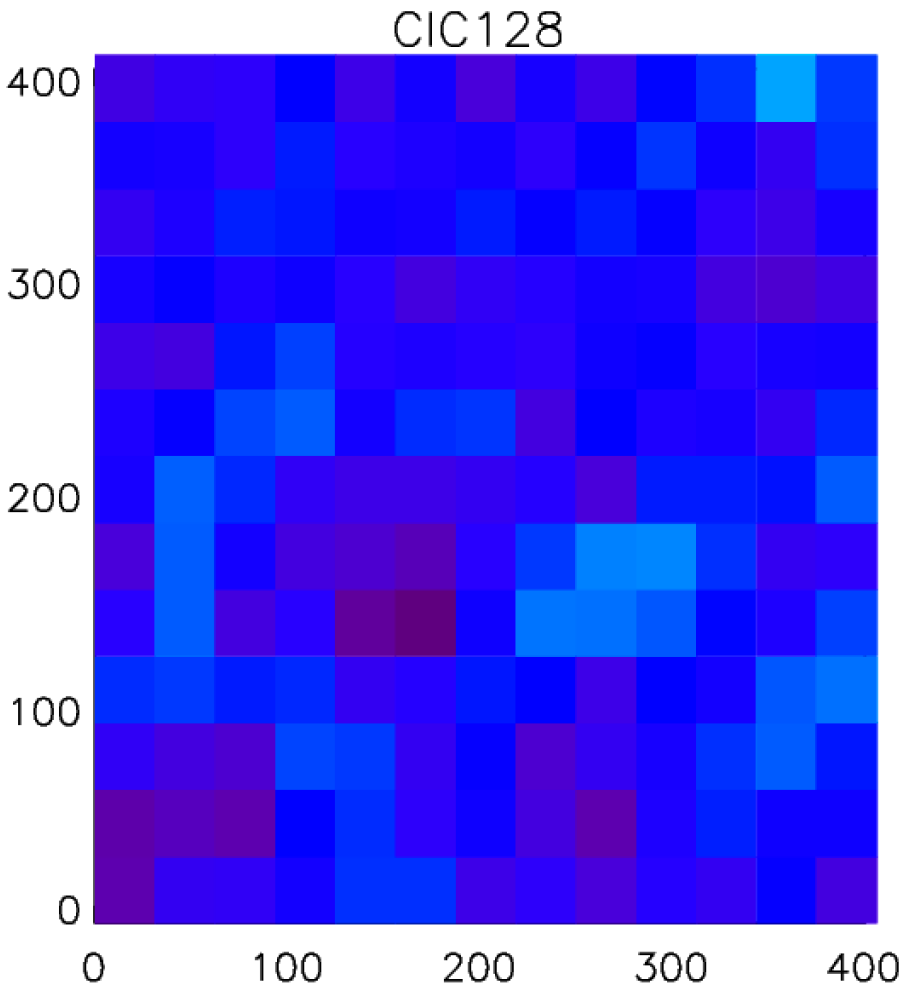
CIC128
400
300
200
100
0
0
100
200
300
400

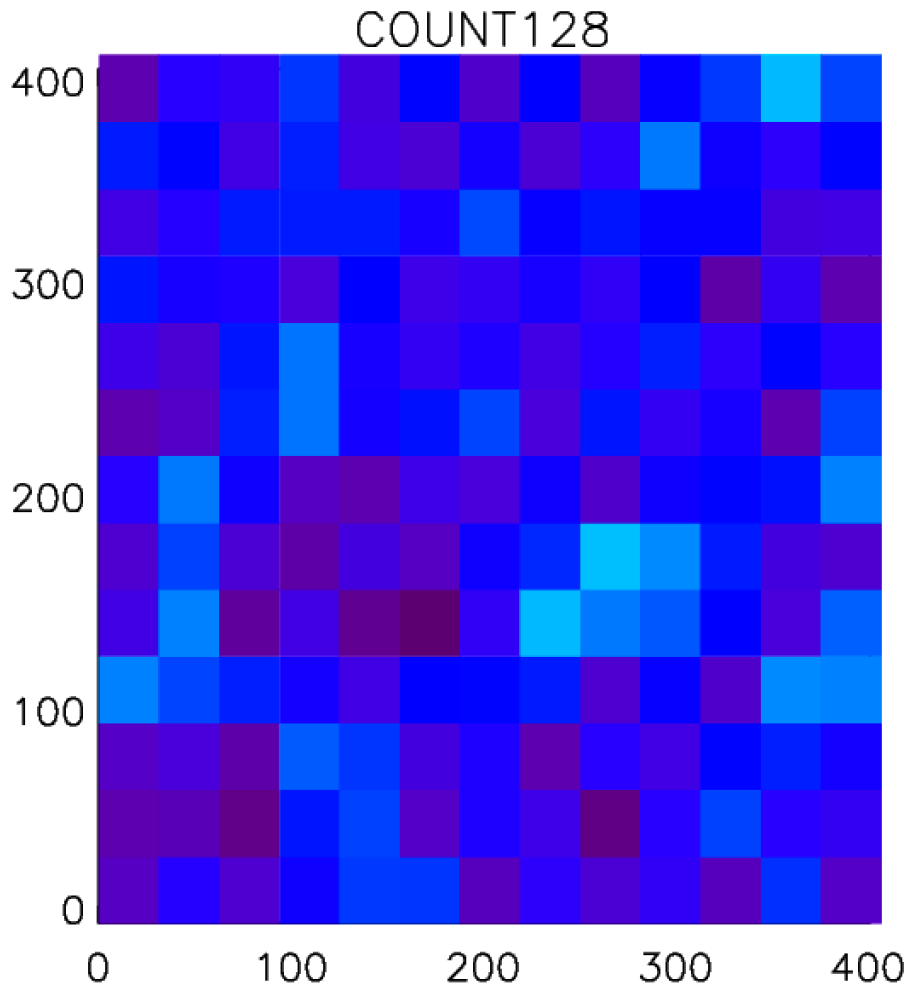
COUNT128
400
300
200
100
0
0
100
200
300
400

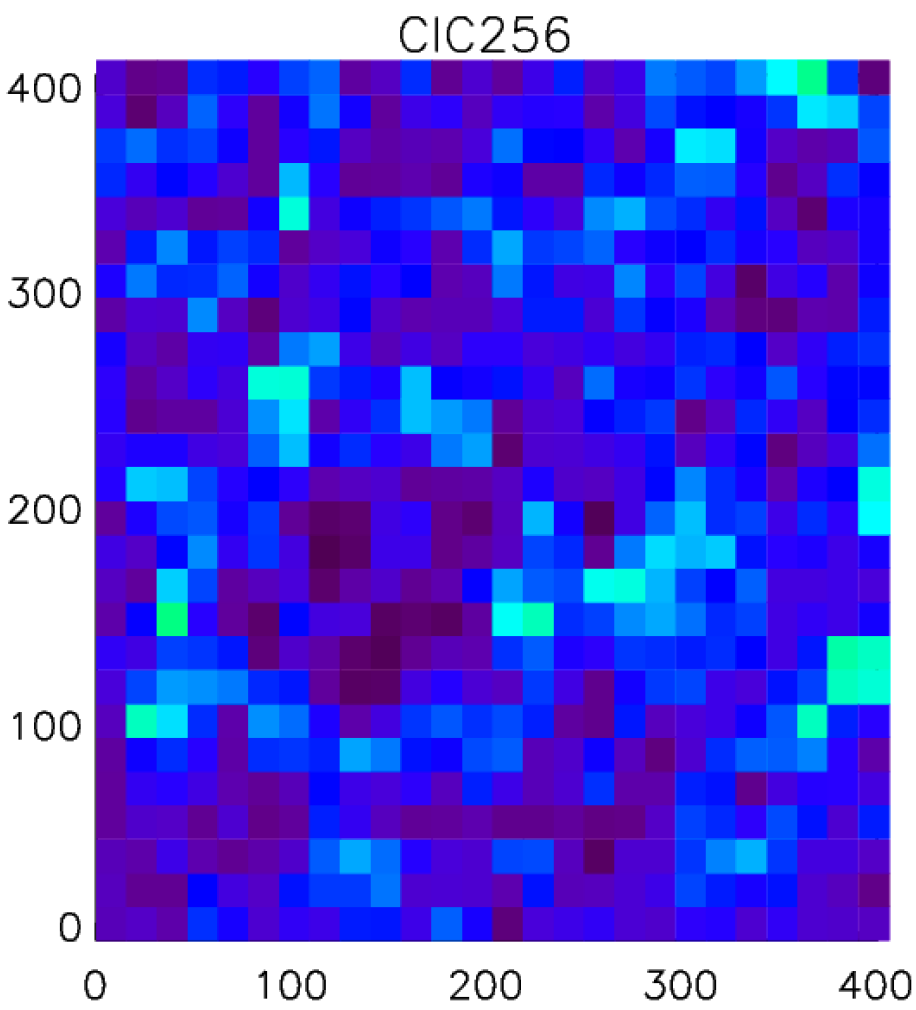
CIC256
400
300
200
100
0
0
100
200
300
400

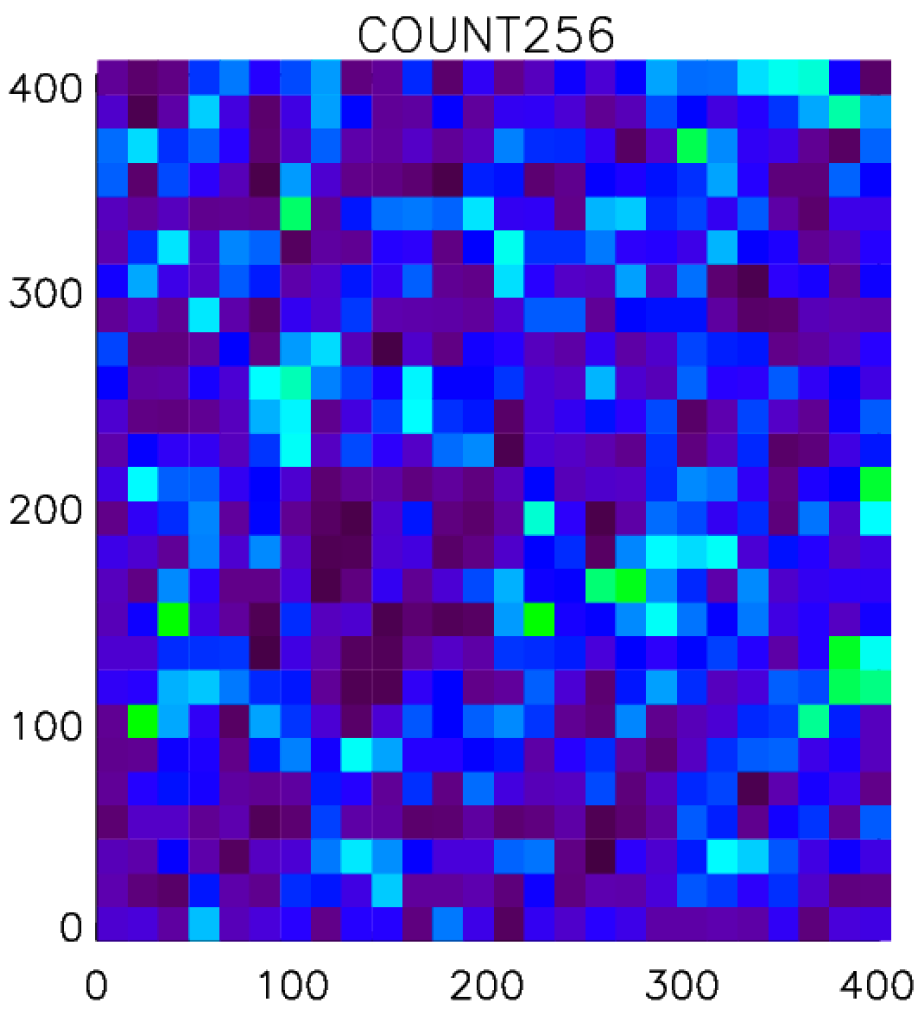
COUNT256
400
300
200
100
0
0
100
200
300
400

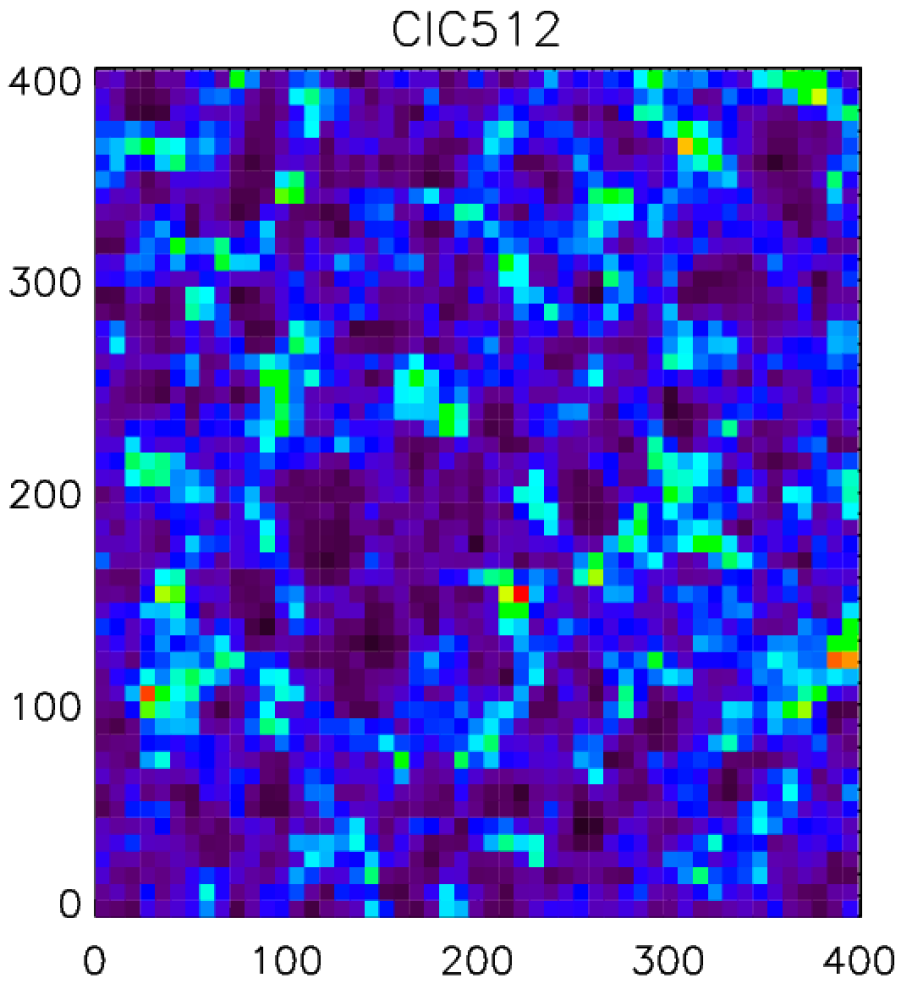
CIC512
400
300
200
100
0
0
100
200
300
400

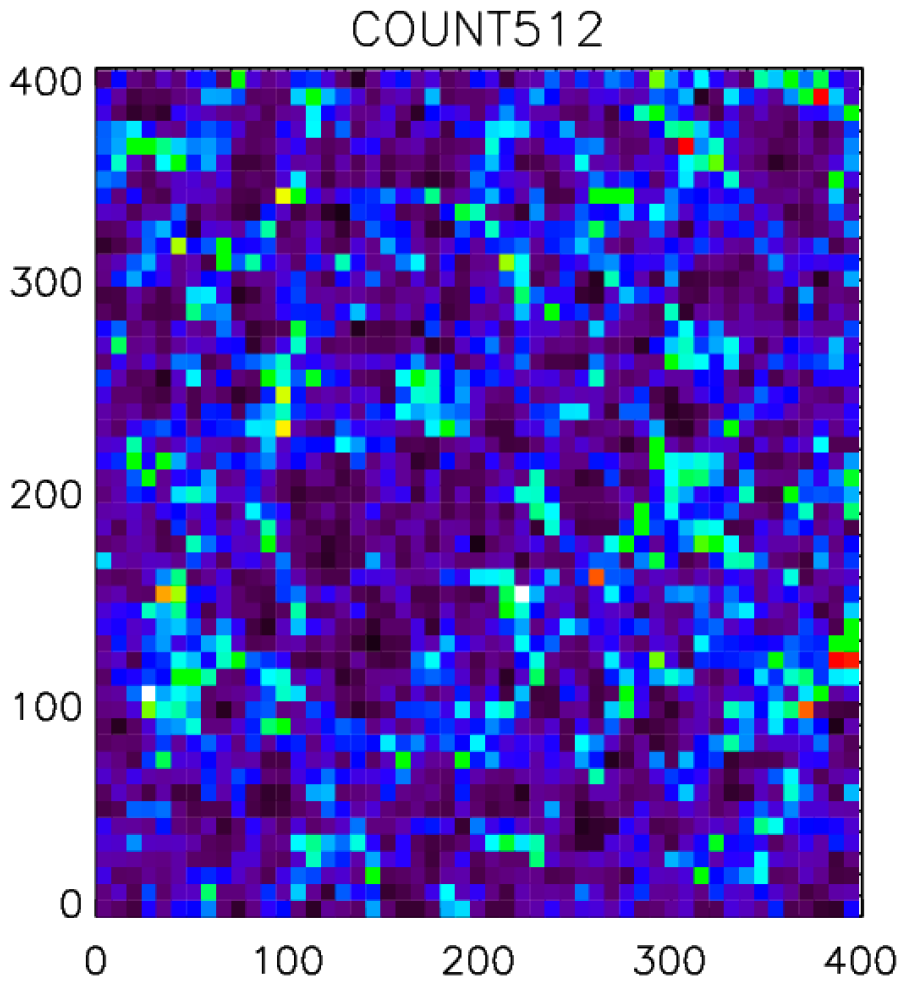
COUNT512
400
300
200
100
0
0
100
200
300
400

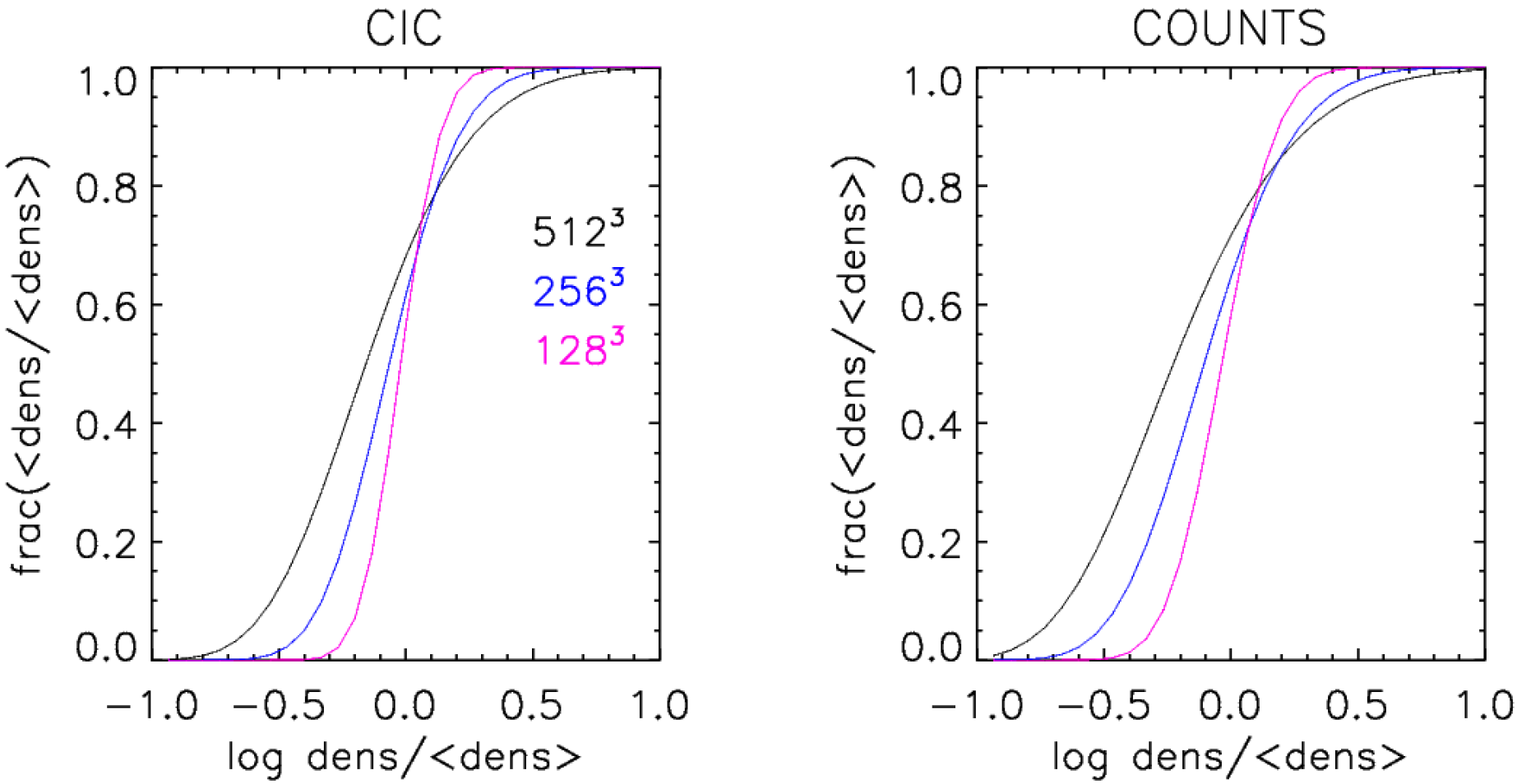
CIC
COUNTS
frac(<dens/<dens>)
log dens/<dens>
1.0
0.8
0.6
0.4
0.2
0.0
−1.0
−0.5
0.0
0.5
1.0
512³
256³
128³

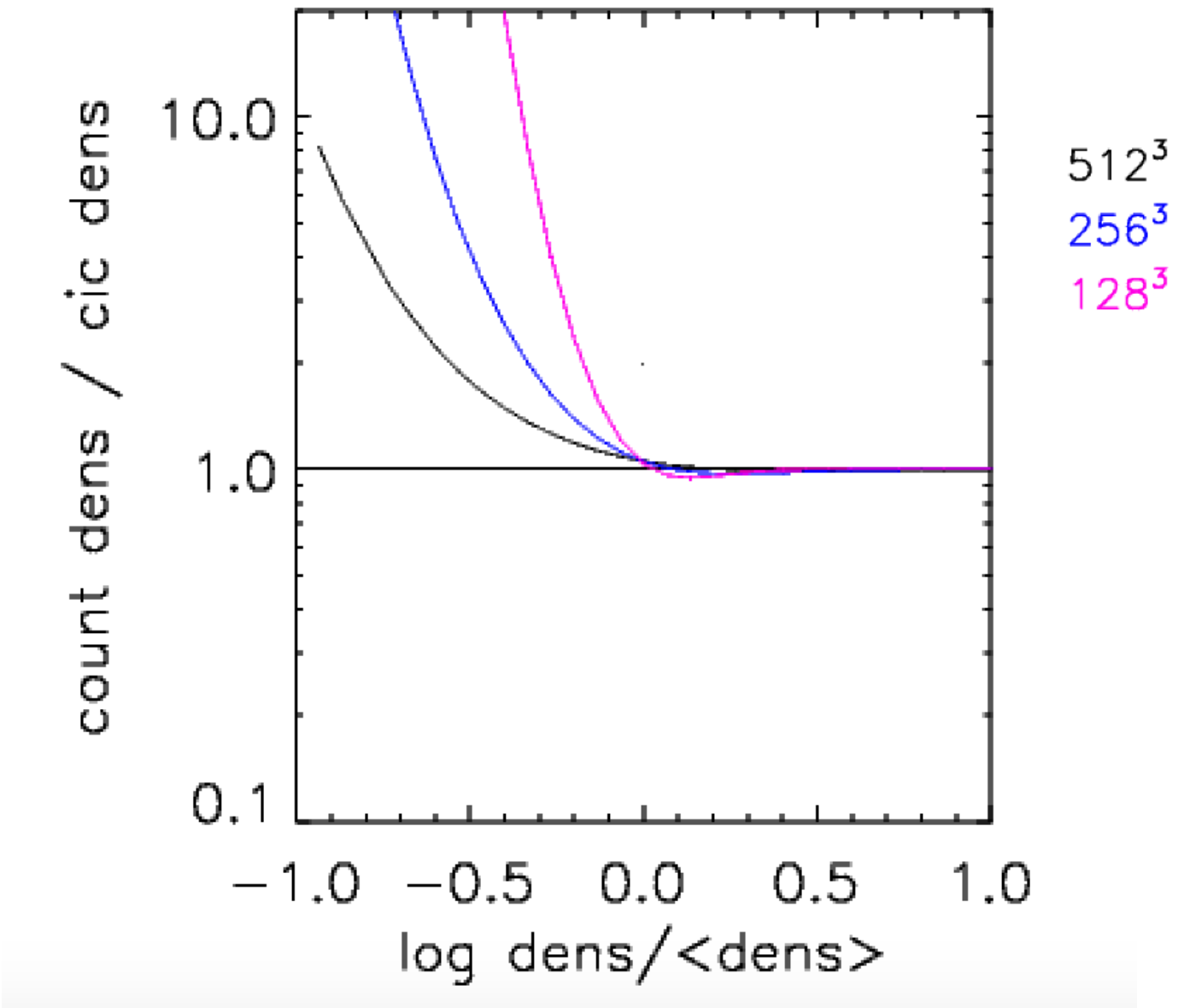
count dens / cic dens
10.0
1.0
0.1
−1.0
−0.5
0.0
0.5
1.0
log dens/<dens>
512³
256³
128³

- numerically integrate Poisson's equation

$$\Delta\Phi(\vec{g}_{k,l,m}) = 4\pi G\left(\rho(\vec{g}_{k,l,m}) - \overline{\rho}\right)$$

$$\vec{F}(\vec{g}_{k,l,m}) = -m\nabla\Phi(\vec{g}_{k,l,m})$$

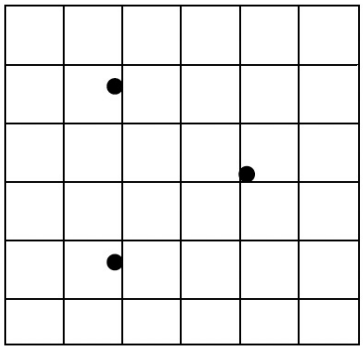

1. calculate mass density on grid $\quad \vec{x}_i \rightarrow \rho(\vec{g}_{k,l,m})$
2. solve Poisson's equation on grid $\quad \Phi(\vec{g}_{k,l,m})$?
3. differentiate potential to get forces $\quad \vec{F}(\vec{g}_{k,l,m})$
4. interpolate forces back to particles $\quad \vec{F}(\vec{g}_{k,l,m}) \rightarrow \vec{F}(\vec{x}_i)$

- numerically integrate Poisson's equation *relaxation technique*

$$\Delta\Phi_{k,l,m} = \rho_{k,l,m}$$

discretized Poisson's equation

$$\Phi_{k,l,m} = \frac{1}{6}(\Phi_{k+1,l,m} + \Phi_{k-1,l,m} + \Phi_{k,l+1,m} + \Phi_{k,l-1,m} + \Phi_{k,l,m+1} + \Phi_{k,l,m-1} - \rho_{k,l,m}H^2)$$

- numerically integrate Poisson's equation *relaxation technique*

$$\Delta\Phi_{k,l,m} = \nabla\cdot\nabla\Phi_{k,l,m}$$

$$= \begin{pmatrix} \frac{\partial}{\partial x} \\ \frac{\partial}{\partial y} \\ \frac{\partial}{\partial z} \end{pmatrix} \cdot \begin{pmatrix} \frac{\partial\Phi_{k,l,m}}{\partial x} \\ \frac{\partial\Phi_{k,l,m}}{\partial y} \\ \frac{\partial\Phi_{k,l,m}}{\partial z} \end{pmatrix}$$

$$= \frac{1}{H}\begin{pmatrix} \frac{\partial}{\partial x} \\ \frac{\partial}{\partial y} \\ \frac{\partial}{\partial z} \end{pmatrix} \cdot \begin{pmatrix} \Phi_{k+\frac{1}{2},l,m} - \Phi_{k-\frac{1}{2},l,m} \\ \Phi_{k,l+\frac{1}{2},m} - \Phi_{k,l-\frac{1}{2},m} \\ \Phi_{k,l,m+\frac{1}{2}} - \Phi_{k,l,m-\frac{1}{2}} \end{pmatrix}$$

$$= \frac{1}{H}\left(\frac{\partial\Phi_{k+\frac{1}{2},l,m}}{\partial x} - \frac{\partial\Phi_{k-\frac{1}{2},l,m}}{\partial x} + \frac{\partial\Phi_{k,l+\frac{1}{2},m}}{\partial y} - \frac{\partial\Phi_{k,l-\frac{1}{2},m}}{\partial y} + \frac{\partial\Phi_{k,l,m+\frac{1}{2}}}{\partial z} - \frac{\partial\Phi_{k,l,m-\frac{1}{2}}}{\partial z} \right)$$

$$= \frac{1}{H^2}\left(\Phi_{k+1,l,m} - 2\Phi_{k,l,m} + \Phi_{k-1,l,m} + \Phi_{k,l+1,m} - 2\Phi_{k,l,m} + \Phi_{k,l-1,m} + \Phi_{k,l,m+1} - 2\Phi_{k,l,m} + \Phi_{k,l,m-1}\right)$$

$$\Delta\Phi_{k,l,m} = \rho_{k,l,m}$$

discretized Poisson's equation

$$\Phi_{k,l,m} = \frac{1}{6}\left(\Phi_{k+1,l,m} + \Phi_{k-1,l,m} + \Phi_{k,l+1,m} + \Phi_{k,l-1,m} + \Phi_{k,l,m+1} + \Phi_{k,l,m-1} - \rho_{k,l,m}H^2\right)$$

- numerically integrate Poisson's equation

$$\Delta\Phi(\vec{g}_{k,l,m}) = 4\pi G\left(\rho(\vec{g}_{k,l,m}) - \overline{\rho}\right)$$

$$\vec{F}(\vec{g}_{k,l,m}) = -m\nabla\Phi(\vec{g}_{k,l,m})$$

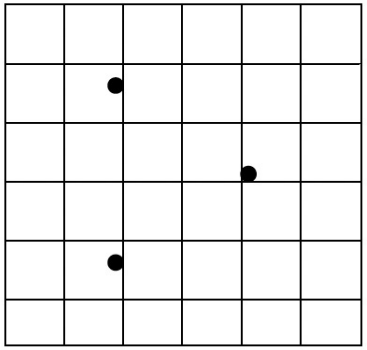

1. calculate mass density on grid $\vec{x}_i \rightarrow \rho(\vec{g}_{k,l,m})$
2. solve Poisson's equation on grid $\Phi(\vec{g}_{k,l,m})$
3. differentiate potential to get forces $\vec{F}(\vec{g}_{k,l,m})$?
4. interpolate forces back to particles $\vec{F}(\vec{g}_{k,l,m}) \rightarrow \vec{F}(\vec{x}_i)$

- discretized Nabla operator

$$\vec{F}(\vec{g}_{k,l,m}) = -m\nabla\Phi(\vec{g}_{k,l,m})$$

$$\downarrow$$

$$F_x(\vec{g}_{k,l,m}) = -m\frac{\Phi(\vec{g}_{k+1,l,m}) - \Phi(\vec{g}_{k-1,l,m})}{2H}$$

$$F_y(\vec{g}_{k,l,m}) = -m\frac{\Phi(\vec{g}_{k,l+1,m}) - \Phi(\vec{g}_{k,l-1,m})}{2H}$$

$$F_z(\vec{g}_{k,l,m}) = -m\frac{\Phi(\vec{g}_{k,l,m+1}) - \Phi(\vec{g}_{k,l,m-1})}{2H}$$

H = (current) grid spacing

- numerically integrate Poisson's equation

$$\Delta\Phi(\vec{g}_{k,l,m}) = 4\pi G\left(\rho(\vec{g}_{k,l,m}) - \overline{\rho}\right)$$

$$\vec{F}(\vec{g}_{k,l,m}) = -m\nabla\Phi(\vec{g}_{k,l,m})$$

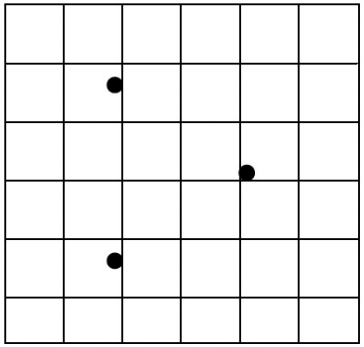

1. calculate mass density on grid $\vec{x}_i \rightarrow \rho(\vec{g}_{k,l,m})$
2. solve Poisson's equation on grid $\Phi(\vec{g}_{k,l,m})$
3. differentiate potential to get forces $\vec{F}(\vec{g}_{k,l,m})$
4. interpolate forces back to particles $\vec{F}(\vec{g}_{k,l,m}) \rightarrow \vec{F}(\vec{x}_i)$?

- interpolating the forces

$$\vec{F}(\vec{g}_{k,l,m}) \rightarrow \vec{F}(\vec{r}_i)$$

use the inverse of the mass assignment scheme

to insure momentum conservation and minimize force anisotropies

$$\vec{F}(\vec{r}_i) = \sum_k \sum_l \sum_m \vec{F}(\vec{g}_{k,l,m}) W(\vec{r}_i - \vec{g}_{k,l,m})$$

exercise...

in practice the triple sum is “only” over 8 (CIC) or 27 (TCS) cells...

- Particle-Mesh (PM) method

$$\Delta\Phi(\vec{g}_{k,l,m}) = 4\pi G\left(\rho(\vec{g}_{k,l,m}) - \overline{\rho}\right)$$

$$\vec{F}(\vec{g}_{k,l,m}) = -m\nabla\Phi(\vec{g}_{k,l,m})$$

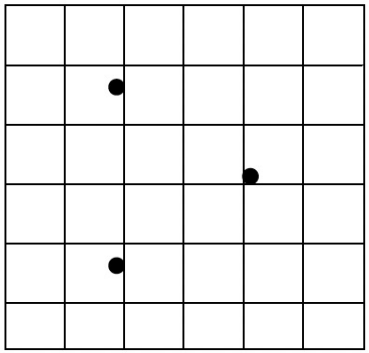

1. calculate mass density on grid $\vec{x}_i \rightarrow \rho(\vec{g}_{k,l,m})$
2. solve Poisson's equation on grid $\Phi(\vec{g}_{k,l,m})$
3. differentiate potential to get forces $\vec{F}(\vec{g}_{k,l,m})$
4. interpolate forces back to particles $\vec{F}(\vec{g}_{k,l,m}) \rightarrow \vec{F}(\vec{x}_i)$

- numerically integrate Poisson's equation

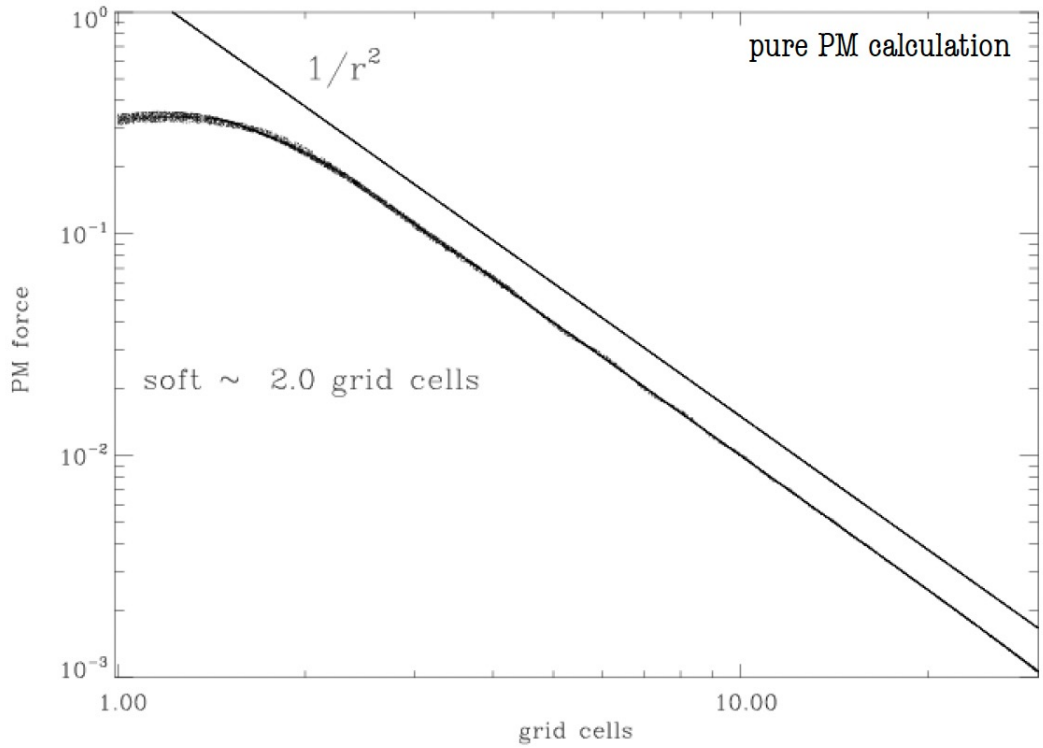

- numerically integrate Poisson's equation

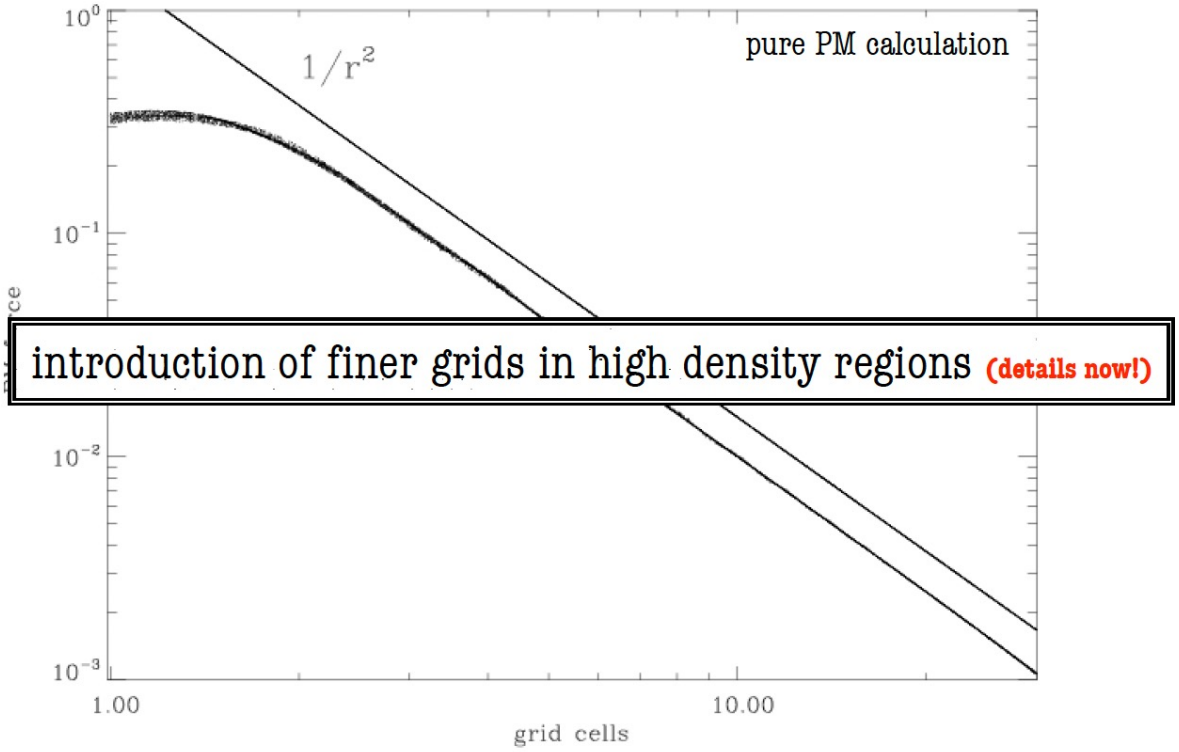

introduction of finer grids in high density regions **(details now!)**

overcoming the spatial resolution limitation

- adaptive mesh refinement

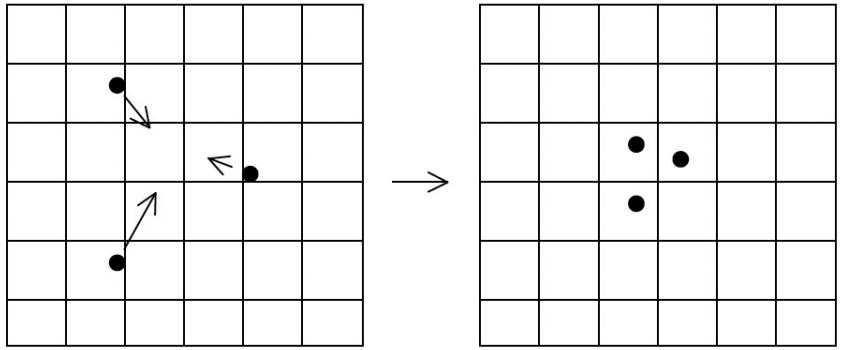

gravity tends to clump matter together...

- adaptive mesh refinement

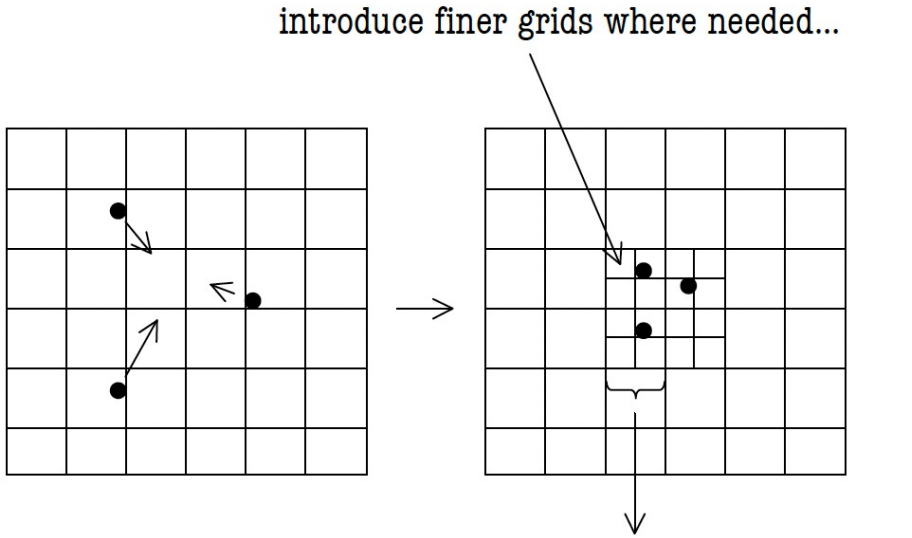

- adaptive mesh refinement

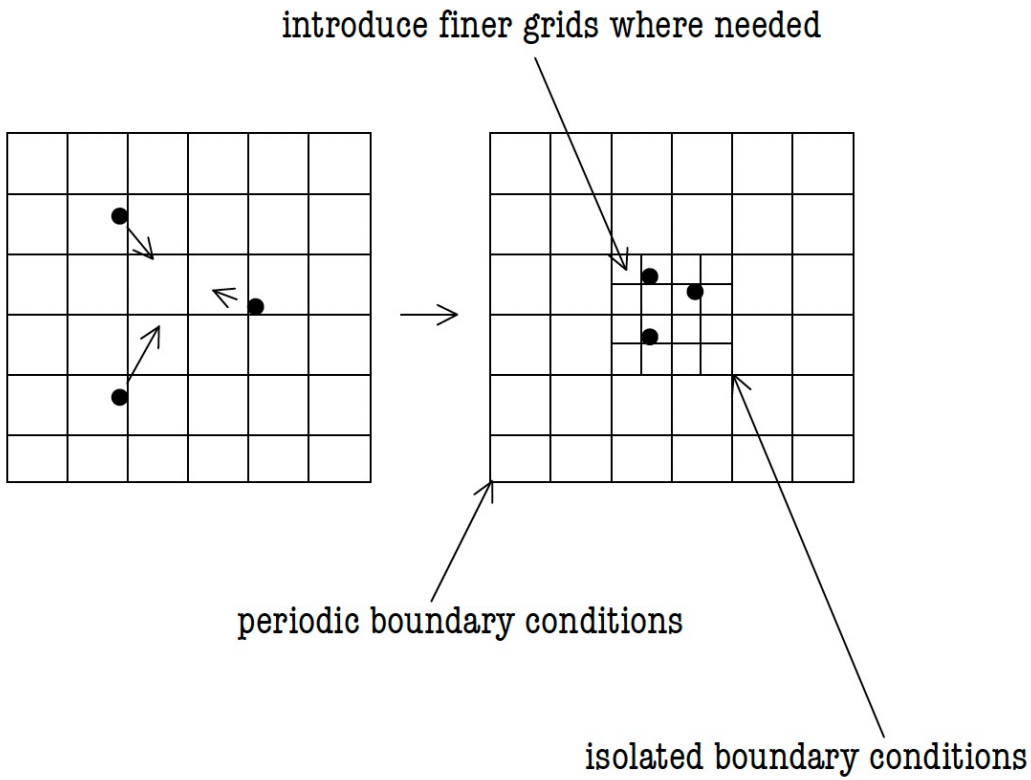

- adaptive mesh refinement

density field of simulated galaxy cluster

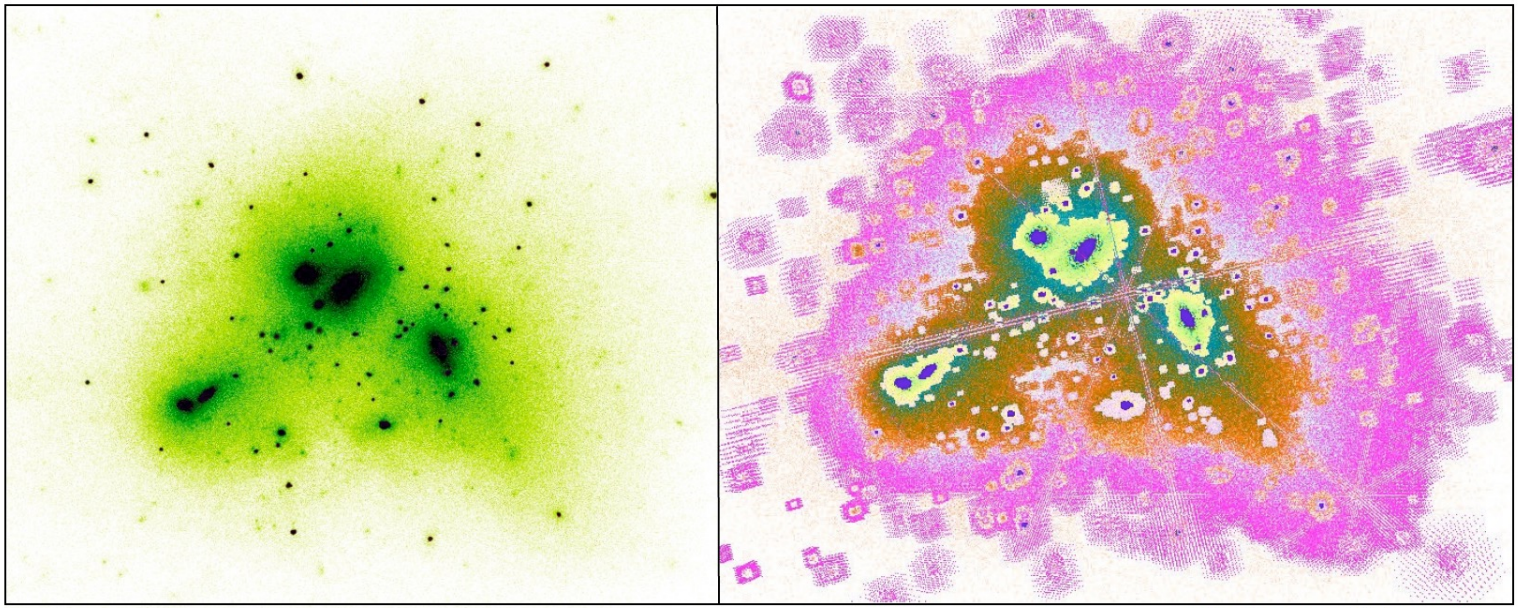

adaptive grid hierarchy

- adaptive mesh refinement

AMR not limited to astrophysics...

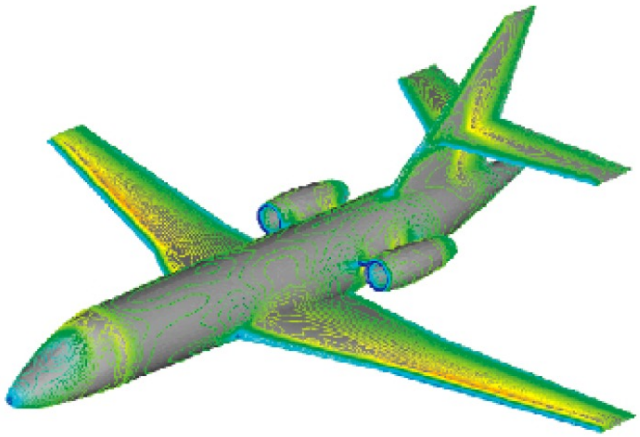

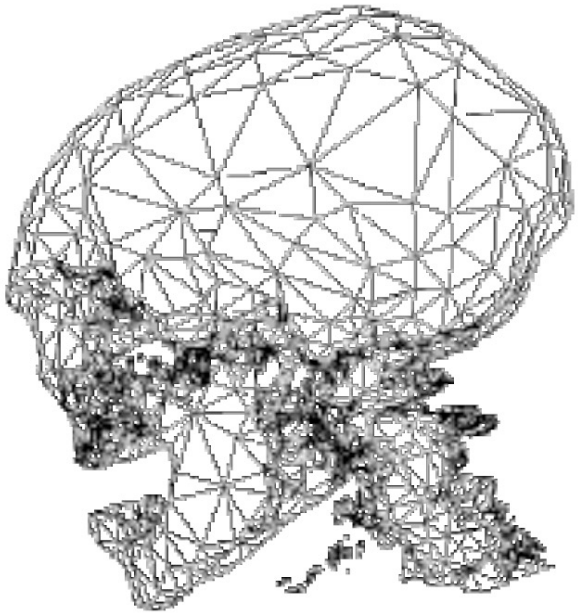

- adaptive mesh refinement
  - cover simulation with regular domain grid
  - create AMR hierarchy:
    - generate fine grid by comparing each node against some refinement criterion...

      –> recursive procedure!
  - assign density on all grids
  - solve Poisson's equation on regular domain grid (FFT is fastest...)
  - loop over all refinement levels:
    - interpolate potential down from parent level
    - relax potential until converged (keeping boundary values fixed)

      –> this will give the correct potential on all (refinement) grids

- generating refinements
  - dark matter only simulations:

number of particles per cell

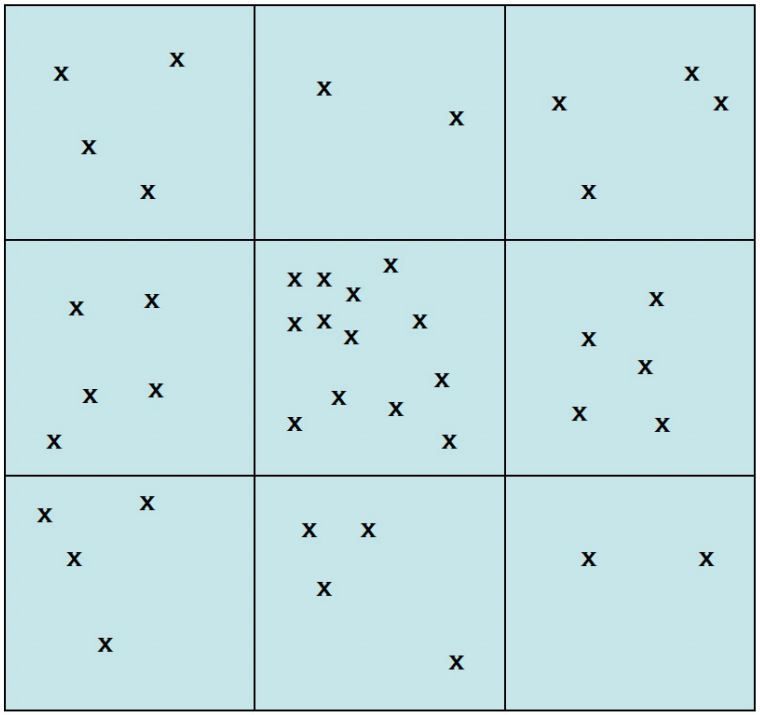

refinement criterion: 6 particles/cell

- generating refinements
  - dark matter only simulations:

number of particles per cell

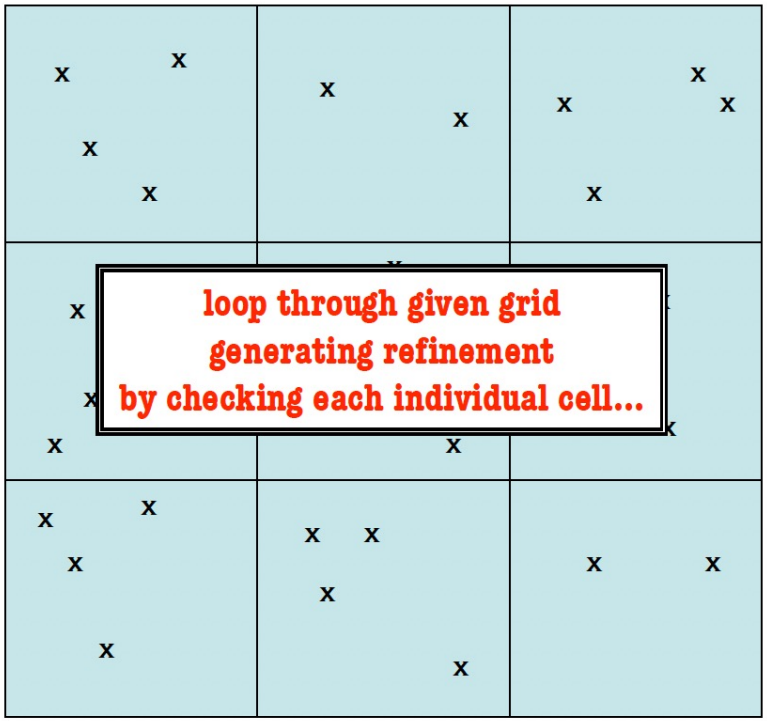

refinement criterion: 6 particles/cell

- generating refinements
  - dark matter only simulations:

number of particles per cell

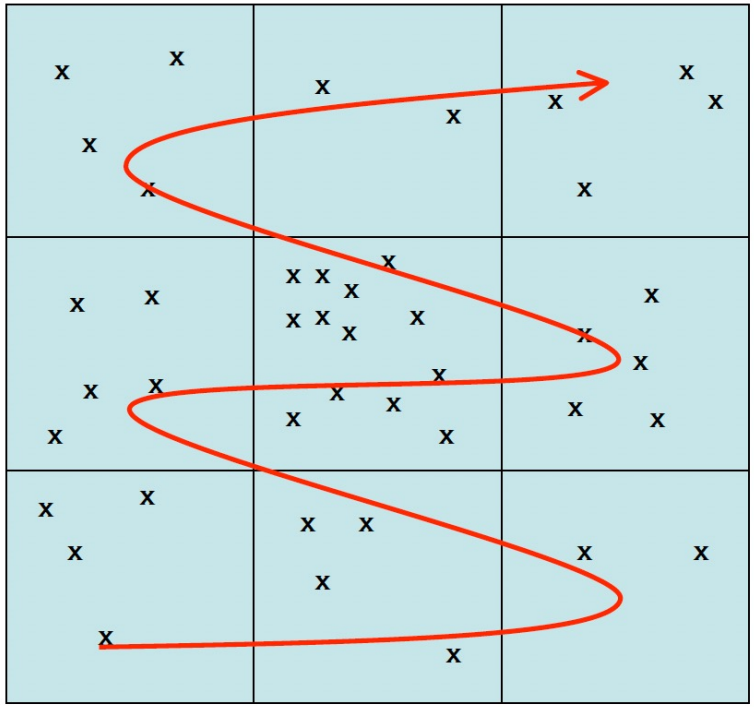

refinement criterion: 6 particles/cell

- generating refinements
  - dark matter only simulations:

number of particles per cell

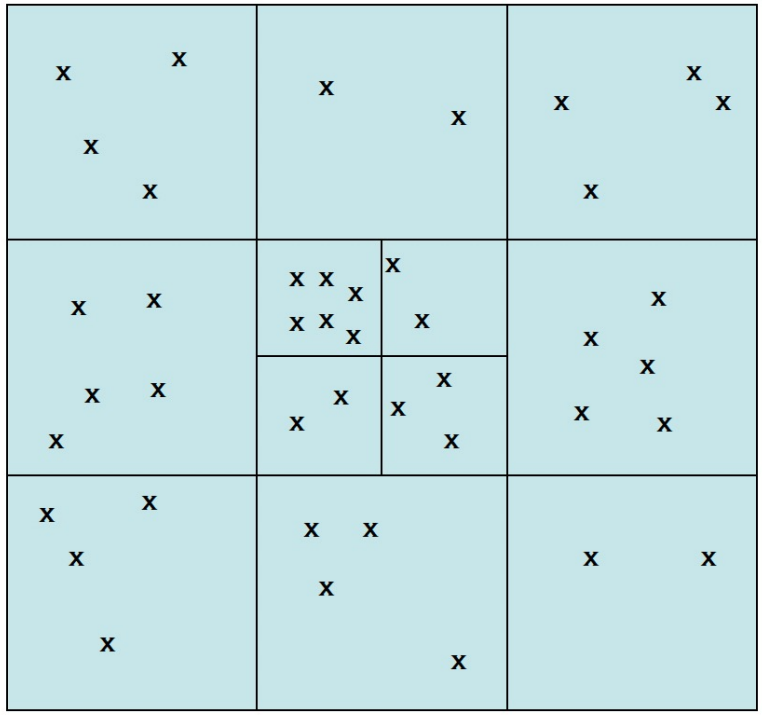

refinement criterion: 6 particles/cell

- generating refinements
  - dark matter only simulations:

number of particles per cell

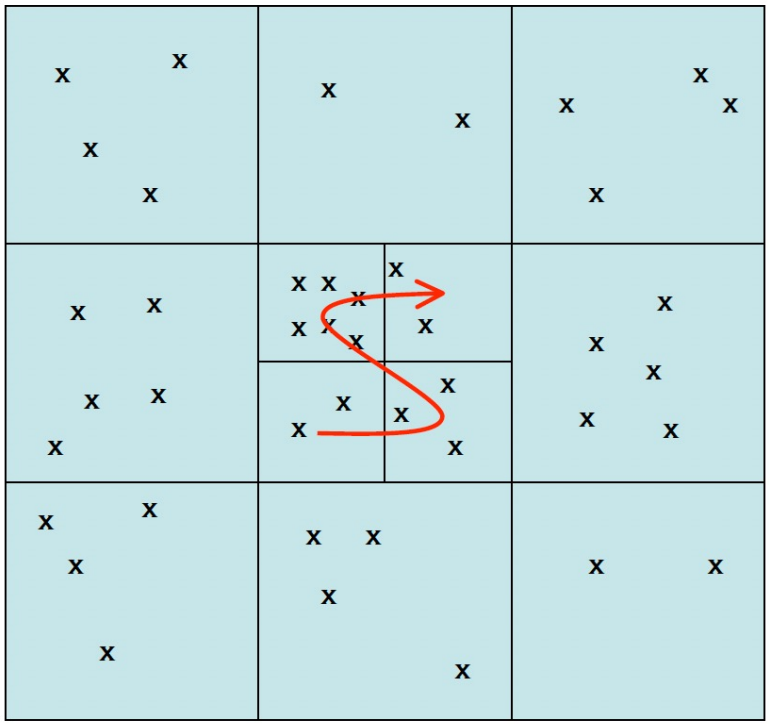

refinement criterion: 6 particles/cell

- generating refinements
  - dark matter only simulations:

number of particles per cell

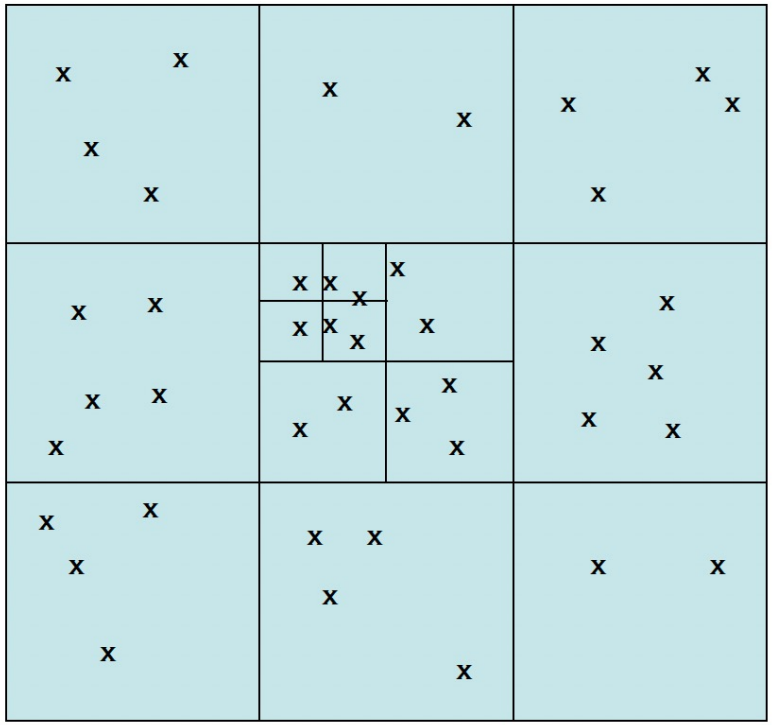

refinement criterion: 6 particles/cell

- generating refinements
  - dark matter only simulations:

number of particles per cell

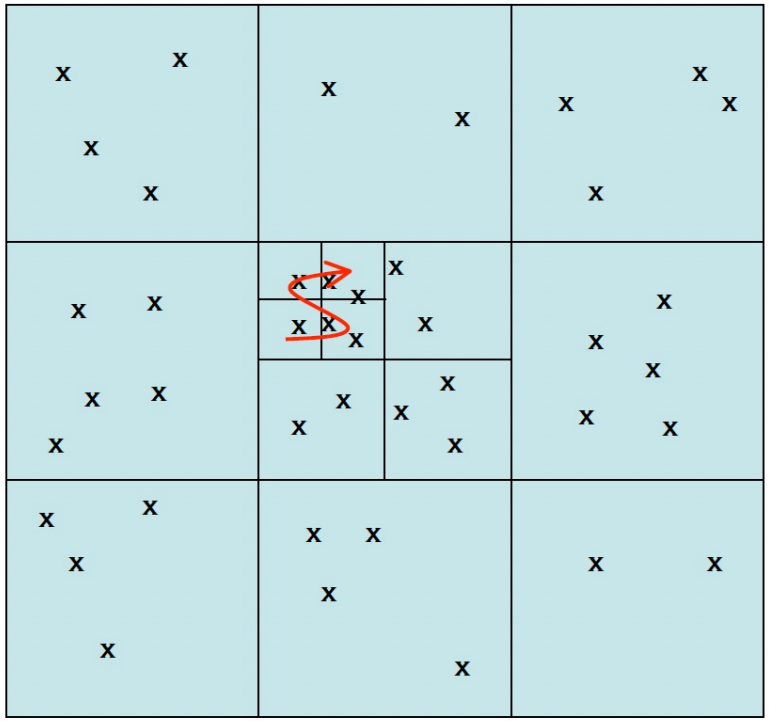

refinement criterion: 6 particles/cell

- generating refinements
  - dark matter only simulations:

number of particles per cell

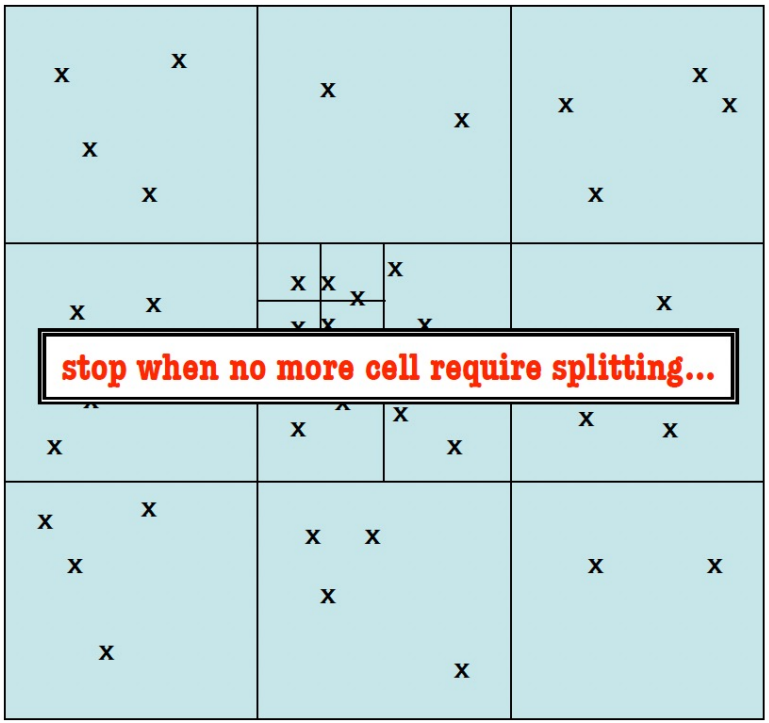

refinement criterion: 6 particles/cell

- density assignment (co-spatial scheme)

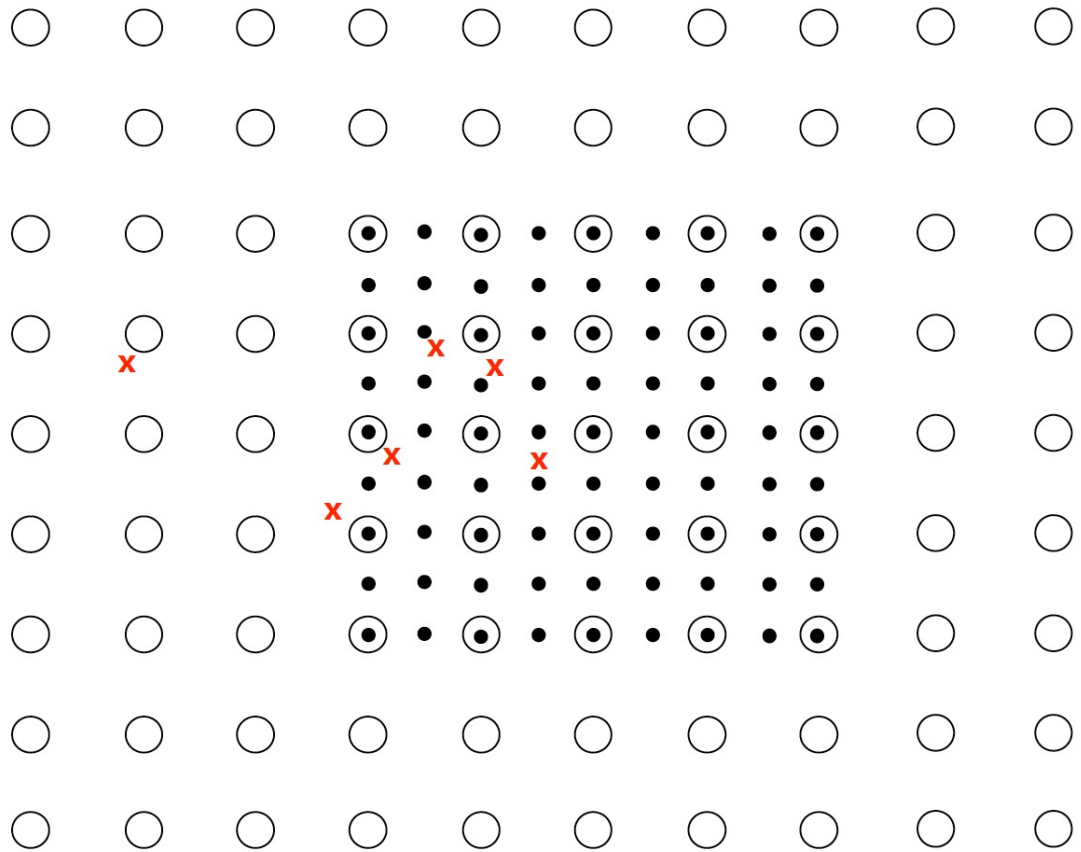

- density assignment (co-spatial scheme)

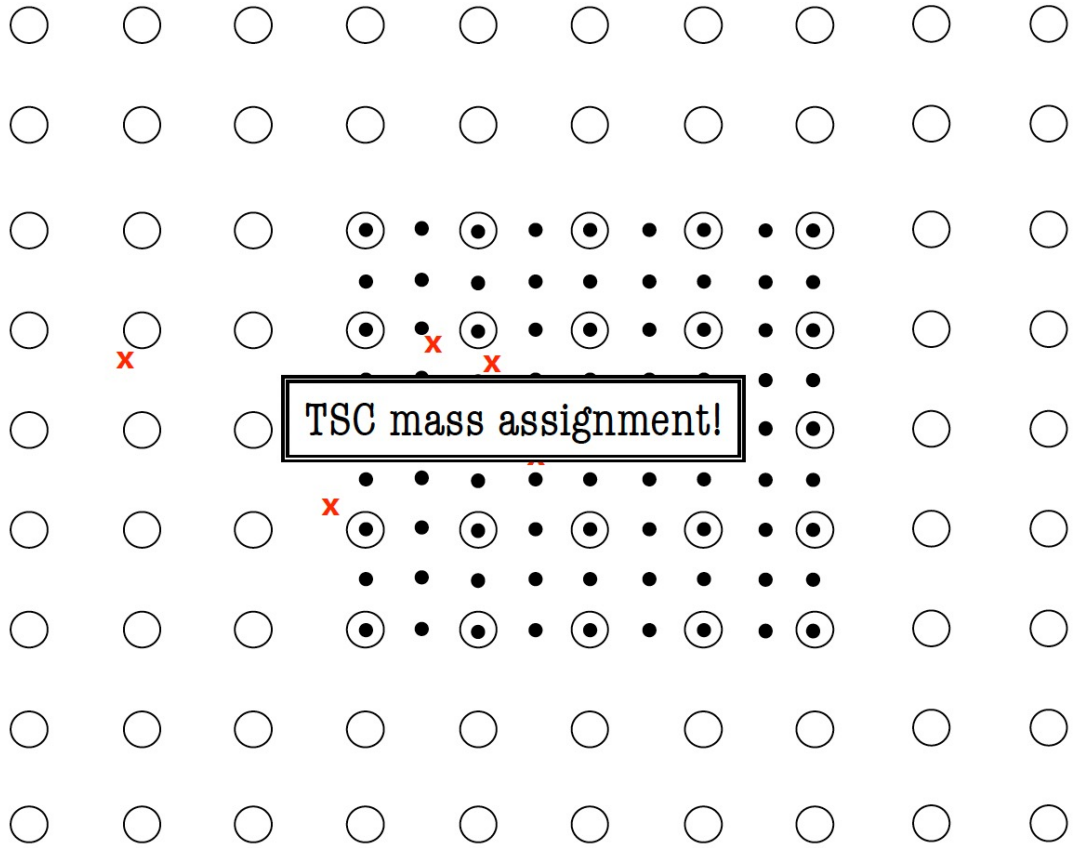

- density assignment (co-spatial scheme)

unproblematic cases:

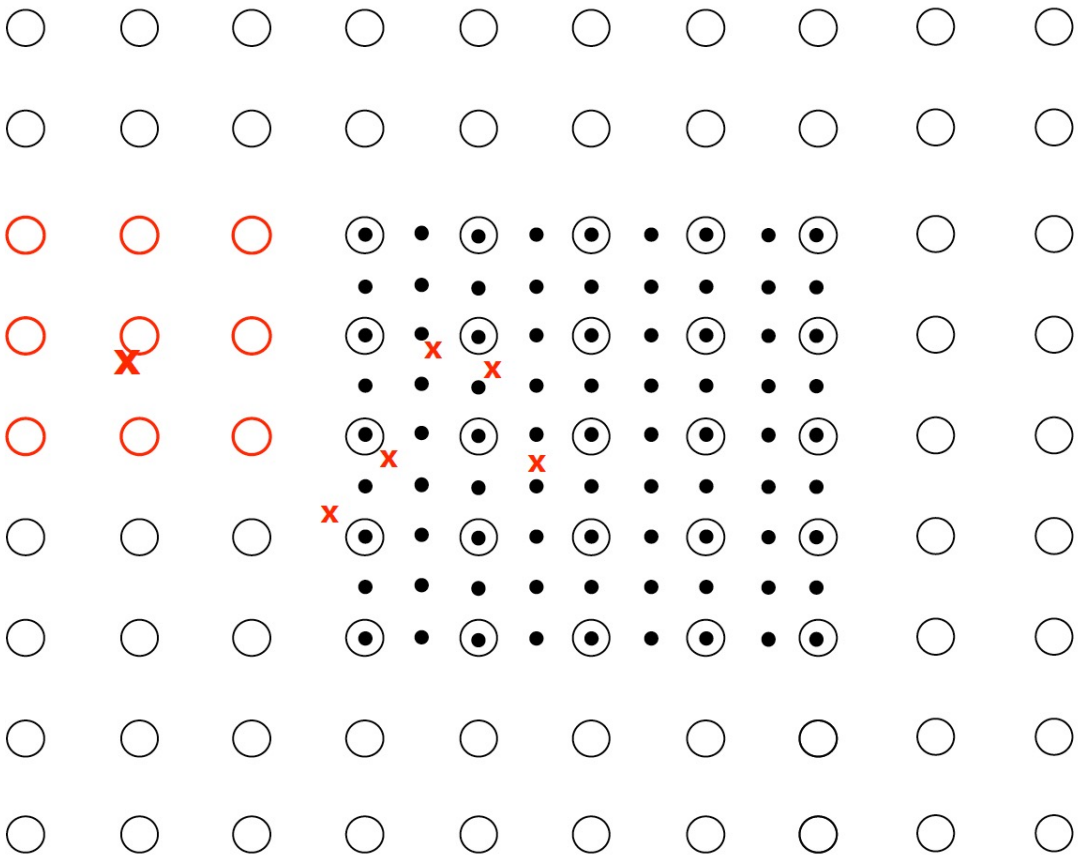

- density assignment (co-spatial scheme)

unprobematic cases:

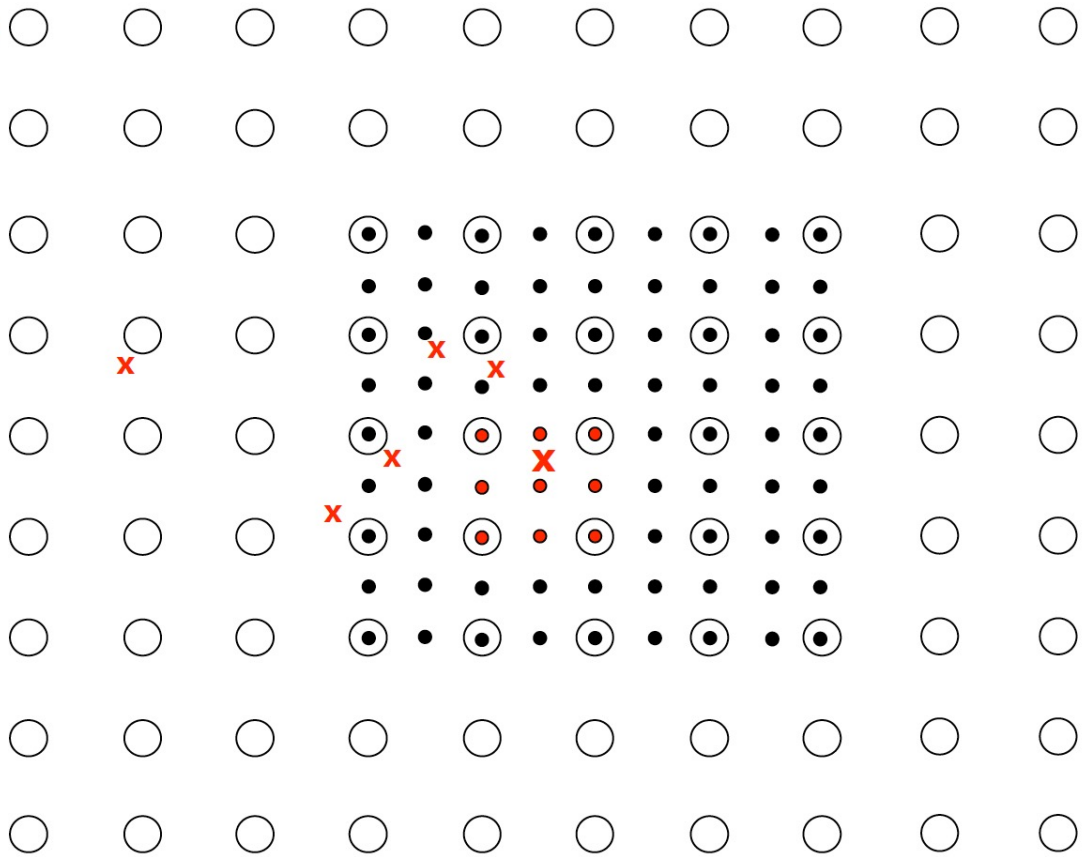

- density assignment (co-spatial scheme)

  - steps required to get density correct on both coarse and fine grid...

    1. assign particles to coarse grid
    2. assign particles to refinement grid

- moving particles on the AMR hierarchy

move particles on fine grids with smaller time step

to better resolve the dynamics, too!

=> natural choice: factor 2 again...

- moving particles on the AMR hierarchy

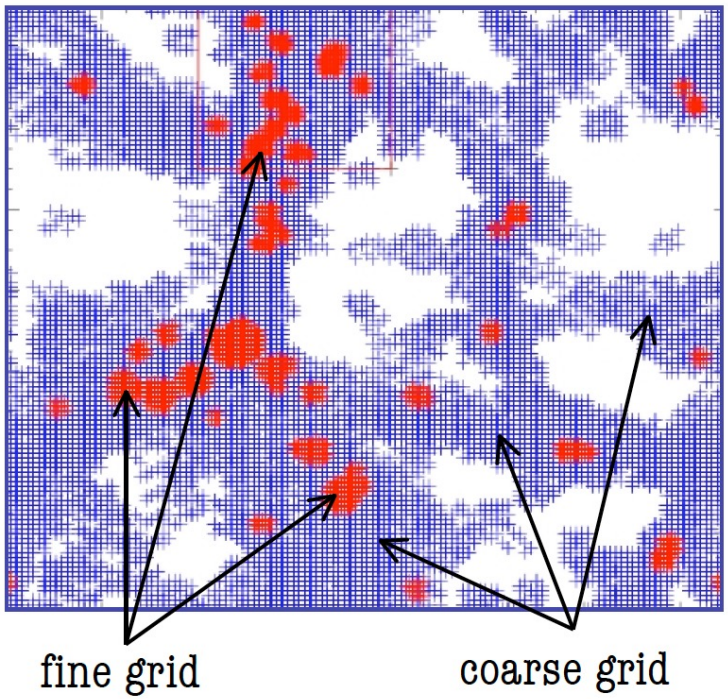

- moving particles on the AMR hierarchy
  - fully recursive approach:

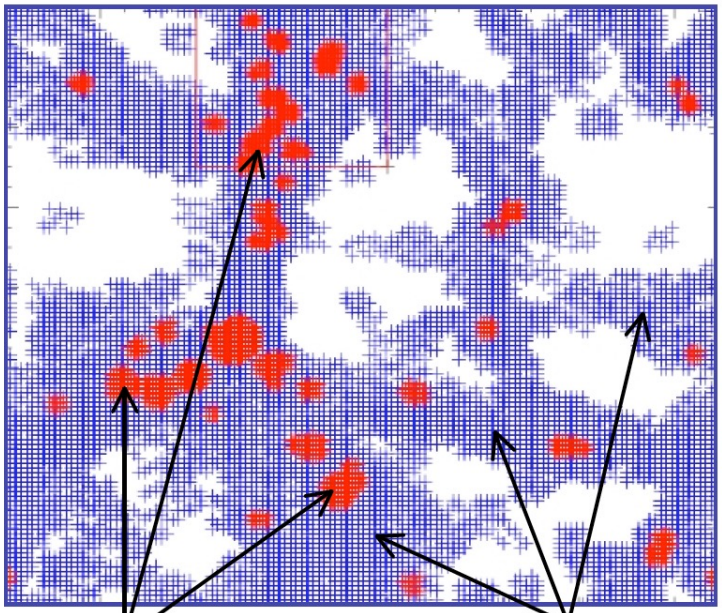

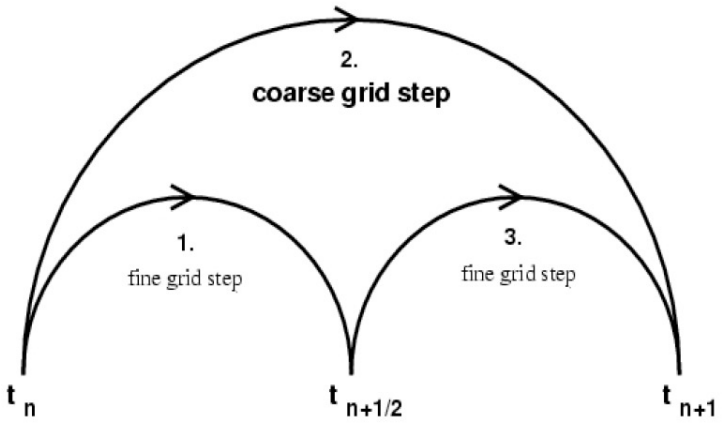

- moving particles on the AMR hierarchy
  - fully recursive approach:

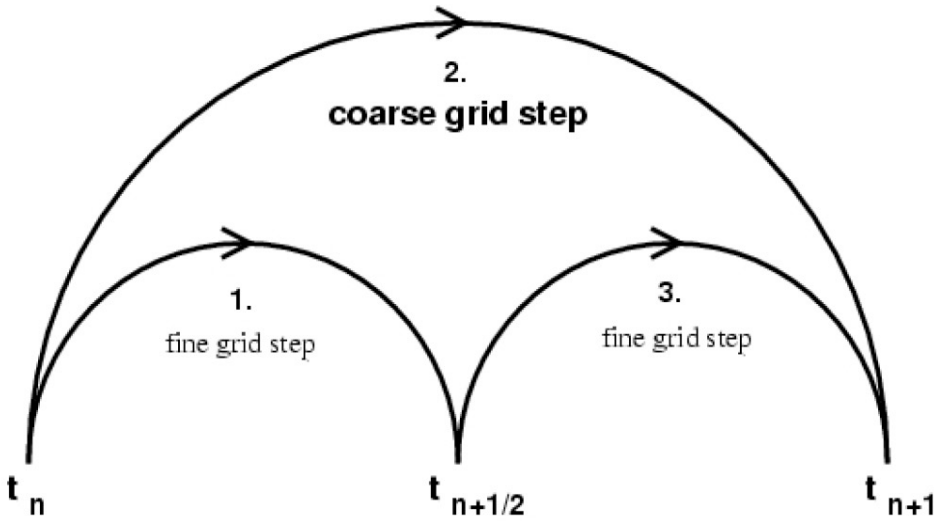

Drift-Kick-Drift variant of the leap-frog integrator:

time synchronisation between different grid levels rather than "leap-frogging"!

- moving particles on the AMR hierarchy
  - fully recursive approach:

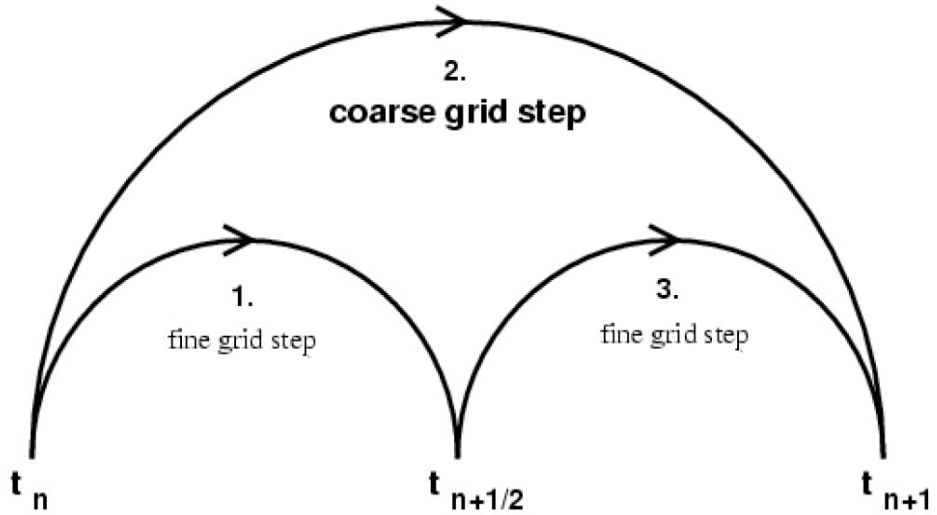

1. fine grid step:

$$\text{Drift}: \quad \vec{x}^{n+1/4} = \vec{x}^{n} + \vec{p}^{n} \int_{t_n}^{t_n+\Delta t/4} \frac{dt}{a^2}$$

$$\leftarrow \quad \text{Kick}: \quad \vec{p}^{n+1/2} = \vec{p}^{n} - \vec{\nabla}\Phi^{n+1/4} \int_{t_n}^{t_n+\Delta t/2} \frac{dt}{a} \quad \rightarrow$$

$$\text{Drift}: \quad \vec{x}^{n+1/2} = \vec{x}^{n+1/4} + \vec{p}^{n+1/2} \int_{t_n+\Delta t/4}^{t_n+\Delta t/2} \frac{dt}{a^2}$$

- moving particles on the AMR hierarchy
  - fully recursive approach:

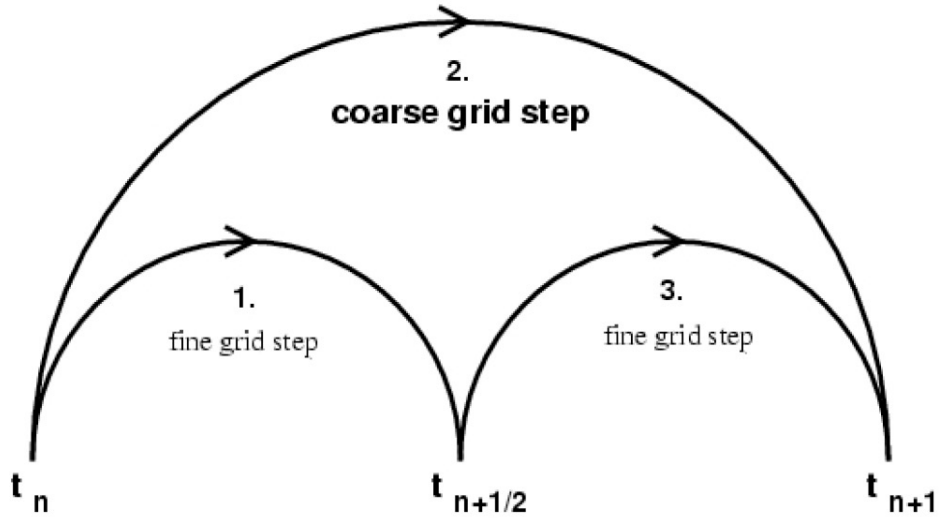

2. coarse grid step:

$$\text{Drift}: \quad \vec{x}^{n+1/2} = \vec{x}^{n} + \vec{p}^{n} \int_{t_n}^{t_n+\Delta t/2} \frac{dt}{a^2}$$

$$\text{Kick}: \quad \vec{p}^{n+1} = \vec{p}^{n} - \vec{\nabla}\Phi^{n+1/2} \int_{t_n}^{t_n+\Delta t} \frac{dt}{a}$$

$$\text{Drift}: \quad \vec{x}^{n+1} = \vec{x}^{n+1/2} + \vec{p}^{n+1} \int_{t_n+\Delta t/2}^{t_n+\Delta t} \frac{dt}{a^2}$$

- moving particles on the AMR hierarchy
  - fully recursive approach:

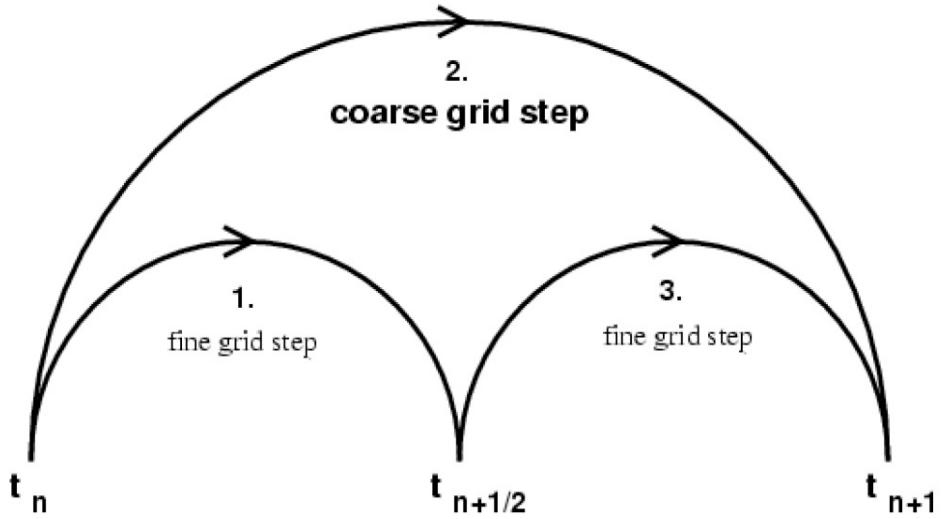

3. fine grid step:

$$\text{Drift}: \quad \vec{x}^{n+3/4} = \vec{x}^{n+1/2} + \vec{p}^{n} \int_{t_n+\Delta t/2}^{t_n+3\Delta t/4} \frac{dt}{a^2}$$

$$\leftarrow \quad \text{Kick}: \quad \vec{p}^{n+1} = \vec{p}^{n+1/2} - \vec{\nabla}\Phi^{n+3/4} \int_{t_n+\Delta t/2}^{t_n+\Delta t} \frac{dt}{a} \quad \rightarrow$$

$$\text{Drift}: \quad \vec{x}^{n+1} = \vec{x}^{n+3/4} + \vec{p}^{n+1} \int_{t_n+3\Delta t/4}^{t_n+\Delta t} \frac{dt}{a^2}$$

- moving particles on the AMR hierarchy

1. fine grid DKD step:

$$\text{Drift}: \quad \vec{x}^{\,n+1/4} = \vec{x}^{\,n} + \vec{p}^{\,n} \int_{t_n}^{t_n+\Delta t/4} \frac{dt}{a^2}$$

$$\text{Kick}: \quad \vec{p}^{\,n+1/2} = \vec{p}^{\,n} - \vec{\nabla}\Phi^{n+1/4} \int_{t_n}^{t_n+\Delta t/2} \frac{dt}{a}$$

$$\text{Drift}: \quad \vec{x}^{\,n+1/2} = \vec{x}^{\,n+1/4} + \vec{p}^{\,n+1/2} \int_{t_n+\Delta t/4}^{t_n+\Delta t/2} \frac{dt}{a^2}$$

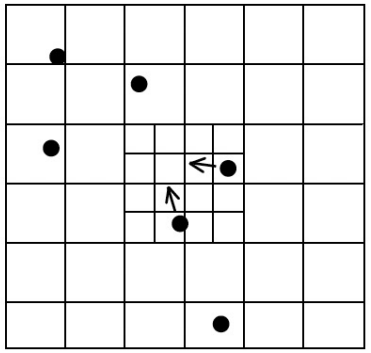

- moving particles on the AMR hierarchy

1. fine grid DKD step:

$$\text{Drift}: \quad \vec{x}^{n+1/4} = \vec{x}^{n} + \vec{p}^{n} \int_{t_n}^{t_n+\Delta t/4} \frac{dt}{a^2}$$

$$\text{Kick}: \quad \vec{p}^{n+1/2} = \vec{p}^{n} - \vec{\nabla}\Phi^{n+1/4} \int_{t_n}^{t_n+\Delta t/2} \frac{dt}{a}$$

$$\text{Drift}: \quad \vec{x}^{n+1/2} = \vec{x}^{n+1/4} + \vec{p}^{n+1/2} \int_{t_n+\Delta t/4}^{t_n+\Delta t/2} \frac{dt}{a^2}$$

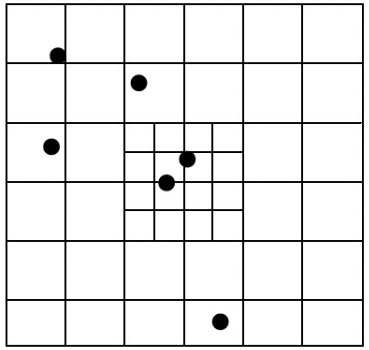

- moving particles on the AMR hierarchy

2. coarse grid DKD step:

$$\text{Drift}: \quad \vec{x}^{n+1/2} = \vec{x}^{n} + \vec{p}^{n} \int_{t_n}^{t_n+\Delta t/2} \frac{dt}{a^2}$$

$$\text{Kick}: \quad \vec{p}^{n+1} = \vec{p}^{n} - \vec{\nabla}\Phi^{n+1/2} \int_{t_n}^{t_n+\Delta t} \frac{dt}{a}$$

$$\text{Drift}: \quad \vec{x}^{n+1} = \vec{x}^{n+1/2} + \vec{p}^{n+1} \int_{t_n+\Delta t/2}^{t_n+\Delta t} \frac{dt}{a^2}$$

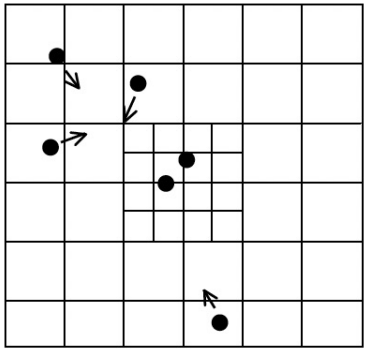

- moving particles on the AMR hierarchy

2. coarse grid DKD step:

$$\text{Drift}: \quad \vec{x}^{\,n+1/2} = \vec{x}^{\,n} + \vec{p}^{\,n} \int_{t_n}^{t_n+\Delta t/2} \frac{dt}{a^2}$$

$$\text{Kick}: \quad \vec{p}^{\,n+1} = \vec{p}^{\,n} - \vec{\nabla}\Phi^{n+1/2} \int_{t_n}^{t_n+\Delta t} \frac{dt}{a}$$

$$\text{Drift}: \quad \vec{x}^{\,n+1} = \vec{x}^{\,n+1/2} + \vec{p}^{\,n+1} \int_{t_n+\Delta t/2}^{t_n+\Delta t} \frac{dt}{a^2}$$

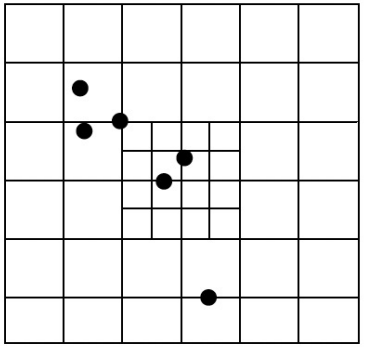

- moving particles on the AMR hierarchy

3. fine grid DKD step:

$$\text{Drift}: \quad \vec{x}^{\,n+3/4} = \vec{x}^{\,n+1/2} + \vec{p}^{\,n} \int_{t_n+\Delta t/2}^{t_n+3\Delta t/4} \frac{dt}{a^2}$$

$$\text{Kick}: \quad \vec{p}^{\,n+1} = \vec{p}^{\,n+1/2} - \vec{\nabla}\Phi^{n+3/4} \int_{t_n+\Delta t/2}^{t_n+\Delta t} \frac{dt}{a}$$

$$\text{Drift}: \quad \vec{x}^{\,n+1} = \vec{x}^{\,n+3/4} + \vec{p}^{\,n+1} \int_{t_n+3\Delta t/4}^{t_n+\Delta t} \frac{dt}{a^2}$$

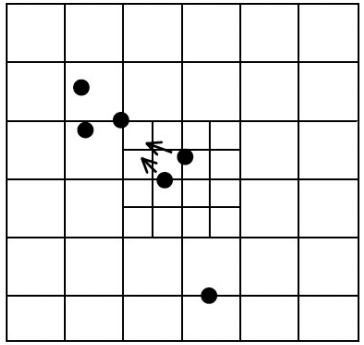

- moving particles on the AMR hierarchy

3. fine grid DKD step:

$$\text{Drift}: \quad \vec{x}^{\,n+3/4} = \vec{x}^{\,n+1/2} + \vec{p}^{\,n} \int_{t_n+\Delta t/2}^{t_n+3\Delta t/4} \frac{dt}{a^2}$$

$$\text{Kick}: \quad \vec{p}^{\,n+1} = \vec{p}^{\,n+1/2} - \vec{\nabla}\Phi^{n+3/4} \int_{t_n+\Delta t/2}^{t_n+\Delta t} \frac{dt}{a}$$

$$\text{Drift}: \quad \vec{x}^{\,n+1} = \vec{x}^{\,n+3/4} + \vec{p}^{\,n+1} \int_{t_n+3\Delta t/4}^{t_n+\Delta t} \frac{dt}{a^2}$$

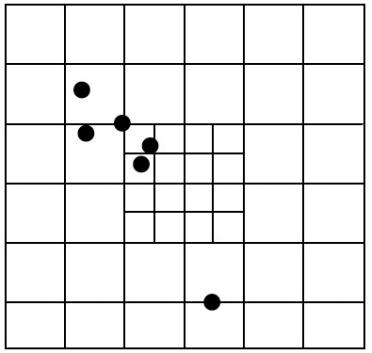

- hierarchical structure formation

  → **the demanding task of identifying halos within halos within halos within...**

- publicly available halo finders

  - FOF
  - AHF
  - BDM
  - SKID

- merger trees vs. halo tracking

- Friends-Of-Friends

a simple geometric grouping of particles...

- mode of operation

  - group all particles together whose distances obey:

$$\boxed{\left|\vec{r}_i - \vec{r}_j\right| \le b\bar{d}} \qquad \bar{d} = \frac{B}{\sqrt[3]{N}}$$

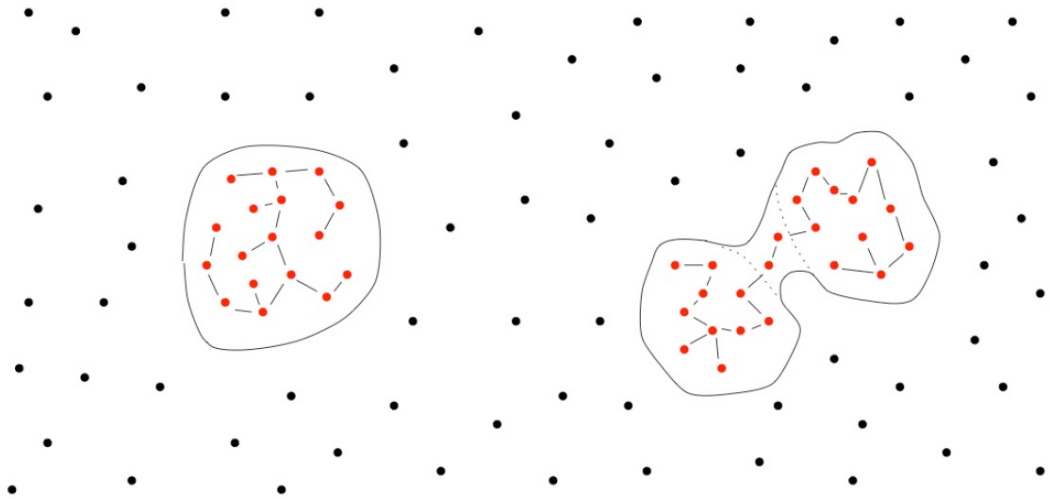

- mode of operation

  - group all particles together whose distances obey:

$$\left|\vec{r}_i - \vec{r}_j\right| \le b\bar{d} \qquad \bar{d} = \frac{B}{\sqrt[3]{N}}$$

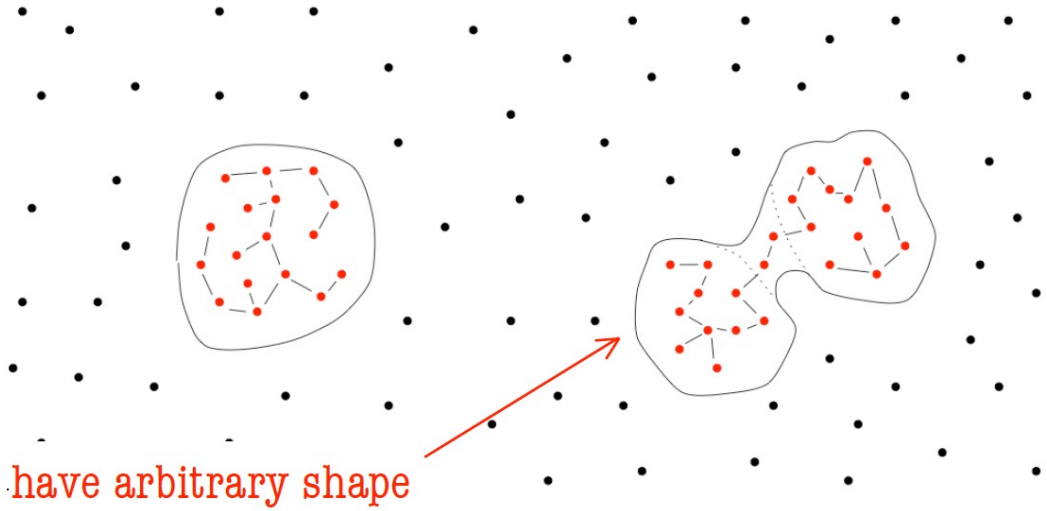

FOF groups have arbitrary shape
and edge defines isodensity contour

- mode of operation

  - group all particles together whose distances obey:

$$\boxed{\left|\vec{r}_i - \vec{r}_j\right| \le b\bar{d}} \qquad \bar{d} = \frac{B}{\sqrt[3]{N}}$$

  - typical "linking-length values:

$$b \approx 0.1 - 0.2$$

$\Rightarrow$intrinsically difficult to find sub-halos:

hierarchical FOF (HFOF), minimal-spanning-tree (MST), ...

- ***AMIGA***'s ***H***alo ***F***inder

the AMR grids naturally locate prospective halo centres

- ***AMIGA***'s ***H***alo ***F***inder

density field of simulated galaxy cluster

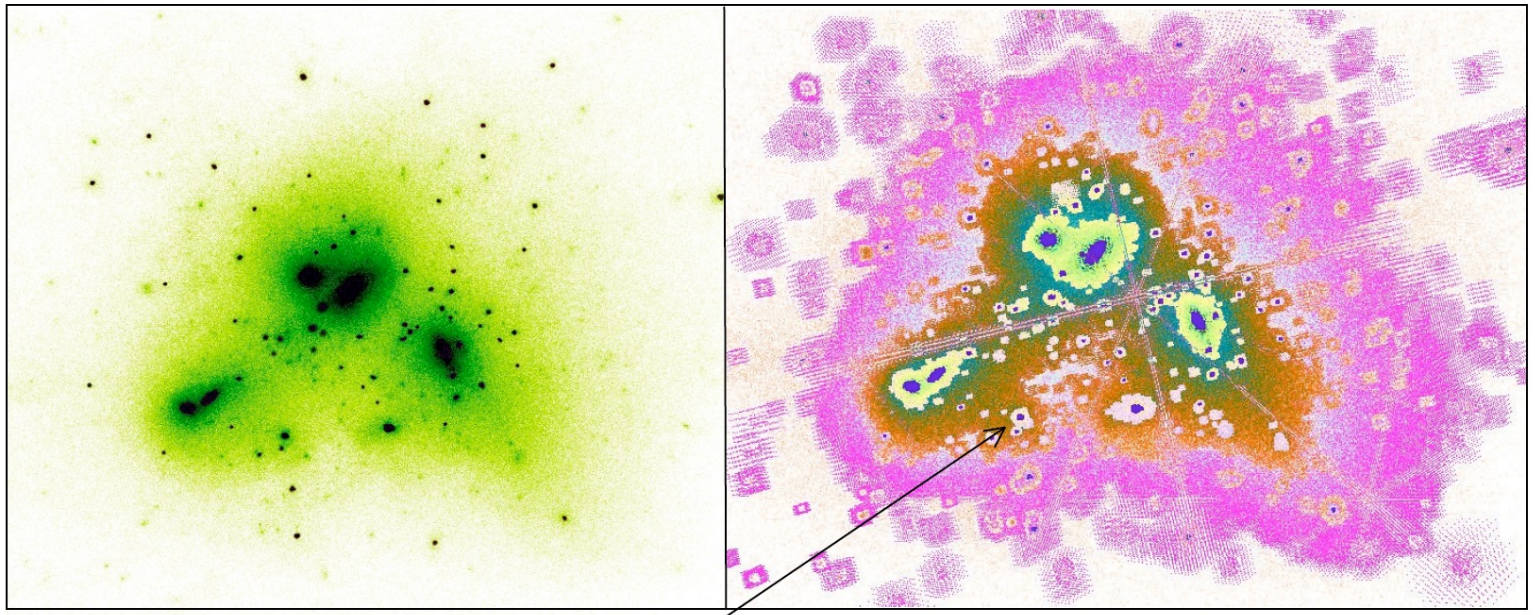

adaptive grid hierarchy

the AMR grids naturally locate centres

- in operation

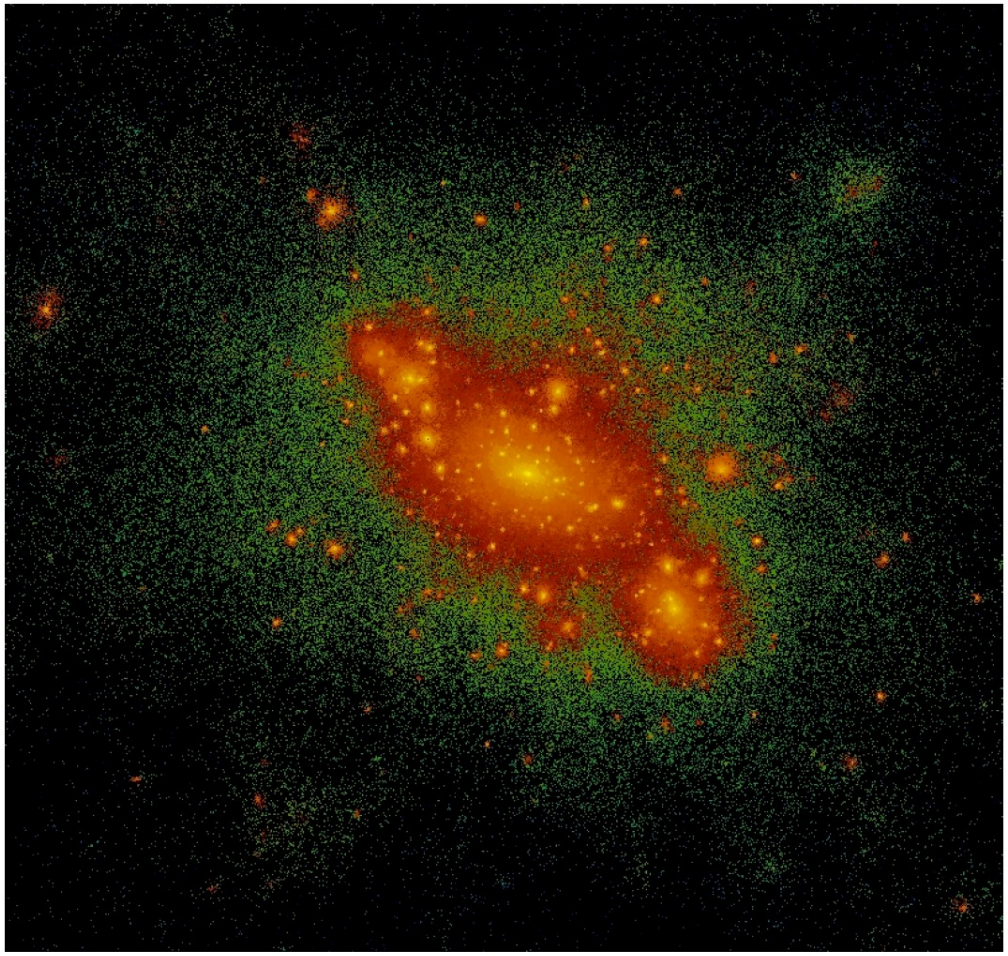

- in operation

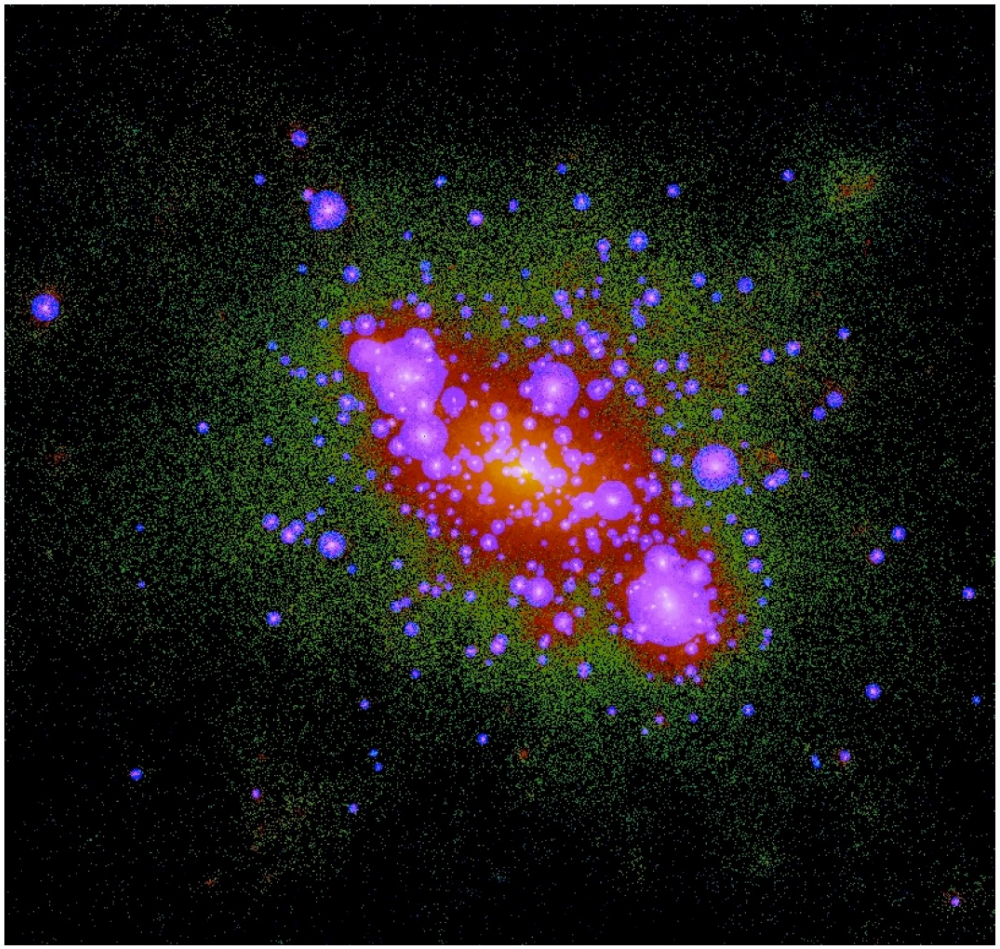

- mode of operation
  - locate potential halo centres via the AMR hierarchy created by ***AMIGA***
  - iteratively remove gravitationally unbound particles
  - calculate integral properties of remaining objects
  - calculate radial profiles of (some) properties

- mode of operation
  - locate potential halo centres via the AMR hierarchy created by ***AMIGA***
  - **iteratively remove gravitationally unbound particles**
  - calculate integral properties of remaining objects
  - calculate radial profiles of (some) properties

- mode of operation

  - iteratively remove gravitationally unbound particles

$$\frac{d\varphi}{dr} = \frac{GM(<r)}{r^2}$$ (Newton's force law)

second integration...

$$\varphi(r) = G\int_0^r \frac{M(<r')}{r'^2}dr' + \varphi(0)$$

unbound particles...

$$v > v_{esc} = \sqrt{2|\varphi|}$$

Halo Finding

Cross Comparison

FOF

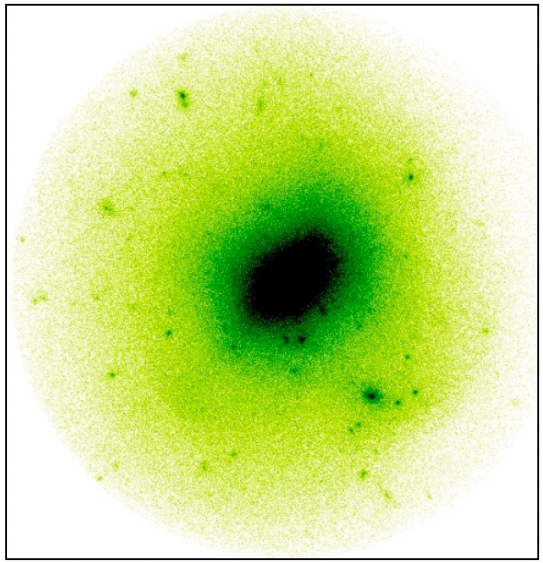

AHF

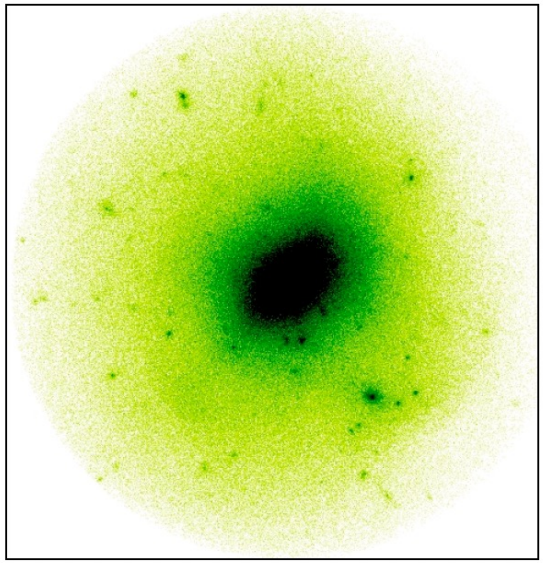

SKID

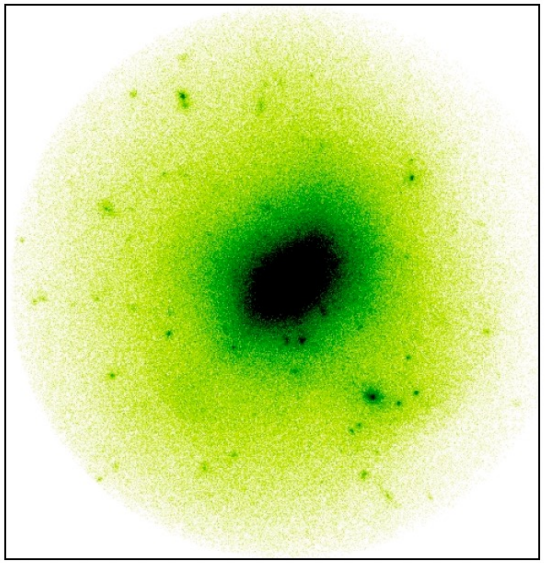

FOF

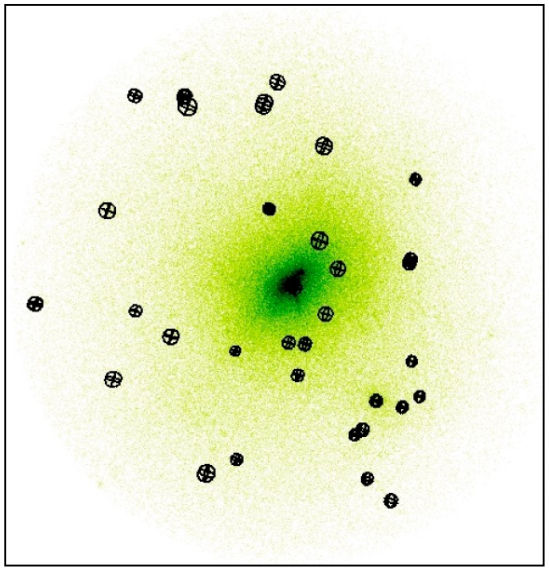

AHF

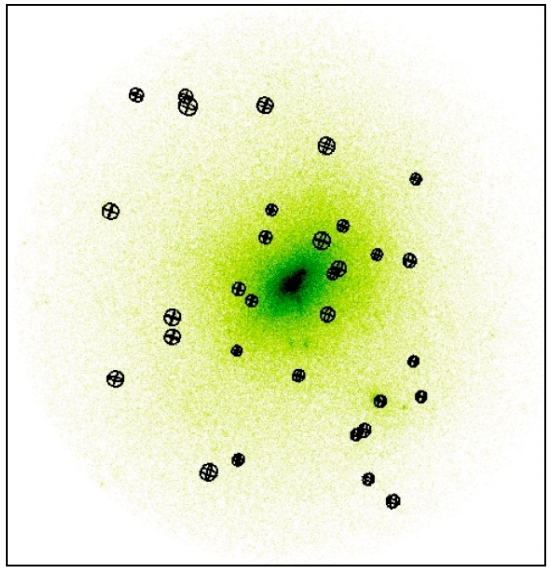

SKID

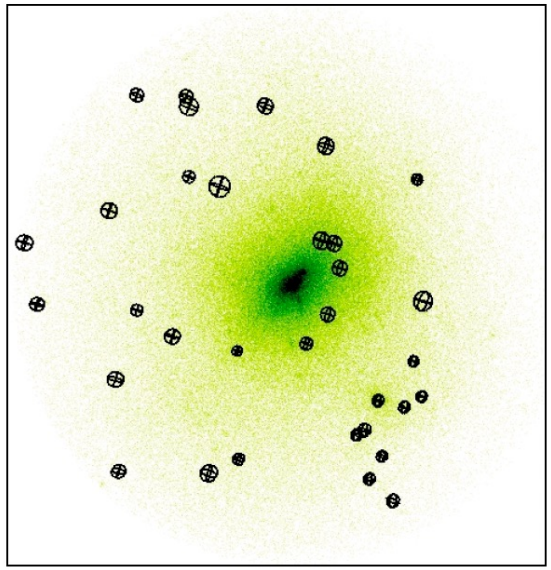

- AHT (**H**alo **T**racking!)

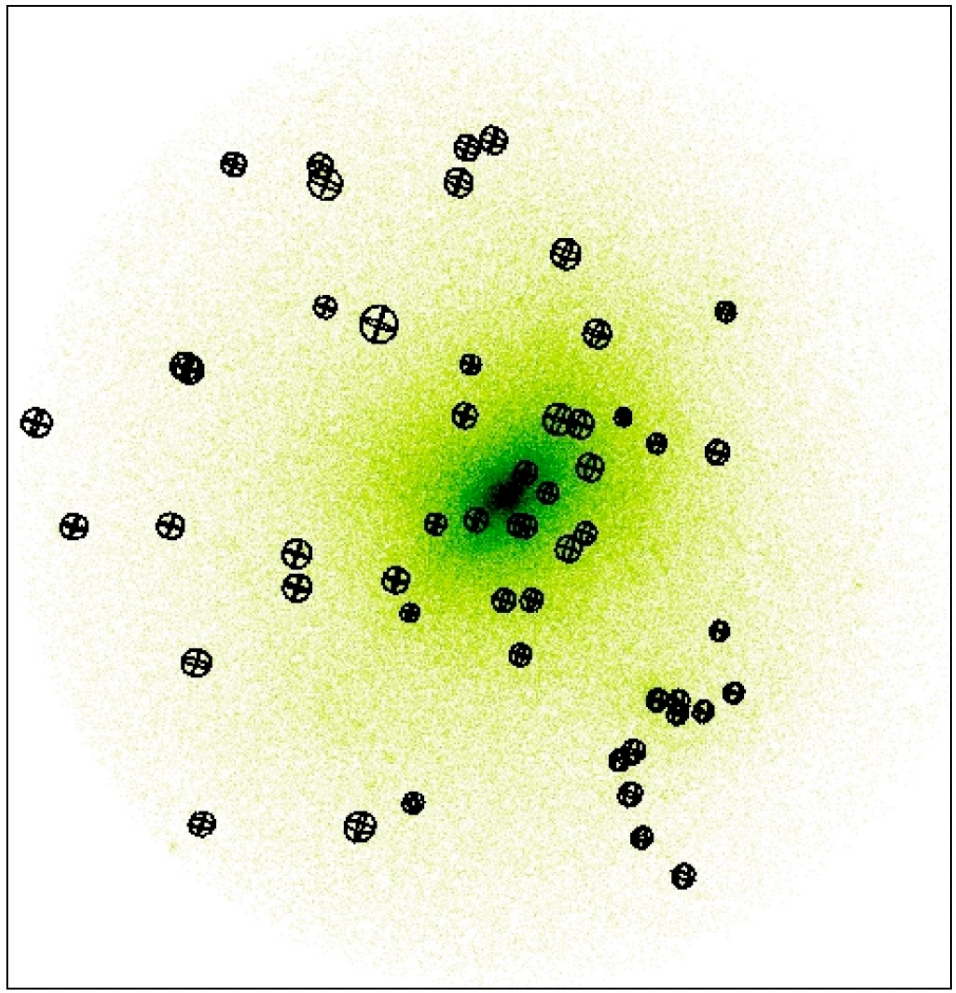

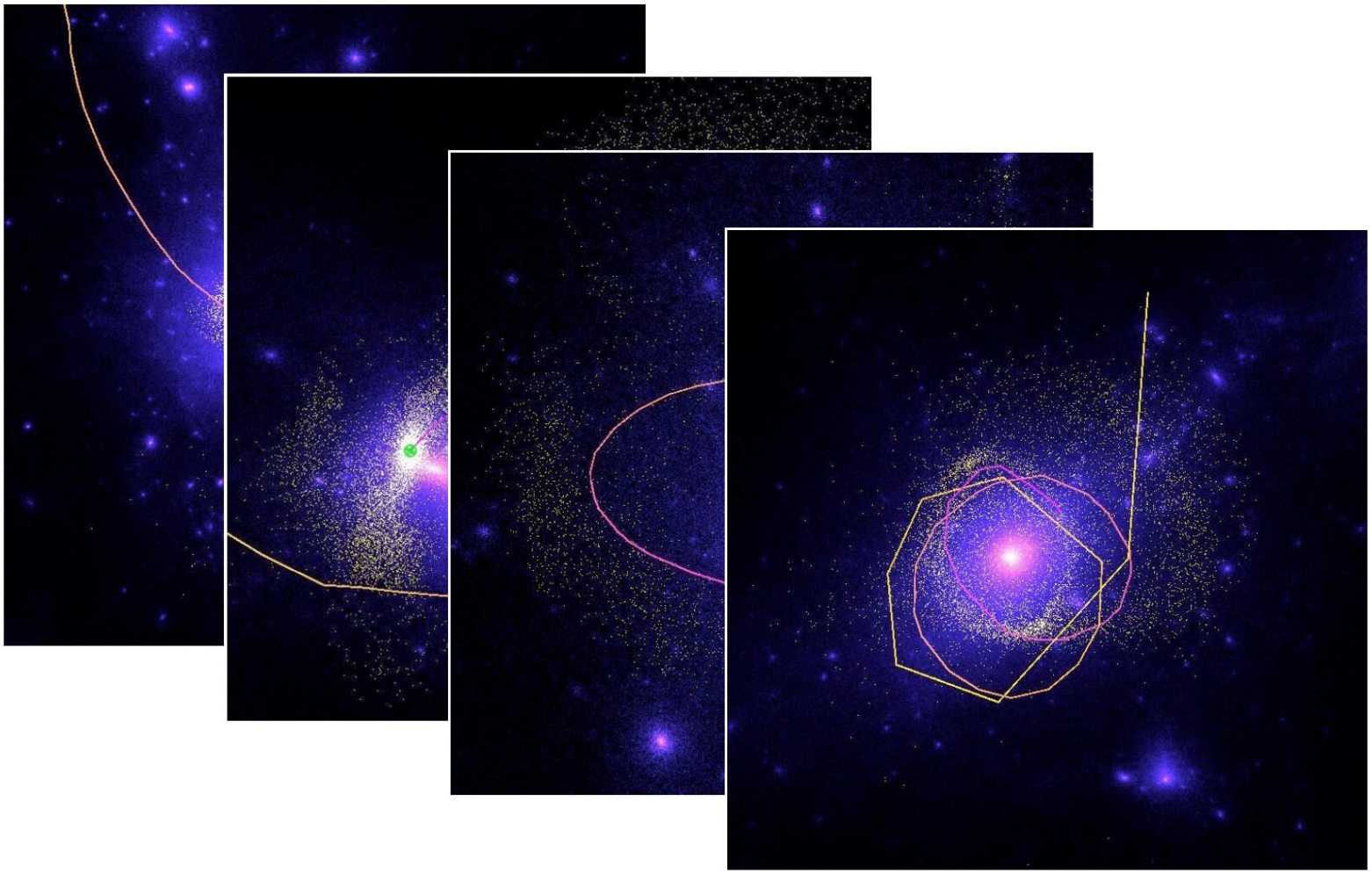

When a halo finder is run on a simulation you will typically get a “halo catalogue”

When a halo finder is run on a simulation you will typically get a “halo catalogue”

This is a list of haloes with some properties (x, y, z, vx, vy, vz, mass, Energy, shape, …)

When a halo finder is run on a simulation you will typically get a “halo catalogue”

This is a list of haloes with some properties (x, y, z, vx, vy, vz, mass, Energy, shape, …)

#ID(1)	hostHalo(2)	numSubStruct(3)	Mvir(4)	npart(5)	Xc(6)	Yc(7)	Zc(8)
127000000000001	0	1752	2.34935e+12	26740085	46441.03505737	49531.24803080	51553.47029923
127000000000002	0	409	1.44086e+12	18906657	47309.23661998	48802.66161311	50002.73253084
127000000000003	0	1069	1.31579e+12	17171289	46793.65378773	49055.29328568	49881.18052007
127000000000004	0	577	1.00862e+12	12063540	47782.36733236	49822.09489433	47597.90234895
127000000000005	0	570	4.16899e+12	6006416	44119.84438277	51643.21753573	52218.96551971
127000000000006	0	187	2.9774e+11	3870341	44549.11847807	50869.39189600	52192.86105408
127000000000007	0	69	2.59742e+11	3605789	46225.65400906	49714.99741077	51828.53203553
127000000000008	0	127	2.23647e+11	3001523	46228.13064692	49834.08915442	49901.28384234
127000000000009	0	140	5.72373e+11	2827996	43315.14396883	52759.86072874	49605.59046165
127000000000010	127000000000003	7	1.84868e+11	2671554	46735.79314672	49126.77516480	49892.31573185
127000000000011	0	172	1.99683e+11	2575597	47850.81529003	48463.41202743	51794.76812120
127000000000012	0	140	1.88151e+11	2498314	45162.67376942	49729.08219575	50359.77686718
127000000000013	0	76	2.0574e+11	2465067	47635.59279811	50609.69999500	47238.87666676
127000000000014	0	166	2.20189e+11	2437113	43958.22313097	47828.14145088	49744.13189623
127000000000015	0	140	1.65608e+11	2167230	46678.17495371	49685.29390661	49249.08703879
127000000000016	0	118	1.49317e+11	2043932	45774.03702962	50216.59548669	49419.30602588
127000000000017	0	122	1.68918e+11	1997509	48719.76524059	50912.02358912	50452.96993940
127000000000018	0	105	1.37485e+11	1730755	45312.70287655	50646.21104134	51758.34982483
127000000000019	0	89	1.19378e+11	1536920	48173.23627230	47832.53453039	52199.31425222
127000000000020	0	117	1.14328e+11	1467379	44212.14349568	48441.63767993	50079.22202349
127000000000021	0	54	9.66642e+10	1451784	46980.39552099	48896.59332602	51692.03046121
127000000000022	0	4	8.64187e+11	1343391	43359.05710856	52952.81949497	49503.10403392

When a halo finder is run on a simulation you will typically get a “halo catalogue”

This is a list of haloes with some properties (x, y, z, vx, vy, vz, mass, Energy, shape, …)

There will also be a file that tells you each particle that belongs to each haloes

```
         162987
26740085 127000000000001
1699593619      4
1592799443      4
1688903932      4
1838057133      4
186690941       1
1285996190      4
1328258335      4
1393158618      4
1264103035      4
1570404843      4
1500575420      4
1560421018      4
1618798338      4
1647224262      4
1648753038      4
1668351832      4
748792458       4
799581810       4
556304099       4
1671967458      4
1854815260      4
1689534454      4
1014113512      4
```

When a halo finder is run on a simulation you will typically get a “halo catalogue”

This is a list of haloes with some properties (x, y, z, vx, vy, vz, mass, Energy, shape, …)

#ID(1)	hostHalo(2)	numSubStruct(3)	Mvir(4)	npart(5)	Xc(6)	Yc(7)	Zc(8)
126000000000001	0	1771	2.33438e+12	26619300	46509.52004646	49470.88449566	51589.10719985
126000000000002	0	424	1.42725e+12	18765241	47368.17615824	48729.10773211	50024.46450771
126000000000003	0	1006	1.26857e+12	16723263	46845.64732588	48990.29740920	49898.32240802
126000000000004	0	579	1.00733e+12	12041501	47843.05870775	49771.65515006	47618.62192359
126000000000005	0	562	4.04505e+12	5694346	44185.18887964	51566.13696790	52265.20203402
126000000000006	0	182	2.98763e+11	3875521	44625.37531161	50796.99874274	52218.40929358
126000000000007	0	65	2.60177e+11	3597227	46270.45812932	49672.35611244	51866.32383953
126000000000008	0	124	2.23063e+11	2994820	46268.64188447	49767.13983663	49918.75617155
126000000000009	126000000000003	19	2.25407e+11	2993682	46769.51447036	49086.89524072	49894.74858219
126000000000010	0	157	5.82901e+11	2877093	43369.13350889	52667.37644371	49602.81409279
126000000000011	0	171	1.99996e+11	2578404	47909.88961494	48399.91587905	51820.16082413
126000000000012	0	137	1.88183e+11	2493869	45203.64186248	49653.88958519	50376.79137410
126000000000013	0	80	2.05885e+11	2452245	47696.97290987	50569.14878514	47258.97801506
126000000000014	0	175	2.16873e+11	2397769	44002.10788375	47755.59243403	49759.09684834
126000000000015	0	156	1.64798e+11	2158312	46727.28340800	49623.15668420	49251.34821636
126000000000016	0	114	1.49291e+11	2039566	45815.68030033	50150.38448559	49427.58085226

When a halo finder is run on a simulation you will typically get a “halo catalogue”

This is a list of haloes with some properties (x, y, z, vx, vy, vz, mass, Energy, shape, …)

There will also be a file that tells you each particle that belongs to each haloes

For each snapshot:

163387	
26619300	126000000000001
1352401101	4
1122106503	4
1559515852	4
1212587238	4
1700457403	4
1832049454	4
1152940510	4
1788826697	4
780514059	4
1427780231	4
1437162399	4
1605198567	4
1650840292	4
1773428268	4
1638650056	4
1840483454	4
1030655781	4
1784262913	4
1146275938	4
574694926	4
1849585096	4
1412941280	4
1636807352	4
930890261	5
1757703349	4
1709521509	4
1698640173	4
1633500826	4
1131192316	4
1609817513	4
1658062679	4
1440606741	4
1668351832	4

162987	
26740085	127000000000001
1699593619	4
1592799443	4
1688903932	4
1838057133	4
186690941	1
1285996190	4
1328258335	4
1393158618	4
1264103035	4
1570404843	4
1500575420	4
1560421018	4
1618798338	4
1647224262	4
1648753038	4
1668351832	4
748792458	4
799581810	4
556304099	4
1671967458	4
1854815260	4
1689534454	4
1014113512	4
186576507	1
1376328380	4
1506037139	4
1416709503	4
555633640	4
213977843	1
1674744109	4
1826558938	4
672147470	4
1563021071	4

When a halo finder is run on a simulation you will typically get a “halo catalogue”

This is a list of haloes with some properties (x, y, z, vx, vy, vz, mass, Energy, shape, …)

There will also be a file that tells you each particle that belongs to each haloes

For each snapshot:

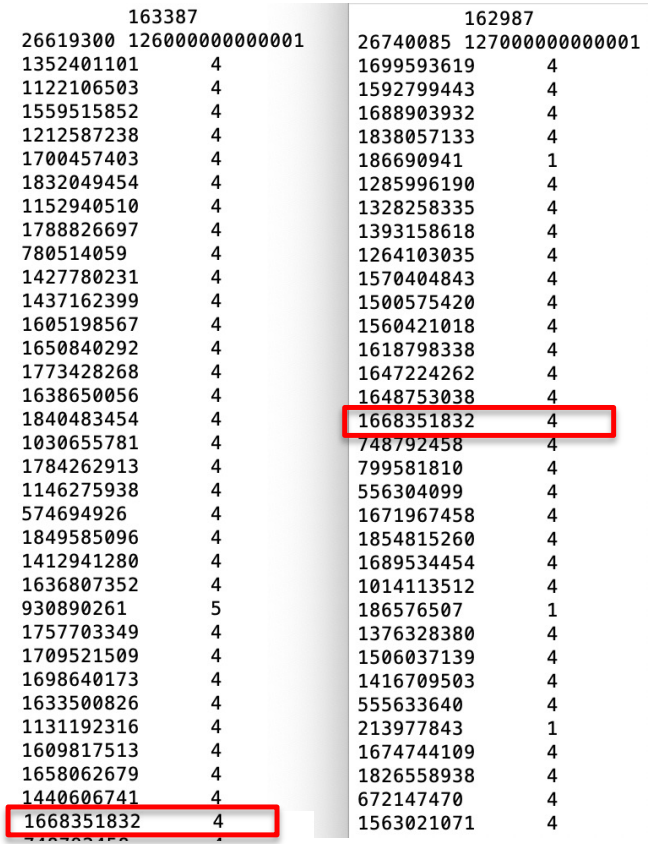

163387	
26619300	126000000000001
1352401101	4
1122106503	4
1559515852	4
1212587238	4
1700457403	4
1832049454	4
1152940510	4
1788826697	4
780514059	4
1427780231	4
1437162399	4
1605198567	4
1650840292	4
1773428268	4
1638650056	4
1840483454	4
1030655781	4
1784262913	4
1146275938	4
574694926	4
1849585096	4
1412941280	4
1636807352	4
930890261	5
1757703349	4
1709521509	4
1698640173	4
1633500826	4
1131192316	4
1609817513	4
1658062679	4
1440606741	4
1668351832	4

162987	
26740085	127000000000001
1699593619	4
1592799443	4
1688903932	4
1838057133	4
186690941	1
1285996190	4
1328258335	4
1393158618	4
1264103035	4
1570404843	4
1500575420	4
1560421018	4
1618798338	4
1647224262	4
1648753038	4
1668351832	4
748792458	4
799581810	4
556304099	4
1671967458	4
1854815260	4
1689534454	4
1014113512	4
186576507	1
1376328380	4
1506037139	4
1416709503	4
555633640	4
213977843	1
1674744109	4
1826558938	4
672147470	4
1563021071	4

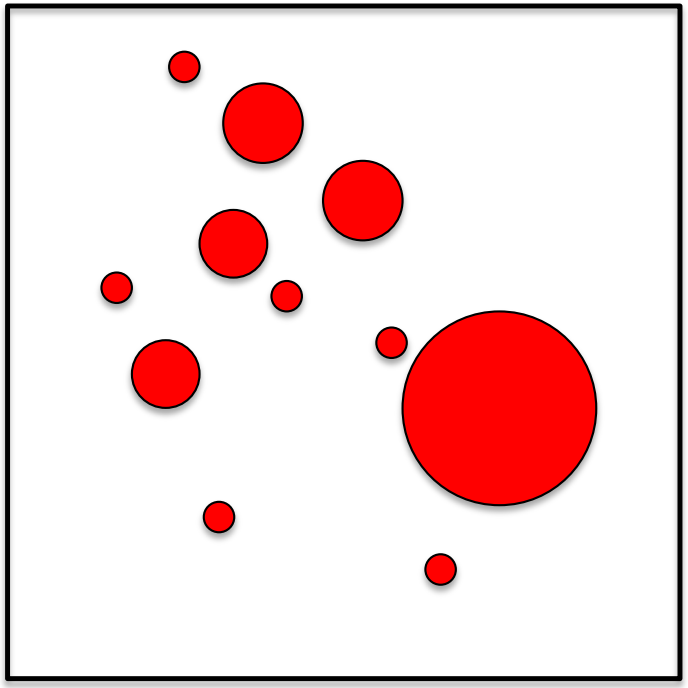

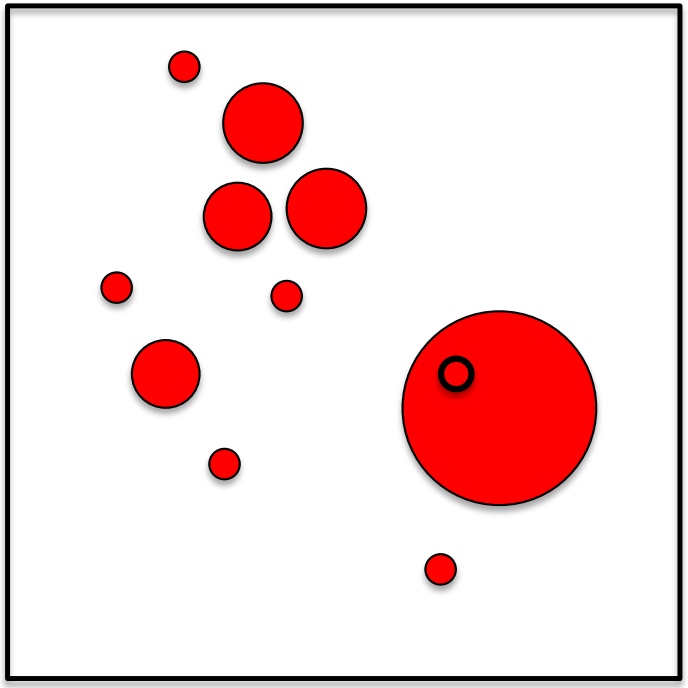

z1

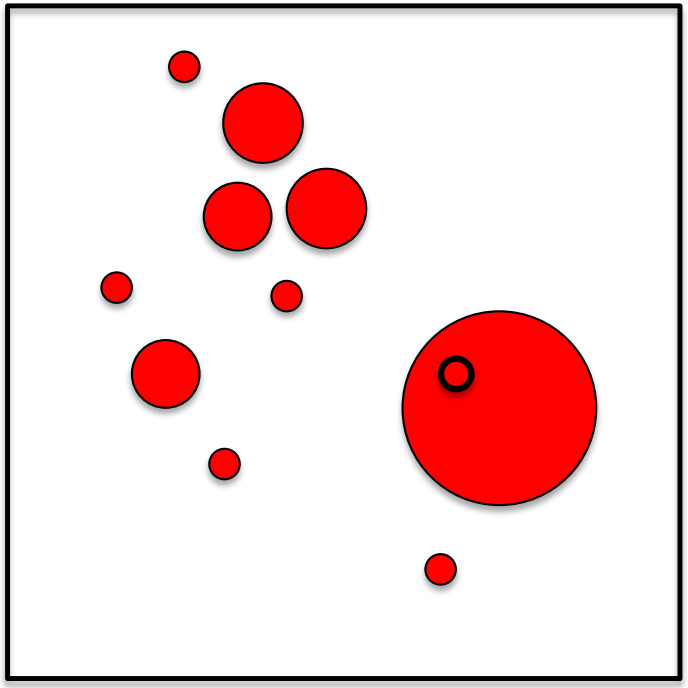

z0

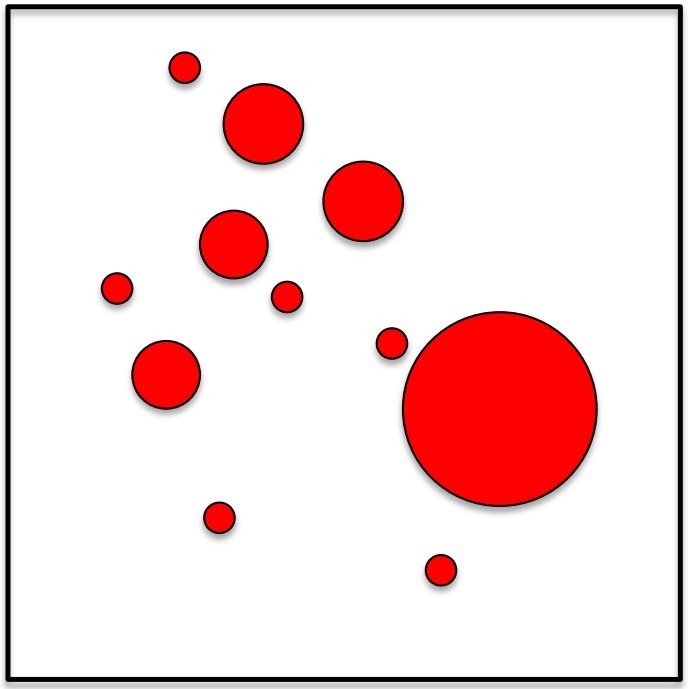

- merger tree for a sample (sub-)halo in file #1

file #1

- merger tree for a sample (sub-)halo in file #1

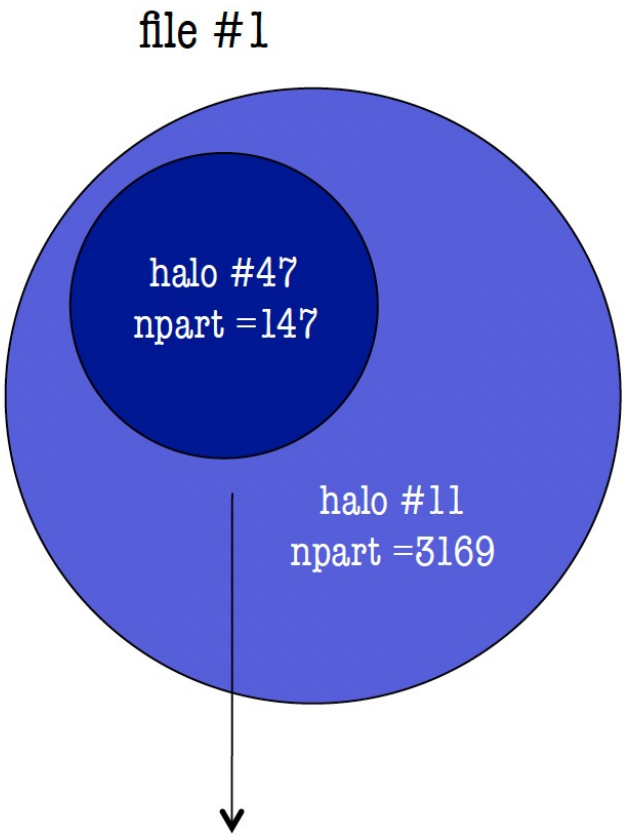

remember, ***AHF*** gives "inclusive" `*_particles` files, i.e. particles belonging to subhalo #47 also belong to host halo #11

- merger tree for a sample (sub-)halo in file #1

file #1

- merger tree for a sample (sub-)halo in file #1

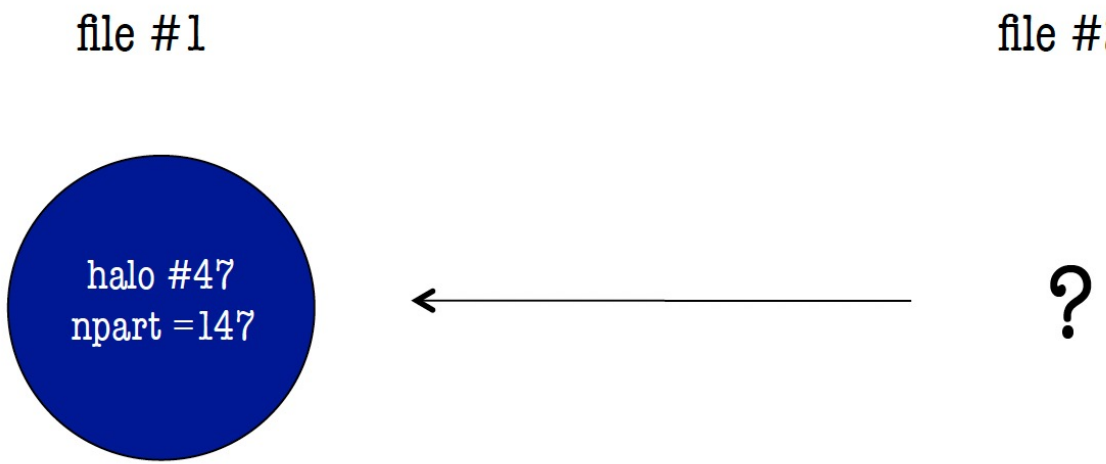

- merger tree for a sample (sub-)halo in file #1

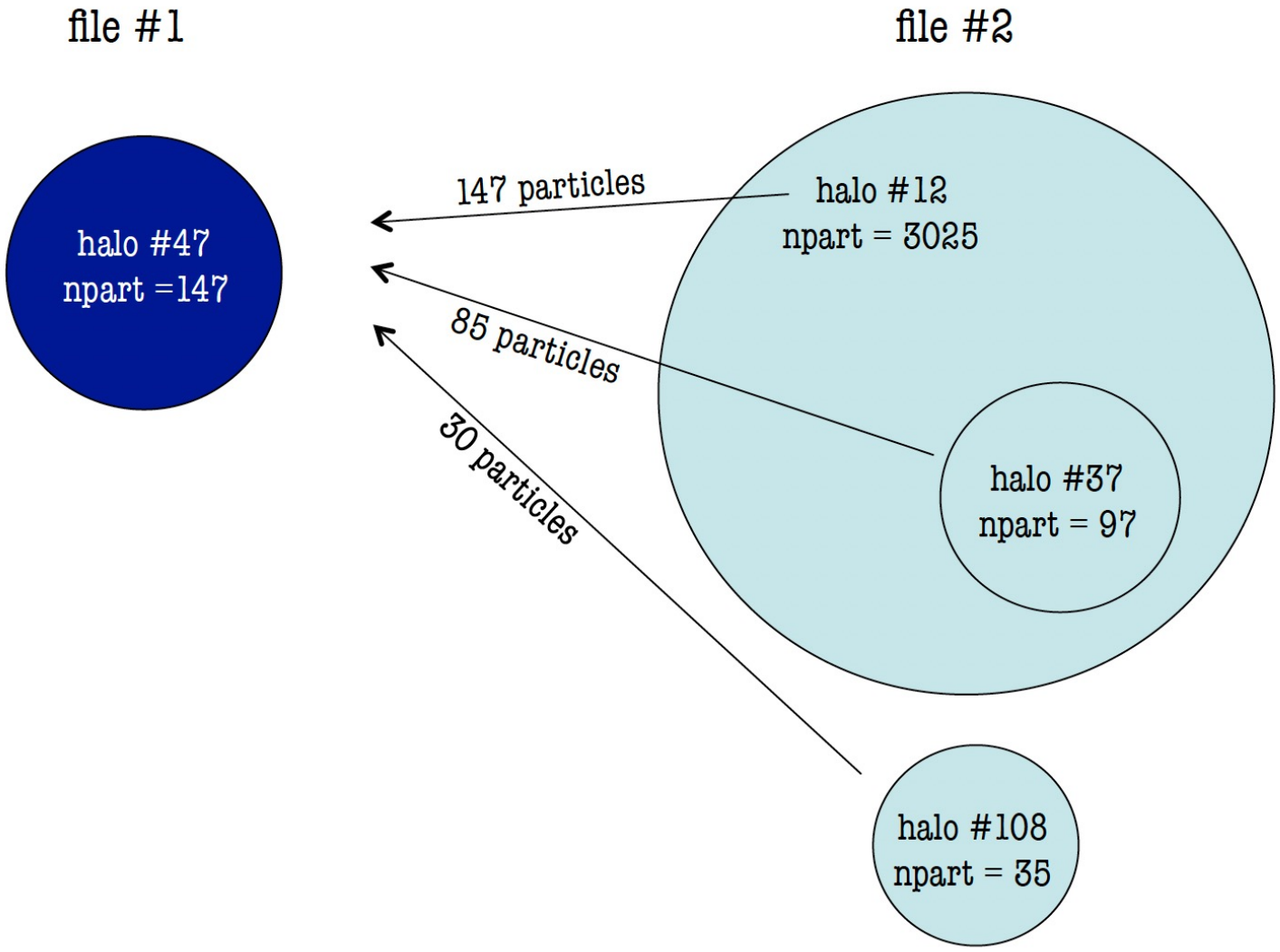

- merger tree for a sample (sub-)halo in file #1

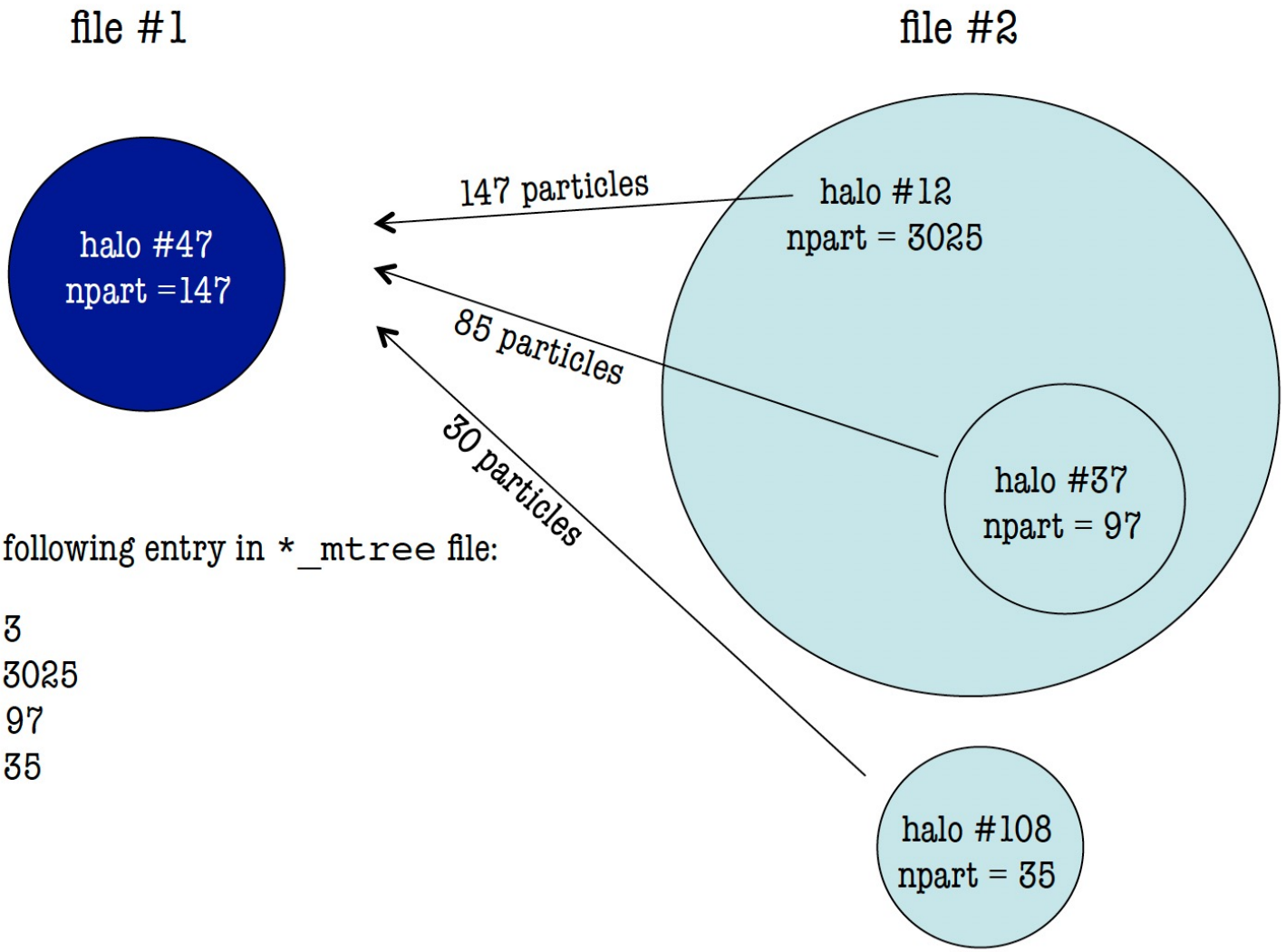

this gives the following entry in `*_mtree` file:

```
47    147    3
  147   12    3025
  85    37    97
  30    108   35
```

- merger tree for a sample (sub-)halo in file #1

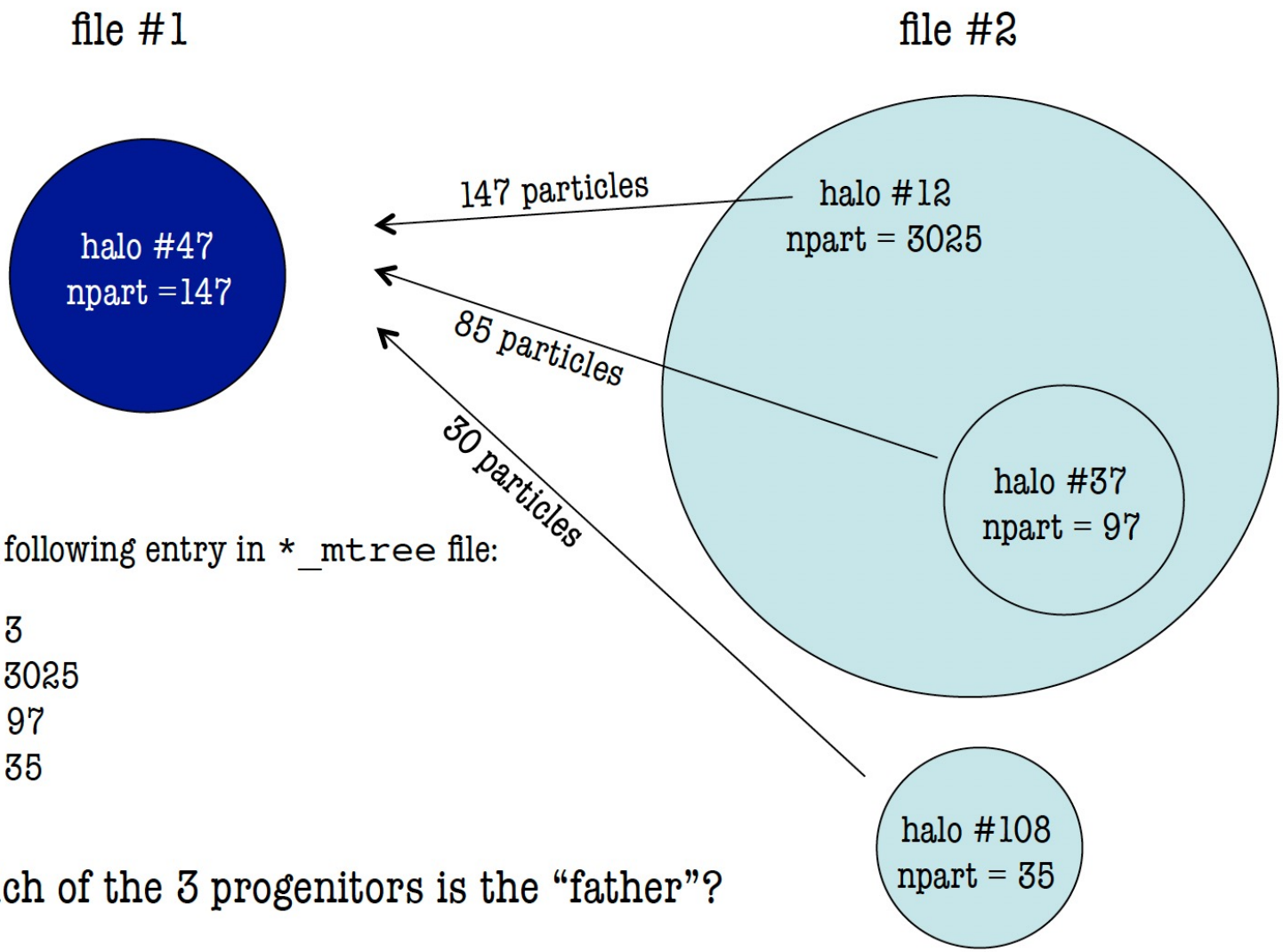

this gives the following entry in `*_mtree` file:

```
47    147    3
  147   12    3025
  85    37    97
  30    108   35
```

but which of the 3 progenitors is the “father”?

- merger tree for a sample (sub-)halo in file #1

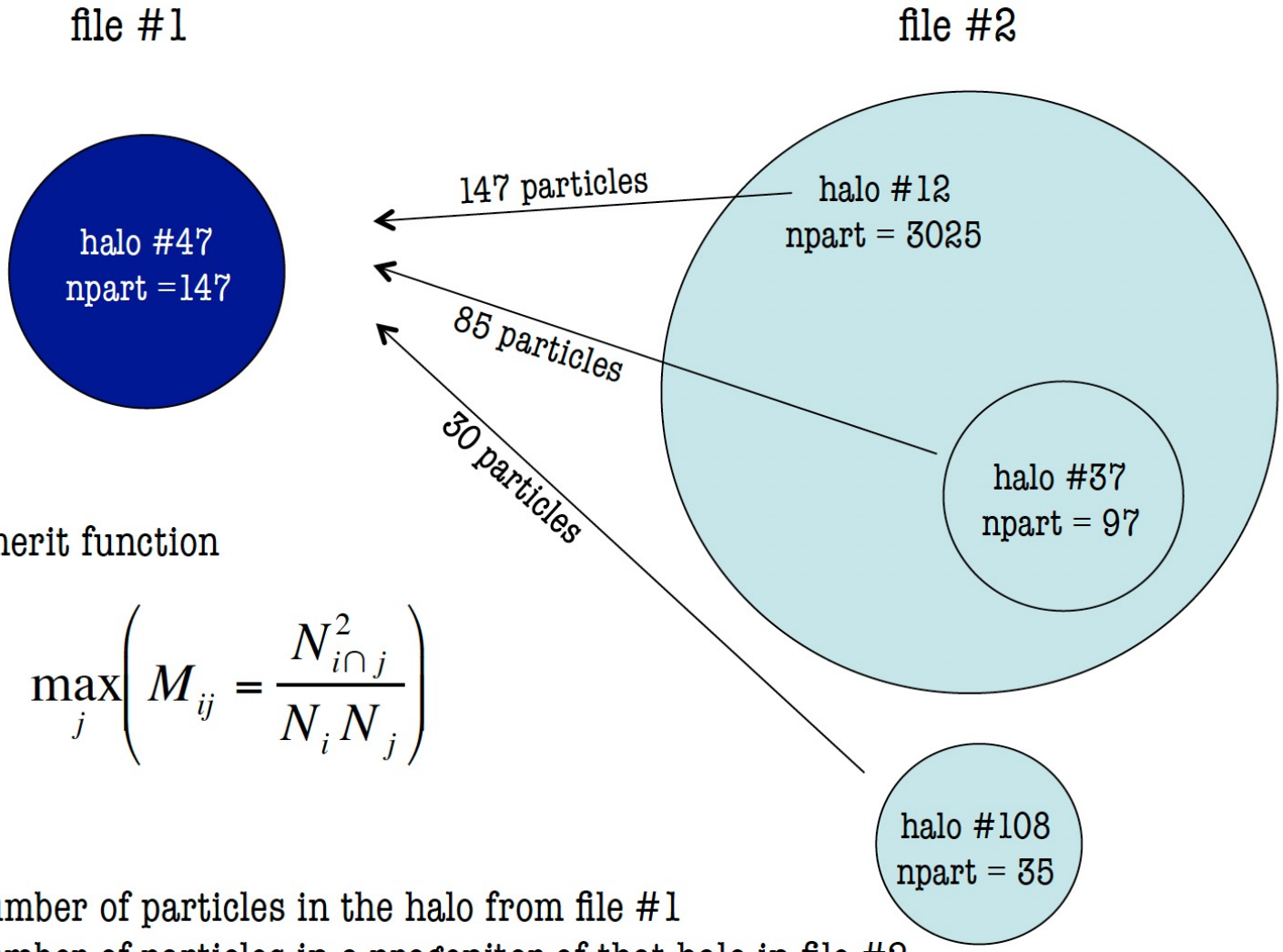

maximize merit function

$$\max_j \left(M_{ij} = \frac{N_{i\cap j}^2}{N_i N_j} \right)$$

where

N_i is the number of particles in the halo from file #1
N_j is the number of particles in a progenitor of that halo in file #2
N_{ij} is the number of shared particles

- merger tree for a sample (sub-)halo in file #1

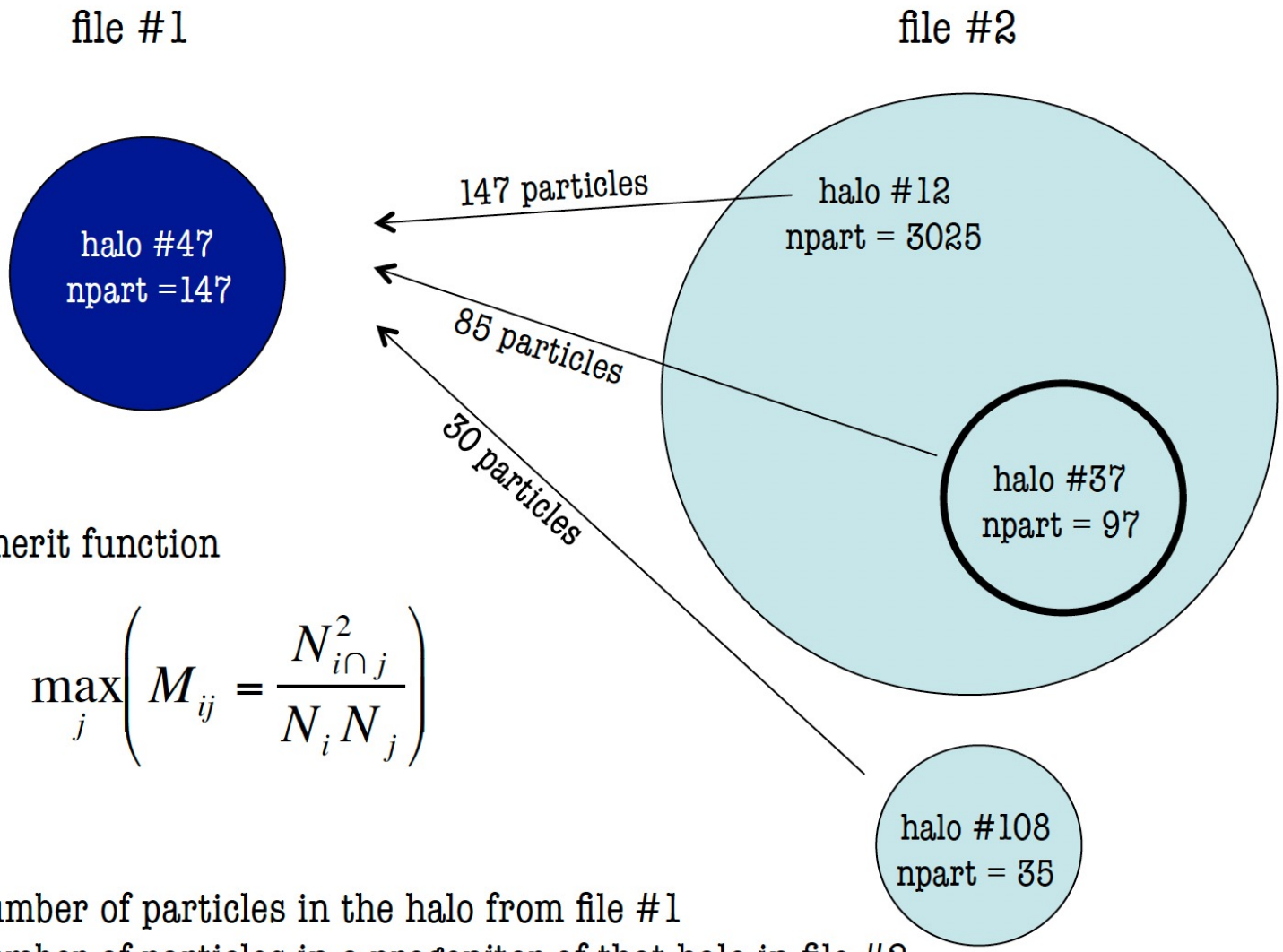

maximize merit function

$$\max_j \left(M_{ij} = \frac{N_{i\cap j}^2}{N_i N_j} \right)$$

where

N_i is the number of particles in the halo from file #1
N_j is the number of particles in a progenitor of that halo in file #2
N_{ij} is the number of shared particles